



PH.D. THESIS
IN THEORETICAL PHYSICS



Resummation of soft and hard gluon radiation in perturbative QCD

by

Marco Bonvini

Supervisors: **Giovanni Ridolfi**
Stefano Forte

Exam date: **February 29, 2012**

DIPARTIMENTO DI FISICA DELL'UNIVERSITÀ DI GENOVA,
VIA DODECANESO 33, 16146 GENOVA.

arXiv:1212.0480v1 [hep-ph] 3 Dec 2012

Abstract

This thesis arises in the context of precision measurements at hadron colliders. The Tevatron and the LHC provide very accurate measurements of many Standard Model processes, such as the production of a lepton pair (Drell-Yan) of high invariant mass. An accurate theoretical prediction of such processes is crucial to be able to distinguish Standard Model physics from possible new physics signals. QCD effects in the computation of the cross-sections at hadron colliders are usually sizable; in particular, in some kinematical regimes they behave in a non-perturbative way. In these cases the resummation of the whole perturbative series is needed for accurate phenomenological predictions. In this thesis the impact of threshold and high-energy resummations for the production of high invariant mass systems (Drell-Yan, Higgs) are studied in detail. In particular, in the threshold case a prescription to deal with the divergent nature of the perturbative series based on Borel summation is presented, and compared with the other prescriptions in the literature. Results for the invariant mass distributions and rapidity distributions are presented. The high-energy resummation formalism is reviewed and improved, and its impact in phenomenological applications at hadron colliders is investigated. In particular, a possible interaction between the two resummation regimes is studied in some detail.

Contents

Introduction	1
1 QCD and the Parton Model.	5
1.1 Basics of QCD	5
1.2 The parton model	7
1.3 GLAP evolution equations	13
1.4 Solving the GLAP equation	20
2 Soft-gluon resummation	27
2.1 Inclusive cross-sections resummation	27
2.2 Rapidity distributions resummation	48
2.3 Numerical implementation.	51
3 High-energy resummation	55
3.1 High-energy factorization	56
3.2 BFKL equation	57
3.3 The Double-Leading approximation	58
3.4 Symmetrization	62
3.5 Running coupling corrections to the BFKL equation.	68
3.6 Resummed anomalous dimensions	76
3.7 Resummed splitting function	83
4 Combining resummations	87
4.1 When is threshold resummation relevant?	87
4.2 Phenomenology of high-energy resummation	97
4.3 Joint effect of both resummations	100
4.4 Toward a joint resummation	103
5 Phenomenology	105
5.1 The Drell-Yan pair production	105

Conclusions	129
A QCD running coupling	131
A.1 The running of α_s	131
B Mellin transformation	137
B.1 Laplace transform	137
B.2 The Mellin transform	138
B.3 Plus distribution	140
B.4 Mellin transformation of logarithms	143
C Analytical expressions	151
C.1 Drell-Yan process at fixed perturbative order	151
C.2 Higgs production at fixed perturbative order	154
C.3 Soft-gluons resummation formulae	156
C.4 High-energy resummation at NLO	160
D Series and divergent series	175
D.1 Series	175
D.2 Divergent series and their sum	178
D.3 Borel summation	180
E Special functions	195
E.1 Euler Gamma and related functions	195
E.2 Riemann Zeta function	198
E.3 Hypergeometric and related functions	199
F Numerical methods	201
F.1 Numerical derivatives	201
F.2 Root finding	202
F.3 Chebyshev polynomials	202
Acknowledgments	207
Bibliography	209

Introduction

This is a very exciting moment for particle physics. After many years of planning and building, LHC and related experiments finally started; in 2010, March 30, the first collision at center-of-mass energy $\sqrt{s} = 7$ TeV took place, setting the beginning of a new era for particle physics. In April 2011, LHC set a new record in collider luminosity (roughly speaking, the number of events per second): the communication by CERN director Rolf Heuer was

Geneva, 22 April 2011. Around midnight this night CERN's Large Hadron Collider set a new world record for beam intensity at a hadron collider when it collided beams with a luminosity of $4.67 \cdot 10^{32} \text{ cm}^{-2}\text{s}^{-1}$. This exceeds the previous world record of $4.024 \cdot 10^{32} \text{ cm}^{-2}\text{s}^{-1}$, which was set by the US Fermi National Accelerator Laboratory's Tevatron collider in 2010, and marks an important milestone in LHC commissioning.

Now, the luminosity peak is $3.65 \cdot 10^{33} \text{ cm}^{-2}\text{s}^{-1}$, one order of magnitude higher than Tevatron. Today, Tevatron has collected an integrated luminosity (the integral of the luminosity over the run time) of about¹ $L_{\text{int}} \simeq 12 \text{ fb}^{-1}$ in more than 10 years (Fig. 1); LHC, instead, has already collected almost $L_{\text{int}} \simeq 6 \text{ fb}^{-1}$, most of which just in the 2011 run (Fig. 2). The integrated luminosity is a measure of how many events are collected by the experiments: a process with cross-section σ is produced roughly σL_{int} times. Hence, the largest the integrated luminosity is, the more events can be registered: this is useful when looking for some new particle, which typically has a very small cross-section.

Along the LHC ring, there are four main experiments: ATLAS (A Toroidal Lhc ApparatuS), CMS (Compact Muon Solenoid), ALICE (A Large Ion Collider Experiment) and LHCb (LHC Beauty). The last two are devoted to the study of high-density hadron matter (quark-gluon plasma) and the physics of b -hadrons (CP-violation), respectively. ATLAS and CMS, conversely, are general purpose experiments, and their main goals are searches of the Higgs boson (the last missing particle to make the Standard Model consistent) and of any kind of signals of new physics beyond the Standard Model (Super SYmmetry, extra-dimensions, ...).

To be able to see such hints of new physics beyond the Standard Model, it is crucial to have very accurate theoretical predictions of what is expected by the Standard Model, in order to be able to distinguish deviation from the expectations with the maximal significance. This thesis arises in this context.

¹The barn is a measure of surface, used in particle physics for the quantity called cross-section, and $1 \text{ b} = 10^{-24} \text{ cm}^2$.

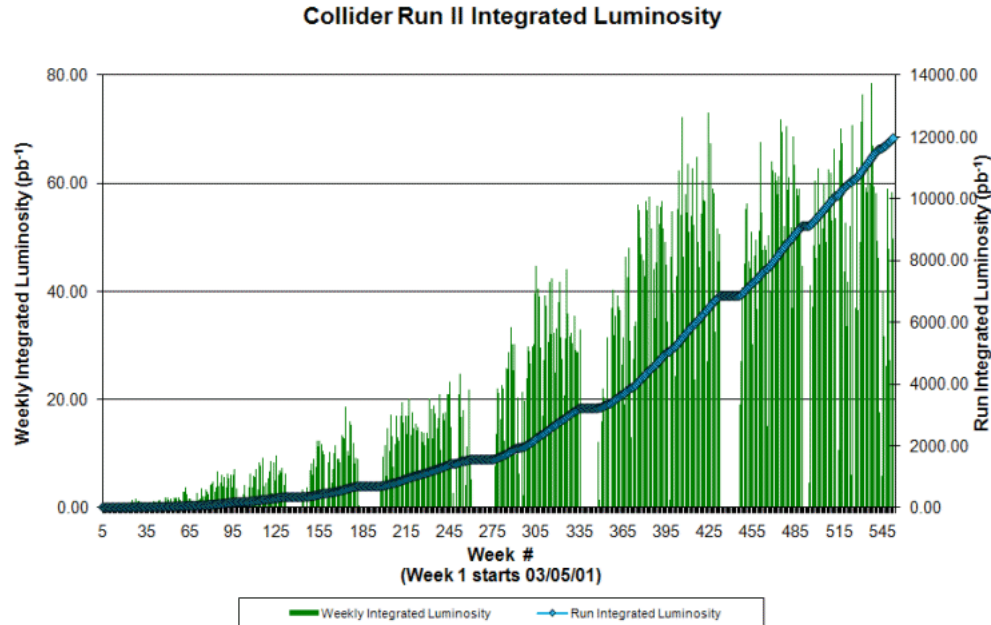


Figure 1. Tevatron integrated luminosity

The cross-sections in particle physics processes are typically computed using perturbation theory. Perturbation theory provides a very powerful tool to predict observable quantities from a quantum field theory. It is based on the assumption that every observable can be defined by a power series in the coupling constant of the theory: then, if such coupling is small, the computation of the first few orders of the power series is sufficient to accurately describe the observable. However, this assumption needs some care: it can be proved very generally that perturbative series are divergent. It is possible to interpret the perturbative expansion in the sense of asymptotic series: the inclusion of higher orders improves the estimate of the physical quantity under study, up to some finite order, thereby saving perturbation theory from a dramatic failure. However, there are situations in which the growth of the series already starts at the level of the first terms in the series: in these cases, a truncation of the series is of no meaning and only a resummed result is reliable.

In QCD this situation quite often appears. A cross-section generically depends on many energy scales, and the dependence is typically in the form of logarithms of ratios of energies. In some kinematical regimes, when two of such scales become very different each other, the logs of their ratio become large: in these cases the coefficients of the perturbative series grow fast, destroying the perturbativity of the series. Then, the entire series of these enhanced terms has to be resummed in order to have an accurate prediction for the observable.

This thesis faces with the problem of resummation of perturbation series in QCD. The processes that will be discussed are the production of high invariant mass systems at hadron colliders, such as the Drell-Yan pair production or the Higgs production. Since at hadron colliders the initial state particles are hadrons, the cross-sections are typically computed using the parton model, which describes the interaction of the

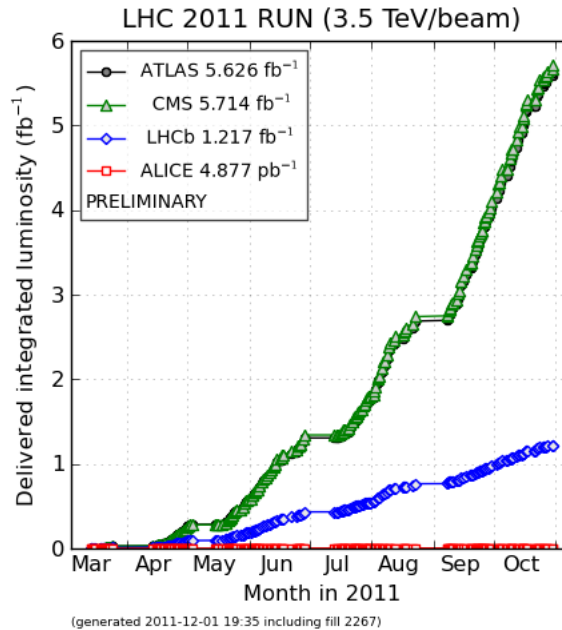


Figure 2. LHC integrated luminosity in the various experiments.

hadron via its partons (quarks and gluons): the parton-level cross-section is then computed in QCD using perturbation theory, and the hadronic cross-section is found from it by convolution with the parton distribution functions, which are non-perturbative objects extracted from data describing the distribution of partons momenta in the hadron. At parton level, the relevant scales are the invariant mass M of the final state and the partonic center-of-mass energy $\sqrt{\hat{s}}$: their ratio $z = M^2/\hat{s}$ appears in the perturbative coefficients of the partonic cross-section. If only the relevant final state were produced, z would be 1; however, even at parton level, also the emission of other particles (in particular, gluons) must be considered, and therefore $z \neq 1$ in general. Gluon emission produces large logarithms in the partonic cross-section: the energy squared carried by the gluons is $\hat{s} - M^2 = (1 - z)\hat{s}$, and in the partonic cross-section powers of $\log(1 - z)$ and $\log z$ appear. These logs are large in the two opposite limits $z \rightarrow 1$, when the gluons have small energy (they become soft), and $z \rightarrow 0$, when the energy of the gluons is large (hard gluons). The soft $\log(1 - z)$ are also referred to as threshold logarithms, as the limit $z \rightarrow 1$ is the threshold for the production of the system with mass M having an energy $\sqrt{\hat{s}} = M/\sqrt{z}$ available. The hard $\log z$ are also referred to as high-energy logarithms, as they are large when the energy \hat{s} is large compared to M^2 . Then, as $z \rightarrow 1$ or 0, the partonic cross-section needs to be resummed.

The thesis is divided in three parts: the first accounts for the resummation of threshold logarithms, the second treats the resummation of high-energy logarithms, and in the last part the effect of both resummations for phenomenology is discussed and some phenomenological results are shown.

Concerning threshold resummation, the main result of the work presented here is the extension and the improvement of a prescription necessary to extract a finite sum from the divergent perturbative series. Such prescription is based on the Borel summation of divergent series, and provides an alternative to another one present in

the literature and widely used, called the minimal prescription. The Borel prescription presents some convenient features, both theoretically and practically. In particular, it is much more suitable than the minimal prescription for phenomenological applications: one of the results presented here is indeed a fast numerical implementation of the Borel prescription by means of Chebyshev polynomials. Another new result is the extension of threshold resummation formalism to the case of rapidity distributions: this is phenomenologically very useful because rapidity distributions are measured with high accuracy at hadron colliders.

In the second part, the high-energy resummation is discussed in some detail. Some improvements are proposed, mainly directed to an efficient numerical implementation. In fact, the most relevant result concerning high-energy resummation is the realization of a fast and stable code which implements the complex procedure of resummation of high-energy logarithms. Such a code was hitherto not available, and it will be useful to increase the accuracy of the parton distribution functions.

Finally the relevance of threshold resummation is discussed quantitatively. As sketched above, the variable which governs threshold resummation is the partonic ratio z , but z is not fixed by the hadron-level kinematics. Conversely, the hadronic process is governed by the variable $\tau = M^2/s$, where \sqrt{s} is the hadronic center-of-mass energy. Then it is not obvious if, for a given τ , the threshold region $z \sim 1$ gives a sizable contribution, thereby determining the need of resummation. An argument based on a saddle-point approximation of the integral defining the hadronic cross-section is then presented, which provides a quantitative way to establish for which values of τ threshold resummation should be included. Such values of τ are found to be unexpectedly small, thereby entering in the region of relevance of high-energy resummation. Then a discussion on the interplay of the two resummations is presented: it turns out that the Drell-Yan process is not strongly affected by high-energy resummation, while the impact on the Higgs production is potentially sizable. Finally, some phenomenological predictions for the Drell-Yan process at the Tevatron and the LHC are presented and compared to data.

Before discussing all these aspects in details, in the first Chapter some basic ingredients concerning QCD are introduced.

1

QCD and the Parton Model

Contents

1.1 Basics of QCD	5
1.1.1 The running of the QCD coupling constant	6
1.2 The parton model	7
1.2.1 Deep-inelastic scattering	9
1.2.2 Radiative corrections and factorization	11
1.3 GLAP evolution equations	13
1.3.1 The non-singlet sector	14
1.3.2 The singlet sector	15
1.4 Solving the GLAP equation	20
1.4.1 Explicit running coupling	20
1.4.2 The non-singlet case	21
1.4.3 The singlet case	22

We will review some basics of QCD, introduce the parton model and describe in more details the GLAP evolution equations. This Chapter is by no means intended as a complete review; in particular we assume the Reader knows the quantum theory of fields. We intend this Chapter as a short introduction useful to fix some notations.

1.1 Basics of QCD

QCD is a gauge field theory with gauge group $SU(3)$. The gauge bosons of the theory are called gluons, and are massless (no Higgs-like mechanism takes place for them). The fermions which carry a $SU(3)$ charge are called quarks, and in the SM they have fractional electric charge which is either $2/3$ or $-1/3$ (and, of course, the opposite sign for the anti-quarks). We know so far six quarks, i.e. three pairs (families) of different charge, as in the following table:

electric charge	family		
	1	2	3
$2/3$	u	c	t
$-1/3$	d	s	b

The different kind of quarks are also usually called flavours. The masses and names of the quarks are as in the following table:

flavour	d	u	s	c	b	t
name	down	up	strange	charm	bottom	top
mass ($\overline{\text{MS}}$)	~ 2.5 MeV	~ 5 MeV	0.1 GeV	1.3 GeV	4.2 GeV	173 GeV

The top quark t , the heaviest one, has been observed directly only recently at Tevatron [1, 2]. The number of quark flavours in the theory is called n_f , and as far as we know $n_f = 6$.

Since the three lightest quarks have very small masses, the QCD lagrangian has an approximate global $U(3)$ symmetry (called a flavour symmetry): it is from this symmetry that the ancient quark model has been built (without knowing anything about QCD). This approximate symmetry is quite rough, but if we consider only the up and down quarks (whose mass are really very small) we get a very good approximate $U(2)$ symmetry. Actually, since the two chiral components of quark fields are completely independent in the massless limit, there are two independent $U(2)$ symmetries for each chiral component, and the global approximate symmetry is $U(2)_L \times U(2)_R$, or, considering vector and axial combinations, $U(2)_V \times U(2)_A$. Now, $U(2)_V = SU(2)_I \times U(1)_B$ is a good symmetry that we see in Nature, since it corresponds to isospin and baryon number. Instead, $U(2)_A = SU(2)_A \times U(1)_A$ is spontaneously broken: hence we expect to find in the spectrum of hadrons the vestiges of the four Goldstone bosons, but only three (the pions, associated with $SU(2)_A$) are present. The absence of a Goldstone boson associated with $U(1)_A$ was known as the $U(1)_A$ problem. Its solution relies on the non-trivial topology of the QCD vacuum. Indeed, the axial current associated with $U(1)_A$ has an anomaly proportional to $\epsilon_{\mu\nu\rho\sigma} G^{\mu\nu} G^{\rho\sigma}$; this term is a total derivative, and then would classically vanish, but due to instanton effects, this term contributes at quantum level, breaking explicitly the $U(1)_A$ symmetry. The axial anomaly induces an effective term in the QCD lagrangian proportional to the anomaly, which clearly violates CP in the strong sector. However we don't see any violation of the CP symmetry in QCD, and why this is the case is still an open question, known as the strong CP problem. An elegant solution comes from Peccei and Quinn [3], who introduced a new axial scalar field (the axion) which couples to the CP-violating term in the QCD lagrangian, dynamically solving the strong CP problem. However, the axion has not been discovered so far.

1.1.1 The running of the QCD coupling constant

Because of renormalization, the QCD coupling constant $\alpha_s = \frac{g_s^2}{4\pi}$ runs. The Callan-Symanzik equation (or renormalization-group equation) for α_s is

$$\mu^2 \frac{d}{d\mu^2} \alpha_s(\mu^2) = \beta(\alpha_s(\mu^2)) \quad (1.1.1)$$

where the β -function is

$$\beta(\alpha_s) = -\alpha_s^2 (\beta_0 + \beta_1 \alpha_s + \beta_2 \alpha_s^2 + \dots) \quad (1.1.2)$$

and the β_i coefficients are known up to 4 loops ($i = 3$). More details on analytic solutions of the equation will be given in App. A. The leading coefficient is

$$\beta_0 = \frac{11C_A - 2n_f}{12\pi} \quad (1.1.3)$$

and it is positive as long as $n_f < 17$. Because of the minus sign in front of the β_0 term, Eq. (1.1.2), as μ^2 increases α_s decreases: QCD is asymptotically free, i.e. it decouples at high energies.¹

Conversely, at low energies the coupling grows, exiting the perturbative regime: then, at such energies the perturbative β -function is no longer good, and we no longer believe the solution of the perturbative renormalization group equation. If we ignore for a moment this fact, and compute the perturbative solution of the renormalization group equation even at low energies, we discover that the running coupling α_s has a singularity at some $\mu^2 = \Lambda^2$, called the Landau pole. The scale Λ , sometimes indicated Λ_{QCD} , is a scale at which QCD is non-perturbative, and it is typically of the order of some hundreds MeV; the exact value depends on the order of the β -function used and on the initial condition for the evolution (typically $\alpha_s(m_Z^2)$ at the Z mass). The Landau pole would probably not be there in a complete non-perturbative solution of the evolution equation: it is something non-physical. However, we will see that it plays an important role in resumming the perturbative series of QCD (see Chap. 2). The non-perturbative region of QCD starts at higher scales, when α_s becomes too large to justify a perturbative expansion, typically around 1 GeV.

Even if we are not able to predict the behaviour of the coupling constant at low energies, it is clear from the renormalization group equation that QCD is strongly coupled at low energies. In Nature, indeed, we don't ever see isolated quarks or gluons, but only hadrons, i.e. composite objects made of quarks and gluons which belong to the singlet representation of the gauge group $\text{SU}(3)$. This fact is known as *confinement*, and it cannot be explained by use of perturbative QCD (pQCD for short); from lattice simulations, there is some evidence that quarks confine, but a complete non-perturbative explanation is still missing. Of course, being composite objects, the description of the interaction between hadrons and other particles is more complicated than for elementary particles: such a description, called the parton model, will be addressed in the following Section.

1.2 The parton model

As just said, hadrons are made of quarks and gluons, generically called *partons*, being the parts of the hadron. Therefore, for studying high-energy processes involving hadrons, a model which describes how a hadron interacts via its partons is generally adopted: the *parton model*. For definiteness, in the following, we will concentrate on protons, but what we will say can be in principle applied to any other hadron.

¹This statement requires a remark: in computing the solution of Eq. (1.1.1) the variable flavour number scheme is generally used, in which n_f is the number of *active* flavours, i.e. flavours whose mass is lower of the current energy μ , see App. A. If the fermion families are not only the three we know (and the corresponding quarks have larger masses), in this scheme they will enter step by step while increasing the energy. If at some point the number of active flavours crosses $n_f = 17$, we would discover that the theory is actually not asymptotically free.

The original (or naive) parton model was proposed by Feynman, and it is formulated in the *infinite momentum frame*, i.e. a reference frame in which the proton is ultrarelativistic. In such frame, we can neglect the mass of the proton ($m_p \sim 0$) and, a fortiori, the masses of the partons. Then, the basic assumption of the model is that each parton i carries a fraction z_i of the proton momentum p ,

$$\hat{p}_i = z_i p, \quad 0 \leq z_i \leq 1, \quad (1.2.1)$$

where \hat{p}_i is the momentum of the parton (we will use often a hat $\hat{}$ to indicate partonic quantities). Note that such a relation can be defined only in the infinite momentum frame, since otherwise the mass of the parton would vary with z_i , as one sees squaring Eq. (1.2.1). The exact momentum fraction z_i for each parton is not fixed by the model; instead, each parton can be picked up from the proton with a given momentum fraction z_i following the distribution

$$f_i(z_i), \quad (1.2.2)$$

called *parton distribution function* (PDF for short). As another assumption, the interaction between a proton and an elementary particle is the incoherent sum of the interaction between each parton and the elementary particle (described by the field theory), weighted with the PDFs. Then, denoting by $\hat{\sigma}_i(\hat{p})$ the cross section for the partonic process, the hadron level cross-section is

$$\sigma(p) = \sum_i \int_0^1 dz f_i(z) \hat{\sigma}_i(zp). \quad (1.2.3)$$

where p is the proton momentum.

The PDFs are defined in such a way that the probability to pick up a parton i with momentum fraction between z and $z + dz$ is $f_i(z)dz$. Some properties (sum rules) follow:

- the difference between quarks and antiquarks PDFs, integrated in z , counts the number of constituents quarks of the proton:

$$\int_0^1 dz [f_u(z) - f_{\bar{u}}(z)] = 2, \quad \int_0^1 dz [f_d(z) - f_{\bar{d}}(z)] = 1, \quad (1.2.4)$$

and all the other partons give zero.

- the sum of the momenta of all partons must equal the proton momentum:

$$\sum_i \int_0^1 dz z f_i(z) = 1. \quad (1.2.5)$$

In Eq. (1.2.3) the partonic cross-section $\hat{\sigma}_i(zp)$ is computable perturbatively from the field theory; the PDFs, instead, are intrinsically non-perturbative objects, and have to be extracted from experimental measures. The sum rules provide important constraints on the extraction process.

This formulation of the parton model is very naive. QCD perturbative corrections induce changes in the model, leading to what is sometimes called the *improved parton model*. In particular, the PDFs acquire a dependence on an energy scale: to see how this happens, we consider now in some detail a prototype process.

1.2.1 Deep-inelastic scattering

The typical process for which the parton model has been built is the deep-inelastic scattering (DIS), the collision of a proton with a lepton. We will concentrate on the case the lepton is charged, see Fig. 1.1. The process is called inelastic because the energy of the collision is such that the proton changes nature, breaking up into pieces which will form something else (possibly other hadrons).

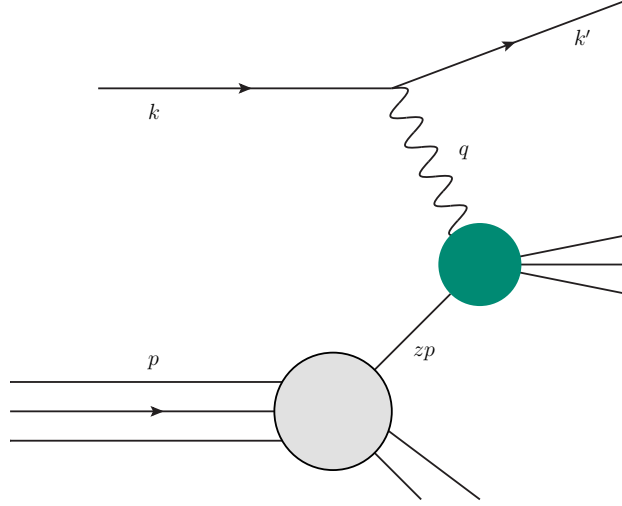


Figure 1.1. The DIS process. The green ball represents the interaction between a parton and the photon, and contains any QCD correction to the process, including real emissions.

Here we will review some results, in order to fix notations which will be useful in the following. For a complete review, see for example [4]. Very generally, we can write the amplitude for the process as

$$\mathcal{M} = e \bar{u}(k') \gamma^\mu u(k) \mathcal{P}_\mu(p, q) \quad (1.2.6)$$

where the momenta are as in Fig. 1.1, and $\mathcal{P}_\mu(p, q)$ contains the information on the hadronic part of the process, including the photon propagator. The amplitude squared, after sum over final states and mean over initial states, can be written as

$$\frac{1}{N_{\text{in, fin}}} \sum |\mathcal{M}|^2 = L_{\mu\nu} W^{\mu\nu} \quad (1.2.7)$$

where $L_{\mu\nu}$ and $W_{\mu\nu}$ are called, respectively, leptonic and hadronic tensors: the first is simply

$$L_{\mu\nu} = e^2 \text{tr} [k' \gamma_\mu k \gamma_\nu], \quad (1.2.8)$$

while the second contains all the information on the hadronic process. Skipping the computations, the final result for the cross-section can be written as

$$\frac{d\sigma}{dx dQ^2} = \frac{4\pi\alpha^2}{Q^4} \left[(1 + (1 - y)^2) F_1(x, Q^2) + \frac{1 - y}{x} (F_2(x, Q^2) - 2x F_1(x, Q^2)) \right] \quad (1.2.9)$$

where we have defined the variables

$$x = \frac{Q^2}{2pq}, \quad y = \frac{qp}{kp}, \quad Q^2 = -q^2 \quad (1.2.10)$$

and introduced the so called *structure functions* F_1 and F_2 . Such structure functions can be obtained via suitable projectors on the hadronic tensor. Note that this result is older than QCD: indeed, we haven't said anything so far about the structure of the hadronic interaction, confining any hadronic information in the structure functions, which could be measured experimentally. It is sometimes useful to define the longitudinal structure function

$$F_L(x, Q^2) = F_2(x, Q^2) - 2x F_1(x, Q^2); \quad (1.2.11)$$

as can be seen from Eq. (1.2.9), the term with F_L corresponds to the absorption of a longitudinally polarized virtual photon, while the term with F_1 corresponds to the absorption of a transversely polarized virtual photon. Since the quarks are spin 1/2, they cannot absorb longitudinal virtual photons, and then they would lead to a vanishing F_L (Callan-Gross relation): this is indeed observed in the limit $Q^2 \rightarrow \infty$ with x fixed (Bjorken limit), confirming the spin 1/2 nature of the quarks.

The hadronic tensor (and, then, the structure functions) can be computed in the parton model framework. We can write

$$F_i(x, Q^2) = x \sum_j \int_x^1 \frac{dz}{z} f_j(z) C_{ij}^{(0)}\left(\frac{x}{z}\right), \quad (1.2.12)$$

where the functions $C_{ij}^{(0)}$ are called *coefficient functions*. The superscript (0) indicates that we are ignoring QCD, i.e. we are not considering QCD corrections: we will discuss them in the next Section. Then, in the naive parton model, we have (choosing F_2 and F_L as the two independent structure functions)

$$C_{2q}^{(0)}(z) = e_q^2 \delta(1-z) \quad C_{2g}^{(0)}(z) = 0 \quad (1.2.13a)$$

$$C_{Lq}^{(0)}(z) = 0 \quad C_{Lg}^{(0)}(z) = 0 \quad (1.2.13b)$$

where e_q is the quark charge in fractions of the electric charge. Then the structure functions are

$$F_2(x, Q^2) = x \sum_q e_q^2 f_q(x), \quad F_L(x, Q^2) = 0, \quad (1.2.14)$$

where there is no actual dependence on Q^2 : this is known as *scaling*, and was observed (in the Bjorken limit) in DIS experiments.

As a final comment, we would like to note that Eq. (1.2.12) (divided by x) has the form of a Mellin convolution

$$(g \otimes h)(x) = \int_x^1 \frac{dz}{z} g(z) h\left(\frac{x}{z}\right). \quad (1.2.15)$$

It is symmetric, i.e. it has the property that, changing variable $z \rightarrow x/z$, it remains in the same form with the arguments of the two functions exchanged. The Mellin convolution diagonalizes under Mellin transform

$$\mathcal{M}[g](N) = \tilde{g}(N) = \int_0^1 dz z^{N-1} g(z), \quad (1.2.16)$$

i.e. in Mellin space we have

$$\mathcal{M}[g \otimes h](N) = \tilde{g}(N) \tilde{h}(N). \quad (1.2.17)$$

The Mellin transformation is related to a Laplace transformation by a change of variable; hence, the inverse Mellin transform is

$$\mathcal{M}^{-1}[\tilde{g}](z) = \frac{1}{2\pi i} \int_{c-i\infty}^{c+i\infty} dN x^{-N} \tilde{g}(N) \quad (1.2.18)$$

where c has to be to the right of the rightmost singularity of $\tilde{g}(N)$ (it always exists because a Mellin (Laplace) transform always has a convergence abscissa). For more details about Mellin transformation and inversion, see App. B. Note that, in the following, by an abuse of notation we will omit the $\tilde{}$ to indicate a Mellin transform, and the Reader can recognize in which space the function is by its argument.

1.2.2 Radiative corrections and factorization

The coefficient functions $C_{ij}^{(0)}(z)$, Eqs. (1.2.13), can be considered as the contribution to the coefficient functions at LO in pQCD. In pQCD, a coefficient function has a perturbative expansion

$$C_{ij}(z, \alpha_s) = C_{ij}^{(0)}(z) + \alpha_s C_{ij}^{(1)}(z) + \alpha_s^2 C_{ij}^{(2)}(z) + \dots \quad (1.2.19)$$

in powers of α_s . When considering QCD corrections to the partonic process, i.e. when computing $C^{(k)}(z)$ with $k \geq 1$, we have to consider both loop corrections and additional emissions of quarks and gluons. The reason for this is that in hadronic process we usually consider inclusive quantities: whatever happens to the proton, we don't care, we simply integrate over it. Indeed the parton model does not give us any information on what happens to the other partons which do not interact in the hard process we are considering. Then, if the "hard parton" emits, let's say, a gluon, how can we distinguish it from the mess of other things coming from the proton? We can't, and that's why we need to consider also emissions to the QCD corrections of the hard process.

The QCD corrections diagrams have both UV and IR divergences: the second ones, called also mass singularities (because they would not be there if partons were massive) appear in two forms, called respectively soft and collinear. Let us trace the origin of these in detail.

The loop diagrams diverge:

- in the UV, and such divergences are treated with renormalization, as usual;
- in the IR, due to the fact that the particles in the loops are massless.

Fortunately, the IR singularities cancel when virtual diagrams are combined with real emission diagrams: when an emitted particle becomes soft (its energy tends to zero) the diagram presents a divergence which is regulated by the divergence of one of the virtual diagrams. This fact is known as Kinoshita-Lee-Nauenberg theorem [5, 6], and can be recast in the sentence that soft divergences always cancel. However, real emission diagrams introduce other singularities, when the transverse momentum of the emitted particle tends to zero (collinear singularities). Such singularities are not canceled by anything, and we have to deal with them.

The way these singularities are treated is similar to what happens in renormalization: since the PDFs are quantities which should be measured, we can imagine that in the naive formulation of the parton model they are bare objects, and that they can be redefined in such a way to reabsorb the collinear divergences: these new PDFs are what we actually measure and they must be finite. Schematically, we have (in N -space for simplicity)

$$C_{ij}(N, \alpha_s) = C_{ij}(N, \alpha_s, \mu^2) c_j^{\text{divergent}}(N, \alpha_s, \mu^2), \quad (1.2.20)$$

where, as usual in any regularization scheme, we have introduced a dependence on a new energy scale μ ; then we can construct the new PDFs as

$$f_j(N, \mu^2) = f_j(N) c_j^{\text{divergent}}(N, \alpha_s, \mu^2), \quad (1.2.21)$$

which acquire a dependence on the new scale μ . Then, the structure functions

$$F_i(N-1, Q^2) = \sum_j f_j(N, \mu^2) C_{ij}(N, \alpha_s(Q^2), \mu^2) \quad (1.2.22)$$

are well defined to all orders in perturbation theory.

In this discussion, we have tacitly assumed three important facts:

- the divergent part of the coefficient functions factorizes;
- it is independent on the observable (independent on the index i) and on the process;
- QCD corrections apply to the parton level process only, i.e. diagrams with additional lines connecting the partonic part of the process directly to the non-perturbative hadronic part (interference terms) do not count.

The first fact is known as *factorization of collinear singularities* and the second represents the *universality* of collinear divergences. The last point is valid for a large class of processes, where in particular such terms are suppressed by powers of the hard scale Q^2 (higher twists). Together, these facts are known as the *(collinear) factorization theorem*, valid at leading twist for all the processes we are interested in. In particular, it allows to reabsorb the collinear divergent terms into the PDFs, and to do it independently on the process or the observable, making the definition of the new PDFs really universal: the hadronic cross-section is then completely factorized into a perturbative part and a non-perturbative part.

Note that in Eq. (1.2.22) there is a dependence on μ on the right-hand-side which however is not present on the left-hand-side: this is correct, since the scale μ (called *factorization scale*) has been introduced arbitrarily by a regularization, and hence physical quantities must not depend on μ . The μ dependence of the coefficient function is fixed by the choice of the *factorization scheme*, analogous to the subtraction scheme in renormalization, i.e. the choice of which finite parts are put into the divergent coefficient $c_j(N, \alpha_s, \mu^2)$ and which are left into the finite coefficient $C_{ij}(N, \alpha_s, \mu^2)$. For example, we could choose a scheme in which the finite coefficient function is

$$C_{2q}(N, \alpha_s, \mu^2) = e_q^2, \quad (1.2.23)$$

which is called the DIS factorization scheme: in such scheme the structure function F_2 corresponds (up to a factor) to the weighted sum of quark PDFs to all orders in

perturbation theory. A more used scheme is the $\overline{\text{MS}}$ scheme, analogous to the same in renormalization, which collects into the divergent term only the ϵ poles of a $d = 4 - 2\epsilon$ dimensional computation and some selected terms; in the following we will always present results in the $\overline{\text{MS}}$ scheme. Once the μ dependence of the coefficient function is fixed, one can compute the μ dependence of the PDFs by imposing μ independence of the structure functions, order by order in perturbation theory. We will elaborate on that in the next Section.

1.3 GLAP evolution equations

Once the factorization scheme is fixed, the μ dependence of the coefficient function is computable in perturbation theory. Moreover, such dependence is again process-independent and observable-independent, since it is strictly related to the divergent piece. Then, μ independence of any physical quantity gives an evolution equation for the PDFs: considering for example the structure functions, the equation

$$\frac{d}{d\mu^2} F_i(N, Q^2) = 0 \quad (1.3.1)$$

allows us to extract an equation for the PDFs

$$\mu^2 \frac{d}{d\mu^2} f_j(N, \mu^2) = \sum_k \gamma_{jk}(\alpha_s(\mu^2), N-1) f_k(N, \mu^2), \quad (1.3.2)$$

which is called the *Altarelli-Parisi* or *Gribov-Lipatov-Altarelli-Parisi (GLAP) evolution equation*. Actually the derivation is not so trivial, but a rigorous proof of the GLAP equation can be done by means of the operator product expansion (OPE). Note in particular that α_s is computed at the scale μ . The functions $\gamma_{jk}(\alpha_s, N)$, called the *Altarelli-Parisi anomalous dimensions*, are computable in perturbation theory as

$$\gamma(\alpha_s, N) = \alpha_s \left[\gamma^{(0)}(N) + \alpha_s \gamma^{(1)}(N) + \alpha_s^2 \gamma^{(2)}(N) + \mathcal{O}(\alpha_s^3) \right] \quad (1.3.3)$$

where we have used a matrix notation (i.e. we have suppressed the indices). In this notation, the anomalous dimensions are $(2n_f + 1)$ -dimensional matrices, acting on a $(2n_f + 1)$ -dimensional vector of PDFs of the form

$$f(x, \mu^2) = \{f_g(x, \mu^2), f_{q_i}(x, \mu^2)\}. \quad (1.3.4)$$

The x -space version of the evolution equation is

$$\mu^2 \frac{d}{d\mu^2} f(x, \mu^2) = \int_x^1 \frac{dz}{z} P\left(\alpha_s(\mu^2), \frac{x}{z}\right) f(z, \mu^2) \quad (1.3.5)$$

where $P(\alpha_s(\mu^2), x)$ is a $(2n_f + 1)$ -dimensional matrix of Altarelli-Parisi *splitting functions*, whose expansion in powers of α_s is

$$P(\alpha_s, x) = \alpha_s \left[P^{(0)}(x) + \alpha_s P^{(1)}(x) + \alpha_s^2 P^{(2)}(x) + \mathcal{O}(\alpha_s^3) \right]. \quad (1.3.6)$$

The LO (1-loop) and NLO (2-loops) splitting functions (and anomalous dimensions) are known for a long time, while the NNLO (3-loops) ones have been computed recently [7, 8]. It has to be noted that the splitting functions are distribution, while the

anomalous dimensions are ordinary functions; however, the knowledge of the anomalous dimensions for complex values of N is needed to compute the inverse Mellin transform and get back the splitting functions.

Note that we use a notation which is slightly different to the common one used in the literature, and which is more suitable for small- x physics: our anomalous dimensions are defined as the Mellin transform of x times the splitting functions,

$$\gamma(\alpha_s, N) = \mathcal{M}[xP(\alpha_s, x)](N). \quad (1.3.7)$$

With this choice, the argument of the anomalous dimensions is shifted by a unity: the usual anomalous dimensions are recovered as $\gamma(\alpha_s, N - 1)$.

The rank of the evolution matrix is not maximal, and we could find several combinations of PDFs which decouple. Such combinations are called non-singlet and evolve independently. There are $2n_f - 1$ independent non-singlet combinations of PDFs. The remaining two degrees of freedom do not decouple and form a rank 2 system of equations, and are called singlet PDFs. Because of $SU(n_f)$ flavour symmetry (remember that in the parton model all partons are treated as massless), the splitting functions satisfy

$$P_{gq_i} = P_{g\bar{q}_i} \equiv P_{gq} \quad (1.3.8a)$$

$$P_{q_i g} = P_{\bar{q}_i g} \equiv P_{qg}/(2n_f) \quad (1.3.8b)$$

$$P_{q_i q_j} = P_{\bar{q}_i \bar{q}_j} \equiv \delta_{ij} P_{qq}^V + P_{qq}^S \quad (1.3.8c)$$

$$P_{q_i \bar{q}_j} = P_{\bar{q}_i q_j} \equiv \delta_{ij} P_{q\bar{q}}^V + P_{q\bar{q}}^S \quad (1.3.8d)$$

where we have defined six of the seven independent splitting functions (the seventh is P_{gg}). At LO, of the four quark splitting functions introduced here, only P_{qq}^V is non-zero.

1.3.1 The non-singlet sector

The non-singlet combinations of PDFs are differences of quarks PDFs, like for example any $f_q - f_{\bar{q}}$. Of course, there are n_f of such combinations, but we can construct other $n_f - 1$ independent combinations whose evolution is decoupled (for more details, see Ref. [4]). The splitting functions governing the evolution of these two kind of non-singlet combinations are called P^- and P^+ respectively, with

$$P^\pm = P_{qq}^V \pm P_{q\bar{q}}^V \quad (1.3.9)$$

in terms of the non-singlet splitting functions defined in (1.3.8). At LO we have $P_{q\bar{q}}^{V(0)} = 0$ and then

$$P^{+(0)}(x) = P^{-(0)}(x) = P_{qq}^{V(0)}(x) = \frac{C_F}{2\pi} \left(\frac{1+x^2}{1-x} \right)_+ \quad (1.3.10)$$

where the plus-distribution is defined in App. B.3. The NLO and NNLO splitting functions and anomalous dimension can be found in [7].

1.3.2 The singlet sector

The remaining degrees of freedom are the gluon PDF and the so called singlet quark PDF defined as

$$f_S = \sum_q (f_q + f_{\bar{q}}). \quad (1.3.11)$$

The evolution of these two PDFs is governed by an evolution matrix

$$\begin{pmatrix} P_{gg} & P_{gq} \\ P_{qg} & P_{qq} \end{pmatrix} \quad (1.3.12)$$

where we have defined

$$P_{qq} = P^+ + n_f (P_{q\bar{q}}^S + P_{\bar{q}q}^S) \quad (1.3.13)$$

in terms of the splitting functions defined in Eqs. (1.3.8) and (1.3.9). At LO, P_{qq} is given by Eq. (1.3.10) and

$$P_{gg}^{(0)}(x) = \frac{C_A}{\pi} \left[\frac{x}{(1-x)_+} + \frac{1-x}{x} + x(1-x) \right] + \frac{11C_A - 2n_f}{12\pi} \delta(1-x) \quad (1.3.14a)$$

$$P_{gq}^{(0)}(x) = \frac{C_F}{2\pi} \left[\frac{1 + (1-x)^2}{x} \right] \quad (1.3.14b)$$

$$P_{qg}^{(0)}(x) = \frac{n_f}{2\pi} [x^2 + (1-x)^2]. \quad (1.3.14c)$$

In N space, the GLAP equation for the singlet sector reads (omitting for ease of notation the α_s and N dependencies)

$$\mu^2 \frac{d}{d\mu^2} \begin{pmatrix} f_g \\ f_S \end{pmatrix} = \begin{pmatrix} \gamma_{gg} & \gamma_{gq} \\ \gamma_{qg} & \gamma_{qq} \end{pmatrix} \begin{pmatrix} f_g \\ f_S \end{pmatrix} \quad (1.3.15)$$

where at LO

$$\gamma_{gg}^{(0)}(N) = \frac{C_A}{\pi} \left[\frac{1}{N} - \frac{1}{N+1} + \frac{1}{N+2} - \frac{1}{N+3} - \psi(N+2) - \gamma_E \right] + \frac{11C_A - 2n_f}{12\pi} \quad (1.3.16a)$$

$$\gamma_{gq}^{(0)}(N) = \frac{C_F}{2\pi} \left[\frac{2}{N} - \frac{2}{N+1} + \frac{1}{N+2} \right] \quad (1.3.16b)$$

$$\gamma_{qg}^{(0)}(N) = \frac{n_f}{2\pi} \left[\frac{1}{N+1} - \frac{2}{N+2} + \frac{2}{N+3} \right] \quad (1.3.16c)$$

$$\gamma_{qq}^{(0)}(N) = \frac{C_F}{2\pi} \left[\frac{3}{2} + \frac{1}{N+1} - \frac{1}{N+2} - 2\psi(N+2) - 2\gamma_E \right]. \quad (1.3.16d)$$

The NLO and NNLO splitting functions and anomalous dimensions $P_{ij}^{(1,2)}$, $\gamma_{ij}^{(1,2)}$ can be found in [8].

1.3.2.1 Eigenvalues of the singlet anomalous dimension matrix

We now study the diagonalization of the evolution matrix: for instance, this can be useful to solve the singlet equations at LO (see Sect. 1.4.3.2). Let's call the evolution matrix Γ :

$$\Gamma = \begin{pmatrix} \gamma_{gg} & \gamma_{gq} \\ \gamma_{qg} & \gamma_{qq} \end{pmatrix}. \quad (1.3.17)$$

The eigenvalues of this matrix are found as solutions of the secular equation

$$\gamma_{\pm}^2 - \gamma_{\pm} \operatorname{tr} \Gamma + \det \Gamma = 0 \quad (1.3.18)$$

leading to

$$\gamma_{\pm} = \frac{1}{2} \left[\operatorname{tr} \Gamma \pm \sqrt{(\operatorname{tr} \Gamma)^2 - 4 \det \Gamma} \right]. \quad (1.3.19)$$

Obviously, γ_+ is the largest eigenvalue for all N . In the case $n_f = 0$, the matrix is triangular (γ_{qg} vanishes to all orders, because it is multiplied by n_f) and the solution has a simpler form

$$\gamma_{\pm} \stackrel{n_f=0}{=} \frac{1}{2} (\gamma_{gg} + \gamma_{qq} \pm |\gamma_{gg} - \gamma_{qq}|). \quad (1.3.20)$$

In this case, the largest eigenvalue γ_+ would be equal to γ_{gg} or γ_{qq} depending on which of the two is the largest; correspondingly, γ_- is the other of the two. This means in particular that in the case $n_f = 0$ for values of N such that $\gamma_{gg} = \gamma_{qq}$ both γ_+ and γ_- as functions of N have a discontinuity in their first derivative with respect to N , see Fig. 1.2. This discontinuity is an artifact, and would be absent if we take

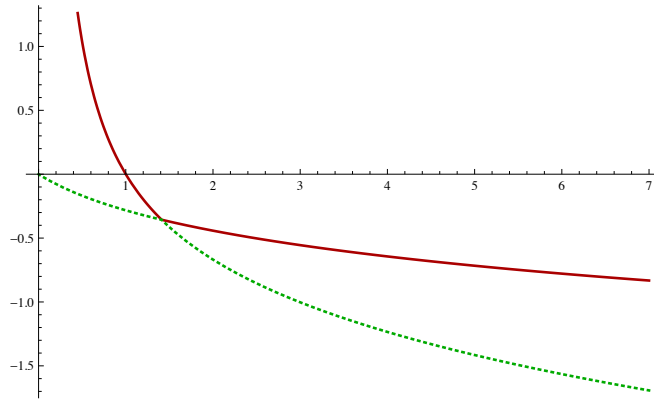


Figure 1.2. The eigenvalues $\gamma_+^{(0)}$ (blue upper curve) and $\gamma_-^{(0)}$ (green lower curve) as functions of N for $n_f = 0$.

separately γ_{gg} and γ_{qq} as eigenvalues. Moreover, when $n_f = 0$, there are no quarks in the game and the only relevant quantity is γ_{gg} . For this reason² in the case $n_f = 0$ we will conventionally choose $\gamma_+ = \gamma_{gg}$. In other words, we choose γ_+ as the largest eigenvalue at small N .

The matrix R that diagonalizes Γ ,

$$R\Gamma R^{-1} = \hat{\Gamma} = \operatorname{diag}(\gamma_+, \gamma_-), \quad (1.3.21)$$

can be written as

$$R = \frac{1}{c_- - c_+} \begin{pmatrix} c_- & -1 \\ -c_+ & 1 \end{pmatrix}, \quad R^{-1} = \begin{pmatrix} 1 & 1 \\ c_+ & c_- \end{pmatrix} \quad (1.3.22)$$

with

$$c_{\pm} = \frac{\gamma_{\pm} - \gamma_{gg}}{\gamma_{gq}} = \frac{\gamma_{qg}}{\gamma_{\pm} - \gamma_{qq}}. \quad (1.3.23)$$

²This choice is also motivated by the fact that in Chap. 3 we will be interested in the largest eigenvalue at small N .

In the diagonal basis, the diagonal evolution matrix can be written as

$$\hat{\Gamma} = \begin{pmatrix} 1 & 0 \\ 0 & 0 \end{pmatrix} \gamma_+ + \begin{pmatrix} 0 & 0 \\ 0 & 1 \end{pmatrix} \gamma_- \quad (1.3.24)$$

where the two matrices are projectors (i.e. idempotent operators) on orthogonal subspaces. When going back to the physical basis, we have the decomposition

$$\Gamma = R^{-1} \hat{\Gamma} R = \mathcal{M}_+ \gamma_+ + \mathcal{M}_- \gamma_- \quad (1.3.25)$$

where the projectors \mathcal{M}_\pm are given by

$$\mathcal{M}_\pm = \pm \frac{1}{c_- - c_+} \begin{pmatrix} c_\mp & -1 \\ c_+ c_- & -c_\pm \end{pmatrix} = \pm \frac{\Gamma - \gamma_\mp}{\gamma_+ - \gamma_-} \quad (1.3.26)$$

or, in terms of the eigenvalues and of γ_{qq} and γ_{qg} ,

$$\mathcal{M}_\pm = \pm \frac{1}{\gamma_+ - \gamma_-} \begin{pmatrix} (\gamma_\pm - \gamma_{qq}) & X \\ \gamma_{qg} & (\gamma_{qq} - \gamma_\mp) \end{pmatrix}, \quad X = \frac{(\gamma_+ - \gamma_{qq})(\gamma_{qq} - \gamma_-)}{\gamma_{qg}}, \quad (1.3.27)$$

and satisfy, being projectors, the relations

$$\mathcal{M}_\pm \mathcal{M}_\pm = \mathcal{M}_\pm, \quad \mathcal{M}_\pm \mathcal{M}_\mp = 0, \quad \mathcal{M}_+ + \mathcal{M}_- = 1. \quad (1.3.28)$$

This projector formalism proves to be useful, for instance, to solve the evolution equations, see Sect. 1.4.

While at LO the eigenvalues (1.3.19) are pure order α_s , the NLO eigenvalues computed using (1.3.19) contain spurious terms of order α_s^3 and higher, due to the presence of the square root. Hence, perturbatively we can write

$$\gamma_\pm = \alpha_s \gamma_\pm^{(0)} + \alpha_s^2 \gamma_\pm^{(1)} + \mathcal{O}(\alpha_s^3) \quad (1.3.29)$$

where

$$\gamma_\pm^{(1)} = \frac{1}{2} \left[\gamma_{gg}^{(1)} + \gamma_{qq}^{(1)} \pm \frac{\gamma_{gg}^{(0)} \gamma_{gg}^{(1)} + \gamma_{qq}^{(0)} \gamma_{qq}^{(1)} - \gamma_{gg}^{(0)} \gamma_{qq}^{(1)} - \gamma_{qq}^{(0)} \gamma_{gg}^{(1)} + 2 \left(\gamma_{gq}^{(0)} \gamma_{qg}^{(1)} + \gamma_{qg}^{(0)} \gamma_{gq}^{(1)} \right)}{\sqrt{(\text{tr } \Gamma^{(0)})^2 - 4 \det \Gamma^{(0)}}} \right]. \quad (1.3.30)$$

Note that this result can be obtained also in the following way: first, we diagonalize the evolution matrix at LO, and we construct the matrix R_{LO} which makes such diagonalization. Then we use R_{LO} to rotate the evolution matrix at NLO: the diagonal entries are exactly the LO eigenvalues *plus* the order α_s^2 term in Eq. (1.3.30), without higher orders. The difference is that with this procedure also non-diagonal entries are generated at NLO.

1.3.2.2 Small- x behaviour

The small- x behaviour of the singlet splitting functions is, up to NLO, (see Ref. [4])

$$P_{gg} \simeq \frac{\alpha_s C_A}{\pi x} + \frac{\alpha_s^2 n_f}{4\pi^2} \frac{6C_F - 23C_A}{9x} \quad (1.3.31a)$$

$$P_{gq} \simeq \frac{\alpha_s C_F}{\pi x} + \frac{\alpha_s^2 C_F}{4\pi^2} \frac{9C_A - 20n_f}{9x} \quad (1.3.31b)$$

$$P_{qg} \simeq \frac{\alpha_s^2 n_f}{4\pi^2} \frac{20C_A}{9x} \quad (1.3.31c)$$

$$P_{qq} \simeq \frac{\alpha_s^2 n_f}{4\pi^2} \frac{20C_F}{9x}. \quad (1.3.31d)$$

In Ref. [8] the small- x behaviour of the order α_s^3 splitting functions can be also found; at that order, also terms of the kind $\frac{\log^k x}{x}$ appear. In general, it can be shown (and will be discussed in details in Chap. 3) that at the order α_s^{k+1} the splitting functions contain terms

$$\alpha_s^{k+1} \frac{\log^j x}{x}, \quad 0 \leq j \leq k \quad (1.3.32)$$

for the gg and gq components, while the others have a power less ($j < k$). It is accidental that at NLO the dominant term $\frac{\log x}{x}$ does not appear. Also at NNLO the dominant term $\frac{\log^2 x}{x}$ accidentally vanishes (while the subdominant one is present, see Ref. [8]).

In N space, the small- x behaviour is determined by the rightmost singularity of the anomalous dimensions, see App. B. In particular, the powers of $\log x$ of Eq. (1.3.32) correspond in N space to multiple poles in $N = 0$,³

$$\alpha_s^{k+1} \frac{1}{N^j}, \quad 0 \leq j \leq k + 1 \quad (1.3.33)$$

for the gg and gq and with $0 \leq j \leq k$ for qg and qq . We can say that the tower of terms with highest power,

$$\left(\frac{\alpha_s}{N}\right)^k, \quad 0 < k < \infty \quad (1.3.34)$$

are the *leading-log* (LL) terms; sometimes the notation LL_x is used, to underline that we are talking about small- x logarithms. If we add, at each order, one power of α_s more, they will be NLL_x terms: in general, the tower of terms

$$\alpha_s^n \left(\frac{\alpha_s}{N}\right)^k, \quad 0 \leq k < \infty \quad (1.3.35)$$

constitute the $\text{N}^n \text{LL}_x$.

Expanding the complete 1- and 2-loops anomalous dimensions at small N , we obtain the small- x contributions in N space, including terms up to order α_s^2 and up to NLL :

$$\gamma_{gg} = \frac{\alpha_s}{2\pi} \left[\frac{2C_A}{N} - \frac{11C_A + 2n_f}{6} + \mathcal{O}(N) \right] + \frac{\alpha_s^2}{4\pi^2} \left[n_f \frac{6C_F - 23C_A}{9N} + \mathcal{O}(1) \right] \quad (1.3.36a)$$

$$\gamma_{gq} = \frac{\alpha_s}{2\pi} \left[\frac{2C_F}{N} - \frac{3C_F}{2} + \mathcal{O}(N) \right] + \frac{\alpha_s^2}{4\pi^2} \left[C_F \frac{9C_A - 20n_f}{9N} + \mathcal{O}(1) \right] \quad (1.3.36b)$$

$$\gamma_{qg} = \frac{\alpha_s}{2\pi} \left[\frac{2n_f}{3} + \mathcal{O}(N) \right] + \frac{\alpha_s^2}{4\pi^2} \left[\frac{20C_A n_f}{9N} + \mathcal{O}(1) \right] \quad (1.3.36c)$$

$$\gamma_{qq} = \alpha_s \mathcal{O}(N) + \frac{\alpha_s^2}{4\pi^2} \left[\frac{20C_F n_f}{9N} + \mathcal{O}(1) \right]. \quad (1.3.36d)$$

³Remember our definition Eq. (1.3.7).

Using the small- N behaviour at NLO, Eq. (1.3.36), and at NNLO, Ref. [8], we can compute the small- N behaviour in the more interesting case of the largest eigenvalue, up to order α_s^3 and up to NLL:

$$\gamma_+^{(0)}(N) = \frac{C_A}{\pi} \frac{1}{N} - \frac{11C_A + 2n_f(1 - 2C_F/C_A)}{12\pi} + \mathcal{O}(N) \quad (1.3.37a)$$

$$\gamma_+^{(1)}(N) = -\frac{n_f(23C_A - 26C_F)}{36\pi^2} \frac{1}{N} + \mathcal{O}(1) \quad (1.3.37b)$$

$$\gamma_+^{(2)}(N) = \frac{C_A^3(54\zeta_3 + 99\zeta_2 - 395) + C_A n_f(C_A - 2C_F)(18\zeta_2 - 71)}{108\pi^3 N^2} + \mathcal{O}(N^{-1}). \quad (1.3.37c)$$

The eigenvalue γ_- , conversely, is not enhanced at small N ; indeed, in Ref. [9, 10] it is shown that using appropriate factorization schemes, specifically DIS and $\overline{\text{MS}}$, the eigenvalue γ_- is free of singularities in $N = 0$ to all orders in α_s .

1.3.2.3 Large- x behaviour

At large x the off-diagonal splitting functions are regular: only the diagonal components are enhanced at large x . It can be proved [11] that the enhancement at large x is given to all orders by

$$P_{ii} \simeq \frac{A_i}{(1-x)_+} + B_i \delta(1-z) \quad (1.3.38)$$

where i is either g or q . The coefficients A_i are related order by order in α_s by the colour-charge relation

$$A_q = \frac{C_F}{C_A} A_g. \quad (1.3.39)$$

Up to 2-loops, we have [4]

$$A_g = \frac{\alpha_s C_A}{\pi} \left[1 + \frac{\alpha_s}{2\pi} \left(C_A \left(\frac{67}{18} - \frac{\pi^2}{6} \right) - \frac{5n_f}{9} \right) + \mathcal{O}(\alpha_s^2) \right] \quad (1.3.40)$$

and

$$B_g = \alpha_s \beta_0 + \frac{\alpha_s^2}{4\pi^2} \left[C_A^2 \left(\frac{8}{3} + 3\zeta_3 \right) - \frac{2}{3} C_A n_f - \frac{1}{2} C_F n_f \right] + \mathcal{O}(\alpha_s^3) \quad (1.3.41)$$

$$B_q = \frac{3\alpha_s C_F}{4\pi} + \frac{\alpha_s^2}{4\pi^2} \left[C_A C_F \left(\frac{17}{24} + \frac{11}{3} \zeta_2 - 3\zeta_3 \right) + C_F^2 \left(\frac{3}{8} - 3\zeta_2 + 6\zeta_3 \right) \right] \quad (1.3.42)$$

$$- C_F n_f \left(\frac{1}{12} + \frac{2}{3} \zeta_2 \right) \Big] + \mathcal{O}(\alpha_s^3). \quad (1.3.43)$$

In N -space, the diagonal anomalous dimensions in the large- N limit are given by

$$\gamma_{ii} = A_i \log \frac{1}{N} + (B_i - A_i \gamma_E) + \mathcal{O}(N^{-1} \log N), \quad (1.3.44)$$

while the off-diagonal entries vanish at $N \rightarrow \infty$ as $N^{-1} \log^{2n-2} N$ at order α_s^n . The order- α_s^3 behaviour can be found in Ref. [8].

1.4 Solving the GLAP equation

First of all, for solving the GLAP equations it is much easier to work in N -Mellin space, where convolutions are simple products. After the solution in Mellin space has been found, an inverse Mellin transform can be performed to obtain a physical x -space PDF.

For convenience, we use here the variable $t = \log \frac{\mu^2}{\mu_0^2}$, where μ_0 is some arbitrary reference scale, because the evolution depends on $\alpha_s(\mu^2)$ and it depends logarithmically on μ^2 ; we may also write for convenience $\alpha_s(t)$. We can define the evolution function $U(t, t_0, N)$ by⁴

$$f(N, \mu^2) = U(t, t_0, N - 1) f(N, \mu_0^2) \quad (1.4.1)$$

where $f(N, \mu_0^2)$ are some input PDFs given at a starting scale μ_0 ($t_0 = 1$). The evolution equation becomes an equation for U :

$$\frac{d}{dt} U(t, t_0, N) = \gamma(\alpha_s(t), N) U(t, t_0, N), \quad U(t_0, t_0, N) = 1. \quad (1.4.2)$$

This equation has a formal solution in terms of the path-ordered integral

$$U(t, t_0, N) = \text{P exp} \int_{t_0}^t dt' \gamma(\alpha_s(t'), N) \quad (1.4.3)$$

$$= 1 + \int_{t_0}^t dt' \gamma(\alpha_s(t'), N) + \int_{t_0}^t dt' \gamma(\alpha_s(t'), N) \int_{t_0}^{t'} dt'' \gamma(\alpha_s(t''), N) + \dots \quad (1.4.4)$$

where the path-ordering symbol accounts for the non-commutativity of the γ 's.

1.4.1 Explicit running coupling

Since the t -dependence of the γ 's is contained in $\alpha_s(t)$, one can recast the evolution equation in terms of an evolution in α_s [12]. In practice, using the renormalization group equation

$$\frac{d}{dt} \alpha_s = \beta(\alpha_s) \quad (1.4.5)$$

we have

$$\frac{d}{dt} = \beta(\alpha_s) \frac{d}{d\alpha_s} \quad (1.4.6)$$

and hence the evolution equation (1.4.2) for U becomes

$$\frac{d}{d\alpha_s} U(\alpha_s, \alpha_s^0, N) = \frac{\gamma(\alpha_s, N)}{\beta(\alpha_s)} U(\alpha_s, \alpha_s^0, N) \quad (1.4.7)$$

with $\alpha_s^0 = \alpha_s(t_0)$ (a notational change for the arguments of U is implicitly understood).

From the practical point of view, using this α_s -evolution equations provides a simple way to insert correctly the appropriate order for the evolution of α_s . Indeed, if we work at N^kLO we need a $(k + 1)$ -loop β -function: here, we simply have to put such

⁴We suppress for simplicity flavour indexes, which are implicitly understood.

β -function, while using the t -evolution we would need an explicit solution⁵ for the α_s evolution equation, which is harder to deal with. Note that, of course, at the end of the computation we still need the explicit evolution for α_s , since we have to compute the results at $\alpha_s(t_0)$ and $\alpha_s(t)$, but in this way the two problems are separated.

Then, everything we will say in the following can be translated without issues in this formalism, by replacing t with α_s and γ with $\gamma/\beta(\alpha_s)$.

1.4.2 The non-singlet case

In this case all the equations are independent, the γ 's are ordinary functions (not matrices) and the path ordering is irrelevant. The solution is then

$$U^{\text{NS}}(t, t_0, N) = \exp \int_{t_0}^t dt' \gamma(\alpha_s(t'), N) \quad (1.4.8)$$

which is well defined.

Perturbatively, the complications of this solution amount to computing t -integrals of functions (integer powers in this case) of $\alpha_s(t)$. We can then recast the t -evolution equation in a evolution equation in α_s using the technique of Sect. 1.4.1. In fact, this amounts to change integration variable from t to α_s , using the renormalization group equation to write the differential

$$dt = \frac{d\alpha_s}{\beta(\alpha_s)}. \quad (1.4.9)$$

The first two powers of α_s (as needed for a NLO computation) give (keeping the β -function up to NLO, i.e. β_0 and β_1)

$$\int_{t_0}^t dt' \alpha_s(t') = \int_{\alpha_s(t_0)}^{\alpha_s(t)} \frac{d\alpha_s}{-\beta_0\alpha_s - \beta_1\alpha_s^2} = -\frac{1}{\beta_0} \left[\log \alpha_s - \log \left(1 + \frac{\beta_1}{\beta_0} \alpha_s \right) \right]_{\alpha_s(t_0)}^{\alpha_s(t)} \quad (1.4.10)$$

$$\int_{t_0}^t dt' \alpha_s^2(t') = \int_{\alpha_s(t_0)}^{\alpha_s(t)} \frac{d\alpha_s}{-\beta_0 - \beta_1\alpha_s} = -\frac{1}{\beta_1} \left[\log \left(1 + \frac{\beta_1}{\beta_0} \alpha_s \right) \right]_{\alpha_s(t_0)}^{\alpha_s(t)}. \quad (1.4.11)$$

At LO we have then (neglecting β_1)

$$U_{\text{LO}}^{\text{NS}}(t, t_0, N) = \left(\frac{\alpha_s(t)}{\alpha_s(t_0)} \right)^{-\gamma^{(0)}(N)/\beta_0} \quad (1.4.12)$$

and at NLO (defining for simplicity $b_1 = \beta_1/\beta_0$)

$$U_{\text{NLO}}^{\text{NS}}(t, t_0, N) = \exp \left[\left(\frac{\gamma^{(0)}(N)}{\beta_0} - \frac{\gamma^{(1)}(N)}{\beta_1} \right) \log \frac{1 + b_1\alpha_s(t)}{1 + b_1\alpha_s(t_0)} \right] \left(\frac{\alpha_s(t)}{\alpha_s(t_0)} \right)^{-\gamma^{(0)}(N)/\beta_0} \quad (1.4.13)$$

$$\simeq \left[1 + \left(\frac{\gamma^{(0)}(N)}{\beta_0} - \frac{\gamma^{(1)}(N)}{\beta_1} \right) b_1 [\alpha_s(t) - \alpha_s(t_0)] \right] \left(\frac{\alpha_s(t)}{\alpha_s(t_0)} \right)^{-\gamma^{(0)}(N)/\beta_0} \quad (1.4.14)$$

⁵This is the case, for example, for the discretized path-ordering (see Sect. 1.4.3.1), or in general for all solutions which involve numerical integration.

where in the last line we have expanded the exponential in front up to NLO (order α_s), to be consistent with the accuracy required.

1.4.3 The singlet case

In this case there are two coupled equations, the evolution matrix Γ is a 2-dimensional matrix, and the path-ordered solution is not of simple usage: in practice, only a discretized form of the path-ordering is viable. The natural way to solve the equations would be the diagonalization of the system, in order to have two independent equations for two linear combinations of gluon (f_g) and singlet-quark (f_S) densities; however, even if in some cases this is simple, in general this solution can be as complicated as solving the original non-diagonal equations. We discuss these methods below.

1.4.3.1 Discretized path-ordering

To obtain a numerical realization of the path-ordered solution, Eq. (1.4.4), we start by separating the evolution from t_0 to t into the product of $n + 1$ subsequent evolution from t_k to t_{k+1} , with $t_{k+1} > t_k$,

$$\begin{aligned} U(t, t_0, N) &= U(t, t_n, N) U(t_n, t_{n-1}, N) \cdots U(t_2, t_1, N) U(t_1, t_0, N) \\ &= \prod_{k=n}^0 U(t_{k+1}, t_k, N), \quad (t_{n+1} \equiv t) \end{aligned} \quad (1.4.15)$$

where the order of the products is such that larger t_k are to the left. A possible sequence of t_k is a linear sequence

$$t_k = t_0 + k \Delta t, \quad \Delta t = \frac{t - t_0}{n + 1}, \quad (1.4.16)$$

but different (possibly optimized) sequences are allowed.

Next we consider the single-step evolution

$$U(t_{k+1}, t_k, N) = \text{P exp} \int_{t_k}^{t_{k+1}} dt' \Gamma(\alpha_s(t'), N) \simeq 1 + \int_{t_k}^{t_{k+1}} dt' \Gamma(\alpha_s(t'), N), \quad (1.4.17)$$

where the second equality holds if the integral is small, i.e. when the separation between t_k and t_{k+1} is small enough.⁶ In this regime we can also approximate the integral with

$$\begin{aligned} \int_{t_k}^{t_{k+1}} dt' \Gamma(\alpha_s(t'), N) &\simeq \Gamma\left(\alpha_s\left(\frac{t_{k+1} + t_k}{2}\right), N\right) (t_{k+1} - t_k) \\ &= \Gamma(\alpha_s(t_k + \Delta t/2), N) \Delta t, \end{aligned} \quad (1.4.18)$$

where the second equality holds if the sequence of Eq. (1.4.16) is adopted. In this particular case, we have finally

$$U(t, t_0, N) \simeq \prod_{k=n}^0 \left[1 + \Gamma(\alpha_s(t_k + \Delta t/2), N) \Delta t \right], \quad (1.4.19)$$

⁶Even if “small enough” is not a mathematical statement, the important thing is that, provided Γ is a smooth function, it is always possible to find a finite separation $t_{k+1} - t_k$ such that the integral is as small (compared to 1) as some precision we would like to reach in our approximate computation.

or, at the same level of accuracy,

$$U(t, t_0, N) \simeq \prod_{k=n}^0 \exp \left[\Gamma(\alpha_s(t_k + \Delta t/2), N) \Delta t \right], \quad (1.4.20)$$

which both provide good numerical implementations of the path-ordered solution. Note, by the way, that the two expressions (1.4.19) and (1.4.20) provide a way to estimate the numerical error in the discretization procedure, which should be of the same order of the difference between the two results.

We have checked numerically that the two expressions converge to the same value, and in the case in which the evolution can be solved exactly, that the asymptotic value is the exact result. It turns out that the exponential expression, Eq. (1.4.20), converges more rapidly, i.e. it gives more accurate results than Eq. (1.4.19) for the same value of n . Indeed, looking more carefully to the single-step evolution Eq. (1.4.17), we see that the first neglected correction can be approximated as

$$\begin{aligned} \int_{t_0}^t dt' \Gamma(\alpha_s(t'), N) \int_{t_0}^{t'} dt'' \Gamma(\alpha_s(t''), N) \\ = \Gamma(\alpha_s(t_k + \Delta t/2), N) \Gamma(\alpha_s(t_k + \Delta t/4), N) \frac{(\Delta t)^2}{2}, \end{aligned} \quad (1.4.21)$$

where the two Γ 's are computed at different values of t . Actually, the point at which the integrand is computed is a matter of choice; we have adopted here a central choice, which is appropriate to reproduce the correct factor 1/2 for this term (however, higher terms do not grow correctly: the next is 1/8 instead of 1/3!). If instead we had chosen the right bound ($t_k + \Delta t$) the argument would be the same, but the factor at each order would be 1. For a left bound choice (t_k), this and higher terms are zero. We conclude that, if we compute all the Γ 's in the nested integrals at the middle point, the discretized single-step path-ordering is better approximated by the full exponential, confirming that the solution Eq. (1.4.20) is more accurate. We have also checked that the central choice of Eq. (1.4.20) provides the faster convergence.

We suggest then to use Eq. (1.4.20); practically, to compute the exponential in each step we need to diagonalize Γ at the given value of t for that step. It is useful here to use the projectors defined in Sect. 1.3.2.1, to write

$$\exp[\Gamma \Delta t] = \mathcal{M}_+ e^{\gamma_+ \Delta t} + \mathcal{M}_- e^{\gamma_- \Delta t} \quad (1.4.22)$$

where everything is computed at $t_k + \Delta t/2$ for the k -th step.

As a final comment, if we had used the α_s evolution, Eq. (1.4.7), we would have found

$$U(\alpha_s, \alpha_s^0, N) \simeq \prod_{k=n}^0 \exp \left[\frac{\Gamma(\alpha_k + \Delta\alpha/2, N)}{\beta(\alpha_k + \Delta\alpha/2)} \Delta\alpha \right], \quad (1.4.23)$$

with

$$\alpha_k = \alpha_s^0 + k \Delta\alpha, \quad \Delta\alpha = \frac{\alpha_s - \alpha_s^0}{n+1}. \quad (1.4.24)$$

This form is easier to use because we don't need to know the explicit solution for the running coupling, but just the β -function up to the desired order.

1.4.3.2 Diagonalization of the system of singlet equations

Introducing a short notation for the vector of singlet PDFs,

$$f = \begin{pmatrix} f_g \\ f_S \end{pmatrix}, \quad (1.4.25)$$

we can write the singlet system, Eq. (1.3.15), in matrix notation

$$\frac{d}{dt}f = \Gamma f \quad (1.4.26)$$

where for simplicity we have suppressed the explicit dependencies on the arguments and we have used the matrix Γ defined in Eq. (1.3.17).

In general, the α_s dependence of Γ is not trivial, and a matrix R which diagonalizes Γ would be α_s -dependent, and hence it does not commute with the t -derivative. Hence the right way to proceed is to introduce some (t -dependent) matrix R and to transform the PDF vector in

$$\hat{f} = Rf; \quad (1.4.27)$$

now, multiplying the evolution equation by R on the left of both sides and expressing everything in terms of \hat{f} , we get

$$\frac{d}{dt}\hat{f} = \left(R\Gamma R^{-1} + \frac{dR}{dt}R^{-1} \right) \hat{f}. \quad (1.4.28)$$

If the matrix (we introduce for simplicity a dot for the t -derivative)

$$\tilde{\Gamma} = R\Gamma R^{-1} + \dot{R}R^{-1} \quad (1.4.29)$$

is diagonal the system (1.4.28) splits into two independent equations, and each can be solved as in the non-singlet case (possibly introducing the evolution function U). So now the problem is to find a matrix R such that $\tilde{\Gamma}$ is diagonal, that is to solve the matrix equation

$$\dot{R} = \tilde{\Gamma}R - R\Gamma \quad (1.4.30)$$

where also the two (diagonal) entries of $\tilde{\Gamma}$ are unknowns. Solving this matrix equation may be as complicated as solving the original system Eq. (1.3.15), so for practical purposes this way may be too complicated.

Let's now consider the LO case. At LO the evolution matrix is given by

$$\Gamma = \alpha_s \Gamma^{(0)} \quad (1.4.31)$$

and hence, since the α_s dependence factorizes, we can diagonalize it by a α_s -independent (t -independent) matrix; we can choose R to be this diagonalizing matrix, and since $\dot{R} = 0$ we get

$$\frac{d}{dt}\hat{f} = \hat{\Gamma}\hat{f} \quad (1.4.32)$$

where

$$\hat{\Gamma} = R\Gamma R^{-1} \quad (1.4.33)$$

with $\hat{\Gamma}$ diagonal. An explicit form of R is given in Eq. (1.3.22). The solution can be easily written by making use of the projectors introduced in Sect. 1.3.2.1; the evolver is

$$U_{\text{LO}}(t, t_0, N) = \mathcal{M}_+(N) \left(\frac{\alpha_s(t)}{\alpha_s(t_0)} \right)^{-\gamma_+(N)/\beta_0} + \mathcal{M}_-(N) \left(\frac{\alpha_s(t)}{\alpha_s(t_0)} \right)^{-\gamma_-(N)/\beta_0} \quad (1.4.34)$$

where we have used the integral (1.4.10).

Now let's move from LO to NLO. In this case Γ is

$$\Gamma = \alpha_s \Gamma^{(0)} + \alpha_s^2 \Gamma^{(1)} \quad (1.4.35)$$

and the α_s -dependence now is non-trivial. Unless $\Gamma^{(0)}$ and $\Gamma^{(1)}$ are diagonalized by the same matrix (and this is not the case) we cannot simply diagonalize Γ but we are in the general case of Eq. (1.4.28). The NLO evolution can alternatively be solved perturbatively, diagonalizing at LO and perturbing around the LO solution (see below).

Consider now the LL case. The matrix Γ in this case is given by

$$\Gamma = \gamma_s \left(\frac{\alpha_s}{N} \right) \Gamma_s, \quad \Gamma_s = \begin{pmatrix} 1 & C_F/C_A \\ 0 & 0 \end{pmatrix} \quad (1.4.36)$$

where again the α_s -dependence has factored out, as in the LO case. Then also in this case we can simply diagonalize the matrix Γ ; the matrix R which implements this diagonalization is the same matrix that diagonalizes the LO matrix, computed in $N = 0$.

As a final comment, we note that using instead the α_s evolution, Eq. (1.4.7), in the LO and LL cases the α_s dependence is still factorized, since the evolution matrix is, respectively,

$$\frac{\alpha_s \Gamma^{(0)}}{\beta(\alpha_s)} = -\frac{\Gamma^{(0)}}{\beta_0 \alpha_s}, \quad \frac{\gamma_s(\alpha_s/N) \Gamma_s}{\beta(\alpha_s)} = -\frac{\gamma_s(\alpha_s/N) \Gamma_s}{\beta_0 \alpha_s^2}, \quad (1.4.37)$$

where we have substituted the 1-loop β -function, as appropriate. Note that, at NLO, the evolution matrix is instead an infinite series in α_s .

1.4.3.3 Hybrid perturbative solution

Now assume the decomposition of Γ into the sum of two pieces

$$\Gamma = \Gamma_0 + \Gamma' \quad (1.4.38)$$

in such a way that we know the solution of the evolution equation for just Γ_0 :

$$U_0(t, t_0, N) = \text{P exp} \int_{t_0}^t dt' \Gamma_0(\alpha_s(t'), N). \quad (1.4.39)$$

This is the case, for example, when the α_s dependence is the same for all the entries of Γ_0 , like in the previously discussed LO and LL cases.

With this setup, we can solve the evolution equation like we do with the Schrödinger equation in the interaction picture. Let's write the full solution U as

$$U(t, t_0, N) = U_0(t, t_0, N) U_I(t, t_0, N); \quad (1.4.40)$$

putting this into the evolution equation we get an equation for U_I

$$\frac{d}{dt} U_I(t, t_0, N) = \tilde{\Gamma}'(t, N) U_I(t, t_0, N) \quad (1.4.41)$$

with

$$\tilde{\Gamma}'(t, N) = U_0(t, t_0, N)^{-1} \Gamma'(\alpha_s(t), N) U_0(t, t_0, N). \quad (1.4.42)$$

Once we have this expression we can either use the discretized path-ordering solution or an approximation (if Γ' can be considered as a perturbation of Γ_0).

This procedure can be used to find, for example, the NLO solution. Indeed, one could identify

$$\Gamma_0 = \alpha_s \Gamma^{(0)}, \quad \Gamma' = \alpha_s^2 \Gamma^{(1)} \quad (1.4.43)$$

and use an approximate solution for the ‘‘perturbation’’ $\Gamma^{(1)}$. However, we have to take care of the running of α_s : indeed, the LO solution would be typically computed with a 1-loop β -function, while the α_s appearing in the NLO equation should be at 2-loops. The easiest way to tackle with this issue is to use the α_s evolution, Eq. (1.4.7), and write the evolution kernel as

$$\frac{\alpha_s \Gamma^{(0)} + \alpha_s^2 \Gamma^{(1)}}{-\beta_0 \alpha_s^2 - \beta_1 \alpha_s^3} = \frac{\Gamma^{(0)}}{-\beta_0 \alpha_s} + \frac{\Gamma^{(1)} - b_1 \Gamma^{(0)}}{-\beta_0 - \beta_1 \alpha_s}, \quad b_1 = \frac{\beta_1}{\beta_0}; \quad (1.4.44)$$

now, we can identify the two contributions in the right-hand-side as the pure LO evolution kernel and the perturbation to it. We could now eventually come back to the t -evolution: we would then have the identifications

$$\Gamma_0 = \alpha_s^{\text{LO}} \Gamma^{(0)}, \quad \Gamma' = (\alpha_s^{\text{NLO}})^2 \left[\Gamma^{(1)} - b_1 \Gamma^{(0)} \right] \quad (1.4.45)$$

where we have written explicitly the order at which α_s must be computed. The pure LO solution is then given by Eq. (1.4.34),

$$U_0(t, t_0, N) = U_{\text{LO}}(t, t_0, N), \quad (1.4.46)$$

and we could take (to NLO accuracy) the first order in the expansion in the path-ordered solution of Eq. (1.4.41)

$$U_I(t, t_0, N) = 1 + \int_{t_0}^t dt' U_{\text{LO}}^{-1}(t', t_0, N) \Gamma'(\alpha_s^{\text{NLO}}(t'), N) U_{\text{LO}}(t', t_0, N) + \dots \quad (1.4.47)$$

leading to a solution which is equivalent to the non-singlet one, Eq. (1.4.14). We don't show here the full result, since we are not interested in it — we will use the discretized path-ordering solution for applications; for a complete solution, equivalent to this up to higher orders in α_s , see Ref. [12].

2 Soft-gluon resummation

Contents

2.1 Inclusive cross-sections resummation	27
2.1.1 Resummation in Mellin space	29
2.1.2 Resummation in physical space: the need of a prescription	33
2.1.3 Minimal prescription	35
2.1.4 Borel prescription	36
2.1.5 Subleading terms	39
2.1.6 Comparison with fixed-order	43
2.2 Rapidity distributions resummation	48
2.3 Numerical implementation.	51
2.3.1 Minimal prescription	51
2.3.2 Borel prescription	52

This Chapter is devoted to a review of some basics on soft-gluon (or threshold or large- x) resummation and in particular to the problem of extracting finite results from the resummation formulae. Indeed, we will see that soft-gluon resummation is performed in N -space, where a closed resummed expression for the inclusive cross-section can be found explicitly; however, the inverse Mellin transform does not exist, and this is related to the divergence of the perturbative series. We will describe then two prescription to deal with such divergence. After that, we will extend the formalism from the inclusive cross-sections to the more interesting case of rapidity distributions. However, we won't cover the as interesting resummation of transverse momentum distributions, for which we refer the Reader to Refs. [13–17].

2.1 Inclusive cross-sections resummation

A generic partonic coefficient function $C(z, \alpha_s)$ is kinematically enhanced when $z \rightarrow 1$, because of gluon emissions. Consider for simplicity the case of a quark parton line which emits n gluons, as in Fig. 2.1. When a gluon is emitted, it carries an energy fraction $1 - z_i$ of the quark from which it is emitted; consequently, the energy of the quark gradually decreases becoming at the end a fraction $z = z_1 z_2 \cdots z_n$ of its initial energy (this z is the argument of the coefficient function). In the coefficient function, for each gluon emission a term enhanced when the corresponding z_i approaches one

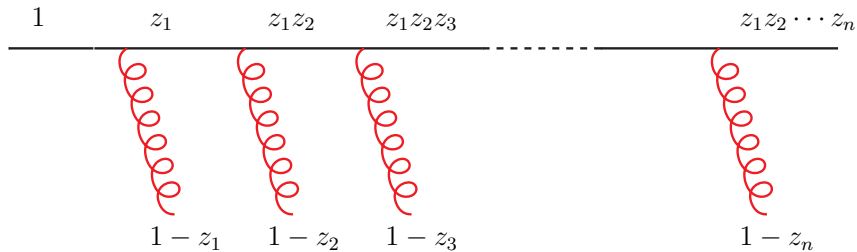


Figure 2.1. Emission of n gluons from a quark parton line. The energy fractions of the gluons refer to the energy of the emitting quark, while the energy fractions in the quark line refer always to its initial energy.

(the i -th gluon becomes *soft*) appears. When integrating over the emitted gluon phase spaces, these enhancements convert into a sequence of terms

$$\frac{\log^k(1-z)}{1-z}, \quad 0 \leq k \leq an - 1 \quad (2.1.1)$$

where a is a process-dependent parameter: $a = 1$ for DIS and $a = 2$ for Drell-Yan and Higgs production.¹ For the sake of exposition, we consider just the case $a = 2$. This choice is motivated phenomenologically: the impact of soft-gluon resummation in DIS is less relevant than in Drell-Yan or Higgs production.

Let's introduce some notations, which will be used extensively in Chap. 5. The variable τ is defined as

$$\tau = \frac{M^2}{s}, \quad (2.1.2)$$

where M is the invariant mass of the target final state (the lepton pair or the Higgs boson) and \sqrt{s} is the hadronic center-of-mass energy. The variable z (the argument of the coefficient function) is the analog of τ at parton level, and then it can be written as

$$z = \frac{M^2}{\hat{s}}, \quad (2.1.3)$$

where $\sqrt{\hat{s}}$ is the partonic center-of-mass energy. This explains why soft-gluon resummation is also called threshold resummation: when z approaches 1, the partonic energy is just sufficient to produce the final state, i.e. the process is close to its threshold (same reasoning holds at hadron level). The inclusive cross-section (differential only in M) can be written in the parton model framework as

$$\frac{1}{\tau} \frac{d\sigma}{dM^2} = \sum_{ij} \int_{\tau}^1 \frac{dz}{z} \mathcal{L}_{ij} \left(\frac{\tau}{z} \right) C_{ij} (z, \alpha_s(M^2)), \quad (2.1.4)$$

where we have defined the so called *parton luminosity*

$$\mathcal{L}_{ij}(x) = c_{ij} \int_x^1 \frac{dy}{y} f_i^{(1)} \left(\frac{x}{y} \right) f_j^{(2)}(y), \quad (2.1.5)$$

where the two PDFs refer to the two incoming hadrons and i, j are flavour indexes. We are omitting renormalization and factorization scale dependence, which will be restored

¹In the Higgs production case, the parton line which emits gluons is a gluon line, since the Higgs is predominantly produced via gluon fusion.

for the sake of phenomenology in Chap. 5. In the rest of this Chapter, we will omit the flavour details (sum over flavours, indexes), concentrating implicitly our attention to those channels which dominate at large z ($q\bar{q}$ for DY, gg for Higgs). Moreover, for convenience, we normalize the coefficient function of such dominant channel in such a way that the LO is simply

$$C^{(0)}(z) = \delta(1-z) \quad \leftrightarrow \quad C^{(0)}(N) = 1; \quad (2.1.6)$$

hence, any numerical factor appearing in the partonic cross section at LO must be included in the definition of the coefficients c_{ij} in front of the luminosity, Eq. (2.1.5).

In a fixed order computation, at LO there are no emissions, by definition; at NLO the contribution from a single gluon emission produces (among others terms not enhanced at large z)

$$\frac{\log(1-z)}{1-z}, \quad \frac{1}{1-z}. \quad (2.1.7)$$

As one sees immediately, when integrating the coefficient function with the PDFs in the convolution (2.1.4) such terms produce a non-integrable singularity in $z = 1$. As already discussed in Sect. 1.2.2, such singularities are regularized by the IR divergence of loop diagrams, giving rise to a plus distribution (see definitions in App. B.3):

$$\left(\frac{\log(1-z)}{1-z}\right)_+, \quad \left(\frac{1}{1-z}\right)_+. \quad (2.1.8)$$

This mechanism takes place also at higher orders (see [5, 6]), producing at the end a tower of terms

$$\alpha_s^n \left(\frac{\log^k(1-z)}{1-z}\right)_+, \quad 0 \leq k \leq 2n-1. \quad (2.1.9)$$

It is now evident why resummation is needed: when z is equal or larger than a value \bar{z} satisfying roughly

$$\alpha_s \log^2(1-\bar{z}) \sim 1, \quad (2.1.10)$$

all terms in the perturbative series are of the same order, and any finite order truncation would be meaningless. Being z an integration variable which extends up to $z = 1$, this condition is always satisfied in a region of the convolution integral Eq. (2.1.4), and in that region the partonic coefficient function needs to be resummed.

2.1.1 Resummation in Mellin space

The resummation task has been achieved long ago [18–20]. The details may be cumbersome because of two complications: the running of the QCD coupling and the non-abelian nature of QCD. It is beyond the purpose of this thesis to investigate the resummation mechanism in such detail: we will therefore limit ourselves to a simplified exposition [21] which nevertheless emphasizes the key ingredients: *factorization* and *exponentiation*.

In the actual computation of the contribution from n gluon emissions, one has first to compute the matrix element and then to integrate over the phase space of the emitted gluons. Concerning the matrix elements, the calculation can be performed in

the *eikonal approximation* (see for example [22]), which reproduces the correct soft limit. In this limit, it can be proved that such matrix element \mathcal{M}_n factorizes as

$$\mathcal{M}_n(z_1, \dots, z_n) \stackrel{\text{soft}}{\simeq} \frac{1}{n!} \prod_{i=1}^n \mathcal{M}_1(z_i) \quad (2.1.11)$$

where \mathcal{M}_1 is the matrix element for the single emission; the proof is rather easy in QED, while in QCD complications arise due to the non-abelian couplings between gluons. However, the phase space in z -space is not factorized, and is proportional to

$$dz_1 \cdots dz_n \delta(z - z_1 \cdots z_n). \quad (2.1.12)$$

Nevertheless, after taking a Mellin transform, also the phase space factorizes,

$$\int_0^1 \frac{dz}{z} z^N \delta(z - z_1 \cdots z_n) = z_1^{N-1} \cdots z_n^{N-1}, \quad (2.1.13)$$

producing the factors z_i^{N-1} which give, upon integration, the Mellin transforms with respect to each individual z_i variable. In N -space, the threshold region $z \sim 1$ corresponds to the region of large N , and in particular the tower of logarithms in Eq. (2.1.9) converts into the tower (see App. B.4)

$$\alpha_s^n \log^k \frac{1}{N}, \quad 0 \leq k \leq 2n. \quad (2.1.14)$$

Hence, in N -space, the coefficient function at order α_s^n is given in the soft limit² by

$$C^{(n)}(N) \stackrel{\text{soft}}{\simeq} \frac{1}{n!} \left[C_{\text{soft}}^{(1)}(N) \right]^n \quad (2.1.15)$$

where $C_{\text{soft}}^{(1)}(N)$ is the Mellin transform of soft terms in the order α_s coefficient. Considering only the leading soft term, it becomes

$$C_{\text{soft}}^{(1)}(N) = \int_0^1 dz z^{N-1} 4A_1 \left(\frac{\log(1-z)}{1-z} \right)_+ \stackrel{N \gg 1}{\simeq} 2A_1 \log^2 \frac{1}{N} \quad (2.1.16)$$

where $A_1 = C_F/\pi$ for the DY case and $A_1 = C_A/\pi$ for the Higgs case.

At this stage it is clear what is going to happen: the soft terms in the perturbative series of the coefficient function can be resummed explicitly, and the results exponentiates:

$$C^{\text{res}}(N, \alpha_s) = \sum_{n=0}^{\infty} \alpha_s^n \left[C^{(n)}(N) \right]_{\text{soft}} = \exp \left[\alpha_s C_{\text{soft}}^{(1)}(N) \right]. \quad (2.1.17)$$

This result is valid only at leading-logarithmic (LL) accuracy: only the highest power $k = 2n$ in the tower of logs in Eq. (2.1.14) is resummed. Moreover, it does not take into account effects due to the running of α_s : hence, in this form, it would be valid in QED, and it would be called *Sudakov* resummation [23]. What needs to be emphasized of this simple argument is that resummation is based on the factorization of multi-gluon

²Including also the virtual contributions which regulate the divergence in $z = 1$.

emissions, and that such factorization can take place only in Mellin space, because the relevant phase space only factorizes in N -space, but not in z -space.

To take into account the running coupling effects, we recall that in the gluon phase space integration there is, besides the energy fractions in Eq. (2.1.12), the transverse momenta of the gluons: such momenta fix the energy scale of the gluon emissions, and then it is the proper energy scale at which α_s should be computed. Then, the exponent of Eq. (2.1.17) becomes

$$\alpha_s C_{\text{soft}}^{(1)}(N) \rightarrow \int_0^1 dz z^{N-1} 2A_1 \left(\frac{1}{1-z} \int_{M^2}^{(1-z)^2 M^2} \frac{dk^2}{k^2} \alpha_s(k^2) \right)_+; \quad (2.1.18)$$

one can immediately verify that, if the coupling is kept fixed, the previous result is obtained again. Note that this expression is ill-defined: indeed, the Mellin transform forces z to take each value from 0 to 1, and hence α_s at some point has to be evaluated in the non-perturbative region, hitting the Landau pole (see App. A). In actual computations, this problem is avoided by expanding in powers of $\alpha_s(M^2)$ the integrand and computing the Mellin transform term-by-term (which is well defined), then taking the large- N approximation and resumming the $\alpha_s(M^2)$ series: such procedure leads to a finite result. In more details, the k^2 integral gives (using the 1-loop β -function)

$$\int_{M^2}^{(1-z)^2 M^2} \frac{dk^2}{k^2} \alpha_s(k^2) = \frac{1}{\beta_0} \log \left(1 + \bar{\alpha} \log(1-z) \right) \quad (2.1.19)$$

having defined for future convenience the variable

$$\bar{\alpha} = 2\beta_0 \alpha_s \quad (2.1.20)$$

(when written without argument, we mean $\alpha_s = \alpha_s(M^2)$). Manifestly, the Mellin transform is divergent, because the log has a branch-cut when $\bar{\alpha} \log(1-z) < -1$, which is always in the integration range. The Mellin transform can be computed term-by-term as

$$\begin{aligned} \mathcal{M} \left[\left(\frac{\log [1 + \bar{\alpha} \log(1-z)]}{1-z} \right)_+ \right] &= - \sum_{k=1}^{\infty} \frac{(-\bar{\alpha})^k}{k} \mathcal{M} \left[\left(\frac{\log^k(1-z)}{1-z} \right)_+ \right] \\ &\simeq - \sum_{k=1}^{\infty} \frac{(-\bar{\alpha})^k}{k(k+1)} \log^{k+1} \frac{1}{N} \\ &= \left(\frac{1}{\bar{\alpha}} + \log \frac{1}{N} \right) \log \left(1 + \bar{\alpha} \log \frac{1}{N} \right) - \log \frac{1}{N} \end{aligned}$$

from which we get

$$C^{\text{res}}(N, \alpha_s) = \exp \left\{ \frac{2A_1}{\beta_0 \bar{\alpha}} \left[\left(1 + \bar{\alpha} \log \frac{1}{N} \right) \log \left(1 + \bar{\alpha} \log \frac{1}{N} \right) - \bar{\alpha} \log \frac{1}{N} \right] \right\}. \quad (2.1.21)$$

In the second equality, we have used Eq. (B.4.9a) in the large- N limit and kept only the highest power of $\log \frac{1}{N}$ for each term in the series, as appropriate for a LL computation; note, however, that it is exactly this approximation which allows to avoid the problem of the Landau pole. Nevertheless, the Landau pole problem has not disappeared, and we will come back later on it.

log approx.	g_i up to	g_0 up to order	accuracy: $\alpha_s^n \log^k \frac{1}{N}$
LL	$i = 1$	$(\alpha_s)^0$	$k = 2n$
NLL	$i = 2$	$(\alpha_s)^1$	$2n - 2 \leq k \leq 2n$
NNLL	$i = 3$	$(\alpha_s)^2$	$2n - 4 \leq k \leq 2n$

Table 2.1. Orders of logarithmic approximations and accuracy of the predicted logarithms.

Eq. (2.1.21), even if it contains the proper running coupling effect, still reproduces only the LL terms. The more general expression is [18–20, 24, 25]

$$C^{\text{res}}(N, \alpha_s) = g_0(\alpha_s) \exp \mathcal{S} \left(\bar{\alpha} \log \frac{1}{N}, \bar{\alpha} \right) \quad (2.1.22)$$

where $g_0(\alpha_s) = 1 + \mathcal{O}(\alpha_s)$ collects all the constant terms, and the exponent, called for similarity Sudakov exponent (or Sudakov form factor), has a logarithmic expansion

$$\mathcal{S}(\lambda, \bar{\alpha}) = \frac{1}{\bar{\alpha}} g_1(\lambda) + g_2(\lambda) + \bar{\alpha} g_3(\lambda) + \bar{\alpha}^2 g_4(\lambda) + \dots \quad (2.1.23)$$

At the next^k-to-leading logarithmic (N^kLL) level functions up to g_{k+1} must be included, and g_0 must be computed up to order α_s^k . Then, the expansion of the resummed coefficient function Eq. (2.1.22) in powers of α_s gives the logarithmically enhanced contributions to the fixed-order coefficient functions $C(N, \alpha_s)$ up to the same order, with, at the N^pLL level, all terms of order $\log^k \frac{1}{N}$ with $2(n-p) \leq k \leq 2n$ correctly predicted; note that at each order also powers of $\log \frac{1}{N}$ less than $2(n-p)$ are generated, but their coefficients are not exact and will change increasing the logarithmic approximation order p . A summary for the first few orders is given in Tab. 2.1.

The inclusion up to the relevant order of the function g_0 is necessary, despite the fact that g_0 contains only constants, because of its interference with the expansion of the exponentiated logarithmically enhanced functions g_i with $i \geq 1$. For example, at NLL we expect, according to Tab. 2.1, to get the correct coefficients for the three leading powers of logarithms at each order: in particular, at order α_s all logarithmic terms (including a constant) should be correct, and at order α_s^2 the coefficients for the powers $k = 4, 3, 2$ of $\log \frac{1}{N}$ are expected to be correctly predicted. By writing

$$g_0(\alpha_s) = 1 + \sum_{j=1}^{\infty} g_{0j} \alpha_s^j, \quad (2.1.24)$$

$$g_k(\lambda) = (2\beta_0)^{2-k} \sum_{j=1}^{\infty} g_{kj} \left(\frac{\lambda}{2\beta_0} \right)^j, \quad g_{11} = 0, \quad (2.1.25)$$

and expanding $C^{\text{res}}(N, \alpha_s)$ in powers of α_s , we get indeed ($L = \log \frac{1}{N}$)

$$\begin{aligned} C^{\text{res}}(N, \alpha_s) = & 1 + \alpha_s [g_{12}L^2 + g_{21}L + g_{01}] \\ & + \alpha_s^2 \left[\frac{g_{12}^2}{2}L^4 + (g_{12}g_{21} + g_{13})L^3 + \left(\frac{g_{21}^2}{2} + g_{22} + g_{12}g_{01} \right)L^2 + \mathcal{O}(L) \right] \\ & + \mathcal{O}(\alpha_s^3). \end{aligned} \quad (2.1.26)$$

log approx.	needs	
	GLAP	fixed-order
LL	1-loop	–
NLL	2-loop	NLO
NNLL	3-loop	NNLO

Table 2.2. Orders of logarithmic approximations and the needed fixed-order accuracy.

The order α_s , as well as the coefficients of the terms L^4, L^3, L^2 at order α_s^2 , depend only on g_1, g_2 and g_{01} , i.e. only NLL contributions, as expected.

Details on the functions g_i ($i \geq 1$) will be given in App. C.3. What we want to emphasize here is that such functions depend on few coefficients: g_1 depends only on the coefficient A_1 introduced in Eq. (2.1.16), g_2 on a couple of other coefficients, and so on. One category (to which A_1 belongs) is fully determined by the GLAP anomalous dimensions: for these coefficients, to compute the N^p LL function g_{p+1} , the $(p+1)$ -loops (N^p LO) anomalous dimension is needed. The other (process dependent) coefficients are then fixed by matching the expansion of $C^{\text{res}}(N, \alpha_s)$ in powers of α_s up to order α_s^p and comparing with a fixed order computation. A summary of these needs for the first few orders is given in Tab. 2.2.

Matched resummed coefficient functions are obtained by combining the resummed result Eq. (2.1.22) with the fixed-order expansion in power of α_s , and subtracting double-counting terms, i.e. the expansion of $C^{\text{res}}(N, \alpha_s(M^2))$ in powers of $\alpha_s(M^2)$ up to the same order:

$$C_{N^k\text{LL}}^{N^p\text{LO}}(N, \alpha_s) = \sum_{j=0}^p \alpha_s^j C^{(j)}(N) + C_{N^k\text{LL}}^{\text{res}}(N, \alpha_s) - \sum_{j=0}^p \frac{\alpha_s^j}{j!} \left[\frac{d^j C_{N^k\text{LL}}^{\text{res}}(N, \alpha_s)}{d\alpha_s^j} \right]_{\alpha_s=0}. \quad (2.1.27)$$

This expression will be used in Chap 5 for phenomenology.

As a final remark, we mention that recently resummation has also been performed using soft-collinear effective theory (SCET) techniques both in N -space [26] and in z -space [27, 28]; in the latter approach the soft scale whose logarithms are resummed is not the partonic scale $M^2(1-z)$ but rather a soft scale μ_s , independent of the parton momentum fraction z , but related to the hadronic scale $M^2(1-\tau)$. As a consequence, the hard coefficient function depends on τ not only through the convolution variable, but also directly through the soft scales: therefore, the resummed result can no longer be factorized by Mellin transformation into the product of a parton density and a hard coefficient. For this reason, a direct comparison between the result obtained through the SCET approach and that based on standard factorization Eq. (2.1.4) is not possible at the parton level [29]. A phenomenological comparison is possible [28], but it requires either assuming a specific form of the parton distribution functions, or switching to the N space version of the SCET result.

2.1.2 Resummation in physical space: the need of a prescription

Once the coefficient function has been resummed in N -space, the inverse Mellin transform of the resummed result has to be computed to get the physical cross-section.

However, it turns out that the inverse Mellin transform of Eq. (2.1.22) does not exist. This fact is strictly related to the divergence of perturbative series: indeed, expanding $C^{\text{res}}(N, \alpha_s)$ in powers of α_s , the inverse Mellin transform exists order by order, but the resulting series is divergent.

This follows from the fact that the functions g_i in Eq. (2.1.23) depend on N through [20]

$$\alpha_s(M^2/N^a) = \frac{\alpha_s(M^2)}{1 + \bar{\alpha}L} (1 + \mathcal{O}(\alpha_s(M^2))), \quad L \equiv \log \frac{1}{N}, \quad (2.1.28)$$

with $\bar{\alpha}$ defined in Eq. (2.1.20). As a consequence, the expansion of the N -space resummed coefficient function in powers of $\alpha_s(M^2)$ has a finite radius of convergence dictated by $|\bar{\alpha}L| < 1$. In fact, $C^{\text{res}}(N, \alpha_s)$ has a branch cut in the complex N -plane along the positive real axis,

$$\text{Re } N > N_L \equiv \exp(1/\bar{\alpha}), \quad \text{Im } N = 0, \quad (2.1.29)$$

as one can see directly from the LL expression, Eq. (2.1.21). But a Mellin transform always has a convergence abscissa, so $C^{\text{res}}(N, \alpha_s)$ cannot be the Mellin transform of any function. The point N_L represents the position of the Landau pole in N -space. Hence, the non-invertibility of the resummed coefficient function is strictly related to the Landau pole of the QCD running coupling.

On the other hand, any finite-order truncation of the series expansion

$$C^{\text{res}}(N, \alpha_s) = \sum_{k=0}^{\infty} \alpha_s^k C_k^{\text{res}}(N) \quad (2.1.30)$$

behaves as a power of $\log N$ at large N and it is thus free of singularities for N large enough. Hence, we can construct the resummed coefficient function in z -space as

$$C^{\text{res}}(z, \alpha_s) = \sum_{k=0}^{\infty} \alpha_s^k C_k^{\text{res}}(z) \quad (2.1.31)$$

where its coefficients are computed as

$$C_k^{\text{res}}(z) = \mathcal{M}^{-1} [C_k^{\text{res}}(N)](z). \quad (2.1.32)$$

It follows, by contradiction, that the series Eq. (2.1.31) must diverge [30]. It turns out [30] that, if the Mellin inversion Eq. (2.1.32) is performed to finite logarithmic accuracy, the series Eq. (2.1.31) acquires a finite but nonzero radius of convergence in z ; however, this does not help given that the convolution integral Eq. (2.1.4) always goes over the region where the series diverges.

Hence, any resummed definition must either explicitly or implicitly deal with the divergence of the perturbative expansion Eq. (2.1.31). We now consider two prescriptions in which this is done by constructing a resummed expression to which the divergent series is asymptotic.

2.1.3 Minimal prescription

In Ref. [31] a simple solution was proposed to avoid cure the Landau pole problem. If the problem were not there, the hadronic cross-section could be constructed as the inverse Mellin of the product of coefficient function and parton luminosity in N -space:

$$\frac{1}{\tau} \frac{d\sigma}{dM^2} = \frac{1}{2\pi i} \int_{c-i\infty}^{c+i\infty} dN \tau^{-N} \mathcal{L}(N) C(N, \alpha_s) \quad (2.1.33)$$

with c , as usual, to the right of all the singularities of the integrand. As already said above, the problem in the resummed case is that such c does not exist because of the cut. The minimal prescription (MP) [31] defines the resummed hadronic cross-section as

$$\frac{1}{\tau} \frac{d\sigma^{\text{MP}}}{dM^2} = \frac{1}{2\pi i} \int_{\text{MP}} dN \tau^{-N} \mathcal{L}(N) C^{\text{res}}(N, \alpha_s). \quad (2.1.34)$$

where the integration path is chosen to pass to the left of the cut but to the right of all the other singularities of the integrand; moreover, the slope of the path is modified as in Fig. 2.2 in order to make the integral convergent numerically.³ It is shown in Ref. [31]

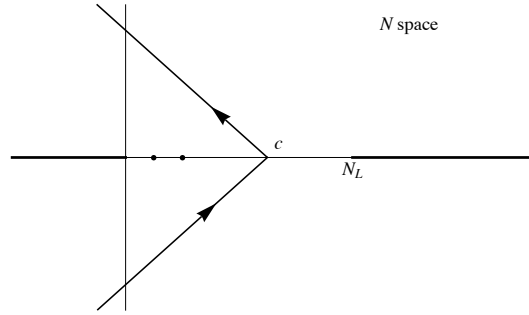


Figure 2.2. Minimal prescription path. In the figure the branch-cut due to the Landau pole is shown, as well as other singularities of the integrand.

that the cross-section obtained in this way is finite, and that it is an asymptotic sum of the divergent series obtained by substituting the expansion Eq. (2.1.30) in Eq. (2.1.34) and performing the Mellin inversion order by order in $\alpha_s(M^2)$. Of course, if the expansion is truncated to any finite order the MP simply gives the exact inverse Mellin transform, namely, the truncation of Eq. (2.1.31) to the same finite order.

Even if the MP is formulated at hadron level, we can build a sort of partonic MP. To obtain it, we start by writing $\mathcal{L}(N)$ as the explicit Mellin transform of $\mathcal{L}(z)$, and then exchanging the integrals:

$$\frac{1}{\tau} \frac{d\sigma^{\text{MP}}}{dM^2} = \int_0^1 \frac{dx}{x} \mathcal{L}(x) \frac{1}{2\pi i} \int_{\text{MP}} dN \left(\frac{\tau}{x}\right)^{-N} C^{\text{res}}(N, \alpha_s). \quad (2.1.35)$$

We can now define the MP partonic resummed coefficient function as

$$C^{\text{MP}}(z, \alpha_s) = \frac{1}{2\pi i} \int_{\text{MP}} dN z^{-N} C^{\text{res}}(N, \alpha_s) \quad (2.1.36)$$

³The result of the integral is independent on the slope, as proved in the original paper [31].

and write, changing variable $x = \tau/z$,

$$\frac{1}{\tau} \frac{d\sigma^{\text{MP}}}{dM^2} = \int_{\tau}^{\infty} \frac{dz}{z} \mathcal{L}\left(\frac{\tau}{z}\right) C^{\text{MP}}(z, \alpha_s). \quad (2.1.37)$$

Note, however, that the integral extends to ∞ . If $C^{\text{res}}(N, \alpha_s)$ was a real Mellin transform (i.e. without the cut) as $z > 1$ one could close the integration in (2.1.36) in the right half N -plane because its contribution vanishes by virtue of the damping z^{-N} , and then by residue theorem one would find that the integral vanishes for $z > 1$, thereby restoring the canonical convolution in (2.1.37). Here, because of the cut, such procedure doesn't work and $C^{\text{MP}}(z, \alpha_s)$ does not vanish in the region $z > 1$. Therefore, the MP *is not a convolution*. However, as shown in Ref. [31], the contribution

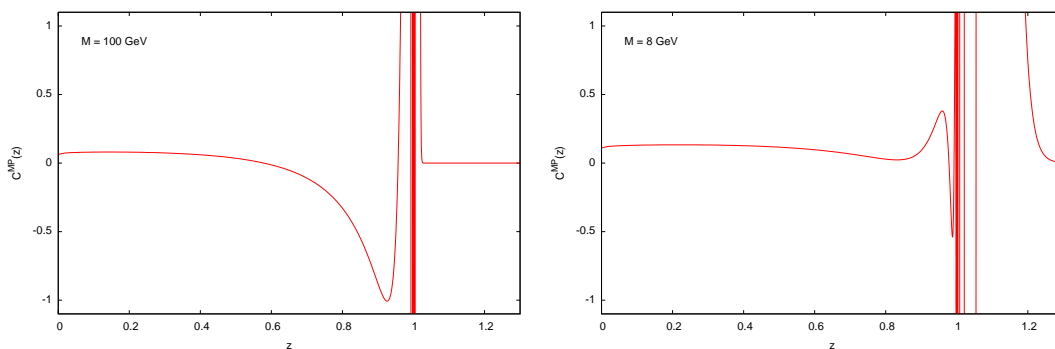


Figure 2.3. The partonic coefficient function $C^{\text{MP}}(z, \alpha_s)$ computed using the minimal prescription, Eq. (2.1.36), evaluated at $M = 100$ GeV (left) and $M = 8$ GeV (right). The curve shown is obtained using the NLL expression for the Drell-Yan coefficient function Eq. (2.1.22), (2.1.23) with only g_1 and g_2 included.

from the $z \geq 1$ region is exponentially suppressed in $\frac{\Lambda_{\text{QCD}}}{M}$. In the vicinity of $z = 1$ the integral oscillates strongly, as shown in Fig. 2.3, where $C^{\text{MP}}(z, \alpha_s)$ is displayed for the Drell-Yan resummed cross-section, evaluated at two scales which are relevant for the phenomenological discussion of Sect. 5.1. When folded with the luminosity, the hadronic cross-section receives a contribution from a region which is unphysical, i.e. when the argument of $\mathcal{L}(z)$ is less than τ : this region would not contribute in any finite order computation. Even if the ensuing integral is finite, the oscillatory behaviour of the partonic cross-section makes its numerical computation difficult. A technical solution to this problem is provided in Ref. [31]; we will propose in Sect. 2.3 a different solution, and use it for phenomenology in Chap. 5.

2.1.4 Borel prescription

An alternative prescription is based on the Borel summation of the divergent series. This prescription was developed in Refs. [30,32]; here we give an equivalent, but much simpler presentation of it [25]. To this purpose, it is convenient to rewrite the resummed coefficient function $C^{\text{res}}(N, \alpha_s)$ Eq. (2.1.22) as

$$C^{\text{res}}(N, \alpha_s) = \Sigma\left(\bar{\alpha} \log \frac{1}{N}, \alpha_s\right), \quad (2.1.38)$$

where the fact that $C^{\text{res}}(N, \alpha_s)$ depends on N via $\log \frac{1}{N}$ is made explicit:

$$\Sigma(\bar{\alpha}L, \alpha_s) = \sum_{k=0}^{\infty} h_k(\alpha_s) (\bar{\alpha}L)^k. \quad (2.1.39)$$

The zeroth term $h_0(\alpha_s)$ contains N -constant terms, i.e. the function $g_0(\alpha_s)$; however, in a matched computation, the constant term (among others) is typically subtracted. We can then compute the inverse Mellin transform term-by-term

$$C^{\text{res}}(z, \alpha_s) = \mathcal{M}^{-1} \left[\Sigma \left(\bar{\alpha} \log \frac{1}{N}, \alpha_s \right) \right] (z) \quad (2.1.40)$$

$$= \sum_{k=0}^{\infty} h_k(\alpha_s) \bar{\alpha}^k c_k(z) \quad (2.1.41)$$

where the $c_k(z)$ are the inverse Mellin transforms of the k -th power of $\log \frac{1}{N}$ and can be written according to Eq. (B.4.19b) as

$$c_k(z) = \mathcal{M}^{-1} \left[\log^k \frac{1}{N} \right] (z) = \frac{k!}{2\pi i} \oint \frac{d\xi}{\xi^{k+1}} \left(\frac{[\log^{\xi-1} \frac{1}{z}]_+}{\Gamma(\xi)} + \delta(1-z) \right), \quad (2.1.42)$$

where the integration path must enclose the origin $\xi = 0$ (the $\delta(1-z)$ term survive only for $k = 0$, and is therefore irrelevant for pure logarithms). This form, among others, is particularly useful. Indeed in this way $\Sigma(z, \alpha_s)$ becomes, exchanging courageously⁴ the sum and the integral,

$$C^{\text{res}}(z, \alpha_s) = \frac{1}{2\pi i} \oint \frac{d\xi}{\xi} \left(\frac{[\log^{\xi-1} \frac{1}{z}]_+}{\Gamma(\xi)} + \delta(1-z) \right) \sum_{k=0}^{\infty} h_k(\alpha_s) \left(\frac{\bar{\alpha}}{\xi} \right)^k k! \quad (2.1.43)$$

where we recognize the power series of Σ with an additional $k!$. Since, because of the cut of Σ , its power series has finite radius of convergence, the series in Eq. (2.1.43) has convergence radius *zero*: we are rediscovering, in another (explicit) form, that the inverse Mellin transform of $C^{\text{res}}(N, \alpha_s)$ does not exist because its perturbative expansion diverges.

Being factorially divergent, we can use the $n = 1$ Borel method (see for details App. D.3) to sum the divergent series. Eq. (2.1.43) becomes then

$$\begin{aligned} C^{\text{res}}(z, \alpha_s) &= \frac{1}{2\pi i} \oint \frac{d\xi}{\xi} \left(\frac{[\log^{\xi-1} \frac{1}{z}]_+}{\Gamma(\xi)} + \delta(1-z) \right) \int_0^{\infty} dw e^{-w} \sum_{k=0}^{\infty} h_k(\alpha_s) \left(\frac{\bar{\alpha}w}{\xi} \right)^k \\ &= \frac{1}{2\pi i} \oint \frac{d\xi}{\xi} \left(\frac{[\log^{\xi-1} \frac{1}{z}]_+}{\Gamma(\xi)} + \delta(1-z) \right) \int_0^{\infty} dw e^{-w} \Sigma \left(\frac{\bar{\alpha}w}{\xi}, \alpha_s \right) \end{aligned} \quad (2.1.44)$$

where the Borel transform of the divergent series coincides with (and has been substituted by) the function Σ . Some comments are in order:

⁴In principle, the exchange of integral and series can be performed only for absolutely convergent series. In fact, since in this case we are looking for a way to obtain a finite result from a divergent expression, such manipulations can be allowed, provided they are interpreted as a *definition* of the result they may bring to. For a more detailed discussion, see App. D.2.

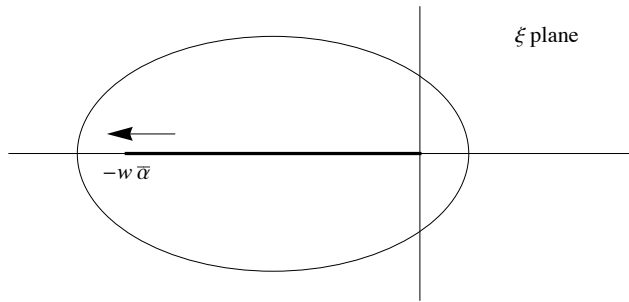


Figure 2.4. Branch-cut in the ξ plane.

- the branch-cut of Σ is mapped in terms of the variable ξ into the region $-\bar{\alpha}w \leq \xi \leq 0$: somehow, the series of $\xi = 0$ poles in the sum has been transformed in this cut;
- since the ξ integration path must encircle the poles in $\xi = 0$ order by order, it must encircle the cut of the sum;
- however, the w integral pushes the lower branch-point to $-\infty$ (see Fig. 2.4), where the oscillatory and factorially growing behaviour of $1/\Gamma(\xi)$ destroys the convergence of the ξ integral.

These considerations hint that the series Eq. (2.1.41) is *not* Borel-summable.

The Borel prescription can be now formulated. To do this, let's rewrite the result Eq. (2.1.44) by changing variable in the w integral as

$$C^{\text{res}}(z, \alpha_s) = \frac{1}{2\pi i} \oint \frac{d\xi}{\xi} \left(\frac{[\log^{\xi-1} \frac{1}{z}]_+}{\Gamma(\xi)} + \delta(1-z) \right) \int_0^\infty \frac{dw}{\bar{\alpha}} e^{-\frac{w}{\bar{\alpha}}} \Sigma \left(\frac{w}{\xi}, \alpha_s \right) \quad (2.1.45)$$

which is valid for $\bar{\alpha} > 0$, which is physically always the case. To make the integrals convergent, an upper cutoff W is put in the w integral:⁵

$$C^{\text{BP}}(z, \alpha_s, W) = \frac{1}{2\pi i} \oint \frac{d\xi}{\xi} \left(\frac{[\log^{\xi-1} \frac{1}{z}]_+}{\Gamma(\xi)} + \delta(1-z) \right) \int_0^W \frac{dw}{\bar{\alpha}} e^{-\frac{w}{\bar{\alpha}}} \Sigma \left(\frac{w}{\xi}, \alpha_s \right). \quad (2.1.46)$$

This results has the following properties:

- the divergent series Eq. (2.1.41) is asymptotic to the BP formula, Eq. (2.1.46): the proof [30] is rather simple, since the damping factor $D_k^{(1)}(W/\bar{\alpha})$, Eq. (D.3.51), tends to 1 faster than any power as $\bar{\alpha} \rightarrow 0^+$;
- even if divergent, the neglected terms due to the cutoff are formally of the form

$$\exp \frac{W}{\bar{\alpha}} = \left(\frac{\Lambda^2}{M^2} \right)^{W/2}, \quad (2.1.47)$$

i.e. they are higher-twist ($\Lambda = \Lambda_{\text{QCD}}$ is the Landau pole scale);

⁵This notation is somewhat misleading: the full coefficient function resummed with the Borel prescription is recovered from C^{BP} by adding $\delta(1-z)$. However, since in any matched result the δ term is always subtracted (being already included in the fixed order result, see Eq. (2.1.27)), this is a minor notation issue.

- such terms correspond to a twist $2 + W$: since the first subleading twist is twist 4, W must be chosen according to $W \geq 2$;
- the parameter W is a degree of freedom which can be used to estimate the ambiguity of the resummation procedure;
- last but not least, this resummed expression is at parton level, and then the convolution structure of the hadronic result is not spoiled as it is in the case of the MP.

As discussed in App. D.3.2, the truncation of the Borel integral effectively cutoff the series (smoothly), making it convergent. The truncation point is regulated by W (in fact by $W/\bar{\alpha}$, see App. D.3.2) and the larger W is the more terms are included in the series. However, since the series is not Borel summable, as W gets large some instabilities should appear: in particular, the integral varies a lot for small changes of W large. Then, a proper choice for W should be a small value: in Chap. 5 we will then choose $W = 2$, the minimal value.

To make contact with the original formulation [32], the BP result can be recast by an integration by parts in the w integral, leading to

$$C^{\text{BP}}(z, \alpha_s, W) = \frac{1}{2\pi i} \oint \frac{d\xi}{\xi} \left(\frac{[\log^{\xi-1} \frac{1}{z}]_+}{\Gamma(\xi)} + \delta(1-z) \right) \times \left[\int_0^W dw e^{-\frac{w}{\bar{\alpha}}} \frac{d}{dw} \Sigma \left(\frac{w}{\xi}, \alpha_s \right) - e^{-\frac{W}{\bar{\alpha}}} \Sigma \left(\frac{W}{\xi}, \alpha_s \right) \right]. \quad (2.1.48)$$

Being higher-twist, the second term in square brackets can be neglected, leading to a new (equivalent) version of the BP. Note that such integration by parts could already have been performed before cutting the integral off: in this case, the boundary contribution vanishes at infinity⁶ only for $\xi < 0$, which is indeed the region which gives contributions to the integral. Putting now the cutoff, we obtain the result of Ref. [32], i.e. Eq. (2.1.48) without the boundary term. Anyway, in practice, the difference between the two results is negligible; nevertheless, in some cases (as for example that of the LL anomalous dimension), this alternative formulation is easier to use, because of the different analytic structure of the derivative of Σ .

2.1.5 Subleading terms

The Borel and minimal prescriptions differ in the way the high-order behaviour of the divergent series is handled. This, as discussed in Refs. [30,32], makes in practice a small difference unless the hadronic τ is close to the Landau pole of the strong coupling,

$$\tau_L = 1 - \frac{\Lambda^2}{M^2}, \quad (2.1.49)$$

which is seldom the case, and never for applications at collider energies that we are mostly interested in. This is a consequence of the fact that for values of α_s in the perturbative region it is only at very high orders that the effect of the various prescriptions kicks in.

⁶To see this, look for example at the LL case, Eq. (2.1.21).

However, prescriptions may also differ in the subleading terms in the z dependence which are introduced when performing the resummation. To understand this, we can simply consider the effect of the prescriptions to the generic term of the expansion of $\Sigma(\bar{\alpha} \log \frac{1}{N}, \alpha_s)$, namely a power of $\log \frac{1}{N}$. The minimal prescription then just gives the exact inverse Mellin transform, since at any finite order there is no cut; then, indicating with $\mathcal{M}_{\text{MP}}^{-1}$ the inverse Mellin à la minimal prescription, we have

$$\mathcal{M}_{\text{MP}}^{-1} \left[\log^k \frac{1}{N} \right] (z) = \mathcal{M}^{-1} \left[\log^k \frac{1}{N} \right] (z). \quad (2.1.50)$$

From Eq. (B.4.19c) we see that the z dependence of such inverse Mellin is via $\log \frac{1}{z}$, and generates terms of the form

$$\left(\frac{\log^j \log \frac{1}{z}}{\log \frac{1}{z}} \right)_+, \quad 0 \leq j < k. \quad (2.1.51)$$

In the large- z limit, these terms coincide⁷ with the right ones,

$$\left(\frac{\log^j (1-z)}{1-z} \right)_+, \quad (2.1.52)$$

which are the terms that are resummed. This mismatch is not surprising: in the resummation procedure, after passing to the N space, the large- N limit was taken, spoiling the exact correspondence between the log terms in z space and their N space counterparts.

Moving to the BP, the inverse Mellin of the k -th power of $\log \frac{1}{N}$ according to Eq. (2.1.46) is ($k > 0$)

$$\mathcal{M}_{\text{BP}}^{-1} \left[\log^k \frac{1}{N} \right] (z) = \frac{1}{2\pi i} \oint \frac{d\xi}{\xi \Gamma(\xi)} \left[\log^{\xi-1} \frac{1}{z} \right]_+ \int_0^{W/\bar{\alpha}} dw e^{-w} \left(\frac{w}{\xi} \right)^k \quad (2.1.53)$$

$$= D_k^{(1)}(W/\bar{\alpha}) \cdot \mathcal{M}^{-1} \left[\log^k \frac{1}{N} \right] (z) \quad (2.1.54)$$

with $D_k^{(1)}(W/\bar{\alpha})$ defined in Eq. (D.3.51) (we have used Eq. (B.4.19b) in the last equality). Then, also the BP produces the same terms of the MP, but multiplied by the damping factor. Being interested in the z dependence, let's forget about the damping factor, since it is actually irrelevant here — the $W \rightarrow \infty$ limit is perfectly safe. Then, in this view, the z dependence of the MP and the BP is the same.

However, one of the features of the BP is that its z dependence is completely under control, as it appears in the term

$$\left[\log^{\xi-1} \frac{1}{z} \right]_+ \quad (2.1.55)$$

which produces the logs (2.1.51) by derivatives with respect to ξ ; this is a crucial difference with respect to the MP, where there is no obvious way to manipulate the z dependence. We can then more conveniently use

$$\left[(1-z)^{\xi-1} \right]_+ \quad (2.1.56)$$

⁷This is not strictly true: indeed, in a hadronic convolution, even if the lower limit τ is large the convolution receives a contribution from an integral with lower limit 0, because of the plus prescription. Then, even at very large τ , the result would be different from the “correct one”.

which generates the right logarithms Eq. (2.1.52). However this simple replacement is not enough. Indeed, in such manipulations one can play with arbitrary subleading terms, provided logarithmically enhanced terms are always the same. In N -space, the terms generated by the two distributions above differ not only by terms of the order $1/N$, but also by a constant term, see App. B.4. Then, to preserve an accuracy up to constant terms in N -space, the appropriate choice for the generating distribution is

$$\left[(1-z)^{\xi-1} \right]_+ + \frac{1}{\xi} \delta(1-z), \quad (2.1.57)$$

as one can read out of Eq. (B.4.21). With this choice the BP

$$C^{\text{BP}_1}(z, \alpha_s, W) = \frac{1}{2\pi i} \oint \frac{d\xi}{\xi \Gamma(\xi)} \left(\left[(1-z)^{\xi-1} \right]_+ + \frac{1}{\xi} \delta(1-z) \right) \times \int_0^W \frac{dw}{\bar{\alpha}} e^{-\frac{w}{\bar{\alpha}}} \Sigma \left(\frac{w}{\xi}, \alpha_s \right) \quad (2.1.58)$$

reproduces the right logarithms Eq. (2.1.52) and does not introduce additional constant terms (in N -space). This is the default Borel prescription of Refs. [30, 32]; however, there the $\delta(1-z)$ term was not taken into account, and therefore the resulting prescription was accurate up to constant terms (in N -space).

Phenomenologically (for realistic τ 's) it will differ by a sizable amount from the MP (or the “old” BP). This point is quite important: indeed, provided the large- z behaviour (or large- N in Mellin space) is respected, all choices of subleading terms are theoretically equivalent, but may lead to large differences in the region far from threshold, eventually spoiling the accuracy of the result. In particular, phenomenologically relevant values of the hadronic τ are typically quite small — of the order of 10^{-3} or less; in the convolution Eq. (2.1.4), values of z in the partonic resummed coefficient function down to $z = \tau$ give contribution, then inadequate choices of subleading terms may produce unphysical contributions to the hadronic cross-section.

To avoid such problems, it has been suggested [33] to (smoothly) truncate the resummed part of the coefficient function below some value of N : in this case, far from the threshold region, potentially large and uncontrolled contributions from subleading terms are suppressed. The price to pay is the introduction of a new, completely arbitrary, degree of freedom.

Then, we prefer and suggest [25] to find some optimal choice for the subleading terms, and in any case use the ambiguity related to different choices as an estimator of the size and the uncertainty of the resummed part of a cross-section. In Sect. 2.1.6 we will investigate several choices by comparing with fixed order results. Here, we propose a more theoretical and general argument.

The key idea is to include subleading terms that we know to appear in the perturbative computation. Coming back to Eq. (2.1.18), we see that the dependence on z is all contained, apart the factor $(1-z)^{-1}$, in the upper integration limit: such limit is determined by the kinematics of gluon emission. A careful computation [20] shows that the upper limit is really

$$k_{\text{max}}^0 = \sqrt{\frac{M^2(1-z)^2}{4z}}, \quad (2.1.59)$$

so that in fact the resummation produces logarithmic terms of the form

$$\log^k \frac{1-z}{\sqrt{z}}. \quad (2.1.60)$$

This suggests to define a new version of the Borel prescription which reproduces such logarithms. The generating distribution can be either

$$\left[z^{-\frac{\xi}{2}} (1-z)^{\xi-1} \right]_+ \quad \text{or} \quad z^{-\frac{\xi}{2}} \left[(1-z)^{\xi-1} \right]_+, \quad (2.1.61)$$

the difference being constant terms in N -space; since for the same reason discussed above the constant terms must be subtracted again, we use the second one and get, according to Eq. (B.4.22),

$$C^{\text{BP}_2}(z, \alpha_s, W) = \frac{1}{2\pi i} \oint \frac{d\xi}{\xi \Gamma(\xi)} \left(z^{-\frac{\xi}{2}} \left[(1-z)^{\xi-1} \right]_+ + \frac{1}{\xi} \delta(1-z) \right) \times \int_0^W \frac{dw}{\bar{\alpha}} e^{-\frac{w}{\bar{\alpha}}} \Sigma \left(\frac{w}{\xi}, \alpha_s \right). \quad (2.1.62)$$

This form of the Borel prescription is more accurate than the default one, Eq. (2.1.58): in Ref. [25] we used it for phenomenology, but there we neglected the $\delta(1-z)$ term. In Chap. 5 we will use here this prescription for phenomenological applications. We finally mention that this choice of subleading terms also arises in a natural way in the context of soft-collinear effective theories, and it was adopted in Ref. [28].

It turns out that these two new Borel prescriptions are closer to the MP (or equivalently to the old BP) than the default one, Eq. (2.1.58), because

$$\log \frac{1}{z} = \frac{1-z}{\sqrt{z}} (1 + \mathcal{O}[(1-z)^2]), \quad (2.1.63)$$

so that

$$\frac{\log^k \log \frac{1}{z}}{\log \frac{1}{z}} = \frac{\sqrt{z}}{1-z} \log^k \frac{1-z}{\sqrt{z}} (1 + \mathcal{O}[(1-z)^2]). \quad (2.1.64)$$

Equation (2.1.64) shows that, amusingly, up to terms suppressed by *two* powers of $1-z$, the minimal prescription effectively also reproduces the logarithms Eq. (2.1.60), though at the cost of also introducing an overall factor \sqrt{z} which is absent in the known perturbative contributions.

2.1.5.1 A discussion on constant terms

We have stressed that the $\delta(1-z)$ term in Eqs. (2.1.58) and (2.1.62) should be there to make the results accurate up to constants in N -space. We would like to show here that in any matched result, the difference between our expression and those used in Refs. [25, 30, 32] is in fact subleading, and therefore does not constitute a real defect.

To prove this, we take the Mellin transform of the Borel prescription. In the three cases of Eqs. (2.1.46), (2.1.58) and (2.1.62) we get

$$C^{\text{BP}}(N, \alpha_s, W) = \frac{1}{2\pi i} \oint \frac{d\xi}{\xi} N^{-\xi} \int_0^W \frac{dw}{\bar{\alpha}} e^{-\frac{w}{\bar{\alpha}}} \Sigma \left(\frac{w}{\xi}, \alpha_s \right) \quad (2.1.65)$$

$$C^{\text{BP}_1}(N, \alpha_s, W) = \frac{1}{2\pi i} \oint \frac{d\xi}{\xi} \frac{\Gamma(N)}{\Gamma(N+\xi)} \int_0^W \frac{dw}{\bar{\alpha}} e^{-\frac{w}{\bar{\alpha}}} \Sigma\left(\frac{w}{\xi}, \alpha_s\right) \quad (2.1.66)$$

$$C^{\text{BP}_2}(N, \alpha_s, W) = \frac{1}{2\pi i} \oint \frac{d\xi}{\xi} \frac{\Gamma(N-\xi/2)}{\Gamma(N+\xi/2)} \int_0^W \frac{dw}{\bar{\alpha}} e^{-\frac{w}{\bar{\alpha}}} \Sigma\left(\frac{w}{\xi}, \alpha_s\right). \quad (2.1.67)$$

By making use of the Stirling approximation, we immediately see that the three equations are equivalent up to terms of order $1/N$, as stressed above.

If we had not included the $\delta(1-z)$ term in Eqs. (2.1.58) and (2.1.62), as done in Refs. [25, 30, 32], the N -dependence of their Mellin transforms would have been, respectively,

$$\left[\frac{\Gamma(N)}{\Gamma(N+\xi)} - \frac{1}{\Gamma(1+\xi)} \right], \quad \left[\frac{\Gamma(N-\xi/2)}{\Gamma(N+\xi/2)} - \frac{1}{\Gamma(1+\xi)} \right]. \quad (2.1.68)$$

Hence, for each power of $L = \log \frac{1}{N}$ in Σ a constant term is produced:

$$L^k \rightarrow L^k + \Delta^{(k)}(1) + \mathcal{O}(N^{-1}), \quad (2.1.69)$$

where $\Delta(\xi) = 1/\Gamma(\xi)$. For definiteness, consider a NLL computation in N space, before the application of any prescription: in this case the at order α_s can be read out of Eq. (2.1.26), and is

$$g_{12}L^2 + g_{21}L + g_{01} \quad (2.1.70)$$

where g_{01} contains all the constants appearing in the Mellin transform of the fixed-order coefficient function $C^{(1)}(z)$; at higher orders, no constants are generated. Indeed, at NLL, the three leading powers of L are correctly predicted at each order, as shown in Tab. 2.1. Using the prescriptions of Refs. [25, 30, 32] we would have obtained instead

$$g_{12}L^2 + g_{21}L + [g_{01} + g_{12}\Delta''(1) + g_{21}\Delta'(1)] + \mathcal{O}(N^{-1}), \quad (2.1.71)$$

and now the constant term (in square brackets) is no longer correctly predicted. However, a NLL resummed result is usually matched with a NLO computation, thereby substituting the order α_s with the correct one: hence, at the end, the three leading powers of L are in fact correctly included in the full result. The same reasoning holds for higher-order resummation: therefore, after matching the generated constant terms are always subleading, and more subleading than other neglected logs.

Having understood that, after matching, the prescriptions of Refs. [25, 30, 32] are as accurate as the ones described here, we now want to stress that the subleading constant terms induced to all orders in α_s by those prescriptions are actually not random: they are exactly the constants coming from the Mellin transform of the distributions. Of course, since not all logarithms are included, not all the constant terms are produced; moreover, these constants are subleading with respect to other logarithmic terms already not included in the resummed expression. Nevertheless, since these constants are there, their inclusion could help somehow the convergence of the perturbative-resummed expansion. We will investigate this at the hadron level in Sect. 5.1.3.

2.1.6 Comparison with fixed-order

In order to assess the impact of these different choices of subleading terms, we compare the complete fixed-order results with the terms produced order by order by a truncation

of the resummed expressions and with the full resummed result, both in N -space and in z -space. For definiteness, we consider the case of the Drell-Yan process, see Sect. 5.1 and App. C.1.

2.1.6.1 N -space comparison

At NLO, the coefficient function for the $q\bar{q}$ channel (the logarithmically enhanced one) is given by Eq. (C.1.13),

$$C^{(1)}(z) = \frac{2C_F}{\pi} \left\{ 2 \left(\frac{\log(1-z)}{1-z} \right)_+ - \frac{\log z}{1-z} - (1+z) \log \frac{1-z}{\sqrt{z}} + (\zeta_2 - 2) \delta(1-z) \right\} \quad (2.1.72)$$

or, in N -space (see App. B.4 for details on the Mellin transforms),

$$C^{(1)}(N) = \frac{2C_F}{\pi} \left\{ \psi_0^2(N) + 2\gamma_E \psi_0(N) + 2\zeta_2 - 2 + \gamma_E^2 + \frac{\psi_1(N+2) - \psi_1(N)}{2} + \frac{\gamma_E + \psi_0(N+1)}{N} + \frac{\gamma_E + \psi_0(N+2)}{N+1} \right\}. \quad (2.1.73)$$

According to Tab. 2.1, a NLL resummed expression, expanded up to order α_s , reproduces all the logarithmically enhanced terms, including constants. Then, consider first the NLL (or higher): the order α_s expansion of the resummed expression in N -space is

$$C_{\text{MP}}^{(1)}(N) = \frac{2C_F}{\pi} \left[\log^2 \frac{1}{N} - 2\gamma_E \log \frac{1}{N} + 2\zeta_2 - 2 + \gamma_E^2 \right] \quad (2.1.74)$$

and coincides to what the minimal prescription would reproduce. The Borel prescription produces different terms: using directly Eqs. (2.1.66) and (2.1.67) in the $W \rightarrow \infty$ limit we would get

$$C_{\text{BP}_1}^{(1)}(N) = \frac{2C_F}{\pi} [\psi_0^2(N) - \psi_1(N) + 2\gamma_E \psi_0(N) + 2\zeta_2 - 2 + \gamma_E^2] \quad (2.1.75)$$

$$C_{\text{BP}_2}^{(1)}(N) = \frac{2C_F}{\pi} [\psi_0^2(N) + 2\gamma_E \psi_0(N) + 2\zeta_2 - 2 + \gamma_E^2] \quad (2.1.76)$$

Of course, they all coincide at large N , but the finest choice of subleading terms is the one which is more accurate even when N is not so large. In Fig. 2.5 we compare these three large- N approximations with the full NLO coefficient for positive real values of N . The MP curve is the closest one to the full order α_s , while the BP_1 is the more distant. To justify this, we expand at large N the differences

$$\frac{C_{\text{MP}}^{(1)}(N) - C^{(1)}(N)}{2C_F/\pi} = \frac{\log \frac{1}{N} - \gamma_E}{N} + \mathcal{O}(N^{-2}) \quad (2.1.77)$$

$$\frac{C_{\text{BP}_1}^{(1)}(N) - C^{(1)}(N)}{2C_F/\pi} = 2 \frac{\log \frac{1}{N} - \gamma_E - \frac{1}{2}}{N} + \mathcal{O}(N^{-2}) \quad (2.1.78)$$

$$\frac{C_{\text{BP}_2}^{(1)}(N) - C^{(1)}(N)}{2C_F/\pi} = 2 \frac{\log \frac{1}{N} - \gamma_E}{N} + \mathcal{O}(N^{-2}) \quad (2.1.79)$$

and note that, actually, the difference between MP and full order α_s is half than the difference between BP_2 and the full order α_s . Anyway, for $N \gtrsim 2$ all choices of

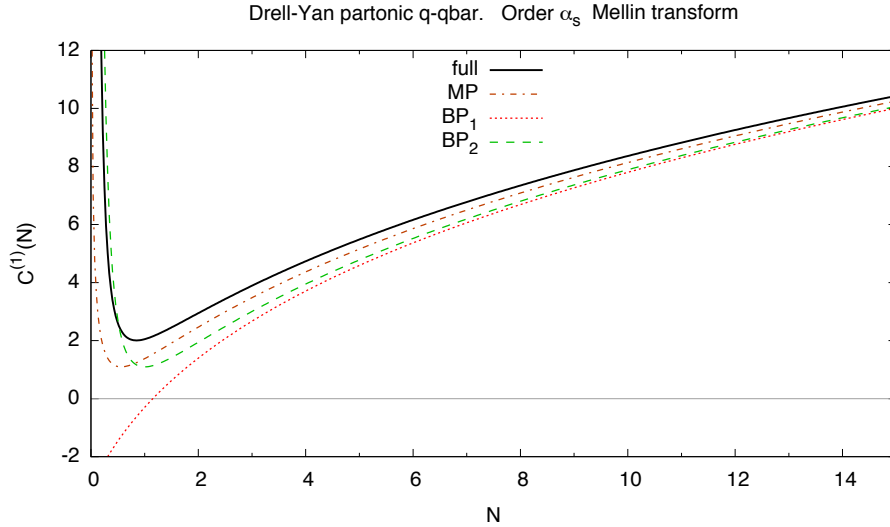


Figure 2.5. The order α_s Drell-Yan partonic coefficient function $C^{(1)}(N)$, Eq. (2.1.73), plotted as a function of N (solid curve) and its logarithmic approximations.

subleading terms are quite close to the full result, the difference being less than 50% of the contribution. Below $N \sim 2$, the BP_1 takes its way, far from fixed order: this confirms that such choice of subleading terms is the worst, and we therefore discard it. The other two curves at small N show a singularity in $N = 0$: the complete order α_s behaves as

$$C^{(1)}(N) = \frac{C_F}{\pi N^2} + \mathcal{O}(N^0) \quad (2.1.80)$$

while the MP has a logarithmic singularity and the BP_2 approximation behaves as

$$C_{BP_2}^{(1)}(N) = \frac{2C_F}{\pi N^2} + \mathcal{O}(N^0). \quad (2.1.81)$$

Then, apart from a factor of 2, the BP_2 reproduces quite well also the behaviour at small N .

The conclusion we may extract from this comparison is that both the MP and the BP_2 have good properties, and reproduce quite well the behaviour of the full fixed-order even far from the threshold region $N \gg 1$.

However, this is of course not enough for saying that the coefficient function is well predicted by the logarithms produced by threshold resummation. Indeed, according to Tab. 2.1 only a tower of dominant logarithms is correctly produced by resummation, while the other subdominant logarithms will have wrong coefficients. For example, at LL only the highest power of log is produced: at order α_s we would then have

$$C_{MP,LL}^{(1)}(N) = \frac{2C_F}{\pi} \log^2 \frac{1}{N} \quad (2.1.82)$$

$$C_{BP_1,LL}^{(1)}(N) = \frac{2C_F}{\pi} [\psi_0^2(N) - \psi_1(N)] \quad (2.1.83)$$

$$C_{BP_2,LL}^{(1)}(N) = \frac{2C_F}{\pi} \psi_0^2(N). \quad (2.1.84)$$

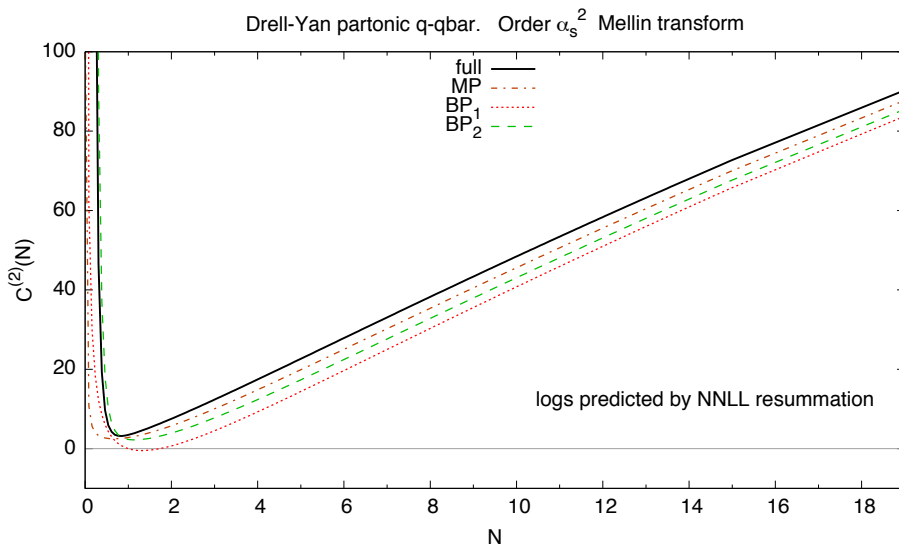


Figure 2.6. The order α_s^2 Drell-Yan partonic coefficient function $C^{(2)}(N)$ plotted as a function of N (solid curve) and its logarithmic approximations.

However, by construction, the difference between these three approximations is never logarithmic, and then no choice of subleading terms can reproduce any of the subleading logarithmic terms. The subleading difference (suppressed by at least one inverse power of N) is subleading with respect to the neglected logs, and therefore a comparison is not that helpful.

The next non-trivial comparison is between the logs produced by a NNLL resummation (or higher) at order α_s^2 (NNLO) and the full NNLO. Without showing the lengthy expression (which can be easily found expanding the expressions in App. C.3) we present the numerical results. In Fig. 2.6, the same curves as in Fig. 2.5 where the various log approximations are computed from NNLL resummation. The leading terms which differ from the full result are logarithms of N suppressed by a factor $1/N$. The first observation we may do is that such terms are quite relevant, because even at quite large N the different logarithmic curves are still quite far from the full NNLO curve.

Concerning the specific difference between each choice of subleading terms in the logarithmic terms, the conclusions drawn at NLO are unchanged. The MP choice is the best at large N , even down to such a small value as $N \sim 1$. At very small N (less than about 1), the BP_2 performs better, reproducing at least qualitatively the small- N behaviour. The BP_1 is the worst at large and intermediate N , confirming our choice of discarding it. Then, for the MP and the BP_2 , we can say that for $N \sim 2$ the logarithmic contribution is already about 50% of the full result, and it rapidly increases as N gets larger. This suggests that indeed the logarithmic contribution provides a sizable or even dominant contribution to it for $N \gtrsim 2$.

As a final comment we note that the region in which we have found logarithmic effects to be important is in fact rather wider than the region in which $\alpha_s \log^2 N \sim 1$. In this region even though logarithmically enhanced terms may lead to a substantial contribution, they behave in an essentially perturbative way, in that $(\alpha_s \log^2 N)^{k+1} <$

$(\alpha_s \log^2 N)^k$, and therefore the all-order behaviour of the resummation is irrelevant. In this intermediate region, the resummation may have a significant impact, but with significant ambiguities related to subleading terms.

2.1.6.2 z -space comparison

We now turn to a comparison in z -space. Since the conclusion would not be different from those in N -space, we perform here a comparison between the fixed order result and the full resummed expressions.

In Fig. 2.7 we compare the matched result Eq. (2.1.27) for the Drell-Yan coefficient function in the quark-antiquark channel obtained by including terms up to NLL in the resummed expression, and either up to order α_s (NLO) or α_s^2 (NNLO) in the fixed-order expansion, with various resummation prescriptions. First, we note that the MP and the BP Eq. (2.1.46) are essentially indistinguishable (for values of z less than about 0.9, where the oscillatory behaviour of the minimal prescription sets in). This is what one expects, since they contain the same subleading terms and they only differ in the treatment of the high-order divergence.

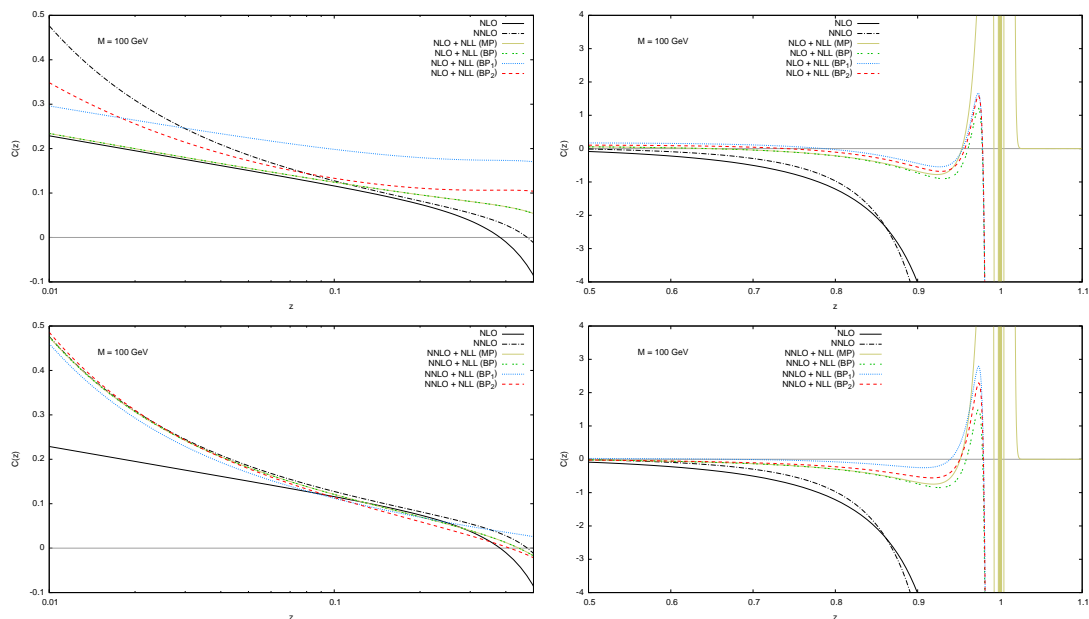


Figure 2.7. The next-to-leading log (NLL) resummed Drell-Yan matched to the fixed next-to-leading order (NLO, top row) or next-to-next-to-leading order (NNLO bottom row), with various resummation prescription. The right plots show the very large z region.

However, the BP₁ Eq. (2.1.58) is seen to differ by a non-negligible amount from the minimal prescription: at large $z \gtrsim 0.3$, where the resummation kicks in, it is small in comparison to the size of the resummation itself, while at small $z \lesssim 0.03$, where the resummation just leads to unreliable subleading contributions, it is smaller than the typical higher order correction, as it is seen by comparing results matched to the NLO and NNLO. However, in the intermediate z region the subleading terms introduced by this prescription are uncomfortably large.

The BP₂ Eq. (2.1.62) as expected differs less from the MP both at large and at small z ; also, it does not introduce unnaturally large subleading terms for any value of z . The difference between MP and this last version of the Borel prescription is not negligible but small in comparison to the size of resummation effects in the region where the resummation is relevant, and it is smaller than typical higher-order terms in the region in which the resummation is not relevant. It can thus be taken as a reliable estimate of the ambiguity in the resummation. It is interesting to observe that the subleading terms which are introduced by the replacement Eq. (2.1.60) grow at small z , and in fact are thus reproducing part of the small- z growth of perturbative coefficient functions. The fact that inclusion of these terms is important in keeping the ambiguities of large z resummation under control suggests that the large z and small z resummation regions are not well separated, and that there might be an interplay between small- and large- z resummation.

2.2 Rapidity distributions resummation

The resummed expression for rapidity distributions was only derived relatively recently in Refs. [34, 35], confirming a conjecture of Ref. [36]. In this Section, after introducing some basics formulae for rapidity distributions, we will briefly review this result, and also compare it to a somewhat different expression later derived in Ref. [28].

The hadronic rapidity Y distribution for a Drell-Yan pair or a Higgs boson of invariant mass M produced in hadronic collisions at center-of-mass energy \sqrt{s} is given by

$$\frac{1}{\tau} \frac{d\sigma}{dM^2 dY} = \sum_{i,j} c_{ij} \int_{x_1^0}^1 \frac{dx_1}{x_1} \int_{x_2^0}^1 \frac{dx_2}{x_2} f_i^{(1)}(x_1) f_j^{(2)}(x_2) C_{ij} \left(\frac{\tau}{x_1 x_2}, y, \alpha_s \right), \quad (2.2.1)$$

where

$$x_1^0 = \sqrt{\tau} e^Y, \quad x_2^0 = \sqrt{\tau} e^{-Y}, \quad \tau = \frac{M^2}{s} \quad y = Y - \frac{1}{2} \log \frac{x_1}{x_2} \quad (2.2.2)$$

and c_{ij} are suitable combination of couplings to make the LO coefficient function simply equal to $C_{ij}^{(0)}(z, y) = \delta(1-z) \delta(y)$ (or zero for channels which do not contribute at LO). The result is conveniently expressed in terms of new variables z, u , defined by

$$x_1 = \sqrt{\frac{\tau}{z}} e^Y \sqrt{\frac{z + (1-z)u}{1 - (1-z)u}}, \quad x_2 = \sqrt{\frac{\tau}{z}} e^{-Y} \sqrt{\frac{1 - (1-z)u}{z + (1-z)u}} \quad (2.2.3)$$

with inverse

$$z = \frac{\tau}{x_1 x_2}, \quad u = \frac{e^{-2y} - z}{(1-z)(1 + e^{-2y})}, \quad e^{-2y} = \frac{x_1}{x_2} e^{-2Y}; \quad (2.2.4)$$

the cross-section then becomes

$$\frac{1}{\tau} \frac{d\sigma}{dM^2 dY} = \sum_{i,j} \int_{\tau}^1 \frac{dz}{z} \int_0^1 du \mathcal{L}_{ij}^{\text{rap}}(z, u) \bar{C}_{ij}(z, u, \alpha_s) \quad (2.2.5)$$

having defined the ‘‘rapidity’’ luminosity

$$\mathcal{L}_{ij}^{\text{rap}}(z, u) = c_{ij} f_i^{(1)}(x_1) f_j^{(2)}(x_2) \quad (2.2.6)$$

(the change of variables Eq. (2.2.3) is understood implicitly) and the coefficient function

$$\bar{C}_{ij}(z, u, \alpha_s) = \left| \frac{\partial(\log x_1, \log x_2)}{\partial(\log z, u)} \right| C_{ij}(z, y(z, u), \alpha_s). \quad (2.2.7)$$

Note that $\mathcal{L}_{ij}^{\text{rap}}(z, u)$ hides a dependence on τ and Y , according to Eq. (2.2.3). The partonic threshold region $M^2 \rightarrow \hat{s} = x_1 x_2 s$ corresponds to $z \rightarrow 1$.

As already mentioned, large threshold logs only appear in the quark-antiquark channel for Drell-Yan and gluon-gluon channel for Higgs, while the contributions from other channels are suppressed by at least one more power of $1 - z$ as $z \rightarrow 1$. Therefore, we suppress flavour indexes, thereby implicitly understanding that we are considering the logarithmically enhanced channel (for the $q\bar{q}$ channel, we also include in \mathcal{L}^{rap} a sum over quark flavours).

Threshold resummation of rapidity distributions is based on the observation [34,35] (conjectured in Ref. [36]) that at large z the coefficient function $C(z, y, \alpha_s)$ factorizes as

$$C(z, y, \alpha_s) = C(z, \alpha_s) \delta(y) [1 + \mathcal{O}(1 - z)], \quad (2.2.8)$$

where $C(z, \alpha_s)$ is the rapidity-integrated coefficient. This is easily proved by rewriting $C(z, y, \alpha_s)$ in terms of its Fourier transform with respect to y :

$$\tilde{C}(z, \omega, \alpha_s) = \int_{-\infty}^{+\infty} dy e^{i\omega y} C(z, y, \alpha_s). \quad (2.2.9)$$

The integration range in Eq. (2.2.9) is restricted by kinematics to $\log \sqrt{z} \leq y \leq -\log \sqrt{z}$. Hence, one may expand the exponential $e^{i\omega y}$ in powers of y ,

$$\tilde{C}(z, \omega, \alpha_s) = \int_{\log \sqrt{z}}^{-\log \sqrt{z}} dy C(z, y, \alpha_s) [1 + \mathcal{O}(y)] = C(z, \alpha_s) [1 + \mathcal{O}(1 - z)], \quad (2.2.10)$$

where $C(z, \alpha_s)$ is the rapidity-integrated coefficient function. Hence, $\tilde{C}(z, \omega, \alpha_s)$ is independent of ω up to terms which as $z \rightarrow 1$ are suppressed by powers of $|\log z| = 1 - z + \mathcal{O}((1 - z)^2)$, and one immediately gets the desired factorized form:

$$C(z, y, \alpha_s) = \int_{-\infty}^{+\infty} \frac{d\omega}{2\pi} e^{-i\omega y} \tilde{C}(z, \omega, \alpha_s) = C(z, \alpha_s) \delta(y) [1 + \mathcal{O}(1 - z)]. \quad (2.2.11)$$

According to Eq. (2.2.3), $y = 0$ corresponds to $u = 1/2$, and noting that

$$\left| \frac{\partial(\log x_1, \log x_2)}{\partial(\log z, u)} \right| \left| \frac{\partial u}{\partial y} \right| = \frac{z^2}{\tau} \left| \frac{\partial u}{\partial y} \left(\frac{\partial x_1}{\partial z} \frac{\partial x_2}{\partial u} - \frac{\partial x_2}{\partial z} \frac{\partial x_1}{\partial u} \right) \right| = 1 \quad (2.2.12)$$

we have immediately

$$\bar{C}(z, u, \alpha_s) = C(z, \alpha_s) \delta\left(u - \frac{1}{2}\right) [1 + \mathcal{O}(1 - z)] \quad (2.2.13)$$

with the same integrated coefficient $C(z, \alpha_s)$. Up to power-suppressed terms we can thus write

$$\frac{1}{\tau} \frac{d\sigma^{\text{res}}}{dM^2 dY} = \int_{\tau}^1 \frac{dz}{z} \int_0^1 du \mathcal{L}^{\text{rap}}(z, u) \delta\left(u - \frac{1}{2}\right) C^{\text{res}}(z, \alpha_s) \quad (2.2.14)$$

$$= \int_{\tau}^1 \frac{dz}{z} \mathcal{L}^{\text{rap}}\left(z, \frac{1}{2}\right) C^{\text{res}}(z, \alpha_s). \quad (2.2.15)$$

Because Eq. (2.2.15) only depends on the rapidity-integrated coefficient function, threshold resummation is simply performed by using for the latter the resummed expressions discussed in Sect. 2.1. Moreover, by inspection of Eq. (2.2.3), we see that, for $u = 1/2$, x_1, x_2 depend on z through the ratio τ/z . Therefore, Eq. (2.2.15) has the form of a convolution product: this greatly simplify its treatment, which is then analogous to that of the resummed integrated cross-section, with the replacement

$$\mathcal{L}\left(\frac{\tau}{z}\right) \rightarrow \mathcal{L}^{\text{rap}}\left(z, \frac{1}{2}\right). \quad (2.2.16)$$

Note that the integration range in Eq. (2.2.15) actually starts from $z = \tau e^{2|Y|}$, because $\mathcal{L}^{\text{rap}}(z, 1/2)$ vanishes for $z < \tau e^{2|Y|}$:

$$\frac{1}{\tau} \frac{d\sigma^{\text{res}}}{dM^2 dY} = \int_{\tau e^{2|Y|}}^1 \frac{dz}{z} C^{\text{res}}(z, \alpha_s) \mathcal{L}^{\text{rap}}\left(z, \frac{1}{2}\right). \quad (2.2.17)$$

This underlines that at large rapidity the threshold region always gives the main contributions, even when the τ is small.

Now we discuss briefly a different way of relating the resummation of rapidity distribution to that of the inclusive cross-section which has been more recently presented in Ref. [28]. Starting from Eq. (2.2.5), the authors observe that at NLO the logarithmically enhanced terms in $\bar{C}(z, u, \alpha_s)$ in the partonic threshold limit $z \rightarrow 1$ appear as coefficients of the combination $\delta(u) + \delta(1-u)$ (see Eq. (C.1.4) to check explicitly). At higher orders, logarithmic terms in general multiply non-trivial functions of u , but Eq. (2.2.3) implies that the u dependence of x_1, x_2 is of order $1-z$, so

$$\bar{C}(z, u, \alpha_s) = [\delta(u) + \delta(1-u)] \frac{C(z, \alpha_s)}{2} [1 + \mathcal{O}(1-z)], \quad (2.2.18)$$

where the factor $1/2$ has been fixed integrating in u from 0 to 1 and comparing with the same integral of Eq. (2.2.13). It follows that

$$\frac{1}{\tau} \frac{d\sigma^{\text{res}}}{dM^2 dY} = \int_{\tau}^1 \frac{dz}{z} \frac{\mathcal{L}^{\text{rap}}(z, 0) + \mathcal{L}^{\text{rap}}(z, 1)}{2} C^{\text{res}}(z, \alpha_s). \quad (2.2.19)$$

Eq. (2.2.19) differs by power suppressed terms from the resummed result previously derived Eq. (2.2.15), as it is easy to check explicitly. Indeed, using Eq. (2.2.3) and expanding $\mathcal{L}^{\text{rap}}(z, 0)$, $\mathcal{L}^{\text{rap}}(z, 1)$ and $\mathcal{L}^{\text{rap}}(z, 1/2)$ in powers of z about $z = 1$ it is easy to check that

$$\frac{\mathcal{L}^{\text{rap}}(z, 0) + \mathcal{L}^{\text{rap}}(z, 1)}{2} = \mathcal{L}^{\text{rap}}\left(z, \frac{1}{2}\right) + \mathcal{O}[(1-z)^2]. \quad (2.2.20)$$

Because the difference is suppressed by two powers of $1-z$ one expects it to be small, and indeed we have checked that (using the Borel prescription) the difference between

Eqs. (2.2.15) and (2.2.19) is negligible, and specifically much smaller than the difference between different choices of subleading terms (see Sect. 2.1.5).

We note that, because $\mathcal{L}^{\text{rap}}(z, 0)$ and $\mathcal{L}^{\text{rap}}(z, 1)$ are not functions of τ/z , the form Eq. (2.2.19) of the resummed result does not have the structure of a convolution and thus would require a separate numerical implementation. For the same reason, a comparison between Eqs. (2.2.15) and (2.2.19) using the minimal prescription cannot be performed, because Eq. (2.2.19) cannot be expressed in terms of the Mellin transform of $C^{\text{res}}(z)$. We will disregard the form Eq. (2.2.19) of rapidity distributions henceforth.

2.3 Numerical implementation

For the sake of phenomenology, Chap. 5, an efficient numerical implementation of resummed results using the various prescriptions is necessary. Such an implementation was hitherto not available and it will be discussed here.

2.3.1 Minimal prescription

The minimal prescription involves the numerical evaluation of the complex integral

$$\frac{1}{2\pi i} \int_{c-i\infty}^{c+i\infty} dN \tau^{-N} \mathcal{L}(N) C^{\text{res}}(N, \alpha_s) \quad (2.3.1)$$

where $\mathcal{L}(N)$ is the Mellin transform of either $\mathcal{L}(z)$, Eq. (2.1.5), for the inclusive cross-section or $\mathcal{L}^{\text{rap}}(z, \frac{1}{2})$, Eq. (2.2.6), for the rapidity distribution. The integration path is usually chosen as in Fig. 2.2 in order to make the integral absolutely convergent. However, parton densities obtained from data analysis are commonly available as functions of z in interpolated form through common interfaces such as LHAPDF [37], and the numerical evaluation of their Mellin transform does not converge along the path of integration (specifically, for $\text{Re } N < 0$) and must be defined by analytic continuation. The option of applying the MP to the partonic cross-section, and then convoluting the result with the parton luminosity in momentum space is not viable, because the MP does not have the structure of a convolution: the partonic cross-section does not vanish for $z \geq 1$, and it oscillates wildly in the region $z \sim 1$, see discussion in Sect. 2.1.3 This problem is discussed in Ref. [31], where it is handled by adding and subtracting the results of the minimal prescription evaluated with a fake luminosity which allows for analytic integration.

Another possibility, adopted for example in Ref. [35], is to use parton distributions whose Mellin transform can be computed exactly at the initial scale. This, however, greatly restricts the choice of parton distributions, and specifically it prevents the use of current state-of-the-art PDFs from global fits. It is thus not suitable for precision phenomenology.

The method adopted here, based on an idea suggested long ago [38], consists of expanding the luminosity in z space, $\mathcal{L}(z)$ or $\mathcal{L}^{\text{rap}}(z, 1/2)$, on a basis of polynomials whose Mellin transform can be computed analytically. We have chosen Chebyshev polynomials, for which efficient algorithms for the computation of the expansion coefficients are available. The details of the procedure are illustrated in Appendix F.3.

The obvious drawback of this procedure is that it must be carried on for each value of the scale μ_F and, in the case of rapidity distribution, for each value of τ and Y .

2.3.2 Borel prescription

We now turn to the discussion of an implementation issue which is specific to the Borel prescription, and has to do with the choice of the cutoff W . As discussed in Sect. 2.1.4 the minimal choice is $W = 2$; however when $W \geq 1$ the ξ integration path in Eq. (2.1.46) includes values of ξ with $\text{Re } \xi < -1$, for which the convolution integral diverges. As discussed in Ref. [32], the integral can be nevertheless defined by analytic continuation, by subtracting and adding back from $\mathcal{L}(\frac{\tau}{z})/z$ its Taylor expansion in z around $z = 1$: the subtracted integrals converge, and the compensating terms can be determined analytically and continued in the desired region.

Here we propose [25] a different method which is numerically much more efficient. The idea is to perform the convolution integral with the luminosity analytically, before the complex ξ -integral. To be able to compute the integral analytically, we will use again Chebyshev polynomials for the relevant combination of luminosity. The actual form of the result depend on whether choice of subleading terms is adopted. Since we have verified numerically that the naive choice of Eq. (2.1.46) coincides with the MP up to very large values of τ , we concentrate first on Eqs. (2.1.58) and (2.1.62). For $\text{Re } \xi > 0$, we can use the identity Eq. (B.3.6) to write

$$\left[(1-z)^{\xi-1} \right]_+ = (1-z)^{\xi-1} - \frac{1}{\xi} \delta(1-z), \quad (2.3.2)$$

and this formula can be analytically extended to all complex values of $\xi \neq 0$. As a result, the $\delta(1-z)$ terms cancel and the resulting z -dependence is contained, respectively, in

$$(1-z)^{\xi-1} \quad \text{and} \quad z^{-\xi/2}(1-z)^{\xi-1} \quad (2.3.3)$$

without plus distribution. In the first case, Eq. (2.1.58), the convolution integral can be written as

$$\int_{\tau}^1 \frac{dz}{z} (1-z)^{\xi-1} \mathcal{L}\left(\frac{\tau}{z}\right) = \int_{\tau}^1 dz (1-z)^{\xi} g(z, \tau) + \mathcal{L}(\tau) \int_{\tau}^1 dz (1-z)^{\xi-1} \quad (2.3.4)$$

where we have defined

$$g(z, \tau) = \frac{1}{1-z} \left[\frac{1}{z} \mathcal{L}\left(\frac{\tau}{z}\right) - \mathcal{L}(\tau) \right]. \quad (2.3.5)$$

The subtraction introduced is justified because the function $g(z, \tau)$ is more easily approximated by an expansion on the basis of Chebyshev polynomials than $\mathcal{L}\left(\frac{\tau}{z}\right)$. Proceeding as in Appendix F.3.2 we find

$$g(z, \tau) = \sum_{p=0}^n b_p (1-z)^p, \quad (2.3.6)$$

where n is the order of the approximation, and the coefficients $b_p = b_p(\tau, \mu_F^2)$ can be computed by numerical methods. We have⁸

⁸Note that the LO is not present in this expression.

$$\frac{1}{\tau} \frac{d\sigma^{\text{BP}_1}}{dM^2} = \frac{1}{2\pi i} \oint \frac{d\xi}{\xi \Gamma(\xi)} \int_0^W \frac{dw}{\bar{\alpha}} e^{-\frac{w}{\bar{\alpha}}} \Sigma\left(\frac{w}{\xi}\right) \times \left[\sum_{p=0}^n b_p \frac{(1-\tau)^{p+\xi+1}}{p+\xi+1} + \mathcal{L}(\tau) \frac{(1-\tau)^\xi}{\xi} \right]; \quad (2.3.7)$$

the term in square brackets has poles in $\xi = 0, -1, \dots, -n$ in correspondence of zeros of $1/\Gamma(\xi)$. Thus, the ξ integrand has only a branch cut in $-w \leq \xi \leq 0$, and the contour in the ξ plane must encircle just the cut. Then this expression is valid for arbitrarily large values of the cutoff W , hence it can also be used in the case $W > 2$, which would require multiple subtractions if the method of Ref. [32] is used.

In fact, this result is applicable for the inclusive cross-section only, while the rapidity distribution requires some care. Indeed, even if the formalism can be the same, since $\mathcal{L}^{\text{rap}}(z, \frac{1}{2})$ is zero below $z = \tau e^{2|Y|}$ it is convenient to compute directly the convolution integral with such lower limit — otherwise, the approximation of $g(z, \tau)$ would be unstable. In practice, it is sufficient to substitute $\mathcal{L}(\tau/z)$ with $\mathcal{L}^{\text{rap}}(z, \frac{1}{2})$ and τ with $\tau e^{2|Y|}$ in the expression above, obtaining

$$\frac{1}{\tau} \frac{d\sigma^{\text{BP}_1}}{dM^2 dY} = \frac{1}{2\pi i} \oint \frac{d\xi}{\xi \Gamma(\xi)} \int_0^W \frac{dw}{\bar{\alpha}} e^{-\frac{w}{\bar{\alpha}}} \Sigma\left(\frac{w}{\xi}\right) \times \left[\sum_{p=0}^n b_p \frac{(1-\tau e^{2|Y|})^{p+\xi+1}}{p+\xi+1} + \mathcal{L}^{\text{rap}}\left(1, \frac{1}{2}\right) \frac{(1-\tau e^{2|Y|})^\xi}{\xi} \right] \quad (2.3.8)$$

where now $b_p = b_p(\tau, \mu_F^2)$ are the coefficient of the expansion (2.3.6) for the function

$$g(z, \tau) = \frac{1}{1-z} \left[\frac{1}{z} \mathcal{L}^{\text{rap}}\left(z, \frac{1}{2}\right) - \mathcal{L}^{\text{rap}}\left(1, \frac{1}{2}\right) \right] \quad (2.3.9)$$

in the range $\tau e^{2|Y|} \leq z \leq 1$ (see App. F.3.2).

The generalization to the other choice of subleading terms, Eq. (2.1.62), is now straightforward: using the same steps for the computation of the convolution integral we find

$$\frac{1}{\tau} \frac{d\sigma^{\text{BP}_2}}{dM^2} = \frac{1}{2\pi i} \oint \frac{d\xi}{\xi \Gamma(\xi)} \int_0^W \frac{dw}{\bar{\alpha}} e^{-\frac{w}{\bar{\alpha}}} \Sigma\left(\frac{w}{\xi}\right) \times \left[\sum_{p=0}^n b_p \text{B}\left(\xi + p + 1, 1 - \frac{\xi}{2}; 1 - \tau\right) + \mathcal{L}(\tau) \text{B}\left(\xi, 1 - \frac{\xi}{2}; 1 - \tau\right) \right], \quad (2.3.10)$$

where

$$\text{B}(b, a; 1 - \tau) = \int_\tau^1 dz z^{a-1} (1-z)^{b-1} \quad (2.3.11)$$

is the incomplete Beta function. The function $\text{B}(b, a; 1 - \tau)$ is singular at $b = 0$. In Eq. (2.3.10) the first argument of the B functions in the integrand vanishes for non positive integer values of $\xi = 0, -1, \dots$, in correspondence of zeros of $1/\Gamma(\xi)$. Thus, again, the remaining singularities are only represented by the branch cut. The rapidity distribution is obtained from this expression with the same changes described above.

Finally, we briefly discuss the case of Eq. (2.1.46). Using for $\text{Re } \xi > 0$ the identity

$$\left[\log^{\xi-1} \frac{1}{z} \right]_+ = \log^{\xi-1} \frac{1}{z} - \Gamma(\xi) \delta(1-z), \quad (2.3.12)$$

we get easily

$$\begin{aligned} \frac{1}{\tau} \frac{d\sigma^{\text{BP}}}{dM^2} &= \frac{1}{2\pi i} \oint \frac{d\xi}{\xi \Gamma(\xi)} \int_0^W \frac{dw}{\bar{\alpha}} e^{-\frac{w}{\bar{\alpha}}} \Sigma \left(\frac{w}{\xi} \right) \\ &\times \left[\sum_{p=0}^n \tilde{b}_p \gamma \left(\xi + p + 1, \log \frac{1}{\tau} \right) + \mathcal{L}(\tau) \gamma \left(\xi, \log \frac{1}{\tau} \right) \right]; \end{aligned} \quad (2.3.13)$$

where $\gamma(\xi, a)$ is the truncated Gamma function (see App. E.1), and with

$$\tilde{g}(z, \tau) = \frac{1}{\log \frac{1}{z}} \left[\frac{1}{z} \mathcal{L} \left(\frac{\tau}{z} \right) - \mathcal{L}(\tau) \right] = \sum_{p=0}^n \tilde{b}_p \log^p \frac{1}{z}, \quad (2.3.14)$$

see App. F.3.2. It would be in principle possible to use the function $g(z, \tau)$, Eq. (2.3.6), but the integral would be complicated a bit; the result would be

$$\begin{aligned} \frac{1}{\tau} \frac{d\sigma^{\text{BP}}}{dM^2} &= \frac{1}{2\pi i} \oint \frac{d\xi}{\xi \Gamma(\xi)} \int_0^W \frac{dw}{\bar{\alpha}} e^{-\frac{w}{\bar{\alpha}}} \Sigma \left(\frac{w}{\xi} \right) \\ &\times \left[\sum_{j=0}^{n+1} \hat{b}_j \gamma \left(\xi, (1+j) \log \frac{1}{\tau} \right) + \mathcal{L}(\tau) \gamma \left(\xi, \log \frac{1}{\tau} \right) \right]; \end{aligned} \quad (2.3.15)$$

with

$$\hat{b}_j = (-)^j \sum_{p=j-1}^n b_p \binom{p+1}{j}. \quad (2.3.16)$$

Extension to rapidity distributions is straightforward.

3 High-energy resummation

Contents

3.1 High-energy factorization	56
3.2 BFKL equation	57
3.3 The Double-Leading approximation	58
3.3.1 Duality relation	59
3.3.2 Double-Leading approximation	60
3.4 Symmetrization	62
3.4.1 The symmetry of the BFKL kernel	62
3.4.2 Off-shell kernels	64
3.4.3 Improved resummation by symmetrization	65
3.5 Running coupling corrections to the BFKL equation	68
3.5.1 Resummation of running coupling effects	71
3.5.2 Quadratic approximation to the kernel	73
3.5.3 On the minimum	75
3.6 Resummed anomalous dimensions.	76
3.6.1 The case $n_f \neq 0$	78
3.6.2 Resummation of quark anomalous dimensions	79
3.6.3 Back to the physical basis	81
3.6.4 Schemes	82
3.7 Resummed splitting function	83
3.7.1 Approximations	84

In this Chapter we will cover the resummation of high-energy logarithms. Such resummation mainly affects the evolution of the gluon, even though also the quark singlet gets contributions at next-to-leading log. We will see that resummation is provided by combining the GLAP evolution equation with the so called BFKL equation: after introducing a first leading resummation, we will show that the result is unstable for perturbative corrections, and it doesn't describe the observed phenomena. Then we will go further by introducing two ingredients: symmetrization and running-coupling resummation. Such ingredients allow to find stable results, which are compatible with the observations. To begin with, we introduce a factorization theorem valid in the high-energy regime, from which the BFKL can be derived.

3.1 High-energy factorization

The mass (or collinear) factorization theorem Eq. (1.2.22) is well established [39, 40]. It is a perturbative factorization, i.e. it is valid order by order in perturbation theory up to terms which are of higher orders and to terms suppressed by negative powers of the hard scale Q^2 , called higher twists. The perturbativity is guaranteed by the condition $Q^2 \gg \Lambda_{\text{QCD}}$, in such a way that $\alpha_s(Q^2)$ is small enough.

However, this is not always enough for realistic applications. Consider for definiteness the DIS process discussed in Sect. 1.2.1: if the available partonic initial energy squared $\hat{s} = 2\hat{p}q = zQ^2/x$ is large, the convergence of the perturbative series is spoiled. Indeed, in the coefficient function logarithms of the ratio of the energies $\sqrt{\hat{s}}$ and Q , i.e. logarithms of x/z , appear at each order, and if $\hat{s} \gg Q^2$ (high-energy regime) all such terms in the perturbative series are equally important. Then, the perturbative result obtained in the context of collinear factorization is not enough for the study of the high-energy regime.

A generalization of the collinear factorization valid in the high-energy regime has been proposed long ago [41–45]. Consider again the DIS: it can be proved that the dominant contributions at high energy are given by diagrams in which a gluon is exchanged in the t -channel, or otherwise stated, from diagrams whose forward amplitude is two-gluon reducible, Fig. 3.1. For such diagrams, the structure function F_2 satisfies

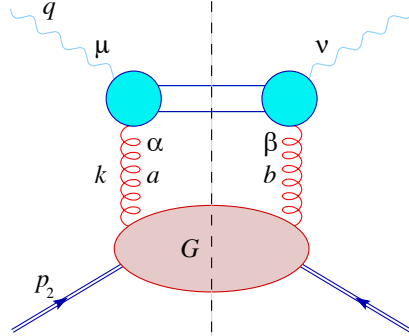


Figure 3.1. Two-gluon reducible diagrams contributing to the high-energy part of DIS structure functions. (Figure taken from Ref. [46].)

the fundamental factorization

$$F_2(x, Q^2) = \int_x^1 \frac{dz}{z} \int d^2\mathbf{k} C\left(\frac{x}{z}, \frac{Q^2}{\mathbf{k}^2}, \alpha_s(Q^2)\right) \mathcal{F}(z, \mathbf{k}) \quad (3.1.1)$$

where $C\left(\frac{x}{z}, \frac{Q^2}{\mathbf{k}^2}, \alpha_s(Q^2)\right)$ is called *off-shell partonic cross-section* and represents the contribution from a partonic diagram in the t -channel where the gluon is off-shell (upper part of the diagram), and $\mathcal{F}(z, \mathbf{k})$ is a non-perturbative contribution analogous to the PDFs (lower part of the diagram, including gluon propagator); the integration limits of the \mathbf{k} integral are set by kinematics. Eq. (3.1.1) is diagonalized by a double Mellin-Laplace transform,

$$F_2(N, M) \equiv \int_0^1 dx x^{N-1} \int_0^\infty \frac{dQ^2}{Q^2} \left(\frac{Q^2}{\Lambda^2}\right)^{-M} F_2(x, Q^2), \quad (3.1.2)$$

where Λ is some reference scale ($F_2(x, Q^2)$ depends logarithmically on Q^2). Then in double Mellin space we have

$$F_2(N, M) = C(N, M, \alpha_s(Q^2)) \mathcal{F}(N, M) \quad (3.1.3)$$

with

$$C(N, M, \alpha_s(Q^2)) = \int_0^1 dz z^{N-1} \int_0^\infty \frac{d\rho}{\rho} \rho^{-M} C(z, \rho, \alpha_s(Q^2)) \quad (3.1.4)$$

$$\mathcal{F}(N, M) = \int_0^1 dz z^{N-1} \int d^2\mathbf{k} \left(\frac{\mathbf{k}^2}{\Lambda^2}\right)^{-M} \mathcal{F}(z, \mathbf{k}). \quad (3.1.5)$$

The high-energy factorization (or k_T -factorization) formula Eq. (3.1.1) is proved to be valid in the high-energy limit

$$\hat{s} \gg Q^2 \quad (3.1.6)$$

regardless the size of the gluon momentum \mathbf{k}^2 , which takes all accessible values in the integral. Conversely, the collinear factorization is valid in the limit $Q^2 \gg \mathbf{k}^2$, because this region (the collinear region) dominates the \mathbf{k} integral. In the limit

$$\hat{s} \gg Q^2 \gg \mathbf{k}^2 \quad (3.1.7)$$

both factorization are reliable, and then in such limit they would coincide. Indeed, it has been proved in Ref. [47] that, in this regime, standard collinear factorization can be derived in a straightforward way from the high-energy factorization theorem.

3.2 BFKL equation

The high-energy factorization formula Eq. (3.1.3) depends on N and M on the same footing. This reflects a symmetry of the factorization formula Eq. (3.1.2) if written in terms of the variables

$$\xi = \log \frac{1}{x}, \quad t = \log \frac{Q^2}{\Lambda^2}. \quad (3.2.1)$$

This suggests, and in fact it is, that an evolution equation in the variable ξ could be derived. Such an equation is called the *Balitsky-Fadin-Kuraev-Lipatov (BFKL) equation* [48–51]

$$\frac{d}{d\xi} f(\xi, q^2) = \int_0^\infty \frac{dk^2}{k^2} K\left(\alpha_s, \frac{q^2}{k^2}\right) f(\xi, k^2), \quad (3.2.2)$$

where $K(\alpha_s, q^2/k^2)$ is a (fixed-coupling) unintegrated kernel (similar to the splitting functions in the case of GLAP). In Ref. [47], with the same technique used to derive the GLAP equation, the BFKL equation is derived from the high-energy factorization.

Taking the Mellin transform with respect to q^2 we get another (more suitable) form of the BFKL equation

$$\frac{d}{d\xi} f(\xi, M) = \chi(\alpha_s, M) f(\xi, M), \quad (3.2.3)$$

where M is the variable conjugate to t and

$$\chi(\alpha_s, M) = \int_0^\infty \frac{dq^2}{q^2} \left(\frac{q^2}{k^2}\right)^{-M} K\left(\alpha_s, \frac{q^2}{k^2}\right) \quad (3.2.4)$$

is the integrated BFKL kernel and

$$f(\xi, M) = \int_0^\infty \frac{dq^2}{q^2} \left(\frac{q^2}{\Lambda^2} \right)^{-M} f(\xi, q^2). \quad (3.2.5)$$

Note that, since a Mellin transform with respect to t is taken, the BFKL equation written in the form of Eq. (3.2.3) is only valid for fixed coupling α_s . Running coupling effects will be discussed in Sect. 3.5.

As the GLAP equation describes the evolution of the PDFs in the t direction, the BFKL equation describes the evolution of f in the direction of the variable ξ (related to x by Eq. (3.2.1)). Then, the BFKL equation resums the small- x (large- ξ) logarithms, as the GLAP equation resums the large- t dependence.

Hence, the PDF appearing in the BFKL equation has to be identified with the largest eigenvector f_+ , since it contains all the small- x singularities. For practical reasons, we have chosen

$$f(\xi, q^2) \equiv x f_+(x, q^2), \quad (3.2.6)$$

since with this factor of x the GLAP equation in Mellin space becomes simply

$$\frac{d}{dt} f(N, q^2) = \gamma(\alpha_s(q^2), N) f(N, q^2), \quad (3.2.7)$$

where $\gamma(\alpha_s, N)$ is

$$\gamma(\alpha_s, N) \equiv \gamma_+(\alpha_s, N). \quad (3.2.8)$$

To further simplify the notations we will write the perturbative expansion of the anomalous dimension as

$$\gamma(\alpha_s, N) = \alpha_s \gamma_0(N) + \alpha_s^2 \gamma_1(N) + \mathcal{O}(\alpha_s^3) \quad (3.2.9)$$

and that of the BFKL kernel as

$$\chi(\alpha_s, M) = \alpha_s \chi_0(N) + \alpha_s^2 \chi_1(N) + \mathcal{O}(\alpha_s^3). \quad (3.2.10)$$

The LO and the NLO contributions to the BFKL kernel are known [52]; the LO is

$$\chi_0(M) = \frac{N_c}{\pi} [2\psi(1) - \psi(M) - \psi(1 - M)] \quad (3.2.11)$$

where ψ is the DiGamma function (see App. E.1), and the NLO is given in App. C.4.1.

3.3 The Double-Leading approximation

As we have seen in Sect. 1.3.2, the singlet splitting functions are unstable at small x ,¹ in the sense that in the generic order α_s^n term a tower of powers of $\log x$ up to n appears: then, if $\alpha_s \log \frac{1}{x} \sim 1$, each term of the perturbative expansion of the splitting functions is equally important and the series must be summed. Note that the condition $\alpha_s \log \frac{1}{x} \sim 1$, the high-energy regime, is often satisfied by the kinematic conditions of HERA.

¹At large x , instead, we have seen that the diagonal terms are enhanced, but such enhancement is the same to all orders in α_s , leaving the perturbative expansion stable at large x .

The leading singularities at small x are contained in the gluon singlet splitting functions P_{gg} and P_{gq} , while the quark splitting functions have singularities suppressed by one power of α_s more, i.e. they are next-to-leading. The coefficient functions are next-to-leading as well: we then conclude that the most significant effect of small- x resummation appears in the gluon splitting functions, and hence in the gluon PDF. Moreover, it is proved in Ref. [45] that resummation of quark splitting functions and of coefficient functions is related to the gluon resummation. We then concentrate our attention to the gluon splitting functions, and we will discuss in Sect. 3.6 the next-to-leading effect of quarks.

To be more precise, we could work in the limit $n_f = 0$, where there are only gluons in the game, and everything would be clean and perfectly well defined, but the inclusion of quarks would be difficult. Then, it is better to work with the eigenvectors of the singlet sector: indeed, in schemes like $\overline{\text{MS}}$ and DIS, the “smallest” eigenvalue is suppressed at small x by one power of x with respect to the “largest”, to all orders in α_s . In the following we will then use the largest eigenvector instead of the gluon: in the limit $n_f = 0$ the two would coincide.

3.3.1 Duality relation

In the region where both GLAP evolution and BFKL evolution are reliable (large t and large ξ respectively), the solution of both equations should coincide (at leading twist). Then, we can take the double Mellin transform and get the equations

$$[M - \gamma(\alpha_s, N)] f(N, M) = F_0(N) \quad (3.3.1a)$$

$$[N - \chi(\alpha_s, M)] f(N, M) = \tilde{F}_0(M) \quad (3.3.1b)$$

where we have defined the boundary conditions

$$F_0(N) = [e^{-Mt} f(N, t)]_{t=-\infty}^{t=+\infty}, \quad \tilde{F}_0(M) = [e^{-N\xi} f(\xi, M)]_{\xi=0}^{\xi=+\infty}. \quad (3.3.2)$$

Note that both Eqs. (3.3.1) are valid only in the fixed-coupling case; the extension of these equations and of the duality we are going to derive will be treated in Sect. 3.5.

The solutions of Eqs. (3.3.1) are, respectively,

$$f(N, M) = \frac{F_0(N)}{M - \gamma(\alpha_s, N)}, \quad f(N, M) = \frac{\tilde{F}_0(M)}{N - \chi(\alpha_s, M)}. \quad (3.3.3)$$

The leading twist behaviour of these solutions is given by the position of the perturbative pole. Indeed, inverting the M -Mellin transform we get, respectively,

$$f(N, t) = \int_{c-i\infty}^{c+i\infty} \frac{dM}{2\pi i} e^{Mt} \frac{F_0(N)}{M - \gamma(\alpha_s, N)} = F_0(N) e^{\gamma(\alpha_s, N)t} \quad (3.3.4)$$

$$f(N, t) = \int_{c-i\infty}^{c+i\infty} \frac{dM}{2\pi i} e^{Mt} \frac{\tilde{F}_0(M)}{N - \chi(\alpha_s, M)} = \frac{\tilde{F}_0(\bar{M})}{-\chi'(\alpha_s, \bar{M})} e^{\bar{M}t} + \text{higher twist} \quad (3.3.5)$$

where \bar{M} is the position of the rightmost² pole of the BFKL solution Eq. (3.3.3) given by

$$\chi(\alpha_s, \bar{M}) = N. \quad (3.3.6)$$

²Rightmost in the “collinear” region, i.e. $M < \frac{1}{2}$.

Hence the consistency of the two solutions at leading twist requires the validity of the duality relation [47]

$$\chi(\alpha_s, \gamma(\alpha_s, N)) = N \quad \leftrightarrow \quad \gamma(\alpha_s, \chi(\alpha_s, M)) = M \quad (3.3.7)$$

(position of the pole) and the relation

$$F_0(N) = -\frac{\tilde{F}_0(\gamma(\alpha_s, N))}{\chi'(\alpha_s, \gamma(\alpha_s, N))} \quad \leftrightarrow \quad \tilde{F}_0(M) = -\frac{F_0(\chi(\alpha_s, M))}{\gamma'(\alpha_s, \chi(\alpha_s, M))} \quad (3.3.8)$$

(pole coefficient matching).

Note that the anomalous dimension and BFKL kernel, if computed both at fixed order, are never dual. To see this we note that, for example, momentum conservation Eq. (1.2.5) requires

$$\gamma(\alpha_s, N = 1) = 0 \quad (3.3.9)$$

to all orders, which in turn implies, by duality

$$\chi(\alpha_s, M = 0) = 1; \quad (3.3.10)$$

however, the BFKL kernel at fixed order is bad behaved in the $M \sim 0$ region, and in particular it has in $M = 0$ a simple pole at LO, and a double pole with opposite sign at NLO (in general, at order α_s^k it behaves as $(-M)^{-k}$). Indeed, the dual of, let's say, the LO anomalous dimension contains all powers of α_s , and therefore it cannot coincide with any fixed-order BFKL kernel.

Therefore, the duality Eq. (3.3.7) is intended to be valid provided all the relevant contributions in the regime of validity (small N and M) are included. Then, in practice, it would be valid only if the small- N contributions to the anomalous dimension are resummed and/or the small- M contributions to the BFKL kernel are resummed. In the following, we will revert this argument and *use* the duality to perform such resummation.

3.3.2 Double-Leading approximation

The duality Eq. (3.3.7) allows us to construct an expansion of γ and χ in powers of α_s at fixed α_s/N and α_s/M respectively [53]:

$$\gamma(\alpha_s, N) = \gamma_s(\alpha_s/N) + \alpha_s \gamma_{ss}(\alpha_s/N) + \dots \quad (3.3.11)$$

$$\chi(\alpha_s, M) = \chi_s(\alpha_s/M) + \alpha_s \chi_{ss}(\alpha_s/M) + \dots \quad (3.3.12)$$

Let's consider χ : all we say applies to γ as well. To derive the relations between χ_s, χ_{ss} and γ_0, γ_1 we insert the expansion (3.3.12) into the duality relation (3.3.7),

$$\gamma_0 \left[\chi_s \left(\frac{\alpha_s}{M} \right) \right] + \alpha_s \gamma_0' \left[\chi_s \left(\frac{\alpha_s}{M} \right) \right] \chi_{ss} \left(\frac{\alpha_s}{M} \right) + \alpha_s \gamma_1 \left[\chi_s \left(\frac{\alpha_s}{M} \right) \right] + \mathcal{O} \left[\alpha_s^2 \left(\frac{\alpha_s}{M} \right)^{\forall k} \right] = \frac{M}{\alpha_s}, \quad (3.3.13)$$

from which we get

$$\chi_s \left(\frac{\alpha_s}{M} \right) = \gamma_0^{-1} \left(\frac{M}{\alpha_s} \right) \quad (3.3.14)$$

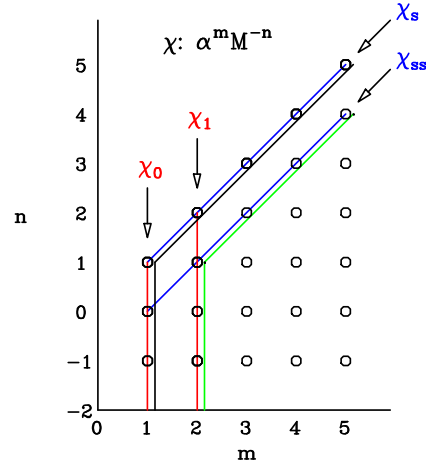


Figure 3.2. Structure of the Double-Leading approximation for the BFKL kernel $\chi(M, \alpha_s)$. (Figure taken from Ref. [53].)

$$\chi_{ss}\left(\frac{\alpha_s}{M}\right) = -\frac{\gamma_1(\chi_s(\alpha_s/M))}{\gamma_0'(\chi_s(\alpha_s/M))} \quad (3.3.15)$$

where γ_0^{-1} is the inverse function of γ_0 . Note that, while at LO $\alpha_s \gamma_0$ and χ_s are exactly dual, at NLO $\alpha_s \gamma_0 + \alpha_s^2 \gamma_1$ and $\chi_s + \alpha_s \chi_{ss}$ are dual up to order α_s^2 corrections (at fixed α_s/M). For this reason, for numerical application it may be better to consider the exact dual also at NLO (or beyond), the difference being subleading. Anyway, for the sake of theoretical discussion, we will continue to consider the singular expansion Eq. (3.3.12).

The singular expansion (3.3.12) allows to produce a Double-Leading (DL) expansion for the BFKL kernel:

$$\begin{aligned} \chi_{\text{DL}}(\alpha_s, M) &= \alpha_s \chi_0(M) + \chi_s\left(\frac{\alpha_s}{M}\right) - \alpha_s \frac{\chi_{0,1}}{M} \\ &+ \alpha_s \left[\alpha_s \chi_1(M) + \chi_{ss}\left(\frac{\alpha_s}{M}\right) - \alpha_s \left(\frac{\chi_{1,2}}{M^2} + \frac{\chi_{1,1}}{M} \right) - \chi_{0,0} \right] \\ &+ \dots \end{aligned} \quad (3.3.16)$$

where the first row represents a LO DL expansion, the second row a NLO DL expansion, and so on. The $\chi_{k,j}$ terms are subtracted to avoid double counting; these coefficients can be read from Eqs. (C.4.21). The structure of the terms which enter this expansion are shown pictorially in Fig. 3.2. A completely analogous expression can be obtained for the anomalous dimension.

The LO DL result resums the leading logarithms of q^2 in the BFKL kernel: therefore, it represents a matched LO+LL resummed kernel (the same for the anomalous dimension, the resummed logarithms being logs of $1/x$). Again, the NLO DL result resums also the next-to-leading logarithms, and therefore represents a matched NLO+NLL resummed kernel. Hence, concerning the double-leading expansion, the notation LO, NLO and so on represents in fact LL, NLL, and so on. The reason for this notation relies on the fact that to accomplish resummation to $N^k\text{LL}$ within the DL expansion one has to simply match a $N^k\text{LO}$ BFKL kernel with a $N^k\text{LO}$ anomalous dimension. We will then continue to talk about LO and NLO resummation, meaning always LO+LL and NLO+NLL matched expressions.

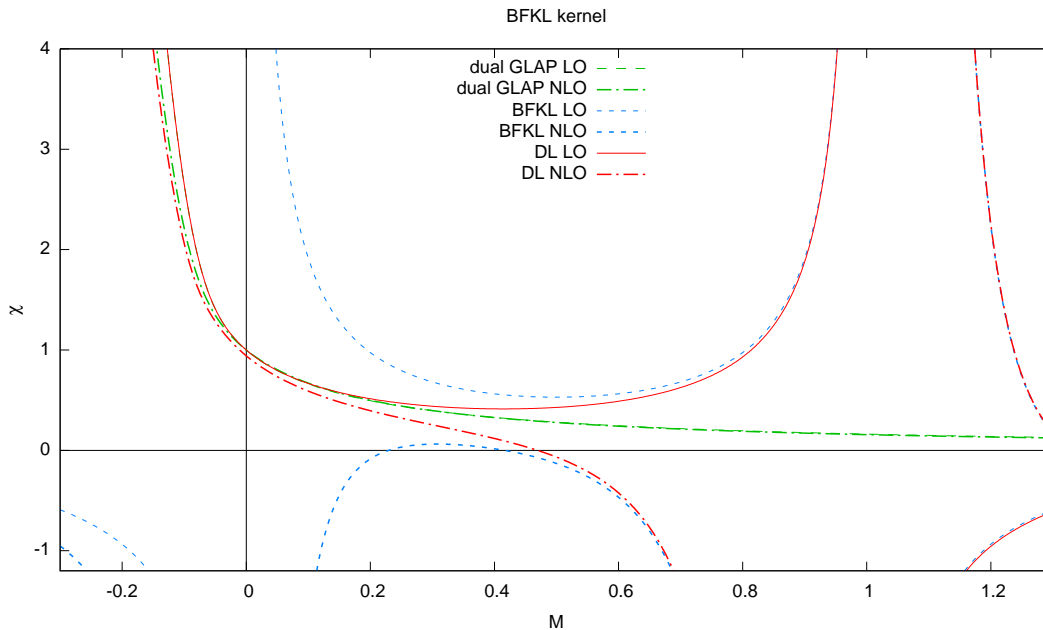


Figure 3.3. Double-Leading approximation for the BFKL kernel $\chi(M, \alpha_s)$. Here we have used $\alpha_s = 0.2$ and $n_f = 4$.

The results for $\alpha_s = 0.2$ and $n_f = 4$ are shown on Fig. 3.3. From the plot, we immediately see that such result is not acceptable: indeed the DL curves (red curves), when mirrored with respect to the main diagonal to give the anomalous dimension, manifest a perturbative instability at small N . The LO DL curve, when inverted, presents a square-root branch-point at some small positive value of N , while the NLO DL curve extends smoothly to all negative values of N . Moreover, from a phenomenological point of view, the LO and NLO anomalous dimensions (which have simple poles in $N = 0$), describe quite well the data, while the DL LO approximation gives a too strong rise at small x , and the DL NLO does not rise at all [53].

Such instability is related to the bad behaviour of the BFKL kernel around $M = 1$: therefore, in order to obtain a stable DL approximation, also the $M = 1$ singularities must be resummed. We will treat such resummation in the next Section.

3.4 Symmetrization

The first ingredient needed to improve the DL result is related to the intrinsic symmetry of the BFKL kernel. We discuss this now.

3.4.1 The symmetry of the BFKL kernel

Since the diagrams involved in the computation of the BFKL kernels are symmetric for the exchange of the incoming gluon momenta, the BFKL kernel should satisfy

$$\frac{1}{q^2} K \left(\alpha_s, \frac{q^2}{k^2} \right) = \frac{1}{k^2} K \left(\alpha_s, \frac{k^2}{q^2} \right) \quad (3.4.1)$$

or, in terms of its Mellin transform,

$$\chi(\alpha_s, M) = \chi(\alpha_s, 1 - M). \quad (3.4.2)$$

However, while the LO kernel Eq. (3.2.11) satisfies this symmetry, the NLO kernel $\chi_1(N)$, Eq. (C.4.3), is no longer symmetric. In fact, this symmetry is broken by two effects:

- the running of the coupling constant α_s
- an asymmetric choice for the variable ξ .

The running of the coupling and the resummation of its effects will be treated in Sect. 3.5; so far, in χ_1 only a perturbative contribution was included, Eq. (3.5.17). The second point is the argument of this Section.

In the computation of the BFKL kernel from gluon-gluon scattering, the value of the variable ξ depends symmetrically on q^2 and k^2 [45, 52]; however, in DIS, the variable ξ is defined as

$$\xi = \log \frac{1}{x} = \log \frac{2pq}{-q^2} \stackrel{\text{small } x}{\simeq} \log \frac{s}{-q^2} \quad (3.4.3)$$

which depends only on q^2 , and hence has no symmetry under the exchange $q^2 \leftrightarrow k^2$. The symmetric choice for the variable ξ is obtained substituting q^2 with $\sqrt{q^2 k^2}$ in the last equality. Then, the BFKL evolution equation for the DIS choice of ξ has to be modified accordingly [52], thereby breaking the symmetry. The transition from one choice to the other is obtained by recasting the double Mellin transform of the BFKL equation: using s as integration variable for the N -Mellin we have (from DIS to symmetric)

$$\int \frac{ds}{s} \int \frac{dq^2}{q^2} \left(\frac{s}{q^2}\right)^N \left(\frac{q^2}{k^2}\right)^{-M} = \int \frac{ds}{s} \int \frac{dq^2}{q^2} \left(\frac{s}{\sqrt{q^2 k^2}}\right)^N \left(\frac{q^2}{k^2}\right)^{-M - \frac{N}{2}}. \quad (3.4.4)$$

Because of the pole condition Eq. (3.3.6), N has to be identified with the current kernel. Therefore, calling for definiteness χ_σ the kernel for the symmetric variable choice and χ that for the usual DIS variables, the two kernels are related by [52, 54]

$$\begin{cases} \chi(\alpha_s, M + \frac{N}{2}) = \chi_\sigma(\alpha_s, M) \\ N = \chi_\sigma(\alpha_s, M), \end{cases} \quad (3.4.5a)$$

or, implicitly,

$$\chi\left(\alpha_s, M + \frac{1}{2}\chi_\sigma(\alpha_s, M)\right) = \chi_\sigma(\alpha_s, M), \quad (3.4.5b)$$

or equivalently

$$\chi_\sigma\left(\alpha_s, M - \frac{1}{2}\chi(\alpha_s, M)\right) = \chi(\alpha_s, M). \quad (3.4.5c)$$

The relation (3.4.5) can be solved iteratively to the desired order. For example, given χ_σ , one can compute χ by writing

$$\chi(\alpha_s, M) = \chi_\sigma\left(\alpha_s, M - \frac{1}{2}\chi_\sigma\left(\alpha_s, M - \frac{1}{2}\chi_\sigma(\alpha_s, M - \dots)\right)\right) \quad (3.4.6)$$

and stopping at the desired level of accuracy. For instance, at LO, it is easy to see that the two kernels are equal. Indeed $\chi_\sigma(\alpha_s, M) = \alpha_s \chi_0(M)$ and hence

$$\chi(\alpha_s, M) = \alpha_s \chi_0 \left(M - \frac{\alpha_s}{2} \chi_0(M + \mathcal{O}(\alpha_s)) \right) = \alpha_s \chi_0(M) + \mathcal{O}(\alpha_s^2). \quad (3.4.7)$$

At fixed NLO, $\chi_\sigma(\alpha_s, M) = \alpha_s \chi_0(M) + \alpha_s^2 \chi_1^\sigma(M)$ and

$$\begin{aligned} \chi(\alpha_s, M) &= \alpha_s \chi_0 \left(M - \frac{\alpha_s}{2} \chi_0(M + \mathcal{O}(\alpha_s)) \right) + \alpha_s^2 \chi_1^\sigma(M + \mathcal{O}(\alpha_s)) \\ &= \alpha_s \chi_0(M) + \alpha_s^2 \left[\chi_1^\sigma(M) - \frac{1}{2} \chi_0(M) \chi_0'(M) \right] + \mathcal{O}(\alpha_s^3). \end{aligned} \quad (3.4.8)$$

Note that the order α_s^2 symmetric term $\chi_1^\sigma(M)$ is modified by adding $-\frac{1}{2} \chi_0(M) \chi_0'(M)$: this is (one of) the non-symmetric term appearing in Eq. (C.4.3).

The relation (3.4.5) is much better written in terms of inverse functions. Since, by duality, the inverse function of χ in asymmetric variables is the anomalous dimension γ , we can introduce the ‘‘symmetric’’ anomalous dimension γ_σ , dual to χ_σ : putting these into one of Eqs. (3.4.5) we get

$$\gamma(N) = \gamma_\sigma(N) + \frac{N}{2}. \quad (3.4.9)$$

This relation is very useful in numerical computations, and also to simply visualize the passage from symmetric variables to asymmetric ones and vice-versa.

3.4.2 Off-shell kernels

We now build a tool that can help us to ‘‘solve’’ the relation Eq. (3.4.5). We introduce the concept of ‘‘off-shell’’ kernel

$$\bar{\chi}(\alpha_s, M, N) \quad (3.4.10)$$

as a function of one more variable N (the name is not a coincidence) defined by the condition that the actual kernel (also ‘‘on-shell’’ kernel from now on) can be obtained by the ‘‘on-shell’’ (or pole) condition

$$\bar{\chi}(\alpha_s, M, \chi(\alpha_s, M)) = \chi(\alpha_s, M). \quad (3.4.11)$$

If $\chi(\alpha_s, M)$ is related by duality to $\gamma(\alpha_s, N)$, Eq. (3.4.11) can be rewritten as

$$\bar{\chi}(\alpha_s, \gamma(\alpha_s, N), N) = N. \quad (3.4.12)$$

More generally, we can consider the ‘‘off-shell’’ relation

$$\bar{\chi}(\alpha_s, M, N) = N \quad (3.4.13)$$

and obtain either Eq. (3.4.11) or Eq. (3.4.12) by putting on-shell respectively N or M , i.e. by setting $N = \chi(\alpha_s, M)$ or $M = \gamma(\alpha_s, N)$.

Geometrically, we have a simple interpretation of the off-shell kernel. Consider a two-dimensional space with coordinates (M, N) : the BFKL kernel is a curve on this plane, provided we identify N with $\chi(\alpha_s, M)$. By duality, the same curve is $\gamma(\alpha_s, N)$, provided now N is considered as the independent variable and we identify M with γ .

In this context, the off-shell kernel $\bar{\chi}(\alpha_s, M, N)$ can be viewed as a function on the (M, N) -plane with the property that the zeros of

$$\bar{\chi}(\alpha_s, M, N) - N, \quad (3.4.14)$$

which form a curve in the plane, are exactly the kernels' curve.

Given $\chi(\alpha_s, M)$, we will call any $\bar{\chi}(\alpha_s, M, N)$ satisfying Eq. (3.4.11) an *off-shell extension* of $\chi(\alpha_s, M)$; of course, there is not a unique way to obtain such an off-shell extension, but there are infinite possibilities. The naive off-shell extension of χ is simply

$$\bar{\chi}(\alpha_s, M, N) = \chi(\alpha_s, M). \quad (3.4.15)$$

Relation (3.4.5) becomes simple from the point of view of off-shell kernels. Given an off-shell extensions of χ and χ_σ

$$\chi(\alpha_s, M) = \bar{\chi}(\alpha_s, M, \chi(\alpha_s, M)), \quad (3.4.16a)$$

$$\chi_\sigma(\alpha_s, M) = \bar{\chi}_\sigma(\alpha_s, M, \chi_\sigma(\alpha_s, M)). \quad (3.4.16b)$$

and putting these equations in Eq. (3.4.5a) we get

$$\bar{\chi}\left(\alpha_s, M + \frac{N}{2}, N\right) = \bar{\chi}_\sigma(\alpha_s, M, N). \quad (3.4.17)$$

Eq. (3.4.17) tells us that given the off-shell kernel, let's say, in asymmetric variables $\bar{\chi}$, we can find immediately the off-shell kernel $\bar{\chi}_\sigma$ in symmetric variables, and vice-versa, by a simple variable shift.

3.4.3 Improved resummation by symmetrization

We can use relation (3.4.5) and the symmetry of $\chi_\sigma(\alpha_s, M)$ under the exchange $M \rightarrow 1 - M$ to cure the instability of $\chi(\alpha_s, M)$ in $M = 1$. The strategy is the following:

- go to symmetric variables using Eq. (3.4.5);
- resum χ in the DL approximation, Eq. (3.3.16), to obtain χ_{DL} ;
- the resulting χ_{DL}^σ is not symmetric: symmetrize it, thereby resumming the $M = 1$ singularities;
- use again Eq. (3.4.5) with the symmetrized χ_{DL}^σ to go back to asymmetric variables, obtaining a kernel which we will call from now on χ_{SDL} (symmetrized double-leading).

The kernel χ_{SDL} obtained with the above procedure is not symmetric (because of the asymmetric choice of the ξ variable) but has a stable DL perturbative expansion. In particular, a minimum near $M = \frac{1}{2}$ is present to all perturbative orders: this is relevant for the running coupling resummation discussed in Sect. 3.5.

3.4.3.1 Practical realization: a toy example

Consider for simplicity the DL expansion Eq. (3.3.16) at LO:

$$\chi_{\text{DL}}(\alpha_s, M) = \alpha_s \chi_0(M) + \chi_s \left(\frac{\alpha_s}{M} \right) - \text{d.c.} \quad (3.4.18)$$

In this equation the χ_0 term is symmetric, while χ_s is not. Following the strategy described above, the next step for resummation consists in going to symmetric variables

$$\chi_{\text{DL}}^\sigma(\alpha_s, M) = \alpha_s \chi_0(M) + \chi_s^\sigma(\alpha_s, M) - \text{d.c.} \quad (3.4.19)$$

where here χ_0 is the same as before, since it was already symmetric at this order, and χ_s^σ is the dual of γ_σ at LO, Eq. (3.4.9). Being in symmetric variables, χ_s^σ should be symmetric, but it is not. A way to obtain χ_s^σ is the approach of Ref. [54], where symmetrization is obtained by defining first the naive off-shell extension of χ_s as

$$\bar{\chi}_s(\alpha_s, M, N) = \chi_s \left(\frac{\alpha_s}{M} \right), \quad (3.4.20)$$

then going to symmetric variables

$$\bar{\chi}_s^\sigma(\alpha_s, M, N) = \chi_s \left(\frac{\alpha_s}{M + N/2} \right), \quad (3.4.21)$$

now symmetrizing it as [54, 55]

$$\bar{\chi}_s^\sigma(\alpha_s, M, N) = \chi_s \left(\frac{\alpha_s}{M + N/2} \right) + \chi_s \left(\frac{\alpha_s}{1 - M + N/2} \right). \quad (3.4.22)$$

The symmetrization procedure, though somewhat arbitrary, satisfies the following constraints:

- the kernel obtained putting on-shell has to be symmetric for $M \leftrightarrow 1 - M$;
- in the $M < \frac{1}{2}$ region, at large N the dual kernel must match with the original LO anomalous dimension;
- no other singularities must be introduced.

However, there are still some bad features in the result: for example, momentum conservation is no longer satisfied. To solve such problem, an additional term [54]

$$\bar{\chi}_{\text{mom}}(N) = c_{\text{mom}} f_{\text{mom}}(N) \quad (3.4.23)$$

is added to $\bar{\chi}_s^\sigma$ to enforce momentum conservation, provided

$$f_{\text{mom}}(\infty) = 0, \quad f_{\text{mom}}(1) = 1, \quad (3.4.24)$$

where c_{mom} is a constant chosen in such a way that momentum conservation is preserved. Specific forms for f_{mom} can be

$$f_{\text{mom}}(N) = \frac{4^k N^k}{(N+1)^{2k}}, \quad \frac{2N^k}{N^{2k} + 1}, \quad k > 0, \quad (3.4.25)$$

which are in particular symmetric for the exchange $N \rightarrow 1/N$ and satisfy additionally

$$f_{\text{mom}}(0) = 0, \quad f'_{\text{mom}}(1) = 0. \quad (3.4.26)$$

In symmetric variables momentum conservation constraint requires

$$M = -\frac{1}{2} \quad \Rightarrow \quad N = 1 \quad (3.4.27)$$

that implies, from Eq. (3.4.22),

$$c_{\text{mom}} = 1 - \bar{\chi}_s^\sigma \left(\alpha_s, -\frac{1}{2}, 1 \right) = -\chi_s \left(\frac{\alpha_s}{2} \right). \quad (3.4.28)$$

With these ingredients at the hand, one can use

$$\bar{\chi}_s^\sigma(\alpha_s, M, N) = \chi_s \left(\frac{\alpha_s}{M + N/2} \right) + \chi_s \left(\frac{\alpha_s}{1 - M + N/2} \right) + \bar{\chi}_{\text{mom}}(N) \quad (3.4.29)$$

to compute $\chi_s^\sigma(\alpha_s, M)$.

Finally, one can add back χ_0 minus the double counting terms, which now should be considered both in $M = 0$ and $M = 1$ for symmetry. This subtraction breaks momentum conservation again, but a simple modification of c_{mom} can cure it.

At the end, one can go back to asymmetric variables; practically, the easier way to do this is to compute the two branches of a resummed $\gamma_\sigma(N)$ and then adding $N/2$ to obtain $\gamma_{\text{SDL}}(N)$, Eq. (3.4.9).

3.4.3.2 Practical realization: the approach of Ref. [54]

Even if the procedure described above seems to be satisfactory, there are still some problems with the other poles of the BFKL kernel, which spoil the matching at large N with the anomalous dimension.

To avoid this, in Ref. [54] an off-shell extension of χ_0 is also considered (see also Ref. [55]). This off-shell $\bar{\chi}_0$ is then added to $\bar{\chi}_s^\sigma$ (after subtracting double counting) and the resulting function is then put on-shell.³

Actually, the off-shell extension of χ_0 performed in Ref. [54] is not really an extension, since it does not lead to the original BFKL kernel when it is put on-shell; nevertheless, it is chosen in such a way that the relevant limits are respected. First, the collinear and anti-collinear parts of χ_0 are separated as

$$\chi_0(M) = \chi_0^L(M) + \chi_0^R(M), \quad (3.4.30)$$

where

$$\chi_0^L(M) = \frac{N_c}{\pi} [\psi(1) - \psi(M)], \quad (3.4.31)$$

$$\chi_0^R(M) = \chi_0^L(1 - M); \quad (3.4.32)$$

³Note that the sum of two off-shell kernel is *not* in general the off-shell kernel for the sum of the kernels.

then, χ_0^L is treated as χ_s before, i.e. the naive off-shell extension of χ_0^L is taken in asymmetric variables, then translated to symmetric variables and symmetrized, obtaining

$$\bar{\chi}_0^\sigma(M, N) = \frac{N_c}{\pi} \left[2\psi(1) - \psi\left(M + \frac{N}{2}\right) - \psi\left(1 - M + \frac{N}{2}\right) \right], \quad (3.4.33)$$

or, in asymmetric variables,

$$\bar{\chi}_0(M, N) = \frac{N_c}{\pi} [2\psi(1) - \psi(M) - \psi(1 - M + N)]. \quad (3.4.34)$$

However, since we don't want to spoil the identification at large N with the anomalous dimension, $\bar{\chi}_0(M, N)$ should vanish at large N . To accomplish this, in Ref. [54] a subleading term is added to $\bar{\chi}_0$ obtaining at the end

$$\bar{\chi}_0(M, N) = \frac{N_c}{\pi} [\psi(1) + \psi(1 + N) - \psi(M) - \psi(1 - M + N)], \quad (3.4.35)$$

which is safe at large N because $\psi(1 - M + N) - \psi(1 + N) \sim 1/N$.

Putting all together, we get (in symmetric variables)

$$\bar{\chi}_{\text{LO}}^\sigma(\alpha_s, M, N) = \bar{\chi}_s^\sigma(\alpha_s, M, N) + \alpha_s \tilde{\chi}_0^\sigma(M, N) + \chi_{\text{mom}}(\alpha_s, N), \quad (3.4.36)$$

where

$$\tilde{\chi}_0^\sigma(M, N) = \frac{N_c}{\pi} \left[\psi(1) + \psi(1 + N) - \psi\left(1 + M + \frac{N}{2}\right) - \psi\left(2 - M + \frac{N}{2}\right) \right] \quad (3.4.37)$$

has subtracted the collinear ($M + \frac{N}{2} = 0$) and anti-collinear ($1 - M + \frac{N}{2} = 0$) doubly counted poles, and the momentum conservation function has been reintroduced. The result of putting on-shell, back to DIS variables, is shown in Fig. 3.4 at LO. The symmetrized DL curve has a minimum, thanks to the fact that the asymptotic behaviour of the curve at large N (large χ) are given by the GLAP anomalous dimension. Then, the minimum is still there also at NLO: symmetrization stabilizes the DL expansion, as expected. The details of the NLO symmetrization are quite cumbersome, and we refer the Reader to App. C.4 or to Ref. [54] for further details.

3.5 Running coupling corrections to the BFKL equation

So far, we have supposed that the strong coupling α_s is fixed; now we want to study the effect of its running. We will find that the inclusion of running coupling effects changes dramatically the small- x behaviour of the anomalous dimension, making the running coupling resummation a crucial ingredient for small- x resummation.

The BFKL equation (3.2.2) has a kernel K which depends on the coupling α_s . If we let the coupling run, we can make several choices for its argument; the most natural ones are $\alpha_s(q^2)$ and $\alpha_s(k^2)$. In both cases, we have that under Mellin transform α_s becomes a differential operator, $\hat{\alpha}_s$, which is constructed by substituting

$$t \rightarrow -\frac{d}{dM} \quad (3.5.1)$$

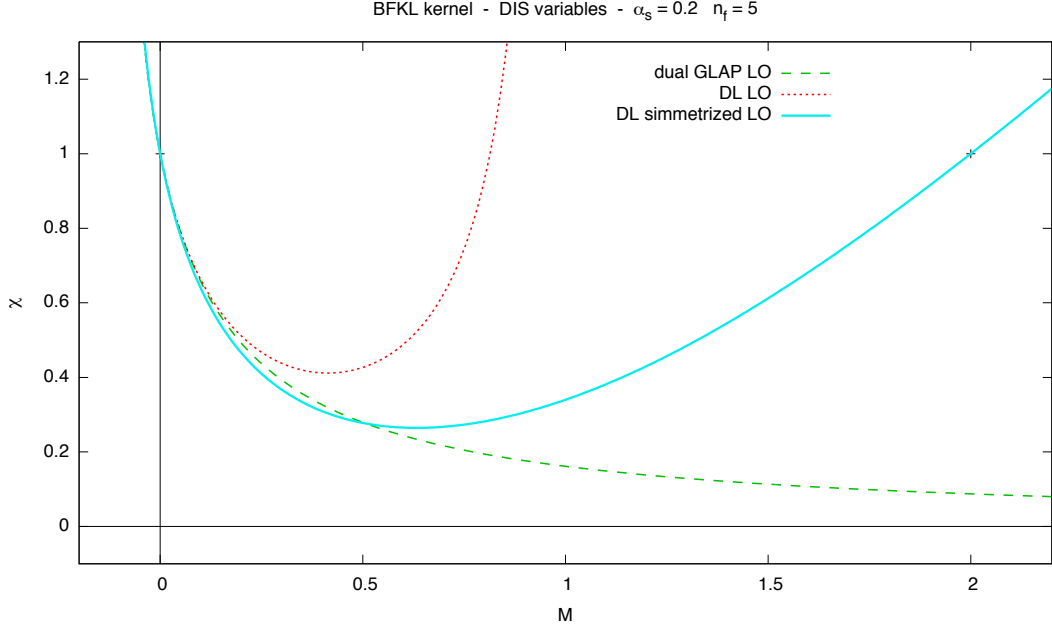


Figure 3.4. The simmetrized Double-Leading approximation at LO. Here we have used $\alpha_s = 0.2$ and $n_f = 5$.

in the explicit form of the running α_s . For example, at 1-loop,

$$\hat{\alpha}_s = \frac{\alpha_s}{1 - \alpha_s \beta_0 \frac{d}{dM}}, \quad (3.5.2)$$

where α_s is now the value of the strong coupling at a given fixed scale μ_0^2 . The difference in choosing the argument q^2 or k^2 in α_s is the resulting operator order. Consider the BFKL equation (3.2.2)

$$\frac{d}{d\xi} f(\xi, q^2) = \int_0^\infty \frac{dk^2}{k^2} \sum_{p=0}^\infty \alpha_s^{p+1}(\cdot) K_p\left(\frac{q^2}{k^2}\right) f(\xi, k^2), \quad (3.5.3)$$

where we have explicitly written the BFKL kernel as a power series in α_s , with argument of α_s not specified. If we choose as argument q^2 , the Mellin transform of the equation becomes

$$\frac{d}{d\xi} f(\xi, M) = \sum_{p=0}^\infty \hat{\alpha}_s^{p+1} \chi_p(M) f(\xi, M), \quad (3.5.4)$$

where $\hat{\alpha}_s$ acts on everything on the right, while choosing k^2 as argument we get

$$\frac{d}{d\xi} f(\xi, M) = \sum_{p=0}^\infty \chi_p(M) \hat{\alpha}_s^{p+1} f(\xi, M), \quad (3.5.5)$$

where now $\hat{\alpha}_s$ acts only on the PDF.

A unique scale choice for α_s inevitably breaks the symmetry of the BFKL equation under the exchange $q^2 \leftrightarrow k^2$, unless we use $\alpha_s(\sqrt{q^2 k^2})$, which however complicates

somewhat the treatment. The most convenient choice is then to compute α_s at the scale q^2 for the collinear part and k^2 for the anti-collinear part:

$$K\left(\alpha_s, \frac{q^2}{k^2}\right) \rightarrow \sum_{p=0}^{\infty} \left[\alpha_s^{p+1}(q^2) K_p^L\left(\frac{q^2}{k^2}\right) + \alpha_s^{p+1}(k^2) K_p^R\left(\frac{q^2}{k^2}\right) \right]. \quad (3.5.6)$$

If symmetric variables are used, the collinear and anti-collinear contributions to the kernel satisfy, order by order, the symmetry relation

$$\frac{1}{q^2} K_p^L\left(\frac{q^2}{k^2}\right) = \frac{1}{k^2} K_p^R\left(\frac{k^2}{q^2}\right) \quad (3.5.7)$$

which is the underlying reason for the symmetry of Eq. (3.4.1). This means that this choice restores the symmetry $q^2 \leftrightarrow k^2$ of the BFKL equation. The Mellin transform of the BFKL kernel with this scale choice is then

$$\chi(\hat{\alpha}_s, M) = \sum_{p=0}^{\infty} [\hat{\alpha}_s^{p+1} \chi_p^L(M) + \chi_p^R(M) \hat{\alpha}_s^{p+1}] \quad (3.5.8)$$

where

$$\chi_p^R(M) = \chi_p^L(1 - M) \quad (3.5.9)$$

and is intended that $\chi(\hat{\alpha}_s, M)$ is an operator itself, and $\hat{\alpha}_s$ in it will act on everything on the right, specifically on the PDF in the BFKL equation. For example, the LO contribution is given by Eq. (3.4.31),

$$\chi_0^L(M) = \frac{N_c}{\pi} [\psi(1) - \psi(M)], \quad (3.5.10)$$

while the NLO will be given in App. C.4.1.

Note that, once we have built the running-coupling kernel Eq. (3.5.8), we can reshuffle the position of $\hat{\alpha}_s$ having care of supplying each switch with the corresponding commutator. If we use the 1-loop beta function Eq. (3.5.2), we get easily

$$[\hat{\alpha}_s^{-1}, M] = -\beta_0. \quad (3.5.11)$$

From this we can compute

$$[\hat{\alpha}_s, M] = \hat{\alpha}_s M - \hat{\alpha}_s \hat{\alpha}_s^{-1} M \hat{\alpha}_s = \hat{\alpha}_s M - \hat{\alpha}_s M \hat{\alpha}_s^{-1} \hat{\alpha}_s - \hat{\alpha}_s [\hat{\alpha}_s^{-1}, M] \hat{\alpha}_s = \beta_0 \hat{\alpha}_s^2. \quad (3.5.12)$$

The commutator of $\hat{\alpha}_s$ (or a function of it) with a function of M can be then built *algebraically* starting from the “fundamental” commutators Eqs. (3.5.11), (3.5.12).

In general, it is quite easy to compute the commutators of $\hat{\alpha}_s^{-1}$ with a function of M , if α_s runs at 1-loop. Indeed

$$[\hat{\alpha}_s^{-1}, g(M)] = -\beta_0 g'(M). \quad (3.5.13)$$

From this, with the same computation as in (3.5.12), we get

$$[\hat{\alpha}_s, g(M)] = \hat{\alpha}_s \beta_0 g'(M) \hat{\alpha}_s. \quad (3.5.14)$$

If we want the $\hat{\alpha}_s$ operator to be on the left we can recursively commute to obtain

$$[\hat{\alpha}_s, g(M)] = \sum_{k=1}^{\infty} (-)^{k+1} \beta_0^k \hat{\alpha}_s^{k+1} g^{(k)}(M). \quad (3.5.15)$$

Now, suppose we want to have all the powers of $\hat{\alpha}_s$ to the left (as we will need it later). Then, at LO, one obtains simply

$$\chi(\hat{\alpha}_s, M) = \hat{\alpha}_s [\chi_0^L(M) + \chi_0^R(M)] + \mathcal{O}(\hat{\alpha}_s^2) \quad (3.5.16)$$

because the commutator Eq. (3.5.15) starts at order $\hat{\alpha}_s^2$. At NLO this commutator gives an effect: indeed we have

$$\chi(\hat{\alpha}_s, M) = \hat{\alpha}_s [\chi_0^L(M) + \chi_0^R(M)] + \hat{\alpha}_s^2 [\chi_1^L(M) + \chi_1^R(M) - \beta_0 \partial_M \chi_0^R(M)] + \mathcal{O}(\hat{\alpha}_s^3) \quad (3.5.17)$$

where

$$\partial_M \chi_0^R(M) = \frac{N_c}{\pi} \psi_1(1-M). \quad (3.5.18)$$

3.5.1 Resummation of running coupling effects

Perturbative inclusion of running coupling effect does not lead to stable results [56], since it produces poles in the BFKL kernel at $M = 1/2$, where it should have a stationary point (in symmetric variables). Then, the leading small- N singularity, which determines the small- x behaviour of the dual anomalous dimension, changes nature whenever the running coupling effects are included at some fixed perturbative order. For this reason, running coupling effects must be resummed to all orders in α_s to get a stable small- N singularity. To do this, let's take the N -Mellin transform of the running-coupling BFKL equation,

$$Nf(N, M) = \chi(\hat{\alpha}_s, M)f(N, M) + \tilde{F}_0(M), \quad (3.5.19)$$

which is the straightforward running-coupling extension of Eq. (3.3.1b). Because of the presence of the operator $\hat{\alpha}_s$, this is a differential equation in M : the solution of this equation incorporates running-coupling effects to all orders, and from this solution we can hence compute a resummed anomalous dimension with full running-coupling dependence.

In Ref. [56] it is proven that a running-coupling resummed anomalous dimension is completely characterized by the inhomogeneous solution of Eq. (3.5.19); nevertheless, up to power suppressed terms, the inhomogeneous solution can be written in the same form of the homogeneous solution, with an appropriate boundary condition $f(N, M_0)$, which however is irrelevant (it cancels out) in the computation of the anomalous dimension. Then from now on we will concentrate on the homogeneous equation

$$Nf(N, M) = \chi(\hat{\alpha}_s, M)f(N, M). \quad (3.5.20)$$

Now, suppose we manipulate $\chi(\alpha_s, M)$ in such a way that the powers of $\hat{\alpha}_s$ are all on the left, using repeatedly the commutator Eq. (3.5.14); if the resulting dependence on

$\hat{\alpha}_s$ is linear we can write⁴

$$\chi(\alpha_s, M) = \hat{\alpha}_s \varphi(M) \quad (3.5.21)$$

and then, for 1-loop beta function,

$$\left(1 - \beta_0 \alpha_s \frac{d}{dM}\right) N f(N, M) = \alpha_s \varphi(M) f(N, M). \quad (3.5.22)$$

The solution of this equation is

$$f(N, M) = f(N, M_0) \exp \int_{M_0}^M dM' \frac{N - \alpha_s \varphi(M')}{N \beta_0 \alpha_s}. \quad (3.5.23)$$

The anomalous dimension which contains resummed running-coupling effects can be found by taking the logarithmic derivative with respect to t of the inverse M -Mellin of the solution Eq. (3.5.23):

$$\gamma_{\text{rc}}(\alpha_s(t), N) = \frac{d}{dt} \log \int_{c-i\infty}^{c+i\infty} \frac{dM}{2\pi i} e^{Mt} \exp \int_{M_0}^M dM' \frac{N - \alpha_s \varphi(M')}{N \beta_0 \alpha_s} \quad (3.5.24)$$

where c must be to the right of all the singularity of the integral. Of course, the ability of computing the integrals depends on the explicit form of $\varphi(M)$; in the next subsection we will show that in the case in which the kernel is quadratic it is possible to find an analytic solution.

Another way to find a general solution for the anomalous dimension can be obtained by taking the N -Mellin transform of Eq. (3.2.2) with running coupling

$$N f(N, t) = \alpha_s(t) \int^t dt' K_\varphi(e^{t-t'}) f(N, t'), \quad (3.5.25)$$

where K_φ is the unintegrated kernel corresponding to φ , and it is typically a distribution. In some cases we may be able to separate the distributional part of K_φ in terms of δ functions and its derivatives, and a finite part:

$$K_\varphi(e^t) = \sum_j k_j \delta^{(j)}(t) + K_\varphi^{\text{fin}}(e^t); \quad (3.5.26)$$

after explicit integration of the δ 's we end up with a integro-differential equation, that we can derive with respect to t to obtain a genuine differential equation,

$$\sum_j (-)^j k_j f^{(j+1)}(N, t) - \frac{N}{\alpha_s(t)} f'(N, t) + \left[K_\varphi^{\text{fin}}(1) - N \beta_0 \right] f(N, t) = 0, \quad (3.5.27)$$

where we have explicitly used the 1-loop β -function and the derivatives are intended with respect to t . This equation may be eventually easier to solve than the inverse Mellin transform in Eq. (3.5.24).

⁴Note that this never happens exactly. Indeed, even at LO, the anti-collinear part has $\hat{\alpha}_s$ to the right, and the reshuffling needed to bring it to the left produces $\mathcal{O}(\hat{\alpha}_s^2)$ terms. Nevertheless, being $\mathcal{O}(\hat{\alpha}_s^2)$, they should be better included in the NLO kernel: hence, up to NLO correction, the LO kernel can be written in the form of Eq. (3.5.21) with $\varphi(M) = \chi_0(M)$.

3.5.2 Quadratic approximation to the kernel

In Ref. [56] it is shown that the small- x behaviour of the running-coupling resummed splitting-functions is determined by the behaviour of the kernel χ in Eq. (3.5.19) around its minimum (which is at $M = 1/2$ in symmetric variables). This result can be simply obtained by means of a saddle point approximation [57] to the M -Mellin inversion integral in Eq. (3.5.24). The saddle point M_s is given by

$$\alpha_s(t)\varphi(M_s) = N; \quad (3.5.28)$$

from this equation it is evident that the region of small N is determined by the smaller values of φ , i.e. by its minimum.

This is pretty useful, because when the kernel is substituted by its quadratic approximation [58]

$$\chi(\alpha_s, M) \rightarrow \chi_q(\alpha_s, M) = c(\alpha_s) + \frac{1}{2}\kappa(\alpha_s) \left(M - \frac{1}{2}\right)^2 \quad (3.5.29)$$

we are able to analytically find a resummed anomalous dimension, provided the α_s dependence of χ (or of the coefficients c and κ) belongs to the following two cases:

$$\text{Airy:} \quad \chi(\hat{\alpha}_s, M) \simeq \hat{\alpha}_s \chi_0(\alpha_s, M) \quad (3.5.30)$$

$$\text{Bateman:} \quad \chi(\hat{\alpha}_s, M) \simeq \chi(\alpha_s, M) + (\hat{\alpha}_s - \alpha_s) \partial_{\alpha_s} \chi(\alpha_s, M) \quad (3.5.31)$$

where $\chi_0(\alpha_s, M)$ may depend on α_s and is not in general the LO kernel $\chi_0(M)$. The coefficients $c(\hat{\alpha}_s)$ and $\kappa(\hat{\alpha}_s)$ satisfy the same expansion. The names Airy [56] and Bateman [54] are due to the fact that in the respective cases the solution is expressed in terms of Airy or Bateman functions (see App. E.3). If the kernel is linear in α_s (as the LO kernel), the Airy solution coincides with the Bateman one; otherwise, if the α_s dependence of χ is non-trivial, the approximation that brings to the Airy solution is not good, and the Bateman solution provides a better approximation.

3.5.2.1 Airy anomalous dimension

Note that a quadratic kernel χ as in Eq. (3.5.29) corresponds, in the case of Airy approximation, to a unintegrated kernel K of the form

$$K(\alpha_s, e^t) = \alpha_s(t) \left[\left(c_0 + \frac{\kappa_0}{8} \right) \delta(t) - \frac{\kappa_0}{2} \delta'(t) + \frac{\kappa_0}{2} \delta''(t) \right]. \quad (3.5.32)$$

Putting this in Eq. (3.5.25) we get

$$f'' - f' = \frac{2}{\kappa_0} \left[\frac{N}{\alpha_s(t)} - c_0 - \frac{\kappa_0}{8} \right] f \quad (3.5.33)$$

where primes denote derivatives with respect to t . Writing

$$f(N, t) \propto g(N, t) \exp \frac{1}{2\beta_0 \alpha_s(t)} \quad (3.5.34)$$

we get

$$g'' = \frac{2}{\kappa_0} \left[\frac{N}{\alpha_s(t)} - c_0 \right] g. \quad (3.5.35)$$

We recognize in this equation the equation for the Airy function,

$$\text{Ai}''(z) - z \text{Ai}(z) = 0, \quad (3.5.36)$$

provided we identify z with

$$z(\alpha_s(t), N) = \left(\frac{2\beta_0 N}{\kappa_0} \right)^{1/3} \frac{1}{\beta_0} \left[\frac{1}{\alpha_s(t)} - \frac{c_0}{N} \right]. \quad (3.5.37)$$

Then, we have found

$$f(N, t) \propto \text{Ai}(z(\alpha_s(t), N)) \exp \frac{1}{2\beta_0 \alpha_s(t)} \quad (3.5.38)$$

from which we immediately compute the anomalous dimension

$$\gamma_A(\alpha_s(t), N) = \frac{1}{2} + \left(\frac{2\beta_0 N}{\kappa_0} \right)^{1/3} \frac{\text{Ai}'(z(\alpha_s(t), N))}{\text{Ai}(z(\alpha_s(t), N))} \quad (3.5.39)$$

which we will call the *Airy anomalous dimension*. The same result can be found by putting the quadratic kernel Eq. (3.5.29) into Eq. (3.5.24), where instead of solving a differential equation you have to compute an inverse Mellin transformation [56].

For comparison with the singular expansion of the fixed-coupling anomalous dimension, we expand Eq. (3.5.39) in powers of α_s at fixed α_s/N and get

$$\gamma_A(\alpha_s, N) = \frac{1}{2} - \sqrt{\frac{N/\alpha_s - c_0}{\kappa_0/2}} - \frac{\beta_0 \alpha_s}{4(1 - c_0 \alpha_s/N)} + \dots \quad (3.5.40)$$

where the dots indicate terms of order α_s^2 at fixed α_s/N . All these terms are divergent in $N = \alpha_s c_0$, but the sum is not; it is instead divergent when the Airy function in the denominator of Eq. (3.5.39) goes to zero, at $z(\alpha_s(t), N) = -2.33811$ (see App. E.3.1).

3.5.2.2 Bateman anomalous dimension

As already mentioned, the Bateman approximation Eq.(3.5.31) is much better than the Airy one, Eq. (3.5.30). Indeed in this approximation the whole sequence of leading-log contributions to α_s is correctly included in the solution [54].

Defining

$$\bar{c}(\alpha_s) = c(\alpha_s) - \alpha_s c'(\alpha_s) \quad (3.5.41)$$

$$\bar{\kappa}(\alpha_s) = \kappa(\alpha_s) - \alpha_s \kappa'(\alpha_s) \quad (3.5.42)$$

we can write, following Ref. [54], the running-coupling BFKL equation Eq. (3.5.19) in the Bateman approximation as

$$\begin{aligned} & \left[N - \bar{c}(\alpha_s) - \frac{1}{2} \bar{\kappa}(\alpha_s) \left(M - \frac{1}{2} \right)^2 \right] f(N, M) \\ & = \hat{\alpha}_s \left[c'(\alpha_s) + \frac{1}{2} \kappa'(\alpha_s) \left(M - \frac{1}{2} \right)^2 \right] f(N, M) + \tilde{F}_0(M). \end{aligned} \quad (3.5.43)$$

The solution to this equation can be found with techniques similar to the Airy case, and we refer the Reader to Ref. [54] for further details. The result can be written in terms of Bateman functions $K_\nu(z)$ (see App. E.3) and reads

$$\gamma_B(\alpha_s(t), N) = \frac{1}{2} - \beta_0 \bar{\alpha}_s + A(\alpha_s, N) \frac{K'_{B(\alpha_s, N)}\left(\frac{A(\alpha_s, N)}{\beta_0 \bar{\alpha}_s}\right)}{K_{B(\alpha_s, N)}\left(\frac{A(\alpha_s, N)}{\beta_0 \bar{\alpha}_s}\right)} \quad (3.5.44)$$

where

$$\frac{1}{\bar{\alpha}_s} = \frac{1}{\alpha_s} + \frac{\kappa'(\alpha_s)}{\bar{\kappa}(\alpha_s)} \quad (3.5.45)$$

$$A(\alpha_s, N) = \sqrt{\frac{N - \bar{c}(\alpha_s)}{\frac{1}{2}\bar{\kappa}(\alpha_s)}} \quad (3.5.46)$$

$$B(\alpha_s, N) = \left(\frac{c'(\alpha_s)}{N - \bar{c}(\alpha_s)} + \frac{\kappa'(\alpha_s)}{\bar{\kappa}(\alpha_s)} \right) \frac{A(\alpha_s, N)}{\beta_0} \quad (3.5.47)$$

We will call this solution the *Bateman anomalous dimension*.

Expanding Eq. (3.5.44) in powers of α_s at small N we get

$$\gamma_B(\alpha_s, N) = \gamma_s^B(\alpha_s, N) + \gamma_{ss}^B(\alpha_s, N) + \dots \quad (3.5.48)$$

with

$$\gamma_s^B(\alpha_s, N) = \frac{1}{2} - \sqrt{\frac{N - c(\alpha_s)}{\frac{1}{2}\kappa(\alpha_s)}} \quad (3.5.49)$$

$$\gamma_{ss}^B(\alpha_s, N) = \gamma_{ss,0}^B(\alpha_s) + \frac{1}{4}\alpha_s^2\beta_0 \frac{c'(\alpha_s)}{c(\alpha_s) - N} \quad (3.5.50)$$

$$\gamma_{ss,0}^B(\alpha_s) = -\beta_0\alpha_s + \frac{3}{4}\alpha_s^2\beta_0 \frac{\kappa'(\alpha_s)}{\kappa(\alpha_s)}. \quad (3.5.51)$$

Note that now, after running coupling resummation, the anomalous dimension behaves as a pole at small N , the position of the pole being determined by the rightmost zero of the Bateman function in the denominator of Eq. (3.5.44). This behaviour is compatible with the observations.

3.5.3 On the minimum

Since the resummation of running coupling effects depends only on the characteristics of the minimum of the symmetric DL BFKL kernel, it is useful to make some comments about its properties.

In symmetric variables, the minimum is always placed in $M = 1/2$, because of the symmetry $\chi_\sigma(\alpha_s, M) = \chi_\sigma(\alpha_s, 1 - M)$. For this reason, the parameter c is easily computed as

$$c(\alpha_s) = \chi_\sigma\left(\alpha_s, \frac{1}{2}\right). \quad (3.5.52)$$

In asymmetric variables, $M \rightarrow M + N/2$, and hence the position of the minimum is

$$M_{\min} = \frac{1}{2} + \frac{c(\alpha_s)}{2}, \quad (3.5.53)$$

and the value at the minimum is the same as in symmetric variables

$$\chi(\alpha_s, M_{\min}) = \chi_\sigma \left(\alpha_s, \frac{1}{2} \right) \equiv c(\alpha_s). \quad (3.5.54)$$

It can be easily shown that also the curvature of the minimum is the same in symmetric and asymmetric variables:

$$\kappa(\alpha_s) = \chi_\sigma'' \left(\alpha_s, \frac{1}{2} \right) = \chi''(\alpha_s, M_{\min}). \quad (3.5.55)$$

In terms of the off-shell kernel $\bar{\chi}_\sigma(\alpha_s, M, N)$ in symmetric variables, the curvature can be written as

$$\kappa(\alpha_s) = \frac{\partial_M^2 \bar{\chi}_\sigma}{1 - \partial_N \bar{\chi}_\sigma} \Big|_{M=\frac{1}{2}, N=c} \quad (3.5.56)$$

as one can easily find by computing the second derivative of the on-shell relation $\chi_\sigma(\alpha_s, M) = \bar{\chi}_\sigma(\alpha_s, M, \chi_\sigma(\alpha_s, M))$,

$$\partial_M^2 \chi_\sigma = \partial_M^2 \bar{\chi}_\sigma + \partial_N \bar{\chi}_\sigma \partial_M^2 \chi_\sigma + \partial_M \chi_\sigma [2\partial_N \partial_M \bar{\chi}_\sigma + \partial_N^2 \bar{\chi}_\sigma \partial_M \chi_\sigma], \quad (3.5.57)$$

where $N = \chi_\sigma$, and at the minimum $\partial_M \chi_\sigma = 0$. The α_s dependence of c can be found in the same way: deriving the duality relation with respect to α_s we get

$$\frac{\partial}{\partial \alpha_s} \chi_\sigma(\alpha_s, M) = \frac{\partial_{\alpha_s} \bar{\chi}_\sigma}{1 - \partial_N \bar{\chi}_\sigma} \Big|_{N=c} \quad (3.5.58)$$

and hence

$$c'(\alpha_s) = \frac{\partial_{\alpha_s} \bar{\chi}_\sigma}{1 - \partial_N \bar{\chi}_\sigma} \Big|_{M=\frac{1}{2}, N=c}. \quad (3.5.59)$$

For κ , one can directly derive Eq. (3.5.56), keeping in mind that c depends on α_s , and obtain

$$\kappa'(\alpha_s) = \frac{\partial_{\alpha_s} \partial_M^2 \bar{\chi}_\sigma + c' \partial_N \partial_M^2 \bar{\chi}_\sigma + \kappa [c' \partial_N^2 \bar{\chi}_\sigma + \partial_{\alpha_s} \partial_N \bar{\chi}_\sigma]}{1 - \partial_N \bar{\chi}_\sigma} \Big|_{M=\frac{1}{2}, N=c}. \quad (3.5.60)$$

Note that in principle all these derivatives can be computed analytically; the more tricky one is the derivative of the χ_s part contained in the off-shell kernel, that can be obtained by deriving duality relation

$$\frac{\partial}{\partial \alpha_s} \chi_s \left(\frac{\alpha_s}{M} \right) = -\frac{M/\alpha_s}{\alpha_s \gamma_0'(\chi_s(\alpha_s/M))}. \quad (3.5.61)$$

These relation are very useful for easily compute derivatives in a numerical code.

3.6 Resummed anomalous dimensions

In the above Sections, we have introduced all the ingredients to obtain stable resummed anomalous dimensions: we summarize the whole procedure here.

- The first crucial ingredient is the duality relation Eq. (3.3.7): strictly speaking, it is valid for fixed coupling, but its extension to the running coupling level (which amounts to the replacement of α_s with $\hat{\alpha}_s$) has been proved to be valid to all orders in Ref. [59]. The duality relates the BFKL kernel to the anomalous dimension, thereby providing a way to resum one of them in terms of the other. This procedure alone gives the Double-Leading approximation introduced in Sect. 3.3.2, which is however unstable for perturbative corrections.
- The way to stabilize the DL expansion is to exploit the intrinsic symmetry of the BFKL kernel, which is however valid for a choice of variables which is not the usual one in DIS. Then, in order to be able to take the advantage of such symmetry we move to symmetric variables, changing also the anomalous dimension via Eq. (3.4.9), and we will get back again to asymmetric variables only at the end. With the help of the off-shell kernel, we symmetrize the DL result, to get a stable perturbative expansion.
- The last ingredient is the resummation of running coupling effects. It produces an anomalous dimension which now has the correct resummed small- N behaviour, which is completely determined by the value and the curvature at the minimum (and their α_s dependence) of the symmetrized DL BFKL kernel. Then, by matching with the symmetrized DL result, and going back to asymmetric variables, we finally get our resummed anomalous dimension.

The result of all this machinery can then be summarized in the following expression,

$$\gamma_{\text{res}}(\alpha_s, N) = \gamma_B(\alpha_s, N) + \gamma_{\text{DL}}^\sigma(\alpha_s, N) - \gamma_{B,s}(\alpha_s, N) - \gamma_{B,ss,0}(\alpha_s) + \frac{N}{2} + \gamma_{\text{mom}}(N), \quad (3.6.1)$$

where:

- $\gamma_B(\alpha_s, N)$ is the Bateman anomalous dimension: it resums running coupling effects and is accurate at small N , while at large N is completely arbitrary;
- $\gamma_{\text{DL}}^\sigma(\alpha_s, N)$ is the symmetrized DL anomalous dimension obtained by solving

$$\bar{\chi}_{\text{DL}}^\sigma(\alpha_s, \gamma_{\text{DL}}^\sigma(\alpha_s, N), N) = N \quad (3.6.2)$$

in symmetric variables: it has the correct large- N behaviour but has a spurious square-root branch-cut at small N ;

- $\gamma_{B,s}(\alpha_s, N)$ subtracts double counting contributions between the two previous contributions, thereby removing the branch-cut in $\gamma_{\text{DL}}^\sigma$ and a part of the spurious large- N behaviour of γ_B ;
- $\gamma_{B,ss,0}(\alpha_s)$ removes the remaining spurious behaviour (a constant) of γ_B ;
- $N/2$ switches back to DIS (asymmetric) variables;
- $\gamma_{\text{mom}}(N) = -\bar{\chi}_{\text{mom}}(N)$ restores momentum conservation (spoiled by running coupling resummation); in particular, since by construction $\gamma_{\text{DL}}^\sigma(\alpha_s, N)$ preserves momentum conservation, here c_{mom} is given by

$$c_{\text{mom}} = \gamma_B(\alpha_s, 1) - \gamma_{B,s}(\alpha_s, 1) - \gamma_{B,ss,0}(\alpha_s). \quad (3.6.3)$$

Actually this scheme is, strictly speaking, valid only at LO at $n_f = 0$.

At NLO there is a mismatch between the parameters in the Bateman and DL pieces, and a supplementary γ_{match} is needed in order to have the correct cancellation of the square-root branch-cut and of the spurious large- N behaviour, see Ref. [54] for more details. Since there are many tricky aspects at NLO which are irrelevant for the discussion, we don't show them here but we collect the results in App. C.4.

Already at LO, when $n_f \neq 0$ some care is needed to avoid an unphysical growth in x -space when Mellin-inverting the anomalous dimension matrix rotated back to the physical basis. We discuss this now.

3.6.1 The case $n_f \neq 0$

The (fixed order) eigenvalues of the anomalous dimension matrix have a branch-cut due to the square-root of the solution Eq. (1.3.19) of the secular equation. This branch-cut is unphysical and indeed is not present in the matrix element of the anomalous dimension matrix in the physical basis.

However, during the resummation procedure, we modify the largest eigenvalue, and typically the cancellation of the branch-cut going back to the physical basis does no longer take place. This is not acceptable because the inverse Mellin of the branch-cut has a spurious huge growth at small x . A simple way to preserve the branch-cut cancellation is to build a

$$\Delta\gamma_{\text{res}} = \gamma_{\text{res}} - \gamma_{\text{fix}} \quad (3.6.4)$$

free of branch-cut, that is to say that the branch-cut in γ_{res} has to be the same of that appearing in the fixed-order anomalous dimension.⁵ However, when $n_f \neq 0$, the function $\Delta\gamma_{\text{res}}$ built as in Eq. (3.6.1) has a cut, inherited from $\gamma_{\text{DL}}^\sigma$.

In [10] the difference between $\Delta\gamma_{\text{res}}$ at a given n_f (which has the cut) and the same computed at $n_f = 0$ (which is free of cut) is substituted with a rational approximation (hence, free of cut); however, increasing the order of the approximation, some oscillations due to the re-appearance of the cut show up, making this procedure unstable.

A better solution is to use in the computation of $\gamma_{\text{DL}}^\sigma$ a fake fixed-order γ_{fix} , which should be accurate at small N but can be arbitrary at large N . In this way $\Delta\gamma_{\text{res}}$ is still good, since at small N it is accurate, and at large N it goes to zero whatever γ_{fix} we use. Moreover, provided γ_{fix} is free of cut, the $\Delta\gamma_{\text{res}}$ we get is free of cut, as required. The easiest way to choose the fake γ_{fix} is to use the complete $n_f = 0$ part plus the leading n_f dependent pieces at small N . By calling this fake function $\tilde{\gamma}_{\text{fix}}$, we have

$$\tilde{\gamma}_{\text{fix}}(\alpha_s, N) = \alpha_s \gamma_0(N)|_{n_f=0} + \alpha_s \left[\alpha_s \gamma_1(N)|_{n_f=0} + c_{10}n_f + c_{11}n_f \frac{\alpha_s}{N} \right] + \text{NNLO}, \quad (3.6.5)$$

where the coefficients

$$c_{10} = \frac{2C_F/C_A - 1}{6\pi}, \quad c_{11} = \frac{26C_F - 23C_A}{36\pi^2} \quad (3.6.6)$$

⁵Actually this constraint is not sufficient to completely cancel the branch-cut; in particular, the gq component of the anomalous dimension would still have the cut. We will see in Sect. 3.6.3 that full cancellation can be still achieved with a minimal modification that is subleading in both α_s and α_s/N expansions.

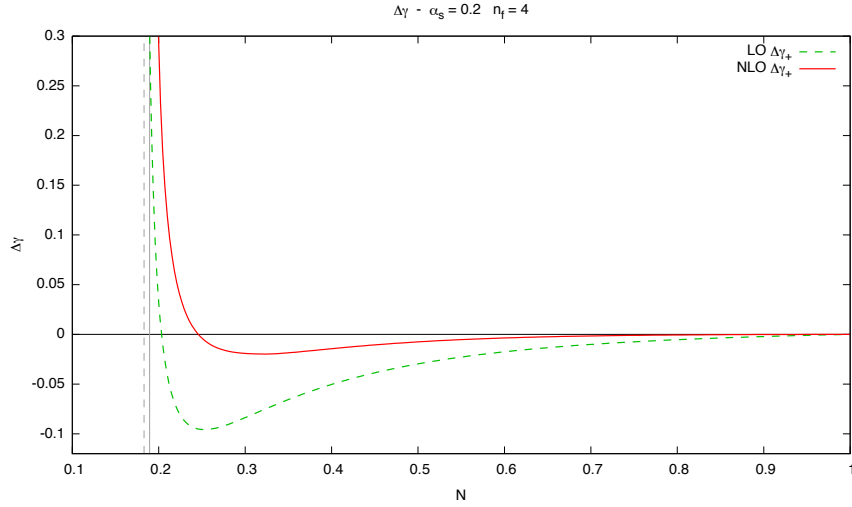


Figure 3.5. $\Delta\gamma_+(\alpha_s, N)$ for $\alpha_s = 0.2$ and $n_f = 4$ at LO and NLO. The Bateman pole position is shown at LO and NLO as well.

can be read from Eq. (1.3.37). Note that at NLO $\tilde{\gamma}_{\text{fix}}$ no longer preserves momentum conservation.

It's a matter of choice if computing the parameters of the Bateman anomalous dimension γ_B from the $\gamma_{\text{DL}}^\sigma$ made of the fake γ_{fix} or of the real one; the difference is subleading. However, since the small- x behaviour of the splitting function is given by the Bateman contribution, one may want to put in γ_B the most accurate parameter as possible. In this way, however, $\gamma_{B,s}$ no longer cancels the small- N branch-cut of $\gamma_{\text{DL}}^\sigma$, because there is a mismatch between the parameters. This mismatch can be cured by a γ_{match} like that used at NLO.

The result for the resummed anomalous dimension at LO and NLO is shown in Fig. 3.5. The Bateman pole is pushed to a somewhat larger value at NLO. The small- N rise is concentrated in the region very close to the Bateman pole. A negative dip dominates instead the intermediate region: this dip is softer in the NLO case.

3.6.2 Resummation of quark anomalous dimensions

At NLL, also the quark anomalous dimensions need to be resummed. Such resummation can be expressed in terms of the resummation of the gluon anomalous dimension [45]. In Ref. [10], the running coupling effects are also taken into account: the (NLL) singular contributions are then given by

$$\gamma_{qq}^{ss}(\alpha_s, N) = h_{qq}([\gamma_s(\alpha_s/N)]) \quad (3.6.7)$$

where h_{qq} is a function defined by its series expansion

$$h_{qq}(M) = \sum_{k=0}^{\infty} h_{qq,k} M^k \quad (3.6.8)$$

and the square brackets mean that each power in the series must be substituted by

$$[\gamma^k] = \left(\frac{\dot{\gamma}}{\gamma}\right)^k \frac{\Gamma(\gamma^2/\dot{\gamma} + k)}{\Gamma(\gamma^2/\dot{\gamma})} = \left(\frac{\dot{\gamma}}{\gamma}\right)^k \left(\frac{\gamma^2}{\dot{\gamma}}\right)_k, \quad (3.6.9)$$

where $(a)_k = \Gamma(a+k)/\Gamma(a)$ is the Pochhammer symbol. However, the series is divergent [10], and then its resummation is needed to get a meaningful result. However, the coefficients $h_{gg,k}$ can be computed only perturbatively, and it is hard to work many of them out. For more details on how to perform such resummation, see App. C.4.3.

The resummed gg anomalous dimension can be written as

$$\gamma_{gg}^{\text{res}}(\alpha_s, N) = \gamma_{gg}^{\text{NLO}}(\alpha_s, N) + \Delta\gamma_{gg}^{\text{res}}(\alpha_s, N) \quad (3.6.10)$$

and has to satisfy the limits

$$\begin{cases} \gamma_{gg}^{\text{res}}(\alpha_s, N) \sim \gamma_{gg}^{\text{NLO}}(\alpha_s, N) & \text{as } N \rightarrow \infty \text{ or } \alpha_s \rightarrow 0 \\ \gamma_{gg}^{\text{res}}(\alpha_s, N) \sim \alpha_s \gamma_{gg}^{\text{ss}}(\alpha_s, N) & \text{as } N \rightarrow 0 \end{cases} \quad (3.6.11)$$

which translate into analogous limits for $\Delta\gamma_{gg}^{\text{res}}(\alpha_s, N)$. These limits are trivially satisfied if we use as argument of h_{gg} the function γ_s :

$$\Delta\gamma_{gg}^{\text{res}}(\alpha_s, N) = \alpha_s h_{gg}([\gamma_s(\alpha_s/N)]) - (\text{small-}x)_{gg}^{\text{NLO}}, \quad (3.6.12)$$

where the subtracted terms are the small- x terms which are already present in the NLO contribution of Eq. (3.6.10), i.e.

$$(\text{small-}x)_{gg}^{\text{NLO}} = \alpha_s \frac{n_f}{3\pi} \left[1 + \frac{5 C_A \alpha_s}{3 \pi N} \right]. \quad (3.6.13)$$

However, this expression inherits the branch-cut of γ_s (which is the naive dual of χ_0), and this would give rise to a spurious small- x growth. To circumvent this, in Ref. [10] γ_s is substituted by the full NLO⁶ resummed anomalous dimension $\gamma_+^{\text{res, NLO}}$, which however introduces also some spurious large- x terms which would spoil the limits in Eq. (3.6.11). Then the expression in Ref. [10] is

$$\begin{aligned} \Delta\gamma_{\text{res}}^{gg}(\alpha_s, N) = \alpha_s \left[h_{gg} \left(\left[\gamma_+^{\text{res, NLO}}(\alpha_s, N) \right] \right) - h_{gg} \left(\left[\gamma_+^{\text{NLO}}(\alpha_s, N) - (\text{small-}x)_+^{\text{NLO}} \right] \right) \right] \\ - (\text{small-}x)_{gg}^{\text{NLO}} + \alpha_s h_{gg}(0), \end{aligned} \quad (3.6.14)$$

where the second term in parenthesis correct the spurious large- x , and the last line eliminates the double counting, but noting that the constant term $h(0)$ has already been eliminated by the subtraction in the first row. The subtracted small- x contribution to the largest eigenvalue is

$$(\text{small-}x)_+^{\text{NLO}} = \frac{C_A \alpha_s}{\pi N} - \alpha_s \left[\frac{11C_A + 2n_f(1 - 2C_F/C_A)}{12\pi} + n_f \frac{23C_A - 26C_F}{36\pi^2} \frac{\alpha_s}{N} \right], \quad (3.6.15)$$

as can be easily extracted from Eqs. (1.3.37).

We propose here a different and easier way to obtain an equivalent result, which possibly differs by subleading contributions. Remember that the expression in Eq. (3.6.12)

⁶In principle one could use the LO resummed anomalous dimension; however, the use of the NLO one guarantees that the leading Bateman pole, which gives the leading small- x behaviour, is at the same position in all the entries of the anomalous dimension matrix. An intermediate solution which preserve this property would be to use the LO resummed anomalous dimension with the Bateman parameters taken from the NLO: this solution coincides up to subleading terms with the NLO one, but has a faster numerical implementation.

is in principle correct, the only problem being the spurious branch-cut. The idea of substituting γ_s with $\gamma_+^{\text{res,NLO}}$ solves the problem introducing differences which are subleading: indeed, from the small- x point of view, $\gamma_+^{\text{res,NLO}}$ has the same leading small- x structure than γ_s . In the same spirit, we propose to use as argument of h_{qg} the difference

$$\gamma_+^{\text{res,NLO}}(\alpha_s, N) - \gamma_+^{\text{NLO}}(\alpha_s, N) + (\text{small-}x)_+^{\text{NLO}}, \quad (3.6.16)$$

which has the requested both small- x and large- x behaviours (the last term restores the NLO small- x terms subtracted by the second term). With this choice we simply have

$$\begin{aligned} \Delta\gamma_{qg}^{\text{res}}(\alpha_s, N) = \alpha_s h_{qg} \left(\left[\gamma_+^{\text{res,NLO}}(\alpha_s, N) - \gamma_+^{\text{NLO}}(\alpha_s, N) + (\text{small-}x)_+^{\text{NLO}} \right] \right. \\ \left. - (\text{small-}x)_{qg}^{\text{NLO}} \right). \end{aligned} \quad (3.6.17)$$

This expression is also simpler for numerical evaluation, since the function h_{qg} must be computed only once.

The same procedure can be used for the resummation of coefficient functions. We do not give many details here; some minimal details are given in App. C.4.4.

3.6.3 Back to the physical basis

The last step to complete the small- x resummation of anomalous dimensions consists in constructing the full anomalous dimension matrix in the physical basis.

At LO, the quark anomalous dimension do not resum, and then we can build the anomalous dimension matrix from the quark anomalous dimensions and the two eigenvectors, one of which is resummed. This can be easily achieved using Eq. (1.3.25), the result being

$$\Gamma = \begin{pmatrix} (\gamma_+ + \gamma_- - \gamma_{qq}) & X \\ \gamma_{qg} & \gamma_{qg} \end{pmatrix}, \quad X = \frac{(\gamma_+ - \gamma_{qq})(\gamma_{qq} - \gamma_-)}{\gamma_{qg}}, \quad (3.6.18)$$

where γ_+ has to be replaced with γ_+^{res} at LL. Then, writing

$$\gamma_+^{\text{res}} = \gamma_+ + \Delta\gamma_+^{\text{res}}, \quad (3.6.19)$$

we obtain for the gluon entries

$$\gamma_{gg}^{\text{res}} = \gamma_{gg} + \Delta\gamma_+^{\text{res}} \quad (3.6.20)$$

$$\gamma_{gq}^{\text{res}} = \gamma_{gq} + \frac{\gamma_{qq} - \gamma_-}{\gamma_{qg}} \Delta\gamma_+^{\text{res}}. \quad (3.6.21)$$

As described above, $\Delta\gamma_+^{\text{res}}$ is built to be free of branch-cuts, in order to avoid spurious small- x enhancements in the physical matrix entries. Indeed, γ_{gg}^{res} does not have any branch-cut. However, γ_{gq} inherit the branch-cut of γ_- ; nevertheless, since $(\gamma_{qq} - \gamma_-)/\gamma_{qg}$ is subleading at small N with respect to $\Delta\gamma_+^{\text{res}}$, we can substitute its value in $N = 0$, which at LO is C_F/C_A , obtaining finally

$$\Gamma_{\text{LO}}^{\text{res}} = \Gamma_{\text{LO}} + \Delta\Gamma_{\text{LO}}^{\text{res}}, \quad \Delta\Gamma_{\text{LO}}^{\text{res}} = \begin{pmatrix} \Delta\gamma_+^{\text{res}} & \frac{C_F}{C_A} \Delta\gamma_+^{\text{res}} \\ 0 & 0 \end{pmatrix}. \quad (3.6.22)$$

Note that this result respects, in the small- N limit, the colour-charge relation Eq. (3.6.33).

At NLO, also the resummation of the quark anomalous dimensions is also needed. Then we define

$$\gamma_{qg}^{\text{res}} = \gamma_{qg} + \Delta\gamma_{qg}^{\text{res}} \quad (3.6.23)$$

$$\gamma_{qq}^{\text{res}} = \gamma_{qq} + \Delta\gamma_{qq}^{\text{res}} \quad (3.6.24)$$

where the two Δ terms satisfy the colour-charge relation

$$\Delta\gamma_{qq}^{\text{res}} = \frac{C_F}{C_A} \Delta\gamma_{qg}^{\text{res}} \quad (3.6.25)$$

coming from Eq. (3.6.34). Then, from Eq. (3.6.17), we have both quark entries, and moreover we know $\Delta\gamma_+^{\text{res}}$ at NLO. In terms of these, the gluon entries become, at NLO,

$$\gamma_{gg}^{\text{res}} = \gamma_{gg} + \Delta\gamma_+^{\text{res}} - \Delta\gamma_{qq}^{\text{res}} \quad (3.6.26)$$

$$\gamma_{gq}^{\text{res}} = \gamma_{gq} + \Delta\gamma_{gq}^{\text{res}} \quad (3.6.27)$$

with

$$\Delta\gamma_{gq}^{\text{res}} = \frac{\gamma_{qq} - \gamma_-}{\gamma_{qg}} \Delta\gamma_+^{\text{res}} + \left[\frac{C_F}{C_A} \frac{\gamma_{gg} - \gamma_{qq}}{\gamma_{qg}} - \frac{\gamma_{gq}}{\gamma_{qg}} \right] \Delta\gamma_{qg}^{\text{res}}, \quad (3.6.28)$$

as one can find expanding X in Eq. (3.6.18) to first power⁷ in $\Delta\gamma_+^{\text{res}}$ and $\Delta\gamma_{qg}^{\text{res}}$ (or, alternatively, using the determinant condition $\gamma_+\gamma_- = \gamma_{gg}\gamma_{qq} - \gamma_{qg}\gamma_{gq}$ at the resummed level). To avoid spurious branch-cuts, as in the LO case, we may substitute the coefficients of the Δ terms with their value in $N = 0$, obtaining

$$\Delta\gamma_{gq}^{\text{res}} = (1 + k\alpha_s) \frac{C_F}{C_A} \Delta\gamma_+^{\text{res}} - \frac{C_F}{C_A} \frac{C_A + n_f}{2n_f} \Delta\gamma_{qg}^{\text{res}} \quad (3.6.29)$$

with

$$k = \frac{1}{12\pi} \left[3C_A + \left(1 - 2\frac{C_F}{C_A} \right) n_f \right]. \quad (3.6.30)$$

The inclusion of the order α_s piece in the first term is needed because it produces NLL terms by interference with the LL part of $\Delta\gamma_+^{\text{res}}$. Then, writing

$$\Gamma_{\text{NLO}}^{\text{res}} = \Gamma_{\text{NLO}} + \Delta\Gamma_{\text{NLO}}^{\text{res}}, \quad (3.6.31)$$

we have finally

$$\Delta\Gamma_{\text{NLO}}^{\text{res}} = \begin{pmatrix} \Delta\gamma_+^{\text{res}} - \frac{C_F}{C_A} \Delta\gamma_{qg}^{\text{res}} & \Delta\gamma_{gq}^{\text{res}} \\ \Delta\gamma_{qg}^{\text{res}} & \frac{C_F}{C_A} \Delta\gamma_{qg}^{\text{res}} \end{pmatrix}. \quad (3.6.32)$$

3.6.4 Schemes

So far, in this Chapter we didn't ever talk about the factorization scheme. Concerning the GLAP equation, we have tacitly used the $\overline{\text{MS}}$ scheme, since it is the most commonly used. However, all the results presented in this Chapter are given in a different scheme which is usually called $Q_0\overline{\text{MS}}$ [10, 60, 61]. This scheme differs to the $\overline{\text{MS}}$ scheme only at

⁷Actually, a term proportional to the product $\Delta\gamma_+^{\text{res}} \Delta\gamma_{qg}^{\text{res}}$ would contribute at NLL, but such a term is not present in the expansion.

small- x , and in particular they coincide at fixed order up to NNLO, while they start differing at N³LO: therefore, all the anomalous dimension used so far are unchanged in $Q_0\overline{\text{MS}}$ scheme.

The theory of small- x scheme changes at the resummed level has been developed in Ref. [9, 62], and we don't want to discuss it here. We simply want to emphasize that the $Q_0\overline{\text{MS}}$ scheme is more suitable for small- x resummation, in particular for the resummation of running-coupling effects [10]. At the end, one could choose to go back to $\overline{\text{MS}}$ scheme, but the price to pay is the introduction of new singularities which should cancel in a hadronic computation, but which are numerically inconvenient. Therefore we prefer to work with the $Q_0\overline{\text{MS}}$ scheme.

Finally, we would like to recall that for all the schemes we are considering the following colour-charge relations are satisfied

$$\gamma_s^{gq}\left(\frac{\alpha_s}{N}\right) = \frac{C_F}{C_A} \gamma_s^{gg}\left(\frac{\alpha_s}{N}\right) \quad (3.6.33)$$

$$\gamma_{ss}^{qq}\left(\frac{\alpha_s}{N}\right) = \frac{C_F}{C_A} \left[\gamma_{ss}^{gg}\left(\frac{\alpha_s}{N}\right) - \gamma_{ss}^{gg}(0) \right], \quad (3.6.34)$$

with

$$\gamma_{ss}^{gg}(0) = \frac{n_f}{3\pi}. \quad (3.6.35)$$

3.7 Resummed splitting function

From $\Delta\Gamma^{\text{res}}$ in N -space we can compute the resummed splitting functions $\Delta P_{ij}^{\text{res}}$ by taking a numerical inverse Mellin transform. Since the resummation affects the small- x region, $\Delta P_{ij}^{\text{res}}$ are normal functions rather than distributions (the distributional nature of the splitting functions regards the $x = 1$ endpoint, which is left unchanged). Hence, they are a more suitable quantity to look at, since they are real and defined in a finite range $0 < x < 1$. Moreover, the computation of $\Delta\Gamma^{\text{res}}$ is not numerically robust, since it needs several root-finding calls for the computation of χ_s and for putting on-shell the off-shell kernels. Therefore, if the goal is the computation of the splitting functions we can specialize the code to be stable along the inverse Mellin integration path.

The fixed Talbot algorithm described in App. B.2.1 turns out to be not the best choice, since the numerical stability decreases going closer to the negative real axis. The straight line of Eq. (B.2.3) provides a better stability. Close to the real axis, the convergence of the root-finding algorithms is still not optimal, and a sampling along the integration path has been adopted to provide good initial guesses for the algorithms.

As an example, we present in Fig. 3.6 the results for the resummed gg and qg components of the splitting function matrix, for $\alpha_s = 0.2$ and $n_f = 4$, which are the values used in Ref. [10]. Concerning P_{gg} , also the LO resummed result is shown: it agrees pretty well to that of Ref. [10], apart in the large- x region, the difference being due to the improved approximation described in Sect. 3.6.1. The NLO resummed result differs a bit more even at small x : however, being ΔP_{gg} built up from ΔP_+ and ΔP_{qg} , Eq. (3.6.26), we can trace this difference in a significant difference in ΔP_{qg} . Indeed, the second plot shows a rather different behaviour for the resummed P_{qg} , even if the asymptotic behaviour at small x seems to be not that different. This difference can be mainly traced in the different matching adopted to obtain the two curves, Eq. (3.6.17)

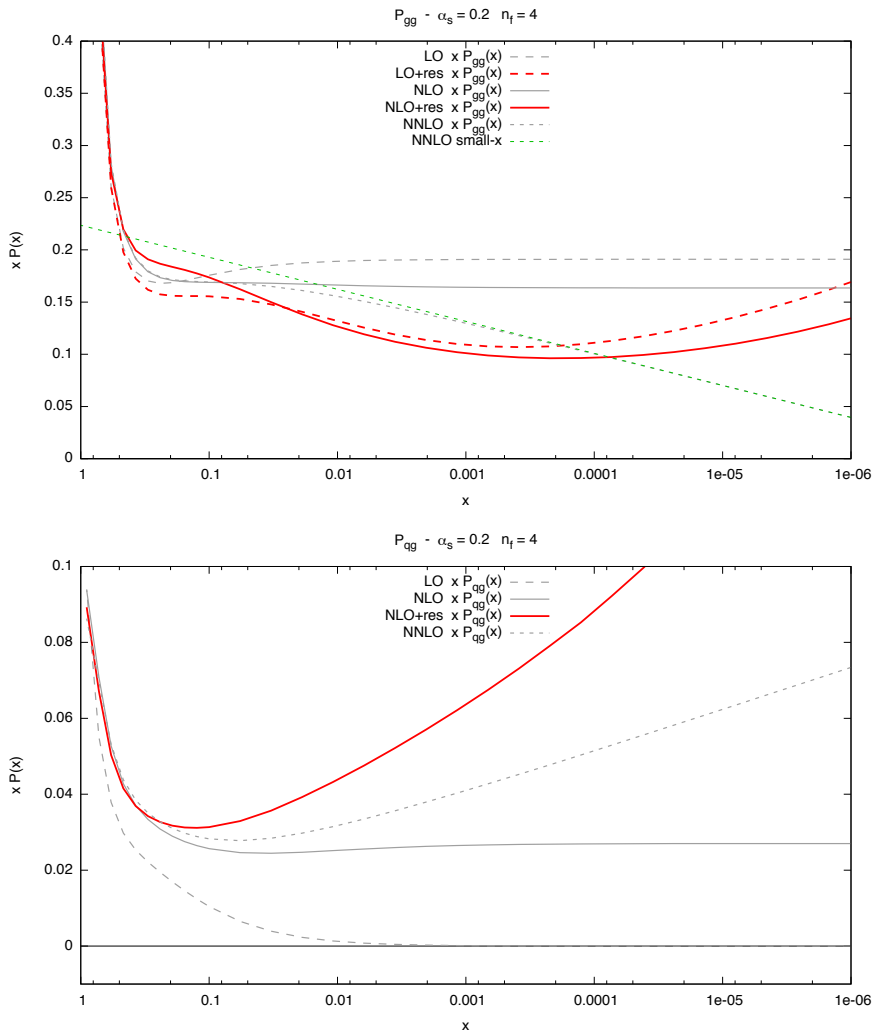


Figure 3.6. Unresummed and resummed $P_{gg}(\alpha_s, x)$ (upper plot) and $P_{qg}(\alpha_s, x)$ (lower plot) for $\alpha_s = 0.2$ and $n_f = 4$. The matching Eq. (3.6.17) has been adopted, and a Padé approximant [8/8] has been used to compute the Borel sum of the series h_{qg} .

here and Eq. (3.6.14) in Ref. [10]. Since both matchings are allowed, the difference could be considered as an estimator of the uncertainty induced by the subleading terms included in the resummation procedure.

3.7.1 Approximations

Once we have $\Delta\Gamma^{\text{res}}$ in the complex plane we could use it to perform the GLAP evolution. However, as described above, numerical stability is hardly achieved, and then for fast numerical applications the use of simple analytic approximation of $\Delta\Gamma^{\text{res}}$ is required.

A good and accurate way to obtain such approximation is to fit the splitting functions ΔP^{res} , computed as the inverse Mellin of $\Delta\Gamma^{\text{res}}$, in terms of an appropriate parametrization. This function appears to be a quite smooth function of $\log x$; moreover, since the convolutions involve the splitting functions in a range that ends at

$x = 1$ but starts at small values of x related to the hadronic scale of the process, we practically need to know the splitting function not really down to $x = 0$, but just down to a small value, making it possible to approximate ΔP^{res} in a finite $\log x$ range.

Since the matrix $\Delta\Gamma^{\text{res}}$ can be built from $\Delta\gamma_+^{\text{res}}$ and $\Delta\gamma_{qg}^{\text{res}}$, it is actually sufficient to fit these two functions (their inverse Mellin), which are the primitive outputs of the resummation code, and build analytically at the end the entire matrix according to Sect. 3.6.3.

Since the asymptotic behaviour (at small x) of ΔP^{res} is given by the the rightmost pole of $\Delta\Gamma^{\text{res}}$,

$$\Delta\Gamma^{\text{res}}(N) = \frac{r_B}{N - N_B} + \dots, \quad (3.7.1)$$

we can fix it and fit the difference (in x -space). For better results, it's actually more accurate to fix the two rightmost poles N_B and N'_B , with residues r_B and r'_B respectively (these are computed numerically from $\Delta\Gamma^{\text{res}}$). Then we can fit a polynomial in x and $\log \frac{1}{x}$, i.e. we use the parametrization

$$x \Delta P^{\text{res}}(\alpha_s, x) = r_B x^{-N_B} + r'_B x^{-N'_B} + \sum_{k, j \geq 0} c_{kj} x^k \log^j \frac{1}{x}. \quad (3.7.2)$$

Note that $\Delta P^{\text{res}}(1) = r_B + r'_B + c_{00}$ is a constant, as it should since $\Delta\Gamma^{\text{res}}(N)$ goes to zero at least as $1/N$ at large N . Its Mellin transform is

$$\Delta\Gamma^{\text{res}}(N) = \frac{r_B}{N - N_B} + \frac{r'_B}{N - N'_B} + \sum_{k, j \geq 0} c_{kj} \frac{j!}{(N + k)^{j+1}}. \quad (3.7.3)$$

For the case of the largest eigenvalue, momentum conservation constraint $\Delta\gamma_+^{\text{res}}(1) = 0$ imposes

$$\frac{r_B}{1 - N_B} + \frac{r'_B}{1 - N'_B} + \sum_{k, j} c_{kj} \frac{j!}{(1 + k)^{j+1}} = 0, \quad (3.7.4)$$

which fixes one of the free parameters in terms of the others.

4 Combining resummations

Contents

4.1 When is threshold resummation relevant?	87
4.1.1 Saddle-point argument	89
4.1.2 The impact of PDFs	91
4.1.3 The resummation region for the Drell-Yan process	92
4.1.4 The resummation region for the Higgs production process	95
4.2 Phenomenology of high-energy resummation	97
4.2.1 Resummed PDFs at the initial scale	98
4.2.2 Resummed evolution	99
4.3 Joint effect of both resummations	100
4.3.1 Joint effect on Higgs production	101
4.4 Toward a joint resummation	103

In this Chapter we will discuss in detail the relevance of threshold resummation. We will establish a quantitative way to assess for which values of the hadronic variables a process is dominated by the threshold logarithms, thereby determining if their resummation is needed or not. We will then show how to get phenomenological implications from the high-energy resummation formalism introduced in Chap. 3. Finally, with specific reference to the Higgs boson production, we will discuss the effect of small- x resummation on the determination of the threshold region.

4.1 When is threshold resummation relevant?

First, we want to establish here a way to assess when threshold resummation is relevant for phenomenology [25]. Of course, when the hadronic ratio $\tau = M^2/s$ is close to threshold, $\tau \rightarrow 1$, all contributions to the cross-section come from the threshold region and threshold resummation cannot be neglected. But in phenomenologically interesting processes, such as those at the LHC and Tevatron, τ is always very small, far from threshold.

However, it has been pointed out since long [63] that because hadronic cross-sections are found convoluting a hard cross-section with a parton luminosity, Eq. (2.1.4), the effect of resummation may be relevant even relatively far from the hadronic threshold. Indeed, in Ref. [35] threshold resummation has been claimed to affect significantly

Drell-Yan production for E866 kinematics, though somewhat different results have been found in Ref. [28]. It is important to observe that Drell-Yan data from E866 and related experiments play a crucial role in the precision determination of parton distributions [64], so their accurate treatment is crucial for precise LHC phenomenology. Furthermore, threshold resummation is known [65] to affect in a non-negligible way standard Higgs production in gluon-gluon fusion at the LHC, even though the process is clearly very far from threshold.

The standard physical argument to explain why resummation may be relevant even when the hadronic process is relatively far from threshold goes as follows [21]. The quantity which is resummed in perturbative QCD is the hard partonic cross-section, which depends on the partonic center-of-mass energy and the dimensionless ratio of the latter to the final state invariant mass. Therefore, resummation is relevant when it is the partonic subprocess that is close to threshold. The partonic center-of-mass energy in turn can take any value from threshold up to the hadronic center-of-mass energy, and its mean value is determined by the shape of the PDFs: therefore, one expects threshold resummation to be more important if the average partonic center-of-mass energy is small, i.e. if the relevant PDFs are peaked at small x (such as gluons or sea quarks, as opposed to valence quarks). This for instance explains why threshold resummation is especially relevant for Higgs production in gluon-gluon fusion.

We will show that this can be made quantitative using a saddle-point argument in Mellin space [25]: for any given value of the hadronic ratio τ , the dominant contribution to the cross-section comes from a narrow range of the variable N , conjugate to τ upon Mellin transform. In Mellin space the cross-section factorizes in the product of a parton luminosity \mathcal{L} and a hard coefficient function C , but it turns out that the position of the saddle is mostly determined by the PDF luminosity. Moreover, the result is quite insensitive to the non-perturbative (low-scale) shape of the parton distribution and mostly determined by its scale dependence, specifically by the low- x (or low- N) behaviour of the relevant Altarelli-Parisi splitting functions: the faster the small- x growth of the splitting function, the smaller the average partonic center-of-mass energy, the farther from the hadronic threshold the resummation is relevant. This is reassuring, because it means that the region of applicability of threshold resummation is controlled by perturbative physics. Moreover, this suggests a connection between threshold (large- z) resummation and high-energy (small- x) resummations: we will come back on this in Sect. 4.3.

The issue of the persistence of sizable soft gluon emission terms even far from threshold was also addressed in Ref. [28] using methods of soft-collinear effective theory, but in the large $\tau \gtrsim 0.2$ region it was related to the (non-perturbative) shape of parton distributions, while for smaller τ values it was also observed, but left unexplained. The treatment of this issue in soft-collinear effective theory issue was revisited in a quantitative way in Ref. [66], where it was related to a parameter determined by the shape of parton distributions.

We now show how we can assess the impact of parton distributions by means of a Mellin-space argument [25]. For a given process and a given value of $\tau = M^2/s$, we determine the region of the variable N which provides the dominant contribution to the cross-section. We show that the such region is mostly determined by the small- x behaviour of the PDFs, which in turn is driven by perturbative evolution. Then, we assess the N region where threshold resummation is relevant, and putting everything

together, we obtain the resummation region for the Drell-Yan process and the Higgs process.

4.1.1 Saddle-point argument

A cross-section for a hadronic process with scale M^2 and center-of-mass energy $s = M^2/\tau$ can be written as a sum of contributions of the form

$$\sigma(\tau, M^2) = \int_{\tau}^1 \frac{dz}{z} \mathcal{L}(z, M^2) C\left(\frac{\tau}{z}, \alpha_s(M^2)\right) \quad (4.1.1)$$

in terms of a partonic coefficient function C and a parton luminosity, in turn determined in terms of parton distributions $f_i(x_i)$ as

$$\mathcal{L}(z, \mu^2) = \int_z^1 \frac{dx}{x} f^{(1)}(x, \mu^2) f^{(2)}\left(\frac{z}{x}, \mu^2\right). \quad (4.1.2)$$

Here we denote generically by σ a suitable quantity (in general, process-dependent) which has the property of factorizing as in Eq. (4.1.1). Such quantities are usually related in a simple way to cross-sections or distributions; for example, in the case of the invariant mass distribution of Drell-Yan pairs, σ is given by Eq. (2.1.4).

In general, the cross-section gets a contribution like Eq. (4.1.1) from all parton channels which contribute to the given process at the given order, but this is inessential for our argument. Indeed, since we are interested on the threshold region, only one channel is enhanced and then contributes: hence, we concentrate on one such contribution.

In Eq. (4.1.1), the partonic coefficient function, which is computed in perturbation theory, is evaluated as a function of the partonic center-of-mass energy

$$\hat{s} = \frac{M^2}{\tau/z} = x_1 x_2 s, \quad (4.1.3)$$

where $x_1 = x$ and $x_2 \equiv z/x$ are the momentum fractions of the two partons. Therefore, the threshold region, where resummation is relevant, is the region in which \hat{s} is not much larger than M^2 . However, all values of x_1, x_2 between τ and 1 are accessible, so whether or not resummation is relevant depends on which region gives the dominant contribution to the convolution integrals Eqs. (4.1.1) and (4.1.2). This dominant region can be determined using a Mellin-space argument [25].

For ease of notation, we temporarily omit the dependence on the energy scale M^2 . The Mellin transform of $\sigma(\tau)$ is

$$\sigma(N) = \int_0^1 d\tau \tau^{N-1} \sigma(\tau), \quad (4.1.4)$$

with inverse

$$\sigma(\tau) = \frac{1}{2\pi i} \int_{c-i\infty}^{c+i\infty} dN \tau^{-N} \sigma(N) = \frac{1}{2\pi i} \int_{c-i\infty}^{c+i\infty} dN e^{E(\tau, N)}, \quad (4.1.5)$$

where in the last step we have defined

$$E(\tau, N) \equiv N \log \frac{1}{\tau} + \log \sigma(N). \quad (4.1.6)$$

We would like to evaluate the integral with a saddle-point approximation: since the integration path in Eq. (4.1.5) has to be to the right of all the singularities of the integrand (see App. B), we must look for a saddle in such region. Since $\sigma(N)$ is a real function¹, we expect that if a saddle-point exists it is on the real axis. The function $\sigma(N)$ has its rightmost (positive) singularity on the real positive axis because of the small- x behaviour of the parton luminosity; to the right of this singularity, it is a decreasing function of N , because $\sigma(\tau)$ is not a distribution and Theorem B.3.1 applies. Conversely, the $N \log \frac{1}{\tau}$ term increases at large N for all $\tau < 1$. As a consequence, $E(\tau, N)$ always has at least one minimum on the real positive N -axis.

We now want to understand if the saddle is unique. If τ is small enough, the growth of the $N \log \frac{1}{\tau}$ sets in at very small N , leaving no space between the rightmost pole of $\sigma(N)$ and the straight line $N \log \frac{1}{\tau}$ for more than one minimum. When τ is larger, we need to supply this argument with other information on the shape of $\sigma(N)$. To clarify, let's write the saddle condition $\frac{d}{dN}E(\tau, N) = 0$ explicitly:

$$\log \frac{1}{\tau} = -\frac{d}{dN} \log \sigma(N). \quad (4.1.7)$$

The condition for the existence of a unique saddle is that the right-hand-side is a monotonically decreasing function of N extending from $+\infty$ down to 0. At small N , this is guaranteed by the positive pole of $\sigma(N)$, as already discussed. Indeed, if $\sigma(N)$ behaves like

$$\sigma(N) \sim \frac{a}{(N - N_p)^\alpha}, \quad a > 0, \quad \alpha > 0 \quad (4.1.8)$$

its logarithmic derivative behaves as

$$-\frac{d}{dN} \log \sigma(N) \sim \frac{\alpha}{N - N_p}, \quad (4.1.9)$$

which has a positive pole in $N = N_p$ and decreases as N increases. In the opposite limit, large N , we can compute the behaviour of $\sigma(N)$ by knowing that $\sigma(\tau)$ vanishes as $\tau \rightarrow 1$: we may assume that

$$\sigma(\tau) \sim b(1 - \tau)^\beta \quad \beta > 0 \quad (4.1.10)$$

as $\tau \rightarrow 1$, whose Mellin transform is

$$\sigma(N) \sim b \frac{\Gamma(N)\Gamma(\beta)}{\Gamma(N + \beta)} \stackrel{N \rightarrow \infty}{\sim} b \Gamma(\beta) N^{-\beta}. \quad (4.1.11)$$

Then,

$$-\frac{d}{dN} \log \sigma(N) \stackrel{N \rightarrow \infty}{\sim} \frac{\beta}{N}, \quad (4.1.12)$$

which is a decreasing function and goes to 0 as $N \rightarrow \infty$. We may guess (and we have verified numerically) that also the intermediate region respect this behaviour: then, the saddle-point is unique for all values of τ .

Then, from now on we will call the saddle-point $N_0 = N_0(\tau, M^2)$, given by the solution of Eq. (4.1.7). From the definition, Eq. (4.1.7), and from the discussion above, we immediately see that the saddle-point N_0 increases with τ : in particular,

¹I.e., $\overline{\sigma(N)} = \sigma(\bar{N})$.

this proves once again that large- τ and large- N regions are mutually related. We will see in the following this relation explicitly for processes like the Drell-Yan process and the Higgs production.

The position of the saddle-point gives us a quantitative way to assess the region of relevance of threshold resummation. Indeed, the Mellin inversion integral, Eq. (4.1.5), is dominated by the region of N around N_0 , and we have exploited the relation between N_0 and τ (and M^2). Then, given τ and M^2 (the hadron-level parameters), we have a precise estimate of the N -region which dominates the hadronic cross-section. If such region (around N_0) is at values of N large enough to be in the threshold region, then we could say that for those τ and M^2 the threshold region gives the dominant contribution, and hence that threshold resummation cannot be neglected.

We have already established in Sect. 2.1.6 that for $N \gtrsim 2$ the threshold logarithms give the main contribution to the coefficient function (for the Drell-Yan case), provided the proper choice of subleading terms is made. Then, we can conclude that the condition $N_0 > 2$ can be considered as a good estimate for the threshold region. This condition translates into $\tau > \tau_0$, with τ_0 being determined by Eq. (4.1.7) with $N = 2$. We have then obtained the desired result: given M^2 , we are able to say for which values of τ resummation is relevant. In the following we will see explicit results.

4.1.2 The impact of PDFs

The position of the saddle-point N_0 is strongly influenced by the rate of decrease of the cross-section $\sigma(N)$ as N grows. Indeed, in Mellin space, the cross-section Eq. (4.1.1) factorizes:

$$\sigma(N) = \mathcal{L}(N) C(N, \alpha_s). \quad (4.1.13)$$

It is then easy to see that the decrease of $\sigma(N)$ with N is driven by the parton luminosity $\mathcal{L}(N)$: in fact, for large N , $C(N, \alpha_s)$ is an *increasing* function of N , because $C(z, \alpha_s)$ is a distribution (see Theorem B.3.2). However, the parton luminosity always offsets this increase if the convolution integral exists, because the cross-section $\sigma(\tau)$ is an ordinary function and its Mellin transform decreases with N . Indeed, because the partonic coefficient function rises at most as a power of $\log N$ as $N \rightarrow \infty$, it is easy to show that a sufficient condition for $\sigma(N)$ to decrease is that the parton luminosity $\mathcal{L}(z)$ vanishes at large z at least as a positive power of $(1 - z)$, as it usually does.

As a consequence, when τ is large, the position of the saddle-point N_0 is completely controlled by the drop of the parton luminosity: indeed, in the absence of parton luminosity, the saddle-point would be very close to the minimum of the coefficient function (which is around $N \simeq 1$ for Drell-Yan, see Fig. 2.5). When τ is smaller, even without PDFs the location of the saddle is controlled by the partonic coefficient function, which in this region is a decreasing function of N . However, this decrease is much stronger in the presence of a luminosity, so the location of the saddle is substantially larger. Hence, in the large τ region the effect of the resummation is made much stronger by the luminosity, while for medium-small τ if the luminosity decreases fast enough, N_0 may be quite large even if $\tau \ll 1$, i.e. far from the hadronic threshold, thereby extending the region in which resummation is relevant.

The position of the saddle-point in the various regions can be simply estimated on the basis of general considerations. At the leading-log level, parton densities can be

written as linear combinations of terms of the form (see Sect. 1.4)

$$f_i(N, \mu^2) = \exp \left[-\frac{\gamma_i^{(0)}(N-1)}{\beta_0} \log \frac{\alpha_s(\mu^2)}{\alpha_s(\mu_0^2)} \right] f_i(N, \mu_0^2) \quad (4.1.14)$$

in terms of initial PDFs $f_i(N, \mu_0^2)$ at some reference scale μ_0^2 . The cross-section is correspondingly decomposed into a sum of contributions, each of which has the form of Eq. (4.1.5), with

$$E(\tau, N; M^2) = N \log \frac{1}{\tau} - \frac{\gamma_i^{(0)}(N-1) + \gamma_j^{(0)}(N-1)}{\beta_0} \log \frac{\alpha_s(M^2)}{\alpha_s(\mu_0^2)} + \log f_i(N, \mu_0^2) + \log f_j(N, \mu_0^2) + \log C(N, \alpha_s(M^2)). \quad (4.1.15)$$

At large N , this expression is dominated by the first term, which grows linearly with N , while at small N the behaviour of $E(\tau, N; M^2)$ is determined by the singularities of the anomalous dimensions, which are stronger than those of the initial conditions if $M^2 > \mu_0^2$, given that low-scale physics is both expected theoretically from Regge theory [67,68] and known phenomenologically from PDF fits [12] to produce at most poles but not essential singularities such as those obtained exponentiating the anomalous dimensions. Indeed, assuming a power behaviour for $f_i(z, \mu_0^2)$ both at small and large z ,

$$f_i(z, \mu_0^2) = z^{\alpha_i} (1-z)^{\beta_i}, \quad (4.1.16)$$

so that

$$f_i(N, \mu_0^2) = \frac{\Gamma(N + \alpha_i) \Gamma(\beta_i + 1)}{\Gamma(N + \alpha_i + \beta_i + 1)}, \quad (4.1.17)$$

$\log f_i(N, \mu_0^2)$ behaves as $\log N$ both at large and small N , and is thus subdominant in comparison to either the τ dependent term or the anomalous dimension contribution in Eq. (4.1.15). A similar argument holds for the partonic coefficient function term $\log C(N, \alpha_s)$.

The position of the minimum is therefore mainly determined by the transition from the leading small- N drop due to the anomalous dimension term and the leading large- N rise due to the τ -dependent term, up to a correction due to the other contributions to Eq. (4.1.15). When τ is large, the rise in the first term is slow, and it only sets in for rather large N so the correction due to the other contributions may be substantial. This is the region in which resummation is surely relevant because the hadronic τ is large. But when τ is not so large, the rise sets in more rapidly, in the region where the second term is dominant and the correction from the initial PDFs and the partonic coefficient function is less important.

Moreover, the small- N region is the one which is sensitive to the high-energy logarithms, Chap. 3. Then, the exact relation between N_0 and τ can be sensibly modified by high-energy resummation: this suggests that there can be an interplay of the threshold region and the high-energy region. We will discuss this in more detail in Sect. 4.3.

4.1.3 The resummation region for the Drell-Yan process

We now assess the relevance of resummation in the specific case of Drell-Yan production. We consider the case of the invariant mass distribution: the quantity $\sigma(\tau, M^2)$

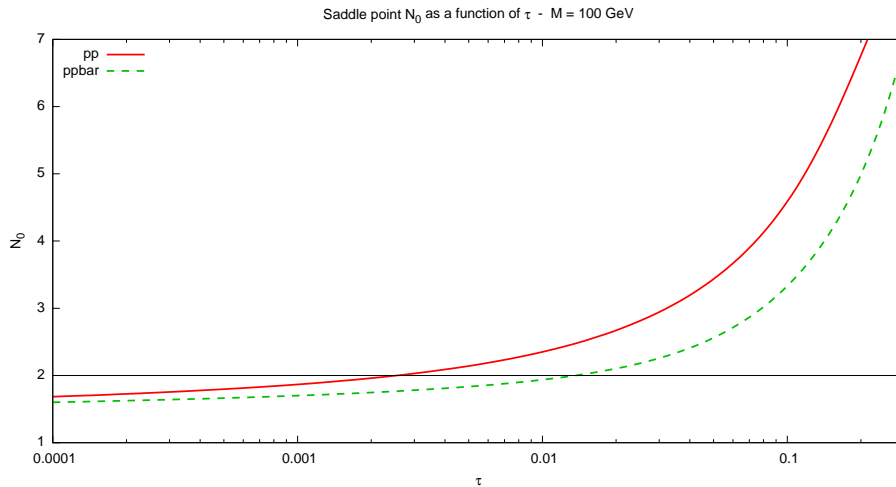


Figure 4.1. The position of the saddle-point N_0 for the Mellin inversion integral Eq. (4.1.5) as a function of τ with the cross-section Eq. (4.1.13) determined using the NLO Drell-Yan cross-section for neutral di-leptons and NNPDF2.0 [64] parton distributions, with $M = 100$ GeV. The two upper curves refer to pp and $p\bar{p}$ collisions.

which appears in Eq. (4.1.1) is given by

$$\sigma(\tau, M^2) = \frac{1}{\tau} \frac{d\sigma_{\text{DY}}}{dM^2}(\tau, M^2), \quad (4.1.18)$$

see App. C.1 for the relevant formulae. The main contribution to the cross-section is given by the $q\bar{q}$ channel, and this is also the only contribution which is enhanced in the threshold region. Then, we concentrate on that from now on — the other channels behaves perturbatively in the threshold region and then there’s no need to investigate them.

We have then determined the position of the saddle-point N_0 in a realistic situation, i.e. using the partonic coefficient function at NLO and the luminosity for the production of a neutral lepton pair of invariant mass $M = 100$ GeV at a pp or $p\bar{p}$ colliders, using NNPDF2.0 [64] parton distributions. In Fig. 4.1 we show the dependence of N_0 on τ in the two cases. The behaviour previously predicted is indeed manifest: at large τ , the saddle-point N_0 increases, going in the region where threshold resummation is more and more relevant, while it decreases at small τ , but slower and slower, because of the lower limit set by the pole of parton luminosity at small N .

Choosing $N = 2$ as the value above which threshold logarithms are relevant, the intersection of the line $N_0 = 2$ (showed in Fig. 4.1) with the curve $N_0(\tau, M^2)$ gives the lower value τ_0 above which resummation is important. It is already surprising that, for pp colliders, τ_0 is as small as 0.003, very far from hadronic threshold. To understand better the result, it is convenient to fix the collider energy \sqrt{s} instead of the mass M . To do this, we first write²

$$\tau_0(M^2) = \exp \left[\left. \frac{d}{dN} \log \sigma(N, M^2) \right|_{N=2} \right] \quad (4.1.19)$$

²Note, by the way, that the dependence on M^2 of τ_0 is completely controlled by perturbative physics, in which it depends naively on the physical anomalous dimension.

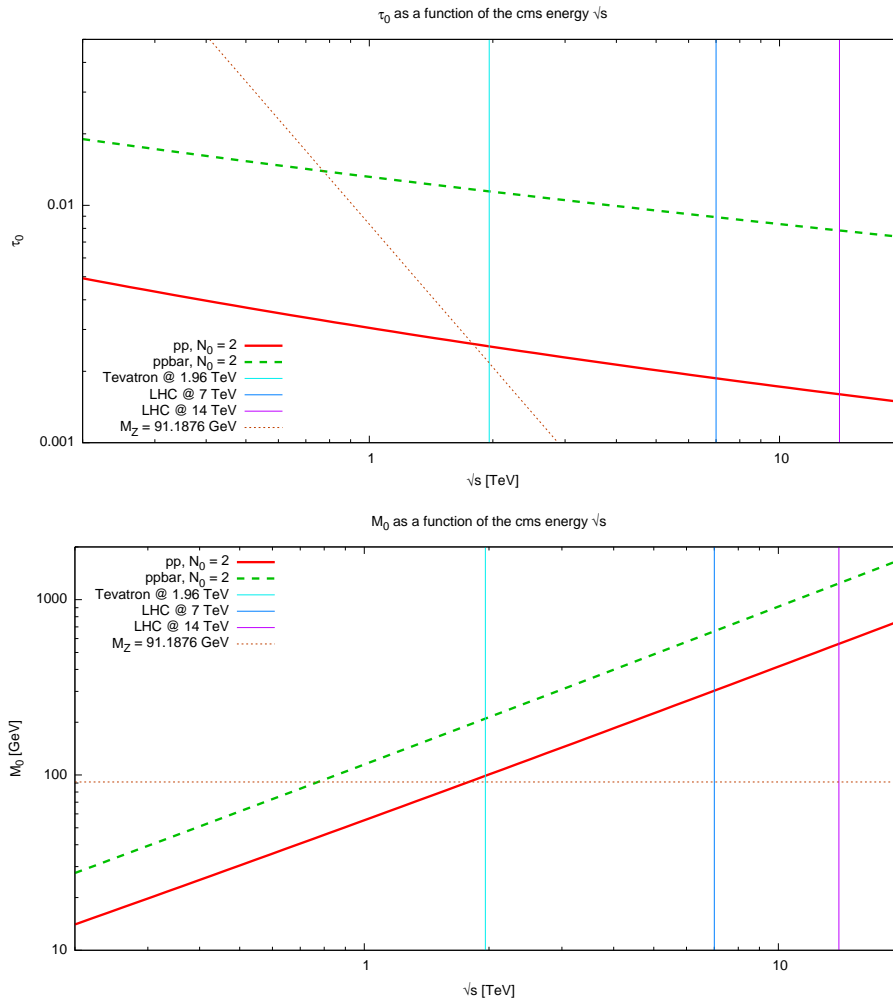


Figure 4.2. Dependence of τ_0 (upper plot) and M_0 (lower plot) on the collider c.m.s. energy \sqrt{s} for the Drell-Yan process. The Z mass is shown as a reference.

and compute it for a sequence of values of M^2 ; then, using the relation of $\tau = M^2/s$, one can either produce a curve $\tau_0(s)$ or even better $M_0(s)$, being M_0 the lower value above which resummation is important. The results are shown in Fig. 4.2, where the upper plot shows τ_0 as a function of \sqrt{s} and the lower plot shows M_0 as a function of \sqrt{s} . For example, by intersection of the solid red curve with the vertical blue curve we can conclude that at LHC at 7 TeV a system of mass larger than about $M_0 \sim 300$ GeV, corresponding to $\tau_0 \sim 0.002$, resummation may be relevant. For Tevatron, we find instead $M_0 \sim 200$ GeV, corresponding to $\tau_0 \sim 0.01$.

These values are, from one side, surprisingly smaller than one could naively expect, since the values of τ_0 are very far from threshold, especially in the LHC case. From the other side, they still tell us that, for practical purposes, threshold resummation does not play a crucial role for phenomenologically relevant Drell-Yan masses. We will see in a moment that in the Higgs case the situation is different.

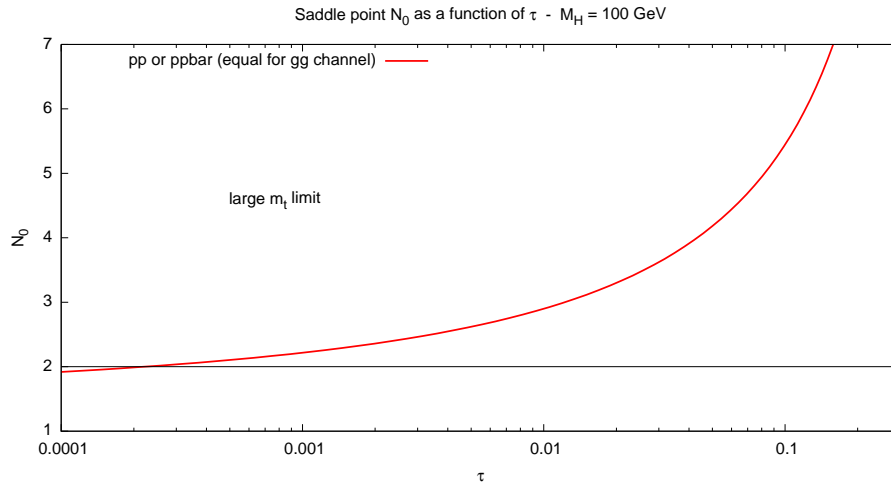


Figure 4.3. The position of the saddle-point N_0 for the Mellin inversion integral Eq. (4.1.5) as a function of τ with the cross-section Eq. (4.1.13) determined using the NLO Higgs production cross-section and NNPDF2.0 [64] parton distributions, with $M = 100$ GeV. The two upper curves refer to pp and $p\bar{p}$ collisions.

4.1.4 The resummation region for the Higgs production process

We now move to the case of Higgs production. For simplicity, we consider the infinite- m_t limit; we will discuss the effect of the top mass in Sect. 4.3. Then, we consider

$$\sigma(\tau, M^2) = \frac{1}{\tau} \frac{d\sigma_H}{dM^2}(\tau, M^2), \quad (4.1.20)$$

see App. C.2 for the relevant formulae. The main (and threshold enhanced) contribution to the cross-section is given by the gg channel: then, as before, we concentrate only on that. Note that the gluon PDF is the same for the proton and an anti-proton: therefore, the gg luminosity is not different between pp and $p\bar{p}$ colliders.

As for the Drell-Yan case, we show in Fig. 4.3 the saddle-point N_0 as a function of τ using a final state mass³ of $M = 100$ GeV. The same PDF set NNPDF2.0 is used. The conclusion we may draw here are pretty much the same as in Drell-Yan case, but here the threshold region is much more extended. Indeed, at the same final state mass $M = 100$ GeV we find here $\tau_0 \sim 0.0002$, one order of magnitude smaller than in the Drell-Yan case. Note that we are assuming that $N \gtrsim 2$ is a good definition for the threshold region also for the Higgs case. To prove this, we make the same comparison we did for the Drell-Yan case. In Fig. 4.4 we present a comparison of the first order coefficient function and its logarithmic approximations (same notations as in Fig. 2.5 are used). We see again that the region $N \gtrsim 2$ is dominated by the logarithms. However, here the small- N behaviour is no longer mimicked by the BP_2 , because the small- N behaviour of the Higgs production in gg channel is dominated by a pole in $N = 1$. However, it turns out that the small- N behaviour in the large- m_t limit is not

³Note that this is not the Higgs mass as a parameter of the SM, but just the invariant mass of the final state produced via a virtual Higgs (two photons, heavy quark pair, ...). The dependence on the parameter m_H does not play any role in the determination of the saddle, being contained in a prefactor with no N dependence.

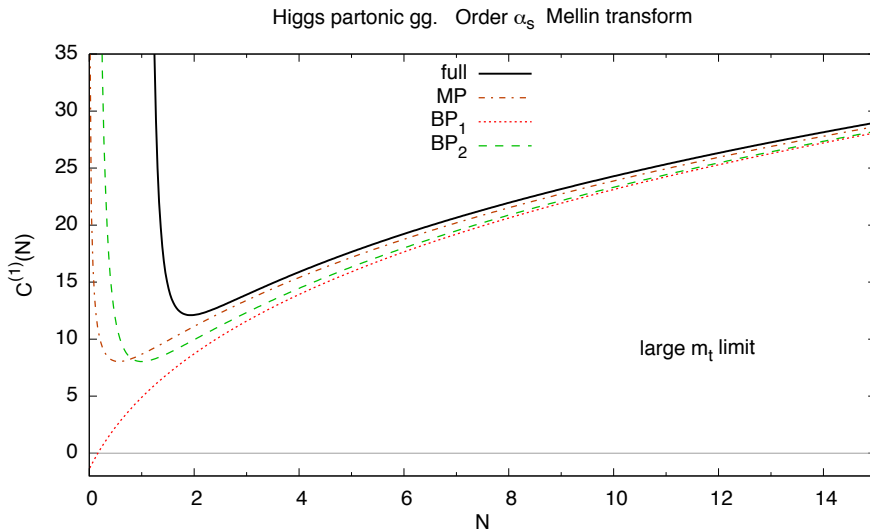


Figure 4.4. The order α_s Higgs partonic coefficient function $C^{(1)}(N)$, Mellin transform of Eq. (C.2.18), plotted as a function of N (solid curve) and its logarithmic approximations. The curves are obtained in large- m_t limit.

correct [69]: therefore, we cannot trust the shape of the complete NLO curve in the region close to $N = 1$. In Sect. 4.3 we will investigate it more in detail. Anyway, the point $N = 2$ seems to be not affected that much from the small- N behaviour: we therefore conclude that $N_0 = 2$ is a good choice also for the Higgs production case.

To present the result in a more convenient way, we perform the same manipulations as before, to obtain the curves for τ_0 and M_0 as functions of \sqrt{s} in Fig. 4.5. The results are even more surprising than in Drell-Yan case: for LHC at 7 TeV, an approximately on-shell Higgs of more than about $M_0 \sim 100$ GeV (corresponding to $\tau_0 \sim 0.0002$) is dominated by the threshold region. It is surprising how small and far from threshold the value of τ_0 is; moreover, this result is phenomenologically relevant, because, if the Higgs boson exists, its mass will be higher than 114 GeV (the limit set by LEP), and then its production is always in the threshold region at LHC 7 TeV. This confirms the well known observation [65] that the Higgs boson production cross-section is dominated by the threshold contributions, but here we are also giving a quantitative evaluation of where and how this is true.

These considerations are even more dramatic in the Tevatron case: there, even an Higgs as light as $M_0 \sim 40$ GeV would be in the threshold region. Then, when looking for a Higgs boson of a reasonable mass at Tevatron, it is not a matter of choice whether to include or not the threshold resummation, since its effect would be non-negligible.

To conclude, we have to recall that, being the Higgs dominated by the gg channel, it is likely to be influenced more than other processes by small- x resummation. In particular, since at small τ the position of the saddle is mainly determined by the rightmost pole of the luminosity, and given that small- x resummation mainly affects the position and shape of such pole, the inclusion of small- x resummation may change quantitatively (even if not qualitatively) our conclusions. We will therefore investigate this in Sect. 4.3.

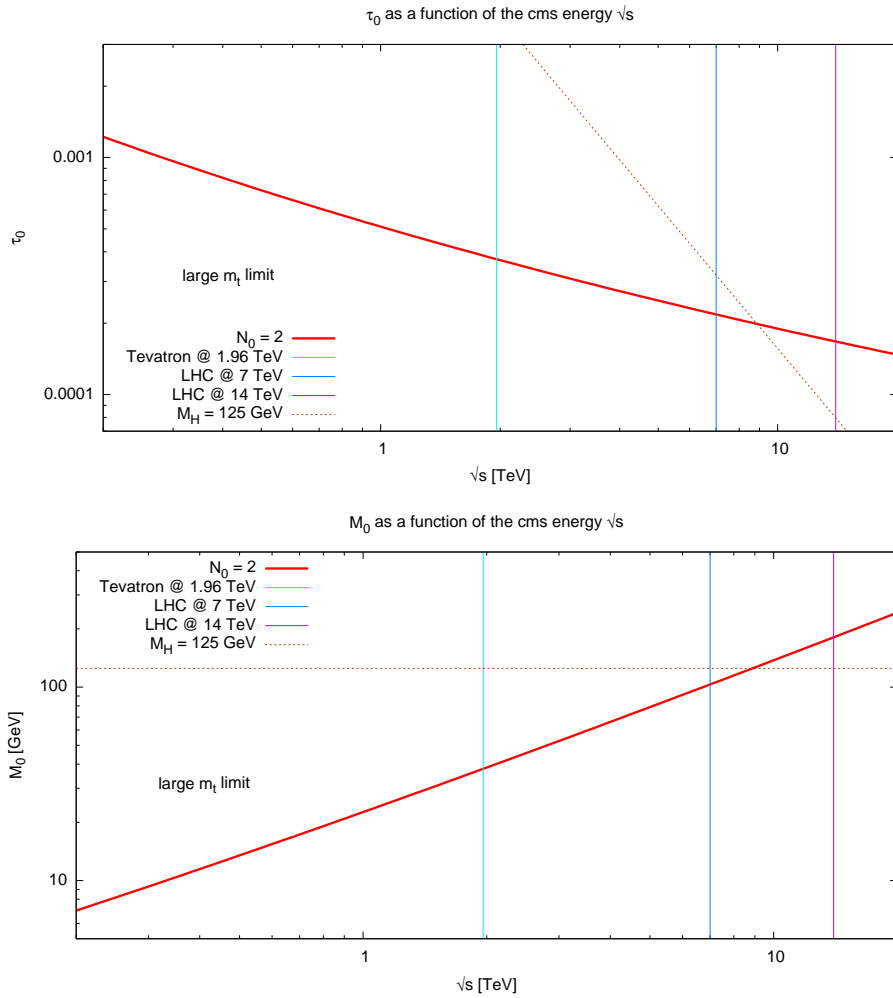


Figure 4.5. Dependence of τ_0 (upper plot) and M_0 (lower plot) on the collider c.m.s. energy \sqrt{s} for the Higgs production process. An hypothetical Higgs mass of 125 GeV is shown as a reference.

4.2 Phenomenology of high-energy resummation

Phenomenology of threshold resummation is rather easy to perform: one simply has to compute resummed coefficient functions and, with those at the hand, compute hadronic cross-sections. In principle, to be perfectly consistent, one should use PDFs fitted with resummed coefficient functions; nevertheless, the effect is expected to be small in the kinematical regions of the data used in the fit, and therefore “unresummed” PDFs can be used without losses of precision.

The case of high-energy resummation is instead very different. Beyond the coefficient functions, small- x resummation affects the anomalous dimensions, and the leading effect is in fact on the gluon anomalous dimensions. Therefore, in this case, one cannot use unresummed PDFs for phenomenological predictions, because in practice most of the effect is contained in the evolution of PDFs. Hence, small- x resummed anomalous dimensions (and coefficient functions) should be included in a PDF fit in order to have resummed PDFs suitable for phenomenology.

However, it is beyond the purpose of this thesis to perform such resummation task. An approximate way to have resummed PDFs is to simply evolve PDFs from a given scale, at which we trust the small- x behaviour, to the scale we are interested in. The smaller- x DIS data ($x \sim 10^{-4}$) were taken by ZEUS and H1 for a very low energy, $Q = 2 \div 3$ GeV, so we can consider this scale as the starting scale for a resummed evolution. Such procedure should be done fixing the data at the reference scale, and not simply the PDFs. To clarify, the procedure should be the following:

- first, we take a current PDF set and evolve the PDFs to the given small reference scale;
- then, we compute structure functions using *unresummed* coefficient functions;
- then, we extract back the PDFs using *resummed* coefficient functions:⁴ we have now initial conditions for the resummed PDFs;
- we evolve to the desired scale using the resummed anomalous dimensions.

Even if this procedure is not as good as a complete resummed fit, it allows to assess in a consistent framework the impact of small- x resummation.

4.2.1 Resummed PDFs at the initial scale

Usually, in PDF fits, the PDFs are extracted from DIS data using F_2 and its derivative with respect to $\log \mu^2$, which gives in particular information on the gluon PDF. We can then use these two quantities as reference at the initial scale. Omitting for simplicity the N and scale dependence (see Eq. (1.2.22) for the correct arguments) we may write

$$F_2 = \sum_i C_{2i} f_i \quad (4.2.1a)$$

$$\begin{aligned} F_2' &= \sum_i C'_{2i} f_i + \sum_{i,j} C_{2i} \gamma_{ij} f_j \\ &= \sum_j \left[C'_{2j} + \sum_i C_{2i} \gamma_{ij} \right] f_j \end{aligned} \quad (4.2.1b)$$

having denoted with a prime the $\mu^2 \frac{d}{d\mu^2}$ derivative.⁵ We can write the two equations in a matrix form

$$F = C f \quad (4.2.2)$$

with

$$F = \begin{pmatrix} F_2 \\ F_2' \end{pmatrix}, \quad f = \begin{pmatrix} f_g \\ f_S \\ (f_{ns}) \end{pmatrix}, \quad (4.2.3)$$

and C can be extracted from Eqs. (4.2.1). Note that we have separated the quark singlet and non-singlet contributions: this can be helpful because resummation affects

⁴For the resummation of coefficient functions see App. C.4.4.

⁵Note that we could also consider the prime as an α_s -derivative, provided we perform the substitution $\gamma_{ij} \rightarrow \gamma_{ij}/\beta(\alpha_s)$.

only singlet quantities. Indeed, we want to extract “resummed” initial PDFs using resummed coefficient function from the known functions F_2 and F_2' : there are many more unknowns than equations, but fortunately we know that the non-singlet PDFs are not affected by resummation, and then the only two unknowns are the “resummed” initial f_g and f_S . To make this more manifest, since the singlet and non-singlet do not interfere each other we may keep fixed just the singlet part of the structure function,

$$F_s = F - F_{\text{ns}}, \quad (4.2.4)$$

since the non-singlet part does not change with small- x resummation. Then, our equations are simplified to

$$F_s = C_s f_s \quad (4.2.5)$$

with

$$C_s = \begin{pmatrix} C_{2g} & C_{2q} \\ C'_{2g} + \sum_i C_{2i} \gamma_{ig} & C'_{2q} + \sum_i C_{2i} \gamma_{iq} \end{pmatrix}, \quad f_s = \begin{pmatrix} f_g \\ f_S \end{pmatrix}. \quad (4.2.6)$$

Then, using the procedure described above, the resummed PDFs at the initial energy are obtained as

$$f_s^{\text{res}}(\mu_0^2) = C_{s,\text{res}}^{-1}(\alpha_s(\mu_0^2)) C_s(\alpha_s(\mu_0^2)) f_s(\mu_0^2), \quad (4.2.7)$$

where $f_s(\mu_0^2)$ should be computed from a fixed-order PDF set.

The fixed-order singlet coefficient functions in the $\overline{\text{MS}}$ scheme are given by [4, 45]

$$C_{2i}(N, \alpha_s) = \frac{1}{n_f} \left(\sum_j e_j^2 \right) \left[\delta_{iq} + \alpha_s C_{2i}^{(1)}(N) + \mathcal{O}(\alpha_s^2) \right] \quad (4.2.8)$$

where e_j are the quark charges in unit of the electric charge and

$$C_{2g}^{(1)}(N) = \frac{n_f}{4\pi} \left[-\frac{\gamma_E + \psi(N+1)}{N} + 2\frac{\gamma_E + \psi(N+2)}{N+1} + 2\frac{\gamma_E + \psi(N+3)}{N+2} + \frac{1}{N^2} - \frac{2}{(N+1)^2} - \frac{2}{(N+2)^2} - \frac{1}{N} + \frac{8}{N+1} - \frac{8}{N+2} \right] \quad (4.2.9)$$

$$C_{2q}^{(1)}(N) = \frac{C_F}{2\pi} \left[\psi^2(N) + \left(2\gamma_E + \frac{3}{2} \right) \psi(N) + \gamma_E^2 - \zeta_2 + \frac{3}{2}\gamma_E - \frac{9}{2} + \psi_1(N+2) + \frac{\gamma_E + \psi(N+1)}{N} + \frac{\gamma_E + \psi(N+2)}{N+1} + \frac{3}{N} + \frac{2}{N+1} \right]. \quad (4.2.10)$$

4.2.2 Resummed evolution

Once the resummed PDFs at the initial scales $f_s^{\text{res}}(\mu_0^2)$ Eq. (4.2.7) has been computed, the evolution to the desired scale must be performed. To do this, we use for the resummed evolution of the singlet sector the discretized path-ordering evolution described in Sect. 1.4.3.1. The resummed anomalous dimensions are given in Sect. 3.6.3. We will see in the next Section the effect of this approximate procedure in the determination of the Higgs threshold region.

4.3 Joint effect of both resummations

As already pointed out in Sect. 4.1, small- x resummation of PDFs may have an effect on threshold resummation of coefficient functions. This fact comes from the observation [21, 25] that in the convolution, Eq. (4.1.1),

$$\sigma(\tau) = \int_{\tau}^1 \frac{dz}{z} \mathcal{L}\left(\frac{\tau}{z}\right) C(z, \alpha_s) \quad (4.3.1)$$

when the argument of the coefficient function is close to threshold, that is, when $z \rightarrow 1$, then the argument of the parton luminosity is small, $\tau/z \sim \tau$. Nevertheless, this simple observation does not tell us if this region gives the dominant contribution to the integral. The naive observation [21] is that, if the luminosity is peaked at small $x = \tau/z$, then it will give the dominant contribution to the integral. The saddle-point argument discussed in Sect. 4.1 had exactly the aim of quantifying this aspect; the price to pay is that the formulation of the argument is done in N space, where the simple relation between the high-energy and the threshold regions is no longer clear. Indeed, in N space the convolution becomes

$$\sigma(N) = \mathcal{L}(N) C(N, \alpha_s) \quad (4.3.2)$$

where both the luminosity and the coefficient function are computed at the same N . Therefore, the naive identification of the threshold and high-energy regions with the large- and small- N regions respectively seems to point out that both functions should contribute in the same region. This is not true, of course: we have proved that the saddle-point, which gives the dominant contribution to the Mellin inversion integral, is pushed to large N because of the small- N shape of the luminosity. Therefore, we recover the conclusion drawn above.

Here, we want to revisit the result in momentum space, to better clarify the relation between the two regions. To begin with, it is convenient to rewrite Eq. (4.3.1) in the form

$$\begin{aligned} \sigma(\tau) &= \int_0^1 dx \int_0^1 dz \delta(xz - \tau) \mathcal{L}(x) C(z, \alpha_s) \\ &= \int_0^1 dx \int_0^1 dz \delta(xz - \tau) \int \frac{dN_1}{2\pi i} e^{N_1 \log \frac{1}{x} + \log \mathcal{L}(N_1)} \int \frac{dN_2}{2\pi i} e^{N_2 \log \frac{1}{z} + \log C(N_2, \alpha_s)}, \end{aligned} \quad (4.3.3)$$

$$(4.3.4)$$

where in the second row we have written the luminosity and the coefficient function as the inverse Mellin transform of their Mellin transforms. We did it because now we want to consider the saddle-points for each inverse Mellin separately:

$$\log \frac{1}{x} + \frac{\mathcal{L}'(\bar{N}_1(x))}{\mathcal{L}(\bar{N}_1(x))} = 0, \quad \log \frac{1}{z} + \frac{C'(\bar{N}_2(z))}{C(\bar{N}_2(z))} = 0; \quad (4.3.5)$$

note that, because of the δ function, x and z always satisfy $xz = \tau$. At some point \bar{x} , the two saddle will coincide

$$\bar{N}_1(\bar{x}) = \bar{N}_2(\bar{z}) \equiv N_0(\tau), \quad \bar{z} = \frac{\tau}{\bar{x}}, \quad (4.3.6)$$

where we have noted that this point is completely determined by τ . It turns out that $N_0(\tau)$ is the saddle-point for $\sigma(\tau)$, since putting together the definitions Eq. (4.3.5) we have

$$\log \frac{1}{\tau} + \frac{\mathcal{L}'(N_0(\tau))}{\mathcal{L}(N_0(\tau))} + \frac{C'(N_0(\tau))}{C(N_0(\tau))} = 0 \quad (4.3.7)$$

which is the saddle-point condition for $\sigma(\tau)$, Eq. (4.1.7). We have already discussed in Sect. 4.1 that the hadronic saddle-point gives the dominant contribution to $\sigma(\tau)$. We conclude from this discussion that, in momentum space, the main contributions to $\sigma(\tau)$ come from the region around $x = \bar{x}$ ($z = \bar{z}$). As discussed in Sect. 4.1.2, the hadronic saddle N_0 is mostly determined by the luminosity, being the contribution from the coefficient function negligible (at least when τ is small). Then, we expect \bar{x} to be rather close to τ , thereby implying that \bar{z} is expected to be rather close to 1. This completes our argument: we have proved that, in fact, in the convolution Eq. (4.3.1) the main contribution comes from the region $z \sim 1$, i.e. when the coefficient function is in the threshold region and the luminosity is in the high-energy region.

Having this in mind, we now turn to the study of the effect of small- x resummation to the determination of the saddle-point. We won't cover the case of Drell-Yan, since $q\bar{q}$ channel (which dominates at threshold) is not expected to get significant contribution from small- x resummation, since the quark PDFs are affected only at NLL level. Conversely, the Higgs production being dominated at threshold by the gg channel, is expected to get sizable contribution from small- x resummation, since the gluon PDF is affected at the LL level.

4.3.1 Joint effect on Higgs production

Using the approximate procedure drawn in Sect. 4.2 to implement small- x resummation, we present here the effect of resummed PDFs in the determination of the threshold region for Higgs production.

The results presented here will differ from those of Sect. 4.1.4 in the following aspects:

- the full m_t dependence is considered (see Ref. [69] and App. C.2.1): this allows to have the correct small- x behaviour of the coefficient function, which is instead wrong in the large- m_t approximation;
- the gluon PDF used for the computation of the luminosity is resummed according to the procedure of Sect. 4.2.

In principle, we should also include the small- x resummed Higgs coefficient function [70]: however, since it affects the coefficient function, the effect should be small compared to the effect of resummation on PDFs. Also the effect of the finite top mass turns out to be almost negligible.

In Fig. 4.6 the same plots of Fig. 4.5 are shown, with the modifications described above. We see that the threshold region now begins at higher masses (higher τ 's): for example, from these plot we discover that actually threshold resummation is not that important even at the LHC at 7 TeV.

The result is rather unexpected: since small- x resummation makes the rise of the gluon PDF stronger at small- x , one naively expects that the saddle-point should move

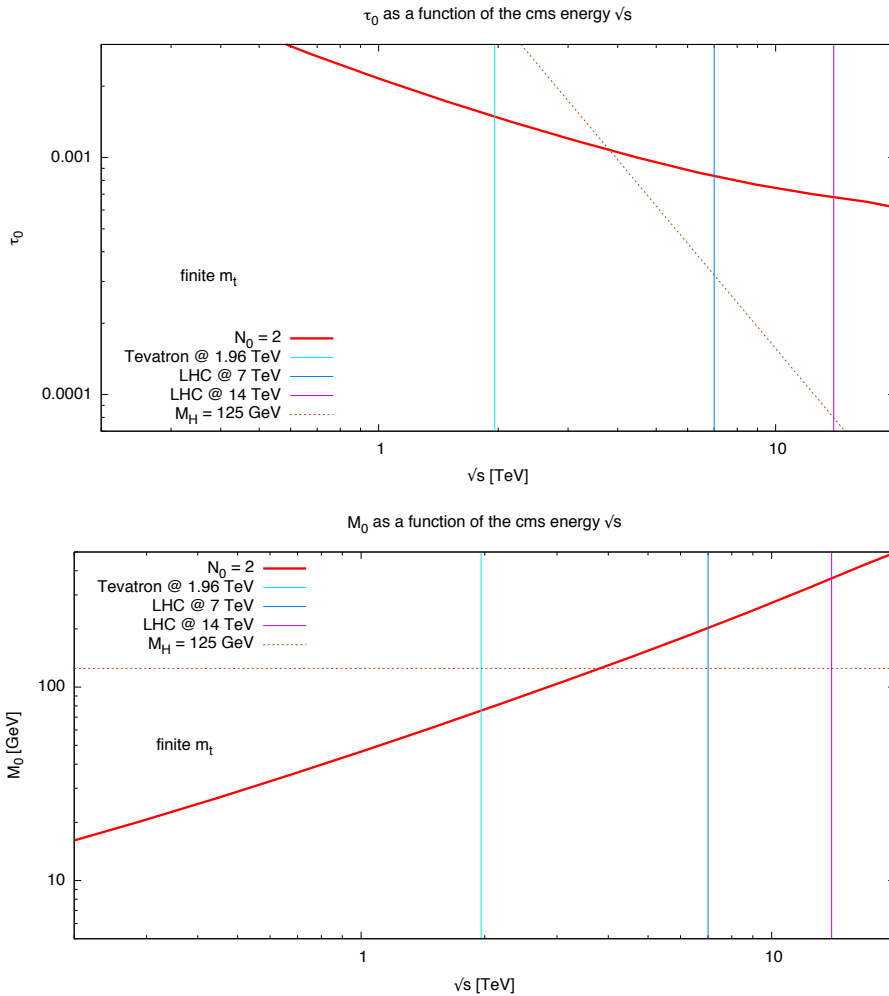


Figure 4.6. Dependence of τ_0 (upper plot) and M_0 (lower plot) on the collider c.m.s. energy \sqrt{s} for the Higgs production process. The approximate resummed PDFs described in Sect. 4.2 are used. The curves are obtained with full m_t dependence.

to larger values of N . However, the small- x rise is located at very small N , very close to the Bateman pole. From Fig. 3.5 one sees indeed that the Bateman pole is located roughly at $N \sim 0.2$: remember however that the anomalous dimension is defined as in Eq. (1.3.7), so that its argument is shifted by a unity with respect to the usual definition for the other quantities, as those used here. Therefore, the Bateman pole affects the cross-section $\sigma(N)$ in the region close to $N \sim 1.2$, which is not relevant for the determination of the saddle-point in $N_0 = 2$. Instead, the saddle-point $N_0 = 2$ is influenced by the region around $N = 1$ in the plot of Fig. 3.5, where momentum conservation constraint imposes $\Delta\gamma_+$ to be zero. In particular, the N -derivative there is negative, thereby justifying the effect of moving the saddle-point to lower values of N , that is to say to move τ_0 Eq. (4.1.19) to larger values.

We emphasize that these results are obtained with the approximate implementation of small- x resummation. It may well be that the proper implementation of small- x resummation in a PDF fit gives a somewhat different result. Be this result correct or wrong, it clearly shows the importance of a good understanding of the impact of small-

x resummation at hadron colliders: this should be a strong motivation for PDF fitter community to include resummed anomalous dimensions and coefficients functions in the fit.

4.4 Toward a joint resummation

As last argument of this Chapter, we discuss the possibility and the implications of a joint resummation of both the high-energy and the threshold logarithms.

What we would like to discover is that a joint resummed cross-section is as close as possible to the “full result”. This sentence is a bit misleading, because the full result, which would correspond to the sum of the full perturbative series, is of course unknown. The way to interpret the sentence is just the requirement that the remaining unresummed pieces behave perturbatively.

As a preliminary test, we consider again the Higgs production, and in particular the NLO coefficient function. Since we are interested in the small- x behaviour, we must work at finite m_t . The large- N logarithms which would be reproduced in a NLL or higher threshold resummation are

$$C_{\text{BP}_2}^{(1)}(N) = \frac{2C_A}{\pi} \left[\psi_0^2(N) + 2\gamma_E \psi_0(N) + 2\zeta_2 + \gamma_E^2 + \frac{11}{12} \right], \quad (4.4.1)$$

where the subscript BP₂ reflects the fact that these logs are those generated by resummation if the Borel prescription of Eq. (2.1.62) is used (see discussion in Sect. 2.1.5). The small- N behaviour has been determined at NLO with full m_t dependence in Ref. [70]: it is

$$C_{\text{sx}}^{(1)}(N) = c \frac{C_A}{\pi} \frac{\alpha_s}{N-1}, \quad (4.4.2)$$

where the coefficient c depends on the Higgs mass, and for $m_H = 125$ GeV it is $c \simeq 4.522$. The sum of these two opposite approximations provides our NLO prototype of a joint resummed coefficient:

$$C_{\text{joint}}^{(1)}(N) = C_{\text{BP}_2}^{(1)}(N) + C_{\text{sx}}^{(1)}(N). \quad (4.4.3)$$

The difference

$$C^{(1)}(N) - C_{\text{joint}}^{(1)}(N) \quad (4.4.4)$$

is the NLO remainder term, i.e. the lowest-order term which would be neglected in a joint resummed coefficient function.

To verify our guess, that the remainder terms behave perturbatively, we start by inspecting the size of this term at NLO. In Fig. 4.7 all the quantities mentioned above are shown. Indeed, the remainder term is absolutely very small for $N \gtrsim 2$, and relatively small everywhere. In particular, at $N \sim 2$ where the relative size of the remainder term is largest, its magnitude is about 3, which multiplied by $\alpha_s \sim 0.1$ (as appropriate at the scale $m_H = 125$ GeV) gives a small contribution 0.3. Assuming that this behaviour is not changed at higher orders, we would conclude that the remainder terms behave indeed perturbatively.

Moreover, the other important observation is that the small- and large- N regions overlap, the first being dominant for $N \lesssim 1.5$ and the second for $N \gtrsim 2$. Therefore,

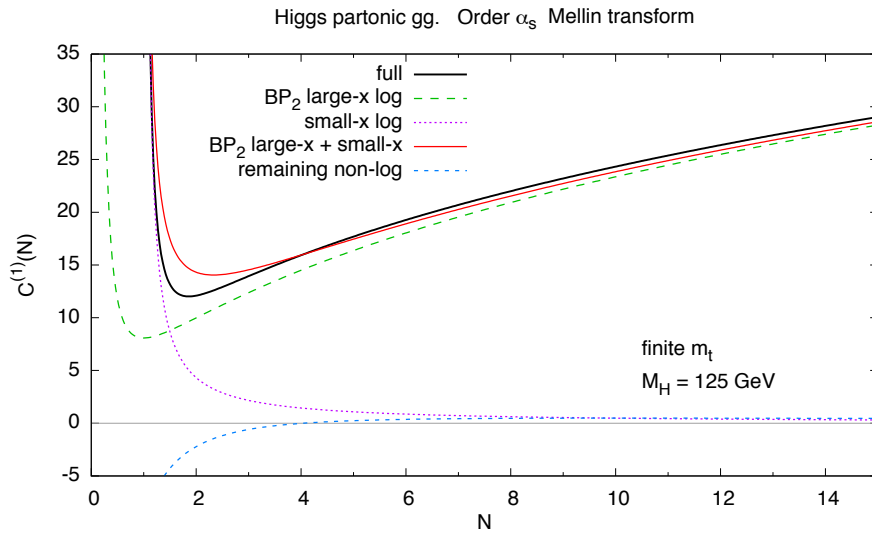


Figure 4.7. The order α_s Higgs partonic coefficient function $C^{(1)}(N)$ plotted as a function of N (black solid curve) and its small- and large- N logarithmic approximations. The curves are obtained with full m_t dependence.

there is a very tight region in which non-log effects may be relevant, enforcing our guess that even at higher orders non-log contributions cannot become too large.

To conclude, we stress that jointly resummed cross-section may be very accurate (at least for the Higgs production case), and that the inclusion of non-logarithmically enhanced terms from fixed-order computations may be considered as a perturbatively stable improvement of such resummed cross-sections.

5 Phenomenology

Contents

5.1 The Drell-Yan pair production	105
5.1.1 Uncertainties	109
5.1.2 Results and comparison with data	114
5.1.3 Comparison of the different prescriptions	126

In this Chapter we will present application of soft-gluon and high-energy resummation for phenomenology. We will present results for the Drell-Yan pair production process. Such process is expected not to get relevant contributions from high-energy logarithms, since the production is dominated by the quark-antiquark channel: we will then show only results from threshold resummation, and compare them to data. It would be more interesting to study the Higgs production process: being dominated by the gluon-gluon channel, it is expected to get a sizable contribution from the high-energy region; moreover it is well known [65] that the main contributions to the Higgs production come from the threshold region. Unfortunately, this is still work in progress, and we will not provide results here.

5.1 The Drell-Yan pair production

The Drell-Yan process is likely to be the standard candle which is both theoretically calculable and experimentally measurable with highest accuracy at hadron colliders, in particular the LHC. It consists in the production of a neutral or charged lepton pair, $\ell\bar{\ell}$ or $\ell\bar{\nu}$, in the collision of two initial hadrons H_1 and H_2 :

$$H_1(p_1) + H_2(p_2) \rightarrow \ell(k_1) + \bar{\ell}(k_2) + X(q) \quad (\text{neutral}) \quad (5.1.1)$$

$$\rightarrow \ell(k_1) + \bar{\nu}(k_2) + X(q) \quad (\text{charged}) \quad (5.1.2)$$

where X is the entire set of other hadronic stuff produced in the event. The process is sketched in Fig. 5.1. A large abundance of events collected at the LHC, combined with a very precise theoretical determination of the process, can be a very powerful test of perturbative QCD. Moreover, the high LHC energy will allow for detailed measurements at a previously unexplored kinematic domain of low parton momentum fraction at a high energy scale, significantly improving the precision on the determination of the PDFs.

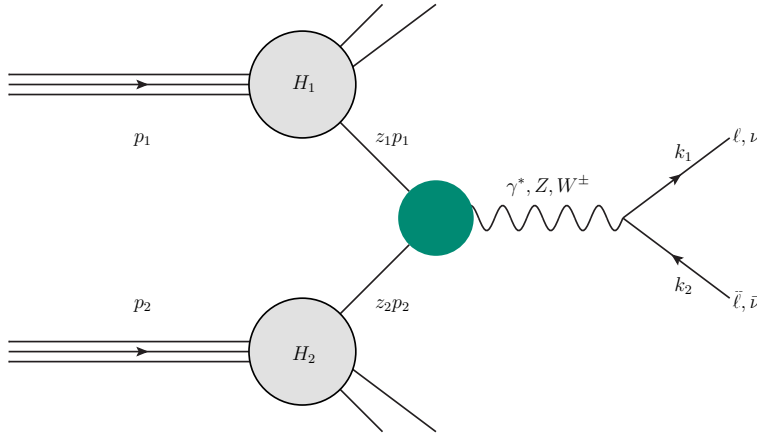


Figure 5.1. The Drell-Yan process at leading order in electroweak interactions. The green ball contains the QCD corrections to the process, including real emissions.

At leading order in both electroweak and QCD the partonic process consists of a quark and an antiquark annihilating into a virtual vector boson γ , Z or W^\pm , which subsequently decays into the lepton pair. At this order all the available partonic center-of-mass energy $\sqrt{\hat{s}}$,

$$\hat{s} = z_1 z_2 s, \quad s = (p_1 + p_2)^2, \quad (5.1.3)$$

goes into the lepton pair invariant mass M ,

$$M^2 = (k_1 + k_2)^2 \quad (5.1.4)$$

(z_1, z_2 are the momentum fractions of the two partons), and the inclusive cross-section is characterized by the variable

$$\tau = \frac{M^2}{s} \quad (5.1.5)$$

which describes the amount of initial hadronic energy going into the relevant final state (the lepton pair). When QCD correction to the initial partons are considered, real emission of gluons and quarks must be taken into account, in order to remove infrared divergences coming from virtual corrections (see discussion in Sect. 1.2.2): in this case the available partonic center-of-mass energy is no longer equal to the final state mass. We can then introduce the variable

$$z = \frac{M^2}{\hat{s}} = \frac{\tau}{z_1 z_2} \quad (5.1.6)$$

which is the partonic analog to τ : the Born amplitude (and its virtual corrections) selects $z = 1$, while in the case of real emissions $0 \leq z \leq 1$. As discussed in Sect. 2.1, in the coefficient function logarithms of $1 - z$ appear: in the soft limit $z \rightarrow 1$ the resummation of the entire perturbative series is needed.

The current QCD theoretical accuracy for this process is NNLO, both for integrated cross-section [71] and rapidity-distributions [72]; explicit formulae up to NLO can be found in App. C.1. Also, small effects such as those related to the coupling of the gauge boson to final-state leptons have been studied recently [73].

Whereas the resummation of contributions related to the emission of soft gluons are routinely included in the computation of Drell-Yan transverse-momentum distributions [74], where they are mandatory in order to stabilize the behaviour of the cross-section at low transverse momenta, their impact on rapidity distributions, as well as inclusive cross-section, has received so far only a moderate amount of attention. This is partly due to the fact that even in fixed-target Drell-Yan production experiments, such as the Tevatron E866 [75–77], let alone LHC experiments, the available center-of-mass energy is much larger than the mass of typical final states, thereby suggesting that threshold resummation is not relevant.

However, we have abundantly discussed in Sect 4.1 that resummation may be relevant even far from hadronic threshold. Indeed, in Ref. [35] threshold resummation has been claimed to affect significantly Drell-Yan production for E866 kinematics, though somewhat different results have been found in Ref. [28]. It is important to observe that Drell-Yan data from E866 and other fixed-target or collider Tevatron experiments play a crucial role in the precision determination of parton distributions such as MSTW08 [78], NNPDF2.0 [64] or CT10 [79], so their accurate treatment is crucial for precise LHC phenomenology. Neither threshold resummation has been so far included in predictions for the LHC, such as those of Ref. [80].

Then, in this Section we will present a detailed phenomenological study [25] of the impact of threshold resummation on inclusive cross-section and rapidity distributions for the Drell-Yan process, and compare it with an analogous study performed in the context of SCET [28].

We will therefore consider three cases: pp collisions at a center-of-mass energy of 38.76 GeV, which corresponds to the case of the experiment E866/NuSea, taken as representative of Tevatron fixed-target experiments; $p\bar{p}$ collisions at the Tevatron collider energy of $\sqrt{s} = 1.96$ TeV; and the LHC case, pp collisions at the intermediate energy of $\sqrt{s} = 7$ TeV. For the Tevatron and LHC configurations, we will consider both charged ($\ell\bar{\nu}$) and neutral ($\ell\bar{\ell}$) Drell-Yan pairs, taking into account in the latter case the interference between virtual Z and γ . Lepton masses will always be neglected. We will show results for both the invariant mass distribution as a function of $\tau = M^2/s$, and for the doubly-differential distribution in invariant mass and rapidity as a function of the rapidity for fixed values of τ . Specifically, for invariant mass distributions we will show results for the K -factor defined as

$$K\left(\tau, \frac{\mu_F^2}{M^2}, \frac{\mu_R^2}{M^2}\right) = \frac{\frac{d\sigma}{dM}\left(\tau, \frac{\mu_F^2}{M^2}, \frac{\mu_R^2}{M^2}\right)}{\frac{d\sigma^{\text{LO}}}{dM}(\tau, 1, 1)}, \quad (5.1.7)$$

where μ_F and μ_R are the factorization and renormalization scale, respectively. Since we will be considering different experimental configurations, the results for the K -factors will be shown for fixed value of s , with M^2 determined by the value of τ , $M^2 = \tau s$. The Born cross-section $\frac{d\sigma^{\text{LO}}}{dM}(\tau, 1, 1)$, which provides the scale for these plots, is shown in Fig. 5.2 for LHC at 7 TeV and Tevatron at 1.96 TeV.

Our aim will be to assess the potential impact of inclusion of resummation effects on cross-sections and their associate perturbative uncertainty, both on experiments which are already used for PDF determinations (and thus, potentially, on the PDF extraction itself), as well as on future LHC measurements, both for real W and Z production as

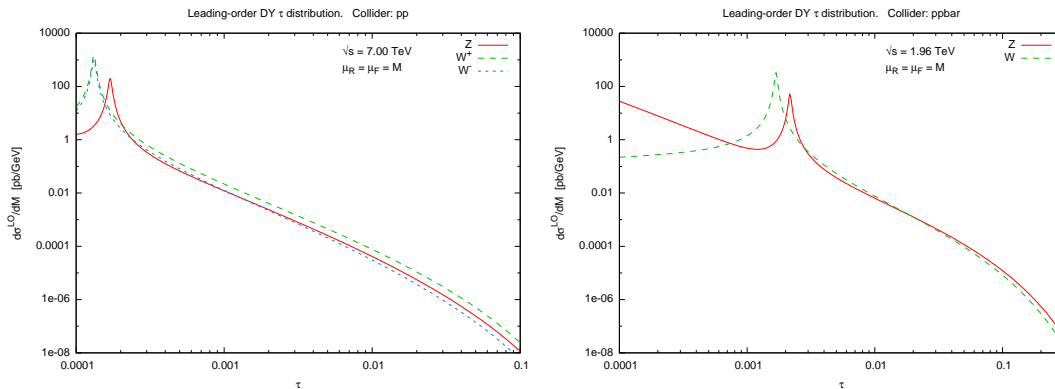


Figure 5.2. The invariant mass distribution of charged and neutral Drell-Yan pairs in pp collisions at $\sqrt{s} = 7$ TeV (left) and in $p\bar{p}$ collisions at $\sqrt{s} = 1.96$ TeV (right) computed at leading order with NNPDF2.0 parton distributions at $\alpha_s(m_Z^2) = 0.118$.

well as for high-mass 1 TeV Drell-Yan pair (relevant for instance as a background to hypothetical Z' production). For each observable, we will show fixed-order predictions at leading, next-to-leading and next-to-next-to-leading order, and, correspondingly, leading, next-to-leading and next-to-next-to-leading log resummed curves.

All curves will be computed using a fixed (NLO) set of parton distributions. In a realistic situation, parton distributions would be refitted each time at the corresponding perturbative order; the effect of the perturbative corrections on the hard cross-section is then partly reabsorbed in the PDFs (with fixed experimental data), and the effect on the Drell-Yan process gets tangled with the effect on other processes which are used for PDF fitting. Hence, a comparative assessment of size of various perturbative corrections on cross-sections and uncertainties, which is our main aim here, can only be done with fixed PDF. It should be born in mind, however, that our predictions will only be fully realistic when considering the NLO case.

In order to assess perturbative uncertainties, we will perform standard variations of factorization and renormalization scales, and furthermore in order to assess the ambiguities related to the resummation procedure we will compare results obtained with the minimal and Borel prescriptions, as discussed in Chap. 2: specifically, for the Borel prescription we will use the modified BP₂ Eq. (2.3.10), which provides a more moderate but realistic estimate of ambiguities as discussed in Sect. 2.1.5, and take $W = 2$ (see Sect. 2.1.4). Actually, we are going to present the results published in Ref. [25], where the constant terms coming from the distributions are resummed as well, see discussion in Sect. 2.1.5.1; we will discuss it in Sect. 5.1.3. Note that we have checked explicitly that also at the hadronic level curves obtained using the Borel prescription Eq. (2.1.46), which contains logarithms of $\frac{1}{2}$, are indistinguishable from those obtained with the minimal prescription, in agreement with the discussion in Sect. 2.1.5, provided τ itself is not too close to threshold: we will come back on that in Sect. 5.1.3.

Other sources of uncertainty will be discussed briefly in Sect. 5.1.1, where we will provide an overall assessment of uncertainties related to the value of the strong coupling and to the parton distributions, and then present and evaluate critically the use of scale

variation to assess perturbative uncertainties. In the remainder of this Section detailed predictions for the three cases of interest will be presented.

5.1.1 Uncertainties

Theoretical predictions for the Drell-Yan process are affected by a number of uncertainties, related to the treatment of both the strong and electroweak interactions. Of course, in a realistic experimental situation further uncertainties arise because of the need to introduce kinematic cuts, which in turns requires comparing to fully exclusive calculations [81]. Here, we will make no attempt to estimate the latter, nor electroweak uncertainties and their interplay with strong corrections (see e.g. Ref. [80] for a recent discussion), and we will concentrate on uncertainties related to the treatment of the strong interactions. Before turning to an assessment of the way higher order corrections can be estimated from scale variation, we discuss uncertainties related to the value of the strong coupling and to the choice of parton distributions (PDFs).

5.1.1.1 Uncertainties due to the parton distributions and α_s

The uncertainty due to PDFs is usually dominant in hadron collider processes. Tevatron Drell-Yan data are used for PDF determination, so PDF uncertainties here reflect essentially the current theoretical uncertainty in knowledge of this process, as well as possible tension between Drell-Yan data and other data which go into global PDF fit (which however seems [64] to be very moderate). Predictions for the LHC are affected by sizable PDF uncertainties because of the need to extrapolate to a new kinematical region, and also, in the case of Drell-Yan, because at the LHC, unlike at the Tevatron, one of the two PDFs which enter the leading-order process is sea-like.

PDF uncertainties for the invariant mass distribution of neutral Drell-Yan pairs at $\sqrt{s} = 7$ TeV are shown in Fig. 5.3 as a function of $\tau = M^2/s$. We use NNPDF2.0 PDFs with $\alpha_s(m_Z^2) = 0.118$; other PDF sets are expected to give similar results [82]. Because we are using a fixed PDF set, the uncertainty does not depend significantly on the perturbative order, or the inclusion of resummation. It ranges between 5% and 15% for $\tau \lesssim 0.1$. For larger values of τ the cross-section becomes essentially undetermined, because there are no data in PDF global fits to constrain PDFs in that region: the few available large- x data are at much lower scale, and the uncertainty due to lack of information at very large $x \gtrsim 0.5$ contaminates PDFs down to $x \gtrsim 0.1$ when evolving up to the LHC scale. Note however that the Drell-Yan cross-section at large $\tau \gtrsim 0.1$ rapidly drops to unmeasurably small values (see Fig. 5.2). The fact that PDF uncertainties blow up for $\tau \gtrsim 0.1$ implies that data in this region would allow a determination of PDFs in a region where they are currently almost unknown; conversely, any signal of new physics in this region would have to be validated by measurements in an independent channel (such as for example jet production) which provides an independent constraint on the relevant PDFs.

In Fig. 5.4 we show the PDF uncertainties for the rapidity distribution of neutral Drell-Yan pairs with $M = 1$ TeV at $\sqrt{s} = 7$ TeV, again using the NNPDF2.0 set with $\alpha_s(m_Z^2) = 0.118$. As in the previous case, the PDF uncertainty does not depend significantly on the perturbative order, and it is typically larger than 5%.

We now turn to the uncertainty due to the value of α_s . The current PDG [83] value

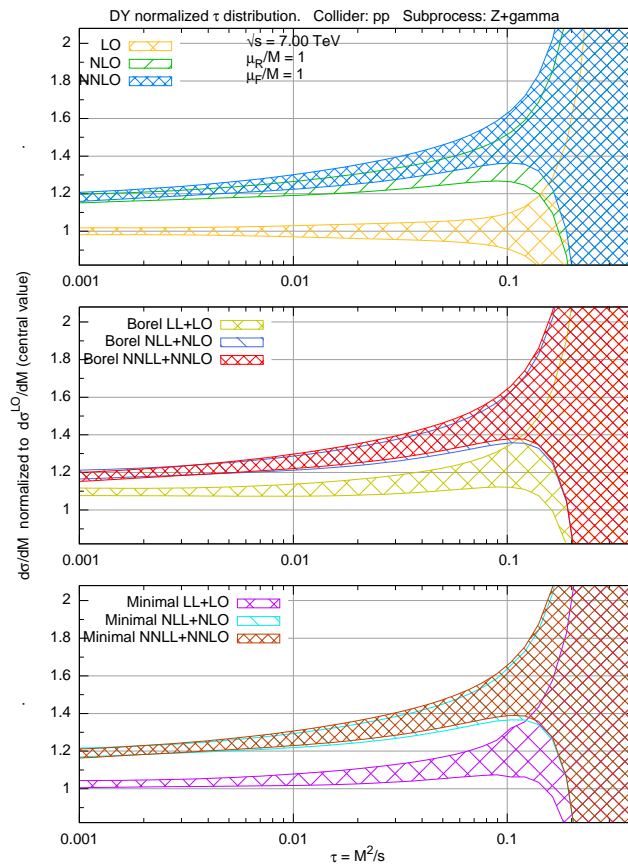


Figure 5.3. Invariant mass distribution of neutral Drell-Yan pairs in pp collisions at $\sqrt{s} = 7$ TeV. The band corresponds to the PDF uncertainty, using the NNPDF2.0 set with $\alpha_s(m_Z^2) = 0.118$.

for $\alpha_s(m_Z^2)$ is taken from Ref. [84] and it is 0.1184 ± 0.0007 . However, this uncertainty seems quite small, especially when taking into account the fluctuation in central values between the determinations that go into it, and the dependence on the perturbative order of some of them: indeed, current recommendations for precision LHC studies from the PDF4LHC group [82] advocate a rather more conservative uncertainty estimate. We thus take

$$\alpha_s(m_Z^2) = 0.118 \pm 0.002 \quad (5.1.8)$$

as a reasonable current range.

The impact of this uncertainty on α_s on the Drell-Yan cross-section at $\sqrt{s} = 7$ TeV can be estimated from Fig. 5.5, where we show the effect on the inclusive Drell-Yan cross-section due to variation in the range Eq. (5.1.8) of the value of $\alpha_s(m_Z^2)$ used both in the computation of the hard matrix element and the PDF evolution. Results are only shown for $\tau < 0.1$, because for larger value the PDF uncertainty blows up and results loose significance, as discussed above. Note that this full dependence of the physical cross-section on α_s is in general somewhat different from the dependence of the hard matrix element alone, because of the dependence on α_s of the relevant parton luminosity. This total dependence might be larger or smaller according to whether the luminosity is correlated or anticorrelated to the value of α_s , either of which might be

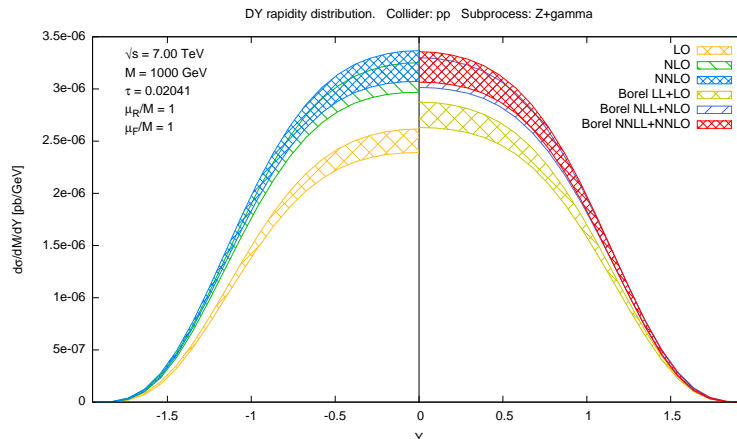


Figure 5.4. Rapidity distribution of neutral Drell-Yan pairs with invariant mass $M = 1$ TeV in pp collisions at $\sqrt{s} = 7$ TeV. Unresummed results are shown for negative Y and resummed results for positive Y . The band corresponds to the PDF uncertainty, obtained by the NNPDF2.0 set with $\alpha_s(m_Z^2) = 0.118$.

the case for a quark luminosity, according to the kinematic region [64]. A priori, the size of the uncertainty due to variation of α_s in the matrix element and that due to the dependence on α_s of the PDFs are likely to be comparable: after all, the Drell-Yan rapidity distribution plays a significant role in the determination of the PDFs themselves.

It appears from Fig. 5.5 that the α_s uncertainty increases with the perturbative order, but it is of similar size at the resummed and unresummed level; at NNLO it is of order of $\sim 1.5\%$ at LHC energies; we have checked that it is about a factor two larger at Tevatron fixed-target experiments. The uncertainty due to α_s on rapidity distributions is clearly of comparable size.

Noting that within the approximation of linear error propagation the PDF and α_s uncertainties should be combined in quadrature [85], we conclude that PDF uncertainties are somewhat larger than α_s uncertainties and the combined effect of PDF and α_s uncertainties is likely to be smaller than about 10% but not much smaller, at least in the region in which PDFs are constrained by presently available data. Once PDF uncertainties will be reduced due to LHC data, it should be possible to keep the combined effect of these uncertainties at the level of few percent. Therefore, perturbative accuracies at the percent level are relevant for precision phenomenology.

5.1.1.2 Perturbative uncertainties: scale variations

A standard way of estimating unknown higher order perturbative corrections is to vary factorization and renormalization scales. We perform this variation by writing the generic factorized cross-section as

$$\sigma(N, M^2) = \mathcal{L}(N, \mu_F^2) C \left(N, \alpha_s(\mu_R^2), \frac{M^2}{\mu_F^2}, \frac{M^2}{\mu_R^2} \right), \quad (5.1.9)$$

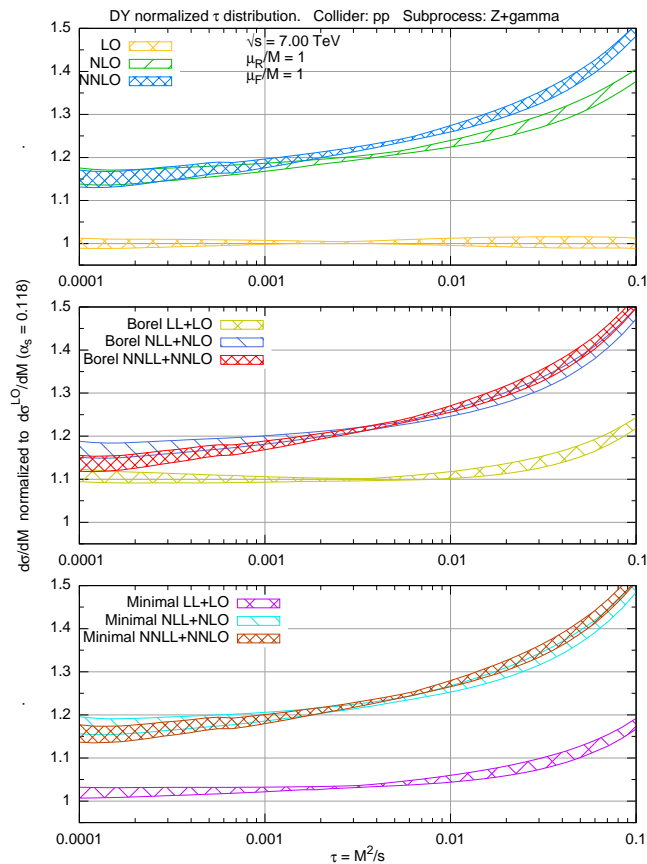


Figure 5.5. Invariant mass distribution of neutral Drell-Yan pairs in pp collisions at $\sqrt{s} = 7$ TeV. The uncertainty bands corresponds to a variation of $\alpha_s(m_Z^2)$ in the range 0.116 to 0.120 in the hard matrix element and in the parton distributions; NNPDF2.0 parton distributions are used.

which is independent of μ_F^2 and μ_R^2 at the order at which the partonic coefficient $\hat{\sigma}\left(N, \alpha_s(\mu_R^2), \frac{M^2}{\mu_F^2}, \frac{M^2}{\mu_R^2}\right)$ is computed. The residual scale dependence is therefore of the first neglected order, and can be used as an estimate of the higher order terms in the perturbative expansion. We vary the two scales in the range

$$\left|\log \frac{\mu_F}{M}\right| \leq \log 2, \quad \left|\log \frac{\mu_R}{M}\right| \leq \log 2, \quad \left|\log \frac{\mu_R}{\mu_F}\right| \leq \log 2, \quad (5.1.10)$$

depicted in Fig. 5.6, which guarantees that both higher-order corrections to the partonic cross-section and to perturbative QCD evolution are generated, with the last condition ensuring that no artificially large scale ratios are introduced.

In the sequel, we will perform scale variation of both unresummed and resummed cross-sections. The interpretation of results deserves a comment. When performing scale variation of a result determined at fixed $\mathcal{O}(\alpha_s^k)$, one generates terms of $\mathcal{O}(\alpha_s^{k+1})$: consequently, the scale uncertainty is reduced as one increases the perturbative order. However, terms generated by scale variation are proportional to those which are present at the given order: therefore, scale variation underestimates the size of higher order corrections when these are enhanced by higher logarithmic powers. For instance,

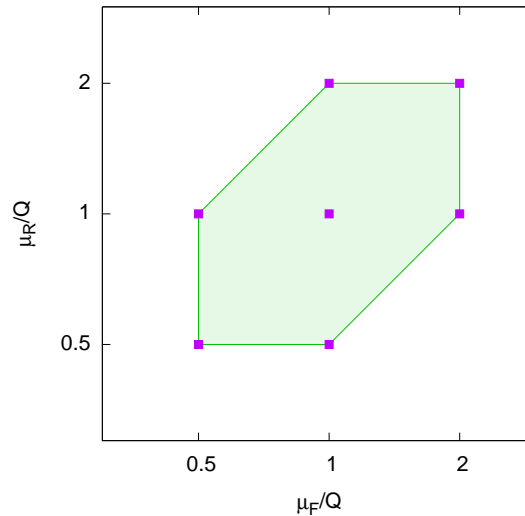


Figure 5.6. Scale variation grid; the cross-section is computed in correspondence of the purple dots.

scale variation of the $\mathcal{O}(\alpha_s)$ Drell-Yan coefficient function $C_1(N)$ Eq. (2.1.73) produces terms which at large N grow at most as $\log^2 N$, whereas the actual $\mathcal{O}(\alpha_s^2)$ $C_2(N)$ coefficient function at large N grows as $\log^4 N$. Hence, if N is so large that these terms dominate the coefficient functions and must be resummed to all orders their impact might be rather larger than the scale variation of the fixed-order result may suggest. Nevertheless, in this case the scale dependence of the resummed result will still be smaller than that of the fixed order result because the resummed result includes the dominant contributions to the cross-section to all orders.

However, in Sect. 4.1.3 we have seen that there is an intermediate kinematic region in which logarithmically enhanced contributions may provide a sizable fraction of the coefficient function even though $\alpha_s \log^2 N \ll 1$: in this case, the resummation improves the fixed-order result in that it includes a sizable fraction of the higher order correction, but it still behaves in a perturbative way, i.e. terms of higher order in α_s included through the resummation give an increasingly small contribution. If so, the scale dependence of the resummed result may well be comparable to or even larger than that of the fixed order result, because the resummation amounts to the inclusion of large terms in the next few higher orders, which are not necessarily seen when performing the scale variation of the lower orders. Furthermore, resummation only affects the quark channel, while fixed-order scale variation mixes the quark and gluon channels: in an intermediate region, the logarithmic terms in the quark channel may be sizable, but with the gluon channel not being entirely negligible. In such case, the scale variation is dominated by subleading terms and thus we expect the residual scale dependence of the resummed result to differ according to the resummation prescription. We will see that this is indeed the case for resummation of Tevatron rapidity distributions, with scale variation of resummed results different according to whether the Borel or minimal prescription is used.

5.1.2 Results and comparison with data

In this Section we present the prediction for the K -factors and the rapidity distributions both at the unresummed level and at the resummed level, using in the latter case both the minimal and Borel prescriptions. When available, we compare our predictions with data. We want to remember again that we use NNPDF2.0 NLO PDFs set: then, our prediction are reliable and comparable with data consistently only at NLO.

5.1.2.1 Tevatron at fixed target: NuSea

We begin by studying the invariant mass distribution of lepton pairs produced by collisions of a proton beam of energy $E = 800$ GeV on a proton or deuteron target, at rest in the laboratory ($\sqrt{s} = 38.76$ GeV). This is the experimental configuration of the experiment E866/NuSea. We first consider the inclusive invariant mass distribution. Results are shown in Fig. 5.7. All uncertainties shown here and henceforth are due to scale variation as described in Sect. 5.1.1.2. As expected, the width of the error bands decreases with increasing perturbative order. Note that for sufficiently small τ the uncertainty blows up, due to the fact that for fixed s the small τ limit corresponds to low scale: for example, at this energy $\tau = 10^{-3}$ corresponds to $M \approx 1.2$ GeV, and varying the scales as in Eq. (5.1.10) the values $\mu_R, \mu_F \approx 0.6$ GeV are reached.

Turning now to the resummed results, we note that the numerical impact of resummation is large for $\tau \gtrsim 0.1$, while for $0.03 \lesssim \tau \lesssim 0.1$ it is moderate but still not negligible. Furthermore, starting with the NLL level, the scale uncertainty band for resummed results is dramatically smaller than in the case of fixed order results. This is because scale variation of the LL result produces NLL terms which beyond the first few orders are not contained in the fixed order result; starting with NLL these terms are already included in the resummed result. It is interesting to note that in the case of the resummed cross-section (with both prescriptions) the NNLL band is almost entirely contained in the NLL band, while the fixed-order NLO and NNLO error bands are only marginally compatible with each other. The ambiguity in the resummation, estimated from the difference between Borel and minimal prescription, is not negligible, but smaller than the scale uncertainty; moreover, it is more evident at small τ , since the different subleading terms give a larger contribution in that region.

The experiment E866/NuSea [75–77] has measured the x_F -distribution Eq. (C.1.14) of lepton pairs with an invariant mass $M = 8$ GeV. The E866 data are displayed in Fig. 5.8, superimposed to the QCD prediction and the corresponding scale uncertainty. The distribution is symmetric about $Y = 0$; the curves shown for $Y < 0$ refer to fixed-order calculations, and those with $Y > 0$ to resummed results. The data agree with the NLO calculation because these data were included in the determination of the NLO PDFs that we are using.

The impact of the resummation is small but not negligible: for instance the difference between NNLO and NNLL is about half of the difference between NNLO and NLO. Furthermore, the scale uncertainty of resummed results is somewhat smaller than that of the unresummed ones. This is consistent with the observation that for this experiment $\tau = 0.04$, which, as discussed in Sect. 4.1, is in the region in which resummation is relevant. However, the difference between resummed results obtained using the Borel and the minimal prescription is almost as large as the size of the re-

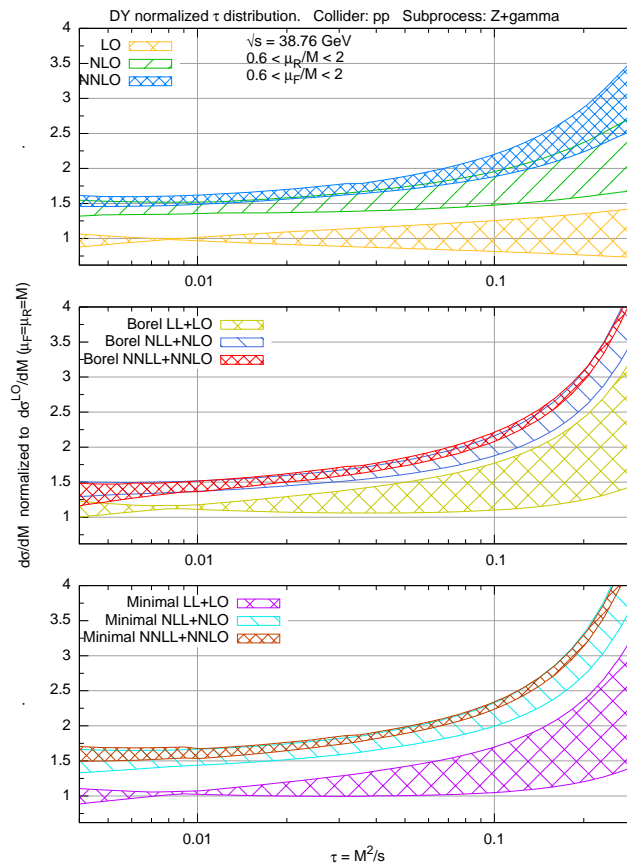


Figure 5.7. Invariant mass distribution of neutral Drell-Yan pairs in pp collisions at $\sqrt{s} = 38.76$ GeV.

summation itself: in fact the NLL Borel results is somewhat lower than the NNLO one, while the NLL minimal prescription result is a bit higher. Hence we conclude that the overall impact of the resummation on these data is essentially negligible. A large and negative NLL resummed correction to the NLO result was claimed in Ref. [35], using the minimal prescription, but we do not confirm it: we find a positive and rather smaller correction. The result of Ref. [35] was first criticized in Ref. [28]. Our result with the Borel prescription is in good quantitative agreement with Ref. [28]; however, the minimal prescription gives a somewhat larger correction, though still positive.

5.1.2.2 Tevatron collider

We now turn to Drell-Yan production in $p\bar{p}$ collisions at a center-of-mass energy $\sqrt{s} = 1.96$ TeV. Results for the invariant mass distribution of neutral and charged Drell-Yan pairs in this configuration are shown in Fig. 5.9.

The behaviour of these curves is similar to that seen in the case of NuSea, Fig. 5.7, but with the impact of the resummation yet a bit smaller, as one would expect both because of the higher energy and because of the collider configuration, as discussed in Sect. 4.1.3 (in particular Fig. 4.1). Interestingly, even when the resummation has a very small impact, it still leads to a non-negligible reduction of the uncertainty: this is

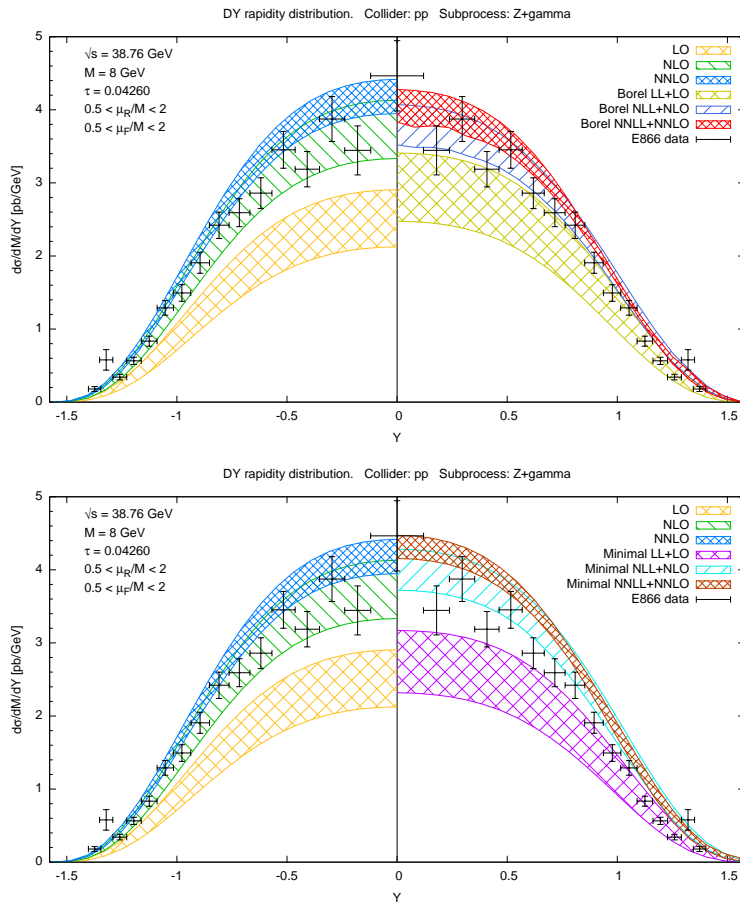


Figure 5.8. Rapidity distribution of neutral Drell-Yan pairs of invariant mass $M = 8$ GeV in pp collisions at $\sqrt{s} = 38.76$ GeV; E866 data are also shown.

consistent with the expectation that for these medium-small values of τ resummation is in fact a perturbative correction, as discussed in the end of Sect. 4.1.3. Note that in these plots the smallness of leading-order uncertainty bands when $\tau \approx 0.002$ (i.e. $M \approx 100$ GeV) is due to the fact that the scale dependence of the parton luminosity, to which the leading-order cross-section is proportional (see Eq. (C.1.3)), is stationary at this scale.

We now turn to rapidity distributions, shown in Figs. 5.10 and 5.11 for neutral Drell-Yan pairs of invariant mass $M = m_Z$ and $M = 200$ GeV respectively. The impact of the resummation is now very small, as one would expect given the smallness of the relevant values of τ . However, interestingly, resummed uncertainty bands are systematically smaller than the unresummed one, with the resummation ambiguity (i.e. the difference between minimal and Borel results) now essentially negligible. Hence, even in this small τ region the resummation leads to perturbative improvement, while behaving of course as a perturbative correction. Again, note that the smallness of leading-order uncertainty bands is due to the fact that the scale here is close to the stationary point of the scale dependence of the parton luminosity already seen in Fig. 5.9.

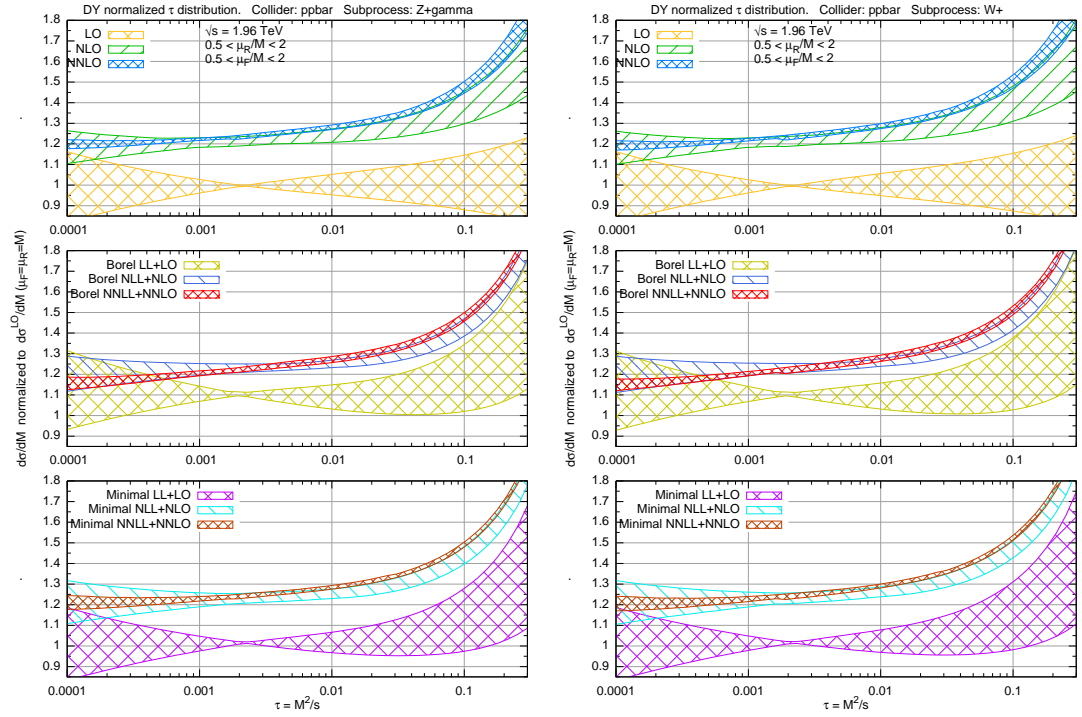


Figure 5.9. Invariant mass distribution of neutral (left) and charged (right) Drell-Yan pairs in $p\bar{p}$ collisions at $\sqrt{s} = 1.960$ TeV.

We can compare these uncertainties to that of typical current data, thanks to recent measurements at the Tevatron. Specifically, the rapidity distribution of e^+e^- pairs with invariant mass in the range $66 \text{ GeV} \leq M \leq 116 \text{ GeV}$ has been recently measured by the CDF collaboration [86]. In principle, the data should be compared with the theoretical prediction for the full process

$$p + \bar{p} \rightarrow e^+ + e^- + X. \quad (5.1.11)$$

For values of M close to the Z mass, however, a good approximation is provided by the Breit-Wigner approximation, which amounts to assuming that the amplitude is dominated by Z exchange, and takes into account the finite width Γ_Z of the Z boson:

$$\frac{d\sigma(\tau, Y, M^2)}{dM^2 dY} = \frac{2m_Z \Gamma_{\ell\bar{\ell}}}{(M^2 - m_Z^2)^2 + m_Z^2 \Gamma_Z^2} \frac{1}{2\pi} \frac{d\sigma_Z}{dY} \quad (5.1.12)$$

where $\Gamma_{\ell\bar{\ell}}$ is the Z decay width into a lepton pair, and $d\sigma_Z$ is the differential cross-section for the production of a real on-shell Z boson. Eq. (5.1.12) gives

$$\frac{d\sigma(\tau, Y, M^2)}{dM^2 dY} = \frac{m_Z^2 \Gamma_Z^2}{(M^2 - m_Z^2)^2 + m_Z^2 \Gamma_Z^2} \frac{d\sigma(\tau, Y, m_Z^2)}{dM^2 dY}, \quad (5.1.13)$$

and therefore

$$\int_{M_{\min}^2}^{M_{\max}^2} dM^2 \frac{d\sigma(\tau, Y, M^2)}{dM^2 dY} = N_Z(M_{\min}^2, M_{\max}^2) \frac{d\sigma(\tau, Y, m_Z^2)}{dM dY}, \quad (5.1.14)$$

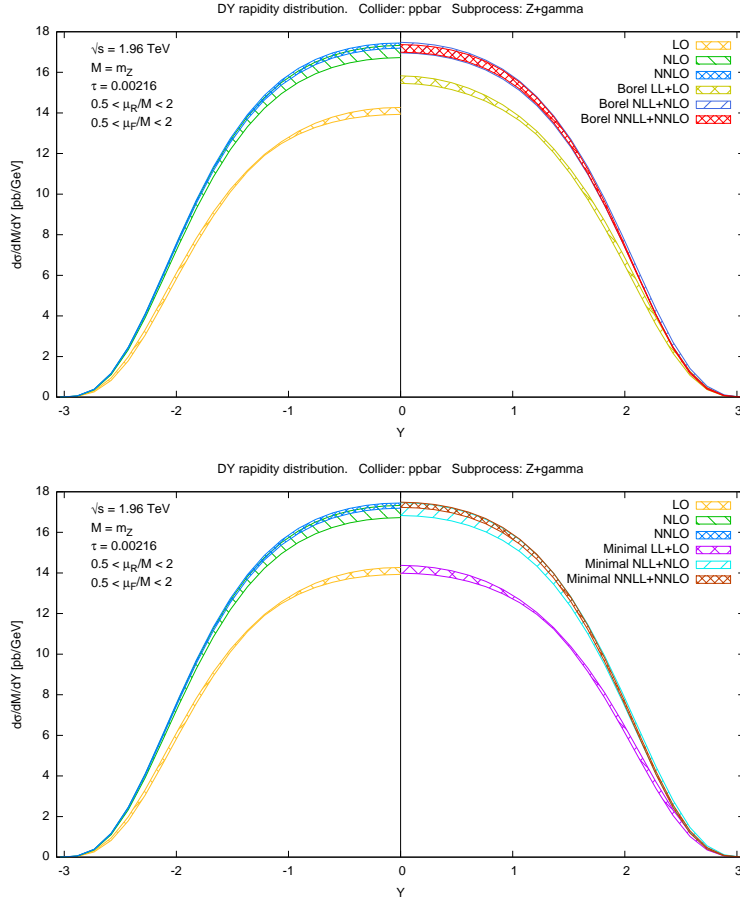


Figure 5.10. Rapidity distribution of neutral Drell-Yan pairs of invariant mass $M = m_Z$ in $p\bar{p}$ collisions at $\sqrt{s} = 1.96$ TeV (the contribution of virtual γ at the Z peak is included).

where

$$\begin{aligned}
 N_Z(M_{\min}^2, M_{\max}^2) &= \frac{m_Z \Gamma_Z^2}{2} \int_{M_{\min}^2}^{M_{\max}^2} dM^2 \frac{1}{(M^2 - m_Z^2)^2 + m_Z^2 \Gamma_Z^2} \\
 &= \frac{\Gamma_Z}{2} \left[\arctan \left(\frac{M_{\max}^2 - m_Z^2}{m_Z \Gamma_Z} \right) + \arctan \left(\frac{m_Z^2 - M_{\min}^2}{m_Z \Gamma_Z} \right) \right] \quad (5.1.15)
 \end{aligned}$$

is just a Y -independent multiplicative factor. A better approximation is obtained including also the contribution from the virtual photon exchange, and neglecting its interference with the Z boson. Schematically, we can separate the contributions as

$$\begin{aligned}
 \sigma(M^2) &= \sigma_Z(M^2) + \sigma_\gamma(M^2) + \sigma_{Z\gamma}(M^2) \\
 &\simeq \frac{m_Z^2 \Gamma_Z^2}{(M^2 - m_Z^2)^2 + m_Z^2 \Gamma_Z^2} \sigma_Z(m_Z^2) + \frac{m_Z^2}{M^2} \sigma_\gamma(m_Z^2) + \frac{M^2 - m_Z^2}{(M^2 - m_Z^2)^2 + m_Z^2 \Gamma_Z^2} \sigma_{Z\gamma}^0 \quad (5.1.16)
 \end{aligned}$$

where the first piece is the Breit-Wigner term used before, the second is the contribution from the virtual photon and the last term is the interference term: since it is

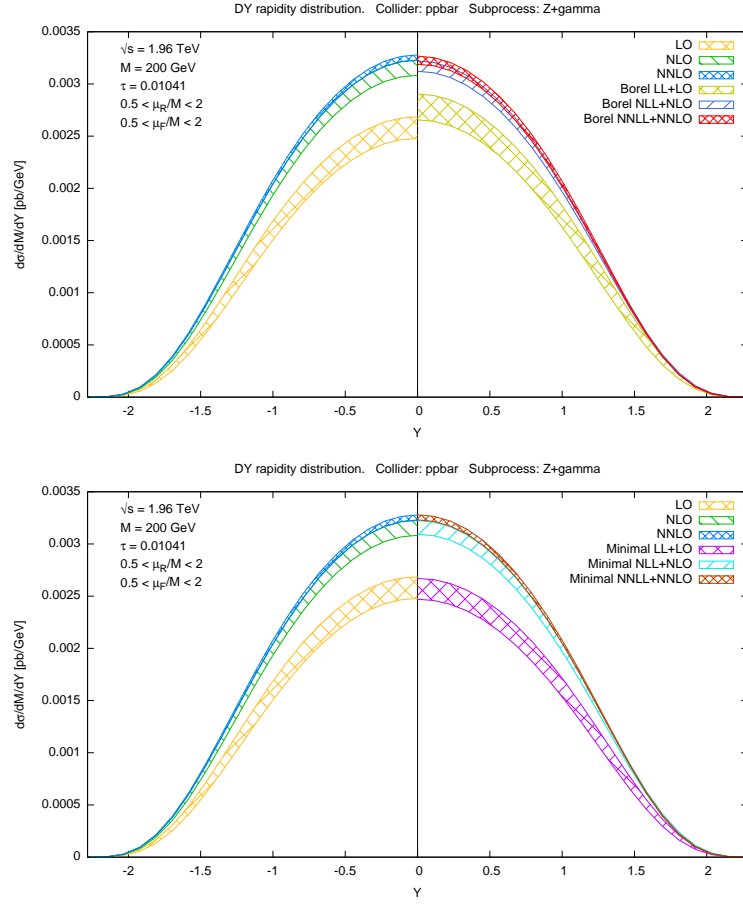


Figure 5.11. Rapidity distribution of neutral Drell-Yan pairs of invariant mass $M = 200$ GeV in $p\bar{p}$ collisions at $\sqrt{s} = 1.96$ TeV.

almost odd in $M^2 - m_Z^2$, its contribution is strongly suppressed in the vicinity of the Z peak and it can be neglected. Note that at the Z peak

$$\sigma(m_Z^2) = \sigma_Z(m_Z^2) + \sigma_\gamma(m_Z^2) \quad (5.1.17)$$

exactly. Then, knowing the relative contributions of Z and γ at the peak the M^2 integral can be estimated to a higher accuracy. Defining

$$R_Z = \sigma_Z(m_Z^2)/\sigma(m_Z^2), \quad R_\gamma = \sigma_\gamma(m_Z^2)/\sigma(m_Z^2), \quad R_Z + R_\gamma = 1, \quad (5.1.18)$$

we have

$$\sigma(M^2) \simeq \sigma(m_Z^2) \left[R_Z \frac{m_Z^2 \Gamma_Z^2}{(M^2 - m_Z^2)^2 + m_Z^2 \Gamma_Z^2} + R_\gamma \frac{m_Z^2}{M^2} \right] \quad (5.1.19)$$

and hence

$$\int_{M_{\min}^2}^{M_{\max}^2} dM^2 \frac{d\sigma(\tau, Y, M^2)}{dM^2 dY} = [R_Z N_Z(M_{\min}^2, M_{\max}^2) + R_\gamma N_\gamma(M_{\min}^2, M_{\max}^2)] \frac{d\sigma(\tau, Y, m_Z^2)}{dM dY}, \quad (5.1.20)$$

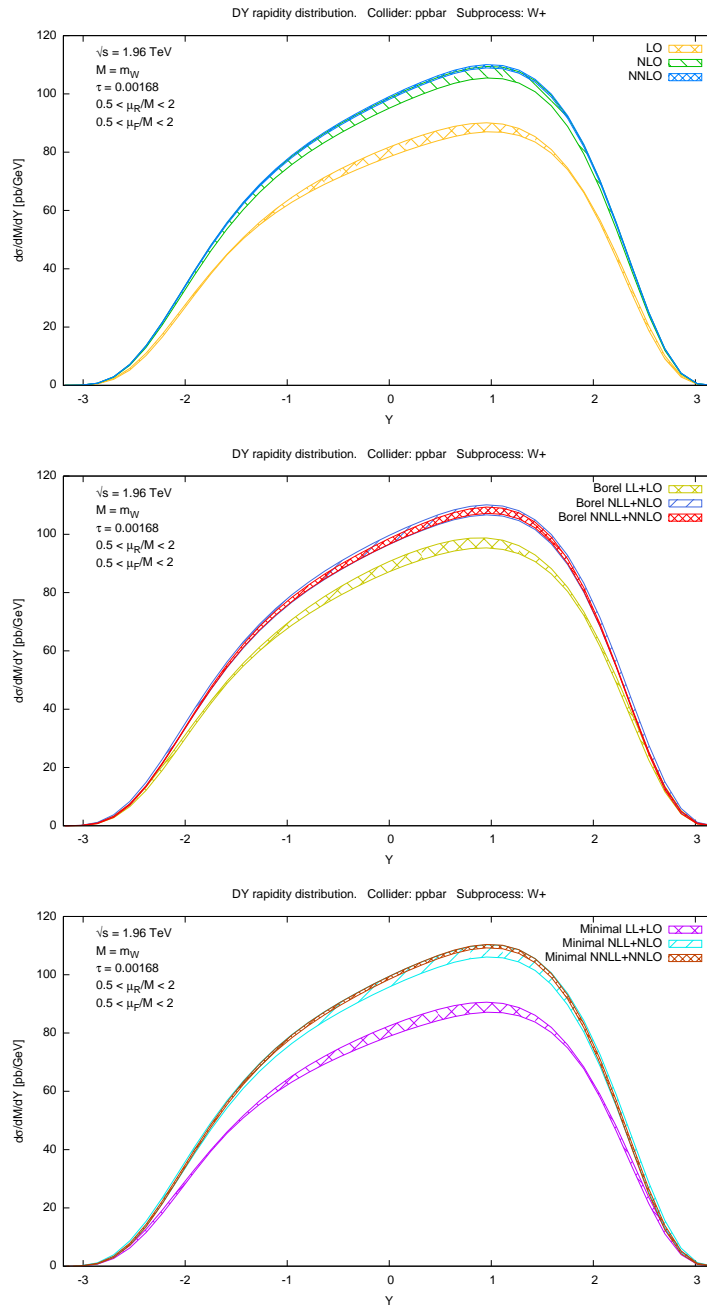


Figure 5.12. Rapidity distribution of charged Drell-Yan pairs of invariant mass $M = m_W$ in $pp\bar{p}$ collisions at $\sqrt{s} = 1.96$ TeV.

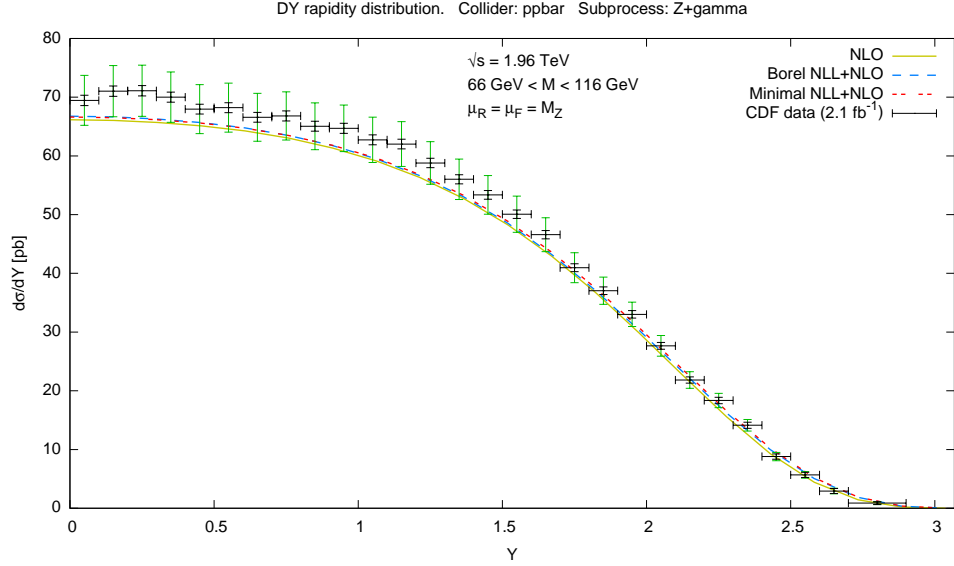


Figure 5.13. Rapidity distribution of Z bosons in $p\bar{p}$ collisions at $\sqrt{s} = 1.96$ TeV (the contribution of virtual γ at the Z peak is included). Data are taken from [86]. The smaller black uncertainty bands are statistical only, while the wider green bands also include normalization uncertainties.

with

$$N_\gamma(M_{\min}^2, M_{\max}^2) = \frac{1}{2m_Z} \int_{M_{\min}^2}^{M_{\max}^2} dM^2 \frac{m_Z^2}{M^2} = \frac{m_Z}{2} \log \frac{M_{\max}^2}{M_{\min}^2} \quad (5.1.21)$$

With a simple electroweak computation one can compute the R -factors

$$R_\gamma = \frac{\alpha_{em}/3m_Z}{\frac{\alpha_{em}}{3m_Z} + \frac{\Gamma_{\ell\bar{\ell}}}{\Gamma_Z^2}} = 0.0021, \quad R_Z = \frac{\Gamma_{\ell\bar{\ell}}/\Gamma_Z^2}{\frac{\alpha_{em}}{3m_Z} + \frac{\Gamma_{\ell\bar{\ell}}}{\Gamma_Z^2}} = 0.9979; \quad (5.1.22)$$

substituting the CDF values, the full factor becomes

$$R_Z N_Z(M_{\min}^2, M_{\max}^2) + R_\gamma N_\gamma(M_{\min}^2, M_{\max}^2) = 3.893 \text{ GeV}, \quad (5.1.23)$$

which is a bit larger than that obtained with the simple Breit-Wigner approximation.

In Fig. 5.13 we show the CDF data [86], corresponding to an integrated luminosity of 2.1 fb^{-1} , compared to the NLO QCD prediction with the inclusion of threshold resummation at NLL, using both Borel and minimal prescriptions. The comparison shows an excellent agreement in shape between the data and the theoretical curves; there is clearly a mismatch in normalization of the total cross-section, which is however consistent with the sizable 6% normalization uncertainty on the cross-section. Also in this case, as for the NuSea experiment, this simply reflects the fact that these data are used in the determination of the PDFs that we are using.

A similar comparison can be performed for the W^\pm asymmetry, defined as

$$A_W(Y) = \frac{\frac{d\sigma_{W^+}}{dY} - \frac{d\sigma_{W^-}}{dY}}{\frac{d\sigma_{W^+}}{dY} + \frac{d\sigma_{W^-}}{dY}}, \quad (5.1.24)$$

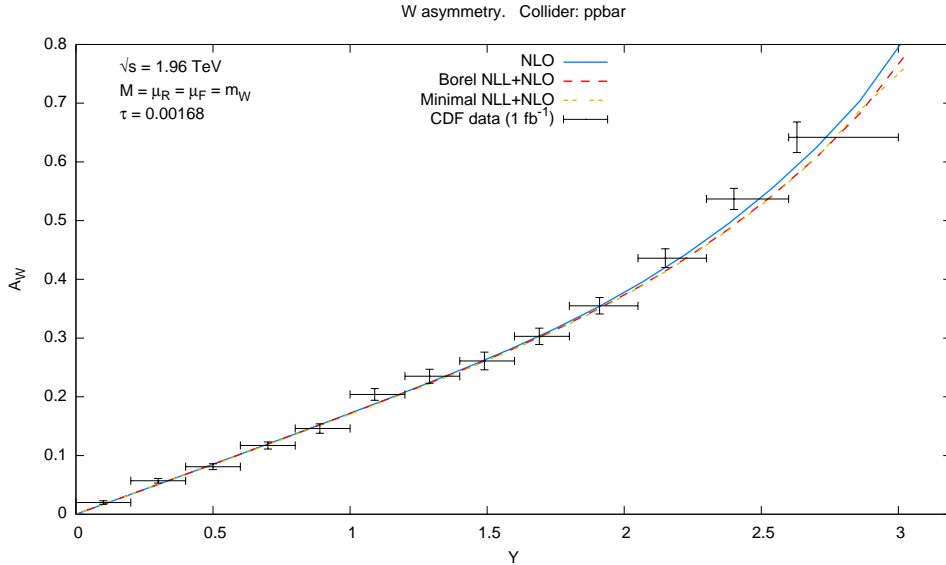


Figure 5.14. W^\pm asymmetry in $p\bar{p}$ collisions at $\sqrt{s} = 1.96 \text{ TeV}$. Data are taken from [87].

also measured by CDF [87]. In this case, normalization uncertainties cancel in the ratio. In Fig. 5.14 we show the measured CDF data [87] compared to the QCD prediction at NLO and resummed NLO+NLL (Borel and minimal prescriptions). Clearly, the accuracy of present-day data is insufficient to appreciate the effect of NNLO or resummation correction, and it is rather comparable to the difference between LO and NLO predictions, which can thus be barely appreciated. However, an improvement of statistical accuracy by an order of magnitude would be sufficient for NNLO and resummation corrections to become significant. The normalization uncertainty has a negligible effect on the shape of the distribution and therefore it does not affect this conclusion

5.1.2.3 LHC

We now consider predictions for Drell-Yan production at the LHC, with the current energy $\sqrt{s} = 7 \text{ TeV}$. Prediction for collider energy $\sqrt{s} = 14 \text{ TeV}$ can be found in Ref. [25]. Very recently, CERN announced the energy upgrade for the 2012 run to $\sqrt{s} = 8 \text{ TeV}$; predictions for such energy are not yet available.

Invariant mass distributions for both neutral and charged Drell-Yan pairs are shown in Figs. 5.15, 5.16. While the impact of fixed-order perturbative corrections is unsurprisingly similar to that at the Tevatron collider shown in Fig. 5.9, interestingly the reduction in uncertainty obtained thanks to the resummation is more marked at the LHC, consistent with the expectation (recall Sect. 4.1) that the effect of the resummation is somewhat more significant at a pp than at a $p\bar{p}$ collider. Moreover, the consistency of the NLO error band with the NNLO prediction is improved by the inclusion of resummation. Of course, as in the case of Tevatron, for realistic values of $\tau \lesssim 0.1$ the impact of the resummation is mostly on the uncertainty but very small or negligible on central values, so the resummation is behaving as a perturbative correc-

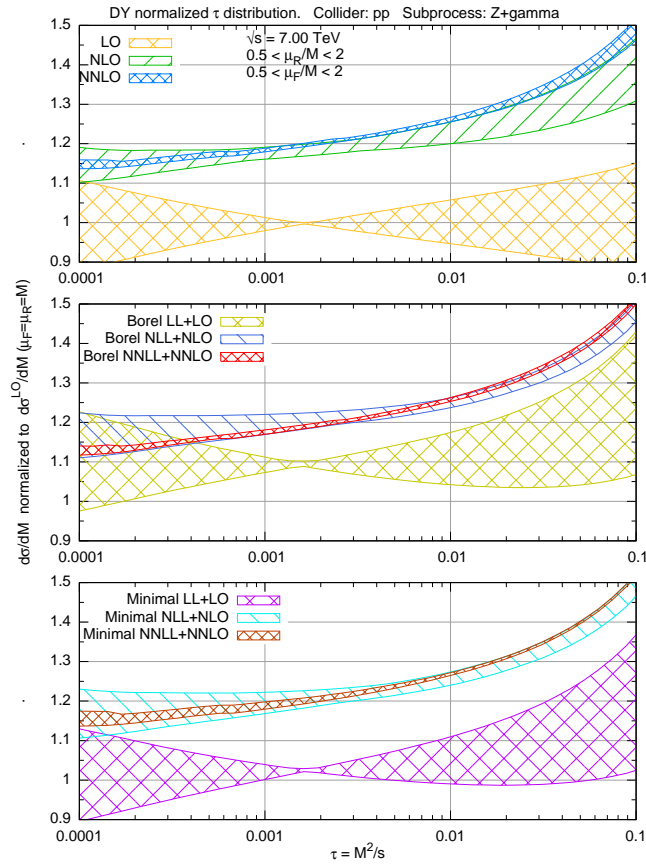


Figure 5.15. Invariant mass distribution of neutral Drell-Yan pairs in pp collisions at $\sqrt{s} = 7$ TeV.

tion.

Turning to rapidity distributions, we present results for the following observables:

- neutral Drell-Yan pairs with invariant mass $M = 1$ TeV, Fig. 5.17;
- neutral Drell-Yan pairs with invariant mass $M = m_Z$, Fig. 5.18;
- positively charged Drell-Yan pairs with invariant mass $M = m_W$, Fig. 5.19;
- negatively charged Drell-Yan pair with invariant mass $M = m_W$, Fig. 5.19.

The first case corresponds to $\tau \sim 0.02$, comparable to the case of a final state with $M = 200$ GeV at the Tevatron shown in Fig. 5.11. As in that case, we clearly see an improvement in uncertainty (with small resummation ambiguities) when going to the resummed result, though also in that case the effect on central value is moderate. On the other hand, the other cases correspond to very small values of τ and indeed in this case the uncertainty on resummed results is larger than that on unresummed ones, indicating that whatever effect is induced by the resummation is related to the inclusion of terms which are not dominant in this region. This is also reflected in a sizable difference between Borel and minimal results.

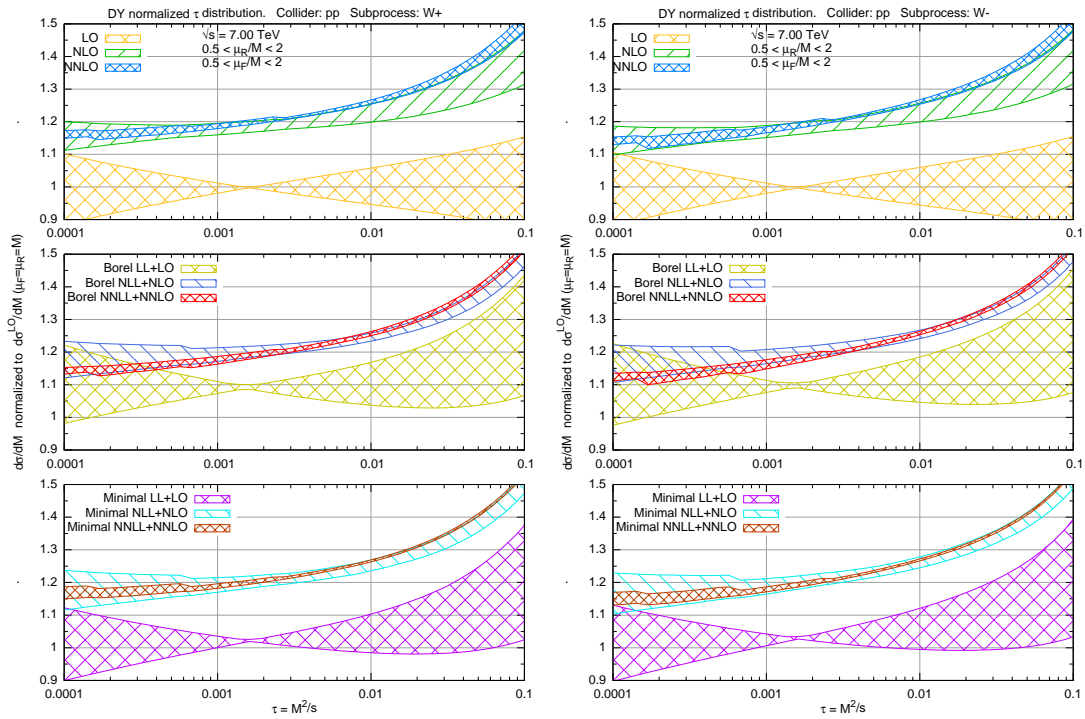


Figure 5.16. Invariant mass distribution of positively (left) and negatively (right) charged Drell-Yan pairs in pp collisions at $\sqrt{s} = 7$ TeV.

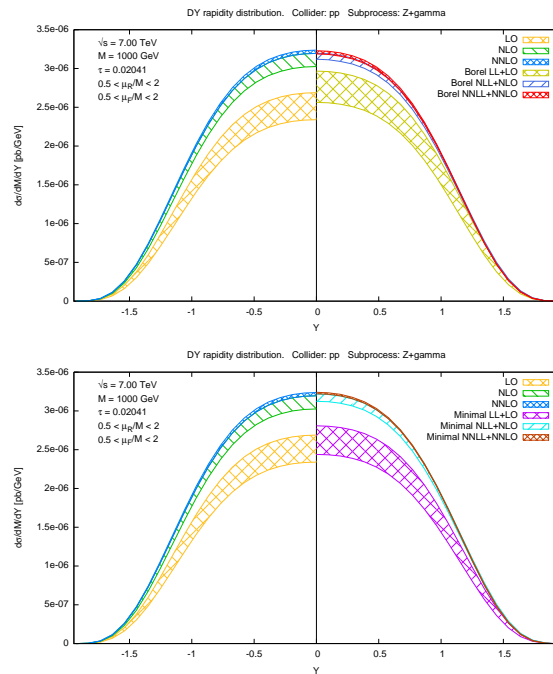


Figure 5.17. Rapidity distribution of neutral Drell-Yan pairs of invariant mass $M = 1$ TeV in pp collisions at $\sqrt{s} = 7$ TeV.

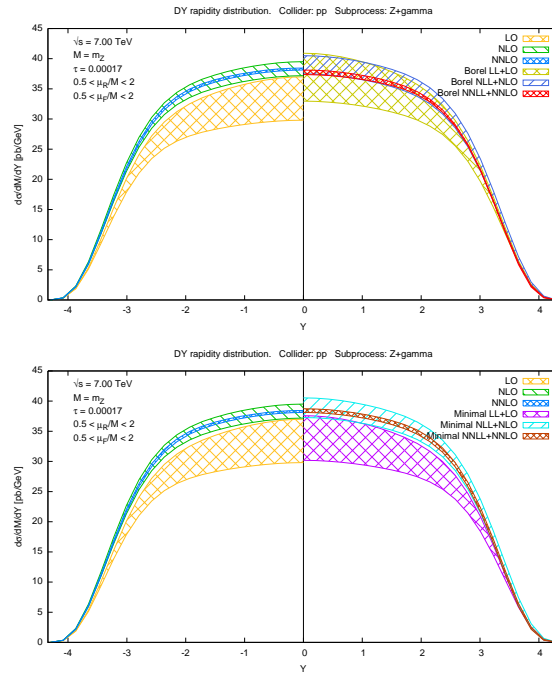


Figure 5.18. Rapidity distribution of neutral Drell-Yan pairs of invariant mass $M = m_Z$ in pp collisions at $\sqrt{s} = 7$ TeV (the contribution of virtual γ at the Z peak is included).

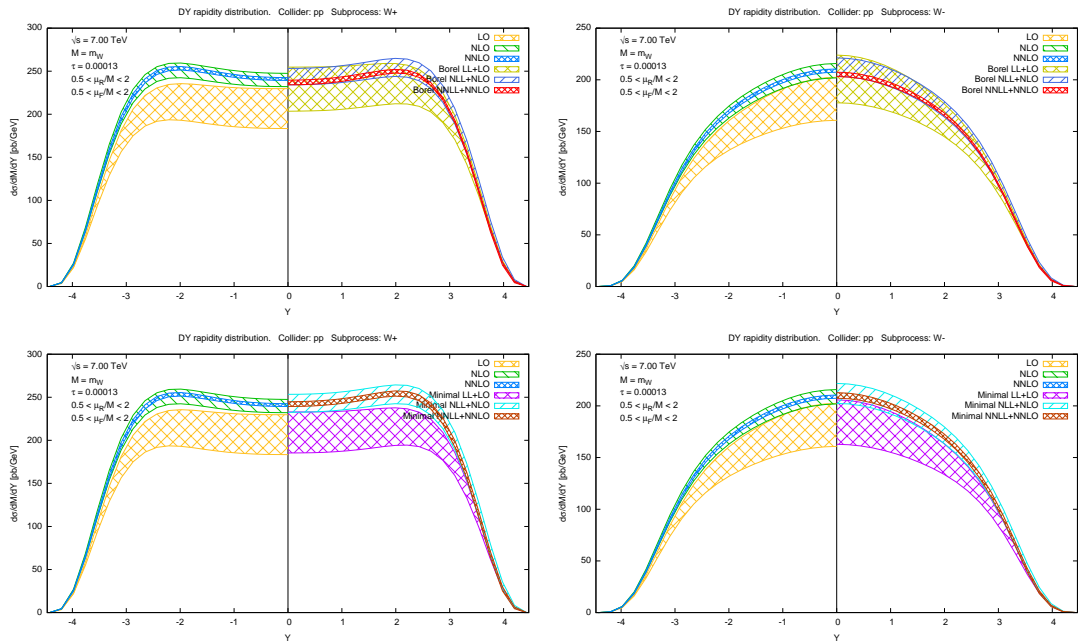


Figure 5.19. Rapidity distribution of positively (left) and negatively (right) charged Drell-Yan pairs of invariant mass $M = m_W$ in pp collisions at $\sqrt{s} = 7$ TeV.

5.1.3 Comparison of the different prescriptions

We finally turn to a comparison of the phenomenological impact of different choices of subleading terms.

First, we want to prove what we claimed several times in the text, i.e. that the “natural” Borel prescription which depends on z via $\log \frac{1}{z}$, Eq. (2.1.46), gives the same result as the Minimal prescription, provided τ is not too large. Therefore, in Fig. 5.20 we plot the predictions for the resummed K -factors as obtained with the Minimal prescription and with the Borel prescription, Eq. (2.3.13). We consider as a reference

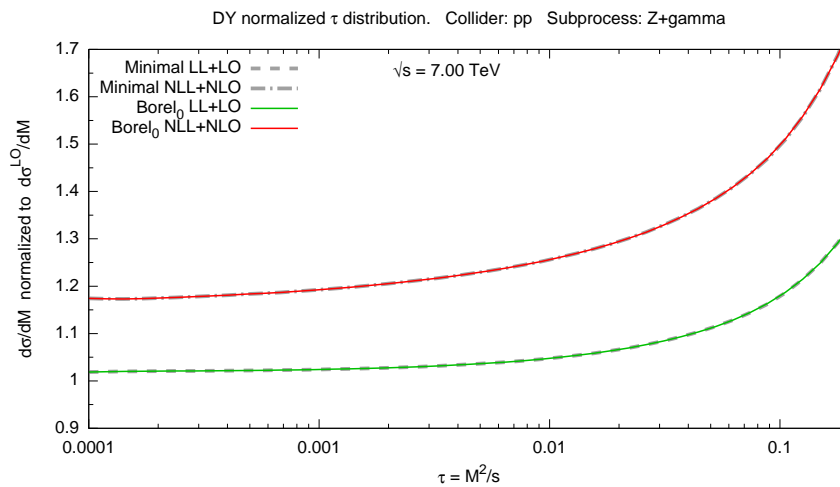


Figure 5.20. Invariant mass distribution of neutral Drell-Yan pairs in pp collisions at $\sqrt{s} = 7$ TeV for central values of the renormalization and factorization scales. The original Borel prescription Eq. (2.3.13) is used.

case the production of neutral DY pairs at the LHC at 7 TeV; since the NNLL+NNLO curves are very close to the NLL+NLO ones, we don’t show them in order to better read the plots. The plot shows the impressive similarity between such Borel prescription and the Minimal prescription: in both the LL and NLL case they are indistinguishable in the whole plotted range.¹ This plot shows clearly that, for experimentally accessible values of τ , the difference in the way the Borel and Minimal prescriptions treat the divergence of the perturbative series is not relevant at all, thereby reassuring who could be worried either by the non-convolutive nature of the Minimal prescription or by the higher-twists included in the Borel prescription. This fact is a consequence of the observation that, for such not too large values of τ , the perturbative series behaves perturbatively, and the divergence of the series (and the details of the treatment of it) does not play a role.

Next, in Fig. 5.21 we compare the different versions of the Borel prescription. The upper plot is a direct comparison of the three choices Eqs. (2.1.46), (2.1.58) and (2.1.62). First, we note that at large τ , where the different subleading terms are less important, all the curves at a given order tend to be very similar each other,

¹This plot is, by the way, a powerful check of the goodness and correctness of the numerical implementation of resummation.

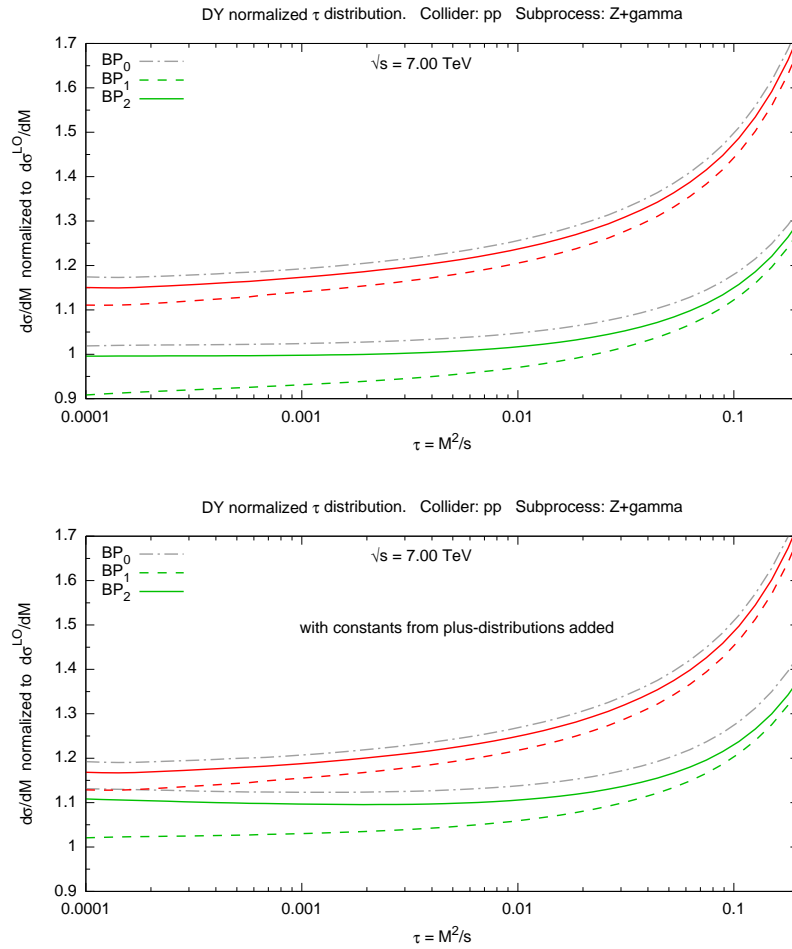


Figure 5.21. Invariant mass distribution of neutral Drell-Yan pairs in pp collisions at $\sqrt{s} = 7 \text{ TeV}$ for central values of the renormalization and factorization scales. Different versions of the Borel prescription are used: BP_0 corresponds to Eq. (2.3.13), BP_1 to Eq. (2.3.7) and BP_2 to Eq. (2.3.10). The upper plot shows the results for these prescriptions, while in the lower plot also the constants from the plus-distributions are added. The upper curves in the plots correspond to NLL+NLO: same style means same prescription.

as expected. Moreover, the BP_0 and BP_2 are rather close each other in the whole range, while the BP_1 is quite different especially at small τ : this is consistent with the discussion in Sect. 2.1.6, and indeed we had decided not to take into account the BP_1 for phenomenology.

The lower plot shows the same curves with the constant terms coming from plus-distributions added: in practice, these prescriptions are obtained by adding

$$-\frac{1}{\xi} \delta(1-z) \quad (5.1.25)$$

to the plus-distribution terms in Eqs. (2.1.46), (2.1.58) and (2.1.62) (see also discussion in Sect. 2.1.5.1). The BP_2 obtained with this modification is the prescription we used in this Chapter for phenomenology [25]. Even if this modification is subleading and somewhat unjustified theoretically, its effect on the Drell-Yan case is to improve the

convergence of the resummed perturbative expansion. Indeed, while the NLL curves do not change too much between upper and lower plot, the LL curves in the lower plot are much closer to the NLL ones.

We conclude noting that, discarding the BP_1 , the other prescriptions, differing for the choices of subleading terms produced, if used as estimators of the uncertainty due to the resummation procedure would give a rather small uncertainty (from NLL+NLO on), comparable to that from scale variation.

Conclusions

We have presented a detailed overview of the current status of soft-gluon and high-energy resummations in perturbative QCD. On the theoretical side, we have obtained several results.

First, concerning soft-gluon resummation, we have presented an alternative prescription, the Borel prescription, to deal with the problem of the Landau pole of the strong coupling, related to the divergence of the perturbative series. The Borel prescription turns out to be very powerful, in which it gives complete control on the subleading terms introduced by the resummation procedure. This property can be either used to estimate the uncertainty due to such subleading terms, or to find the best choice of these terms, in such a way that the threshold logarithms could best reproduce the partonic coefficient even far from the threshold region.

We have then discussed the resummation of high-energy logarithms, providing several improvements in the whole procedure. The most important result on this subject is the development of a code implementing all the machinery of high-energy resummation, providing for the first time publicly available small- x resummed splitting functions and coefficient functions.

One of the main achievements is that we have provided a way to estimate the value of hadronic variable $\tau = M^2/s$ at which resummation of threshold logarithms is expected to provide an improvement over fixed-order calculations. This result has been accomplished through a determination of the relevant partonic center-of-mass energy, whose distance from threshold determines the impact of resummation. This estimate relies on the singularity structure of the anomalous dimensions which drive M^2 evolution of parton distributions in perturbative QCD. Using this technique, we have shown that resummation is expected to be relevant down to fairly small values of τ , very far from hadronic threshold. For example, at the LHC at 7 TeV the Drell-Yan process is expected to be influenced by threshold resummation for $\tau \gtrsim 0.002$, corresponding to $M \gtrsim 300$ GeV. More interestingly, the Higgs boson production at LHC at 7 TeV is expected to get contributions from the threshold region down to values of τ as small as $\tau \gtrsim 0.0002$, corresponding to $M \gtrsim 100$ GeV.

Being such values of τ so small, we have investigated the modifications in our predictions induced by high-energy resummation, in particular for the Higgs boson production, being it dominated by gluon fusion. By a preliminary analysis, based on an approximate implementation of small- x resummation, it seems that the threshold region is reduced, in the sense that threshold logarithms are dominant only for higher masses. This observation needs to be clarified: this request enforces the need of a complete inclusion of small- x resummation in PDF fits for precision phenomenology

at hadron colliders.

At the phenomenological level, we have shown how to use different versions of the Borel resummation prescription and their comparison to the minimal prescription as a means to assess the ambiguities related to the resummation, and in particular to the treatment of the subleading terms. The application of these tools to the Drell-Yan process at Tevatron and LHC has shown that resummation is relevant for the production of states of mass as light as W and Z vector bosons at the Tevatron, and for the production of heavy dileptons of mass in the TeV range at the LHC: in all these cases threshold resummation leads to a significant improvement in perturbative accuracy. The impact of resummation on Tevatron fixed-target rapidity distributions is less clear, in that, despite being larger, the effect of resummation may be marred by its ambiguities.

Our general conclusion is that the impact of threshold resummation at hadron colliders even for significantly small values of τ is comparable to that of NNLO corrections, and it should thus be included both in the determination of parton distributions and in precision phenomenology, though care should be taken in also estimating carefully the ambiguity which is intrinsic in the resummation procedure.

A QCD running coupling

Contents

A.1 The running of α_s	131
A.1.1 Solutions of the renormalization-group equation	132
A.1.2 Quark masses thresholds	133

In this Appendix we review some features of the QCD running coupling and we compute the solutions to its renormalization-group equation.

A.1 The running of α_s

The QCD coupling α_s satisfies the renormalization-group equation

$$\mu^2 \frac{d}{d\mu^2} \alpha_s(\mu^2) = \beta(\alpha_s(\mu^2)) \quad (\text{A.1.1})$$

where the β -function in the right-hand-side has the perturbative expansion

$$\beta(\alpha_s) = -\alpha_s^2 (\beta_0 + \beta_1 \alpha_s + \beta_2 \alpha_s^2 + \dots) \quad (\text{A.1.2})$$

$$= -\beta_0 \alpha_s^2 (1 + b_1 \alpha_s + b_2 \alpha_s^2 + \dots) \quad (\text{A.1.3})$$

where $\beta_k = b_k \beta_0$ for $k \geq 1$. The k -th coefficient β_k can be computed by a $(k+1)$ -loop calculation, and so far are known up to 4 loops [88, 89]. Here, we present the first three, which are those that will be used for resummation:

$$\beta_0 = \frac{11C_A - 4T_F n_f}{12\pi} = \frac{33 - 2n_f}{12\pi} \quad (\text{A.1.4})$$

$$\beta_1 = \frac{17C_A^2 - (10C_A + 6C_F)T_F n_f}{24\pi^2} = \frac{153 - 19n_f}{24\pi^2} \quad (\text{A.1.5})$$

$$\begin{aligned} \beta_2 &= \frac{1}{(4\pi)^3} \left[\frac{2857}{54} C_A^3 + \left(2C_F^2 - \frac{205}{9} C_F C_A - \frac{1415}{27} C_A^2 \right) T_F n_f \right. \\ &\quad \left. + \left(\frac{44}{9} C_F + \frac{158}{27} C_A \right) T_F^2 n_f^2 \right] \\ &= \frac{1}{128\pi^3} \left[2857 - \frac{5033}{9} n_f + \frac{325}{27} n_f^2 \right] \end{aligned} \quad (\text{A.1.6})$$

where in the second equality we have substituted the numerical values

$$C_A = N_c = 3, \quad C_F = \frac{N_c^2 - 1}{2N_c} = \frac{4}{3}, \quad T_F = \frac{1}{2}, \quad (\text{A.1.7})$$

which are appropriate for the gauge group $SU(N_c)$ with $N_c = 3$ of QCD.

As already discussed in Chap. 1, as long as $n_f < 17$ (and so far we know 6 flavours) β_0 is positive, and because of the minus sign in front of the perturbative expansion of the β -function the solution of the renormalization-group equation is decreasing as μ^2 increases. We now show explicit solutions where this fact, known as asymptotic freedom, is manifest.

A.1.1 Solutions of the renormalization-group equation

The renormalization-group equation can be easily solved, because the μ^2 dependence appear only as argument of α_s , and in general we have then

$$\int \frac{d\mu^2}{\mu^2} F(\alpha_s(\mu^2)) = \int \frac{d\alpha_s}{\beta(\alpha_s)} F(\alpha_s) \quad (\text{A.1.8})$$

with the appropriate integration limits. At one loop, the only coefficient of the β -function is β_0 and the solution is

$$\alpha_s(\mu^2) = \frac{\alpha_s(Q^2)}{1 + \beta_0 \alpha_s(Q^2) \log \frac{\mu^2}{Q^2}} \quad (\text{A.1.9a})$$

$$= \frac{1}{\beta_0 \log \frac{\mu^2}{\Lambda^2}}, \quad (\text{A.1.9b})$$

where in the first line we have used an initial condition for α_s at the scale Q^2 , while in the second one the initial condition is chosen at the scale Λ^2 at which α_s goes to infinity (Landau pole). At this order, then, the Landau pole μ_L can be written as

$$\mu_L^2 = \Lambda^2 = \mu^2 \exp\left(-\frac{1}{\beta_0 \alpha_s(\mu^2)}\right) \quad (\text{A.1.10})$$

valid for every choice of μ^2 , then in particular for $\mu^2 = Q^2$, making the connection between the two solutions Eqs. (A.1.9).

Note that the first form of the solution, Eq. (A.1.9a), shows explicitly that the renormalization group equation resums all powers of $\log \frac{\mu^2}{Q^2}$. In particular, we may write an expansion of $\alpha_s(\mu^2)$ in powers of $\alpha_s(Q^2)$ at $\alpha_s(Q^2) \log \frac{\mu^2}{Q^2}$ fixed,

$$\alpha_s(\mu^2) = \alpha_0 f_1(\alpha_0 \ell) + \alpha_0^2 f_2(\alpha_0 \ell) + \dots, \quad (\text{A.1.11})$$

where we have defined for simplicity $\alpha_0 = \alpha_s(Q^2)$ and $\ell = \log \frac{\mu^2}{Q^2}$. The functions f_1, f_2, \dots contain all powers of their argument; therefore, such expansion is valid provided only $\alpha_s(Q^2) \ll 1$, regardless the value of ℓ . The functions f_j can be found for all $j = 1, \dots, k$ solving the renormalization-group equation with a k -loop β -function, i.e. including all the coefficients β_i in the range $0 \leq i \leq k - 1$.

The 1-loop solution indeed predicts f_1 :

$$f_1(\alpha_0 \ell) = \frac{1}{1 + \beta_0 \alpha_0 \ell}. \quad (\text{A.1.12})$$

At two loops, we must include $\beta_1 = b_1 \beta_0$ and we find

$$\left[\frac{1}{\beta_0 \alpha_s} - \frac{b_1}{\beta_0} \log \left(\frac{1}{\alpha_s} + b_1 \right) \right]_{\alpha_s(Q^2)}^{\alpha_s(\mu^2)} = \log \frac{\mu^2}{Q^2}. \quad (\text{A.1.13})$$

Solving for $\alpha_s(\mu^2)$ and expanding in order to take terms up to the second order in the expansion (A.1.11) we then obtain

$$\alpha_s(\mu^2) = \frac{\alpha_s(Q^2)}{X} \left[1 - \frac{b_1 \alpha_s(Q^2)}{X} \log X \right] \quad (\text{A.1.14})$$

where $X = 1 + \beta_0 \alpha_s(Q^2) \log \frac{\mu^2}{Q^2}$. With the same technique, it is easy to find also the three loops solution, which reads

$$\begin{aligned} \alpha_s(\mu^2) = & \frac{\alpha_s(Q^2)}{X} - b_1 \frac{\alpha_s^2(Q^2)}{X^2} \log X \\ & + \frac{\alpha_s^3(Q^2)}{X^3} \left[b_1^2 (\log^2 X - \log X - 1 + X) + b_2 (1 - X) \right]. \end{aligned} \quad (\text{A.1.15})$$

Note that the Landau pole is still present in the two- and three-loops solutions, and it is always given by Eq. (A.1.10). This is indeed a general feature: the Landau pole is always present in any perturbative solution to the running coupling equation.

Typically, the initial condition for α_s is given at the Z mass $Q^2 = m_Z^2$, because many measurements were made at LEP and more recently at colliders with high precision. Then, at the Z mass

$$m_Z = 91.18 \text{ GeV}, \quad (\text{A.1.16})$$

the current better estimate of α_s is [83, 84]

$$\alpha_s(m_Z^2) = 0.1184 \pm 0.0007. \quad (\text{A.1.17})$$

From this value we could compute the Landau pole; however, we have to choose the value of n_f , i.e. the number of flavours, which appears in the coefficient β_0 . With the two extreme choices $n_f = 0$ and $n_f = 6$ we get, respectively,

$$\mu_L(n_f = 0) \sim 730 \text{ MeV}, \quad \mu_L(n_f = 6) \sim 47 \text{ MeV}. \quad (\text{A.1.18})$$

These two results are quite different each other, but nevertheless they set the order of magnitude of the non-perturbative scale of QCD, which is of the order of some hundreds MeV. The proper choice for the value of n_f is a matter of renormalization scheme choice. We are going to discuss the most common scheme in the next Section.

A.1.2 Quark masses thresholds

The number of flavours n_f is generically not kept fixed. What is usually adopted is the so called *variable flavour number scheme*,¹ a renormalization scheme in which the number of *active* flavours depends on the energy scale μ . This choice is motivated by the computation of the β function: the 1-loop coefficient β_0 is computed by the diagrams of Fig. A.1, where in the second diagram the fermions running in the loop

¹More precisely, this is the *zero-mass* variable flavour number scheme; there are several extensions of this scheme, but their discussion is beyond the purpose of this Appendix.

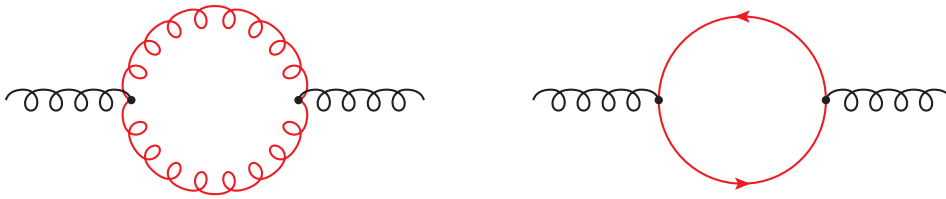


Figure A.1. Diagrams contributing to the 1-loop β -function.

are the quarks. If they were real, there would be a threshold for the diagram given by

$$\mu > 2m_q, \quad (\text{A.1.19})$$

being m_q the mass of the quark. Then, a natural choice would be to use as number of active flavours the numbers of quarks which have a mass less than half of the current energy μ . Since however such procedure is somehow arbitrary (quarks in the loop are virtual and the threshold is not really there) a simpler choice is to use just the mass, and not twice the mass, of the quarks to set the number of active flavours.

Then, starting as usual from $\alpha_s(m_Z^2)$ with $n_f = 5$ (only the top quark is heavier than the Z), one can build $\alpha_s(\mu^2)$ with n_f changing with μ^2 , by requiring continuity of the solution and then using as initial condition for any new branch the value of α_s at the quark thresholds. The resulting solution has a discontinuous derivative: one could imagine to perform a smearing to eliminate this problem, but this goes beyond the purpose of this Appendix. In Fig. A.2 we show explicitly the 1- and 2-loops solutions; the Landau pole at low energies and the asymptotic freedom at large energies are both evident.

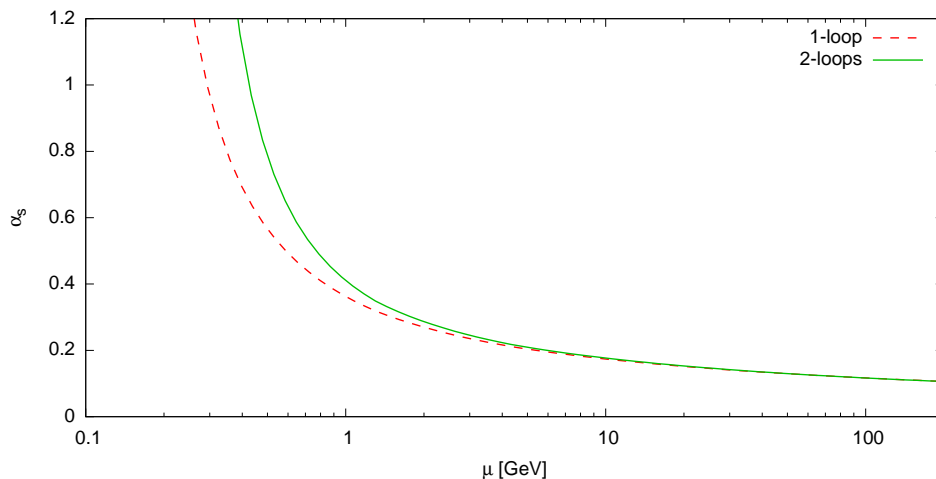


Figure A.2. The running coupling α_s as a function of μ at 1- and 2-loops.

As a final comment, we want to show where the Landau pole is located using this variable flavour number scheme. We first note that, because of the patching of $\alpha_s(\mu^2)$ at quark thresholds, the position of the Landau pole now will be different for different orders of the solution. We then take as representative examples the 1- and 2-loops solution Eq. (A.1.14) and find

$$\mu_L^{1\text{-loop}} \sim 150 \text{ MeV}, \quad \mu_L^{2\text{-loop}} \sim 180 \text{ MeV}, \quad (\text{A.1.20})$$

where we have used the quarks masses given in Sect. 1.1. Note that the two predictions are of the same order, even if they are in the non-perturbative region of QCD where the running is no longer under control. From Fig. A.2 it is clear that indeed perturbation theory in QCD breaks down at a scale around 1 GeV, where the coupling starts growing fast and the two curves become very different.

B Mellin transformation

Contents

B.1 Laplace transform	137
B.2 The Mellin transform	138
B.2.1 Fixed Talbot Algorithm	139
B.2.2 Convolution	139
B.3 Plus distribution.	140
B.3.1 Convolution	141
B.3.2 Mellin transform of plus distributions	141
B.4 Mellin transformation of logarithms	143
B.4.1 Explicit computation of Mellin transforms for the first few orders	148

In this Appendix we collect some useful definitions and results concerning Mellin transformations. In particular, we concentrate our attention to the case of logarithms, which are the main subject of this thesis.

B.1 Laplace transform

The Mellin transform is a particular case of a Laplace transform. Hence we first start considering some definitions and results about Laplace transforms, which remains also in the case of Mellin transforms.

The (unilateral) Laplace transform of a function $f(t)$ is defined as

$$\tilde{f}(s) \equiv \int_0^{\infty} dt e^{-st} f(t). \tag{B.1.1}$$

If the function $\tilde{f}(s)$ exists, then it is regular for $\text{Re } s > k$ for some value of k depending on $f(t)$. This is because, in order for the transform to exist, the function $f(t)$ can grow at most as e^{kt} as $t \rightarrow \infty$, and then the integral is convergent for $\text{Re } s > c$.

The inverse is given by ($c > k$)

$$f(t) = \frac{1}{2\pi i} \int_{c-i\infty}^{c+i\infty} ds e^{st} \tilde{f}(s). \tag{B.1.2}$$

The proof is easy:

$$\begin{aligned}
\frac{1}{2\pi i} \int_{c'-i\infty}^{c'+i\infty} ds e^{st} \tilde{f}(s) &= \int_0^\infty dt' f(t') \frac{1}{2\pi i} \int_{c-i\infty}^{c+i\infty} ds e^{s(t-t')} \\
&= \int_0^\infty dt' f(t') \delta(t-t') \\
&= \begin{cases} f(t) & t \geq 0 \\ 0 & t < 0. \end{cases}
\end{aligned} \tag{B.1.3}$$

Note that, if we had taken the bilateral transform, i.e. with lower limit $-\infty$, the inverse transform Eq. (B.1.2) would have reproduced $f(t)$ in the whole range $-\infty < t < \infty$. Hence, the unilateral transform is suitable for functions defined only for $t > 0$, while the bilateral for functions defined everywhere.

If $f(t)$ is real, then $\tilde{f}(s)$ is a real function, i.e. it satisfies

$$\tilde{f}(s^*) = \tilde{f}(s)^* \tag{B.1.4}$$

where $*$ indicates complex conjugation, as one can immediately verify from the definition Eq. (B.1.1).

B.2 The Mellin transform

When a function $f(x)$ is defined in the range $0 < x < 1$ (as many of the functions in this thesis) a Laplace transform can be taken by using $x = e^{-t}$. The resulting transform,

$$\tilde{f}(N) \equiv \mathcal{M}[f](N) \equiv \int_0^1 dx x^{N-1} f(x), \tag{B.2.1}$$

is called *Mellin transform*. Even if we changed name, N is the same variable as s , and then the inverse, according to Eq. (B.1.2), is

$$f(x) \equiv \mathcal{M}^{-1}[\tilde{f}](x) = \frac{1}{2\pi i} \int_{c-i\infty}^{c+i\infty} dN x^{-N} \tilde{f}(N), \tag{B.2.2}$$

where c must be greater than the real part of the rightmost singularity (which must exist, because again $\tilde{f}(N)$ has a convergence abscissa). The integration contour can be deformed at will, provided it does not cross any singularity — all the singularities must be at the left of the contour. Being $x < 1$, a typical deformation consists in giving a phase to the upper and lower parts of the integration path in such a way that the real part of N be negative and increasing as its absolute value goes to infinity. In particular, when $\tilde{f}(N)$ is a real function (see definition in Eq. (B.1.4)), we can perform the following manipulations

$$\begin{aligned}
f(x) &= \frac{1}{2\pi i} \int_{c-i\infty}^{c+i\infty} dN x^{-N} \tilde{f}(N) \\
&= \frac{1}{\pi} \operatorname{Im} \int_c^{c+i\infty} dN x^{-N} \tilde{f}(N) \\
&= \frac{1}{\pi} \int_0^{+\infty} dt \operatorname{Im} \left[(i - \epsilon) x^{-c-(i-\epsilon)t} \tilde{f}(c + (i - \epsilon)t) \right]
\end{aligned}$$

$$= \frac{x^{-c}}{\pi} \int_0^{+\infty} du \operatorname{Im} \left[\frac{\epsilon - i}{\log x} e^{(i-\epsilon)u} \tilde{f} \left(c - (i-\epsilon) \frac{u}{\log x} \right) \right] \quad (\text{B.2.3})$$

where in the last two steps we have deformed the integration contour according to $N = c + (i - \epsilon)t$, $\epsilon > 0$, to guarantee numerical convergence.

B.2.1 Fixed Talbot Algorithm

An alternative and numerically powerful way to compute the inverse Mellin transform is to use the Talbot contour [90], where

$$N = N(\theta) = r\theta (\cot \theta + i) \quad (\text{B.2.4})$$

with r a free parameter. Then the inverse Mellin integral becomes

$$f(x) = \frac{1}{2\pi i} \int_{-\pi}^{\pi} d\theta x^{-N(\theta)} \tilde{f}(N(\theta)) N'(\theta) \quad (\text{B.2.5})$$

or, using the reality of \tilde{f} ,

$$f(x) = \frac{r}{\pi} \int_0^{\pi} d\theta \operatorname{Re} \left[x^{-N(\theta)} \tilde{f}(N(\theta)) [1 + i\sigma(\theta)] \right] \quad (\text{B.2.6})$$

where $N'(\theta) = ir[1 + i\sigma(\theta)]$ and

$$\sigma(\theta) = \theta + (\theta \cot \theta - 1) \cot \theta. \quad (\text{B.2.7})$$

For numerical applications, the integral can be computed using a trapezoidal rule using the points $\theta_k = k\pi/K$ with K a constant: the resulting expression

$$f(x) \simeq \frac{r}{K} \left[\frac{1}{2} x^{-r} \tilde{f}(r) + \sum_{k=1}^K \operatorname{Re} \left(x^{-N(\theta_k)} \tilde{f}(N(\theta_k)) [1 + i\sigma(\theta_k)] \right) \right] \quad (\text{B.2.8})$$

is known as the *fixed Talbot algorithm* [90]. In Ref. [90] an optimal choice for r is suggested:

$$r = \frac{2K}{5 \log \frac{1}{x}}; \quad (\text{B.2.9})$$

then, the relative precision is approximately $10^{-0.6K}$.

B.2.2 Convolution

Let us define the convolution product \otimes

$$(f \otimes g)(x) = \int_x^1 \frac{dy}{y} f(y) g\left(\frac{x}{y}\right). \quad (\text{B.2.10})$$

$$= \int_0^1 dy \int_0^1 dz f(y) g(z) \delta(x - yz) \quad (\text{B.2.11})$$

In the second form, it is clear that it is commutative

$$f \otimes g = g \otimes f \quad (\text{B.2.12})$$

and it can be easily extended to many functions

$$(f_1 \otimes \dots \otimes f_n)(x) = \int_0^1 dy_1 \cdots \int_0^1 dy_n f_1(y_1) \cdots f_n(y_n) \delta(x - y_1 \cdots y_n). \quad (\text{B.2.13})$$

Under Mellin transformation, the convolution product diagonalizes:

$$\begin{aligned} \mathcal{M}[f \otimes g](N) &= \int_0^1 dx x^{N-1} \int_0^1 dy \int_0^1 dz f(y) g(z) \delta(x - yz) \\ &= \int_0^1 dy y^{N-1} f(y) \int_0^1 dz z^{N-1} g(z) = \tilde{f}(N) \tilde{g}(N) \end{aligned} \quad (\text{B.2.14})$$

B.3 Plus distribution

The plus distribution arises from the cancellation of soft divergences, and is defined as

$$\int_0^1 dz [f(z)]_+ g(z) = \int_0^1 dz f(z) [g(z) - g(1)]. \quad (\text{B.3.1})$$

From the definition it follows that, formally,

$$[f(z)]_+ = f(z) - \delta(1-z) \int_0^1 dz f(z), \quad (\text{B.3.2})$$

but, if $f(z)$ diverges as $z \rightarrow 1$, this expression makes sense only in a regularized form:

$$[f(z)]_+ = \lim_{\eta \rightarrow 0^+} \left[\Theta(1-\eta-z) f(z) - \delta(1-z) \int_0^{1-\eta} dz f(z) \right], \quad (\text{B.3.3})$$

where the limit is intended to be performed *after* the integration over the test function $g(z)$.

The plus distribution defined in Eq. (B.3.1) regularizes functions which diverge as $z \rightarrow 1$ at most as

$$(1-y)^{-\alpha}, \quad \alpha < 2 \quad (\text{B.3.4})$$

in the sense that the integral (B.3.1) over any test function $g(z)$ is finite. In particular, the usual logarithms

$$\frac{\log^k(1-z)}{1-z} \quad (\text{B.3.5})$$

are properly regularized.

Some useful identities can be derived directly from the definition; if $g(z)$ is a regular function as $z \rightarrow 1$, then

$$[g(z) f(z)]_+ = g(z) [f(z)]_+ - \delta(1-z) \int_0^1 dy g(y) [f(y)]_+ \quad (\text{B.3.6})$$

$$g(z) [f(z)]_+ = g(1) [f(z)]_+ + [g(z) - g(1)] f(z). \quad (\text{B.3.7})$$

In the last term of second line, the plus distribution is no longer necessary since $g(z) - g(1)$ regularizes $f(z)$. One interesting consequence is the following relation

$$\left(\frac{\log z}{1-z} \right)_+ = \frac{\log z}{1-z} + \zeta_2 \delta(1-z) \quad (\text{B.3.8})$$

where we have noted that $\log 1 = 0$ and we have used

$$\begin{aligned}
\int_0^1 dy \frac{\log z}{1-z} &= \lim_{b \rightarrow 0} \frac{d}{da} \int_0^1 dy z^a (1-z)^{b-1} \Big|_{a=0} \\
&= \lim_{b \rightarrow 0} [\psi_0(1+a) - \psi_0(1+a+b)] \frac{\Gamma(1+a)\Gamma(b)}{\Gamma(1+a+b)} \Big|_{a=0} \\
&= \lim_{b \rightarrow 0} \frac{\psi_0(1) - \psi_0(1+b)}{b} \\
&= -\psi_1(1) = -\zeta_2
\end{aligned} \tag{B.3.9}$$

(for details about Γ and ψ functions, see App. E.1).

B.3.1 Convolution

Now we want to investigate how a convolution appear when extended to distributions. This is not trivial, because the definition of the plus distribution Eq. (B.3.1) involves an integral from 0 to 1, while a convolution written as Eq. (B.2.10) is an integral from x to 1. The obvious way to extend the definition is to use instead Eq. (B.2.11):

$$\begin{aligned}
([f]_+ \otimes g)(x) &= \int_0^1 dy \int_0^1 dz [f(y)]_+ g(z) \delta(x-yz) \\
&= \int_0^1 dy \int_0^1 dz f(y) g(z) [\delta(x-yz) - \delta(x-z)] \\
&= \int_0^1 dy f(y) \left[\int_0^1 dz g(z) \delta(x-yz) - g(x) \right] \\
&= \int_x^1 dy f(y) \left[\frac{1}{y} g\left(\frac{x}{y}\right) - g(x) \right] - g(x) \int_0^x dy f(y).
\end{aligned} \tag{B.3.10}$$

The last form could be grouped in the more natural way

$$\int_x^1 \frac{dy}{y} f(y) g\left(\frac{x}{y}\right) - g(x) \int_0^1 dy f(y), \tag{B.3.11}$$

as one would have immediately obtained using Eq. (B.3.2), but in this form both integrals are not convergent, and can be interpreted only as a limit

$$\lim_{\eta \rightarrow 0^+} \left[\int_x^{1-\eta} \frac{dy}{y} f(y) g\left(\frac{x}{y}\right) - g(x) \int_0^{1-\eta} dy f(y) \right]. \tag{B.3.12}$$

It must be noticed that the 0 to x region contributes to the result of the convolution: this is not surprising, because it was already intrinsically included in the definition of the plus distribution, but it can be relevant for applications.

B.3.2 Mellin transform of plus distributions

From the definition, the Mellin transform of a distribution is

$$\mathcal{M}[(f)_+] (N) = \int_0^1 dz (z^{N-1} - 1) f(z). \tag{B.3.13}$$

The behaviour in N space of a distribution is qualitatively different from that of an ordinary function. To see this, we prove first the following

Theorem B.3.1. *If $f(z)$ is real, then $|\mathcal{M}[f](N)|$ for real $N > 0$ is bounded by a decreasing function which tends to 0 as $N \rightarrow \infty$.*

Proof. First, we see that $|\mathcal{M}[f](N)|$ is bounded by

$$|\mathcal{M}[f](N)| \leq \int_0^1 dz |z^{N-1} f(z)| = \mathcal{M}[|f|](N) \quad (\text{B.3.14})$$

where in the last equality we used the fact that z^{N-1} is positive for N real. The rest of the proof consists in showing that $\mathcal{M}[|f|](N)$ is a decreasing function:

$$\frac{d}{dN} \mathcal{M}[|f|](N) = - \int_0^1 dz \log \frac{1}{z} z^{N-1} |f(z)| \leq 0 \quad (\text{B.3.15})$$

because $\log \frac{1}{z}$ is positive in the integration range. The last part of the theorem is proved by noting that, in the $N \rightarrow \infty$ limit, the integrand tends to 0 almost everywhere: by using the monotone convergence theorem we have the hypothesis.

The proof shows in particular that if $f(z)$ is positive in the whole integration range then the Mellin transform monotonically decreases. This is not true for distributions. For example, the Mellin transform of $\delta(1-z)$ is 1, a constant for all values of N , and in particular it does not go to 0 as N gets large. For the interesting case of plus distributions, we can prove the following

Theorem B.3.2. *For real $N > 1$, if $f(z)$ is real and singular in $z = 1$ then $|\mathcal{M}[(f)_+](N)|$ is bounded by an increasing function of N and it diverges as $N \rightarrow \infty$.*

Proof. As before, we note first that

$$|\mathcal{M}[(f)_+](N)| \leq \int_0^1 dz |(z^{N-1} - 1) f(z)| \stackrel{N \geq 1}{=} -\mathcal{M}[(|f|)_+](N) \quad (\text{B.3.16})$$

where now the minus sign comes from the fact that $z^{N-1} - 1 < 0$ for $N > 1$. Then, $|\mathcal{M}[(f)_+](N)|$ is bounded by $-\mathcal{M}[(|f|)_+](N)$; note that, in this case, the Mellin transform is positive is $f(z) < 0$. The derivative of the bounding function is

$$-\frac{d}{dN} \mathcal{M}[(|f|)_+](N) = \int_0^1 dz \log \frac{1}{z} z^{N-1} |f(z)| \geq 0 \quad (\text{B.3.17})$$

and hence it is an increasing function. Using again the monotone convergence theorem, we can pass the limit $N \rightarrow \infty$ under the integral and see that the result is

$$|\mathcal{M}[(f)_+](N)| \stackrel{N \rightarrow \infty}{\rightarrow} \left| \int_0^1 dz f(z) \right| \quad (\text{B.3.18})$$

which is divergent.

Note that, since the monotonically increase applies only to the bound, this theorem does not limit the Mellin transform from being small for a wide range in N ; however, since $|\mathcal{M}[(f)_+](N)|$ diverges in the limit $N \rightarrow \infty$, it must start increasing at some point. Anyway, for simple functions which have the same sign in $0 < z < 1$, the bounds are saturated and the monotonically increase applies.

Then, we can conclude that the difference between the Mellin transform of a function and that of a plus distribution of a $z = 1$ singular function is that the first is limited and goes to zero at larger N , the second instead at some point increases and goes to infinity at large N .

B.4 Mellin transformation of logarithms

In this Section we compute explicitly the Mellin transforms of logarithms, which appear in (or are related to) perturbative computations of coefficients functions. To begin with, we consider the following distributions:

$$\left(\frac{\log^k(1-z)}{1-z}\right)_+, \quad \left(\frac{\log^k \log \frac{1}{z}}{\log \frac{1}{z}}\right)_+, \quad \left(\frac{\log^k \frac{1-z}{\sqrt{z}}}{1-z}\right)_+ \quad (\text{B.4.1a})$$

and also

$$\left(\frac{\log^k \frac{1-z}{\sqrt{z}}}{1-z}\right)'_+ = \sum_{j=0}^k \binom{k}{j} \left(\frac{\log^{k-j}(1-z)}{1-z}\right)_+ \log^j \frac{1}{\sqrt{z}} \quad (\text{B.4.1b})$$

where the $'$ denotes that the plus distribution has to be put only around $\frac{\log^{k-j}(1-z)}{1-z}$; note that in the sum only the first term needs the plus symbol, since $\log \sqrt{z} = 0$ in $z = 1$. These distributions can be obtained, respectively, as the k -th ξ -derivative of the following generating distributions, computed in $\xi = 0$:

$$\left[(1-z)^{\xi-1}\right]_+, \quad \left[\log^{\xi-1} \frac{1}{z}\right]_+, \quad \left[z^{-\xi/2}(1-z)^{\xi-1}\right]_+, \quad z^{-\xi/2} \left[(1-z)^{\xi-1}\right]_+. \quad (\text{B.4.2})$$

Their Mellin transforms can be computed easily, and are

$$\mathcal{M} \left[\left((1-z)^{\xi-1} \right)_+ \right] = \Gamma(\xi) \left[\frac{\Gamma(N)}{\Gamma(N+\xi)} - \frac{1}{\Gamma(1+\xi)} \right] \quad (\text{B.4.3a})$$

$$\mathcal{M} \left[\left(\log^{\xi-1} \frac{1}{z} \right)_+ \right] = \Gamma(\xi) \left[N^{-\xi} - 1 \right] \quad (\text{B.4.3b})$$

$$\mathcal{M} \left[\left(z^{-\xi/2} (1-z)^{\xi-1} \right)_+ \right] = \Gamma(\xi) \left[\frac{\Gamma(N-\xi/2)}{\Gamma(N+\xi/2)} - \frac{\Gamma(1-\xi/2)}{\Gamma(1+\xi/2)} \right] \quad (\text{B.4.3c})$$

$$\mathcal{M} \left[z^{-\xi/2} \left((1-z)^{\xi-1} \right)_+ \right] = \Gamma(\xi) \left[\frac{\Gamma(N-\xi/2)}{\Gamma(N+\xi/2)} - \frac{1}{\Gamma(1+\xi)} \right]. \quad (\text{B.4.3d})$$

Since $\Gamma(\xi)$ has a simple pole in $\xi = 0$, the limit $\xi \rightarrow 0$ of these functions needs the computation of a derivative. To be precise, we note that every Mellin transform above is written in the form

$$\Gamma(\xi) F_N(\xi) = \frac{1}{\xi} \Gamma(1+\xi) F_N(\xi) \equiv \frac{1}{\xi} G_N(\xi) \quad (\text{B.4.4})$$

with $F_N(0) = G_N(0) = 0$, which has the power expansion

$$\frac{1}{\xi} G_N(\xi) = \sum_{k=0}^{\infty} \frac{G_N^{(k+1)}(0)}{(k+1)!} \xi^k. \quad (\text{B.4.5})$$

Hence, the k -th derivative of the generic Mellin transform Eqs. (B.4.3) is

$$\frac{G_N^{(k+1)}(0)}{k+1} = \frac{1}{k+1} \sum_{j=0}^k \binom{k+1}{j} \Gamma^{(j)}(1) F_N^{(k+1-j)}(0) \quad (\text{B.4.6})$$

where the $(k+1)$ -th term in the sum has been omitted because $F_N(0) = 0$. In the case of the first and the last of Eqs. (B.4.3), a somewhat simpler expansion can be found by noting that for them $G_N(\xi)$ has the form

$$G_N(\xi) = \Gamma(1 + \xi) H_N(\xi) - 1, \quad (\text{B.4.7})$$

and then the derivatives are

$$\frac{G_N^{(k+1)}(0)}{k+1} = \frac{1}{k+1} \sum_{j=0}^{k+1} \binom{k+1}{j} \Gamma^{(j)}(1) H_N^{(k+1-j)}(0) \quad (\text{B.4.8})$$

where now the $(k+1)$ -th term is not null. We can now show explicitly the Mellin transforms of Eqs. (B.4.1):

$$\begin{aligned} \mathcal{M} \left[\left(\frac{\log^k(1-z)}{1-z} \right)_+ \right] &= \frac{1}{k+1} \sum_{j=0}^k \binom{k+1}{j} \Gamma^{(j)}(1) \left[\Gamma(N) \Delta^{(k+1-j)}(N) - \Delta^{(k+1-j)}(1) \right] \\ &= \frac{1}{k+1} \sum_{j=0}^{k+1} \binom{k+1}{j} \Gamma^{(j)}(1) \Gamma(N) \Delta^{(k+1-j)}(N) \end{aligned} \quad (\text{B.4.9a})$$

$$\mathcal{M} \left[\left(\frac{\log^k \log \frac{1}{z}}{\log \frac{1}{z}} \right)_+ \right] = \frac{1}{k+1} \sum_{j=0}^k \binom{k+1}{j} \Gamma^{(j)}(1) \log^{k+1-j} \frac{1}{N} \quad (\text{B.4.9b})$$

$$\mathcal{M} \left[\left(\frac{\log^k \frac{1-z}{\sqrt{z}}}{1-z} \right)_+ \right] = \frac{1}{k+1} \sum_{j=0}^k \binom{k+1}{j} \Gamma^{(j)}(1) \left[\Upsilon_{k+1-j}(N, 0) - \Upsilon_{k+1-j}(1, 0) \right] \quad (\text{B.4.9c})$$

$$\begin{aligned} \mathcal{M} \left[\left(\frac{\log^k \frac{1-z}{\sqrt{z}}}{1-z} \right)'_+ \right] &= \frac{1}{k+1} \sum_{j=0}^k \binom{k+1}{j} \Gamma^{(j)}(1) \left[\Upsilon_{k+1-j}(N, 0) - \Delta^{(k+1-j)}(1) \right] \\ &= \frac{1}{k+1} \sum_{j=0}^{k+1} \binom{k+1}{j} \Gamma^{(j)}(1) \Upsilon_{k+1-j}(N, 0) \end{aligned} \quad (\text{B.4.9d})$$

where we have defined

$$\Delta(\xi) = 1/\Gamma(\xi) \quad (\text{B.4.10a})$$

$$\Upsilon_0(N, \xi) = \Gamma(N - \xi/2) \Delta(N + \xi/2) \quad (\text{B.4.10b})$$

and denoted with $\Upsilon_k(N, \xi)$ the k -th derivative of $\Upsilon_0(N, \xi)$ with respect to ξ . The equivalence of the two expressions in the first and last of Eqs. (B.4.9) is encoded in the relation

$$- \sum_{j=0}^k \binom{k+1}{j} \Gamma^{(j)}(1) \Delta^{(k+1-j)}(1) = \Gamma^{(k+1)}(1); \quad (\text{B.4.11})$$

indeed, grouping all terms on the same side we recognize the $(k+1)$ -th derivative of $\Gamma(\xi) \Delta(\xi) = 1$, which trivially vanishes.

At large N , all the expressions in Eqs. (B.4.9) are equivalent up to constant terms or terms suppressed by inverse powers of N . Indeed, the dominant terms in each first line of Eqs. (B.4.9) coincide at large N

$$\Gamma(N) \Delta^{(k+1-j)}(N) \simeq \log^{k+1-j} \frac{1}{N} \simeq \Upsilon_{k+1-j}(N, 0) \quad (\text{B.4.12})$$

up to corrections of order $1/N$. This can be verified using the Stirling approximation Eq. (E.1.8) on the generating functions, i.e.

$$\frac{\Gamma(N)}{\Gamma(N+\xi)} = N^{-\xi} + \mathcal{O}(N^{-1}) \quad (\text{B.4.13a})$$

$$\frac{\Gamma(N-\xi/2)}{\Gamma(N+\xi/2)} = N^{-\xi} + \mathcal{O}(N^{-1}). \quad (\text{B.4.13b})$$

The first subleading difference between Eqs. (B.4.9) is a constant: indeed in Eq. (B.4.9b) there are no constants, while in Eqs. (B.4.9a) and (B.4.9d) there is a $\Gamma^{(k+1)}(1)/(k+1)$, and finally in Eq. (B.4.9c) there is a constant term given by

$$-\frac{1}{k+1} \sum_{j=0}^k \binom{k+1}{j} \Gamma^{(j)}(1) \Upsilon_{k+1-j}(1, 0). \quad (\text{B.4.14})$$

The difference between these two non-zero constants can be better computed by taking the difference of the generating functions Eqs. (B.4.3c) and (B.4.3d):

$$\begin{aligned} \mathcal{M} \left[\left(\frac{\log^k \frac{1-z}{\sqrt{z}}}{1-z} \right)_+ - \left(\frac{\log^k \frac{1-z}{\sqrt{z}}}{1-z} \right)'_+ \right] &= \frac{d^k}{d\xi^k} \left[\Gamma(\xi) \left(\frac{1}{\Gamma(1+\xi)} - \frac{\Gamma(1-\xi/2)}{\Gamma(1+\xi/2)} \right) \right]_{\xi=0} \\ &= \frac{d^k}{d\xi^k} \left[\frac{1-C(\xi)}{\xi} \right]_{\xi=0} \\ &= -\frac{C^{(k+1)}(0)}{k+1} \end{aligned} \quad (\text{B.4.15})$$

having defined

$$C(\xi) = \frac{\Gamma(1+\xi)\Gamma(1-\xi/2)}{\Gamma(1+\xi/2)}. \quad (\text{B.4.16})$$

In threshold resummation (see Chap. 2), only the large- N part of the coefficient function, i.e. powers of $\log N$, is resummed. This is the reason why we computed also the Mellin transforms Eq. (B.4.9b): even if those z -space logarithms never appear in perturbative computations, their Mellin transform produces instead the resummed logarithms. From Eq. (B.4.3b), we can then find the inverse Mellin transforms of powers of $\log \frac{1}{N}$, since $N^{-\xi}$ is their generating function. We have

$$N^{-\xi} = 1 + \frac{1}{\Gamma(\xi)} \mathcal{M} \left[\left(\log^{\xi-1} \frac{1}{z} \right)_+ \right] \quad (\text{B.4.17})$$

and therefore

$$\mathcal{M}^{-1} [N^{-\xi}] = \delta(1-z) + \left(\frac{\log^{\xi-1} \frac{1}{z}}{\Gamma(\xi)} \right)_+. \quad (\text{B.4.18})$$

Taking k derivatives with respect to ξ at $\xi = 0$ we get either one of the following expressions

$$\mathcal{M}^{-1} \left[\log^k \frac{1}{N} \right] = \delta_{k0} \delta(1-z) + \left(\frac{d^k}{d\xi^k} \frac{\log^{\xi-1} \frac{1}{z}}{\Gamma(\xi)} \Big|_{\xi=0} \right)_+ \quad (\text{B.4.19a})$$

$$= \delta_{k0} \delta(1-z) + \frac{k!}{2\pi i} \left(\oint \frac{d\xi}{\xi^{k+1}} \frac{\log^{\xi-1} \frac{1}{z}}{\Gamma(\xi)} \right)_+ \quad (\text{B.4.19b})$$

$$= \delta_{k0} \delta(1-z) + \left(\frac{1}{\log \frac{1}{z}} \sum_{j=1}^k \binom{k}{j} \Delta^{(j)}(0) \log^{k-j} \log \frac{1}{z} \right)_+ , \quad (\text{B.4.19c})$$

where we have used again $\Delta(\xi) = 1/\Gamma(\xi)$ and $\Delta(0) = 0$. The derivatives of $\Delta(\xi)$ in $\xi = 0$ can be related to those in $\xi = 1$ using Eq. (E.1.14); equivalently, we can write directly $\Delta(\xi) = \xi\Delta(1+\xi)$ before computing the derivatives, obtaining

$$\mathcal{M}^{-1} \left[\log^k \frac{1}{N} \right] = \delta_{k0} \delta(1-z) + \left(\frac{k}{\log \frac{1}{z}} \sum_{j=0}^{k-1} \binom{k-1}{j} \Delta^{(j)}(1) \log^{k-1-j} \log \frac{1}{z} \right)_+ . \quad (\text{B.4.19d})$$

Note that the result is a distribution, consistently with the fact that $\log^k N$ is an increasing function of N , see Theorem B.3.2. In the second form, directly related to the first by Cauchy theorem, the integration contour is any closed curve in the complex ξ plane which encircles the origin $\xi = 0$.

Starting from one of the other of Eqs. (B.4.3), we can use the same procedure to find the inverse Mellin transform of the analogous of a power of $\log \frac{1}{N}$, according to the large- N equivalence Eq. (B.4.12). At the level of the generating functions, we have then, respectively,

$$\mathcal{M}^{-1} \left[\frac{\Gamma(N)}{\Gamma(N+\xi)} \right] = \frac{1}{\Gamma(1+\xi)} \delta(1-z) + \left[\frac{(1-z)^{\xi-1}}{\Gamma(\xi)} \right]_+ \quad (\text{B.4.20a})$$

$$\mathcal{M}^{-1} \left[\frac{\Gamma(N-\xi/2)}{\Gamma(N+\xi/2)} \right] = \frac{\Gamma(1-\xi/2)}{\Gamma(1+\xi/2)} \delta(1-z) + \left[\frac{z^{-\xi/2}(1-z)^{\xi-1}}{\Gamma(\xi)} \right]_+ \quad (\text{B.4.20b})$$

$$= \frac{1}{\Gamma(1+\xi)} \delta(1-z) + \frac{z^{-\xi/2}}{\Gamma(\xi)} \left[(1-z)^{\xi-1} \right]_+ . \quad (\text{B.4.20c})$$

The left-hand-side of each equation can be confused, up to terms of order $1/N$, with the inverse Mellin of $N^{-\xi}$, Eq. (B.4.13). Moreover, since the last two lines are different forms of the same inverse Mellin, we can choose to use one and discard the other: the second, Eq. (B.4.20c), is somewhat simpler and then we use it. By computing the ξ -derivatives in $\xi = 0$ in the left-hand-side we get powers of $\log \frac{1}{N}$ up to terms suppressed as $1/N$. Then, up to this accuracy, using the derivative and the Cauchy notations we have in the first case, Eq. (B.4.20a),

$$\mathcal{M}^{-1} \left[\log^k \frac{1}{N} \right] \simeq \Delta^{(k)}(1) \delta(1-z) + \left(\frac{d^k}{d\xi^k} \frac{(1-z)^{\xi-1}}{\Gamma(\xi)} \Big|_{\xi=0} \right)_+ \quad (\text{B.4.21a})$$

$$= \frac{k!}{2\pi i} \oint \frac{d\xi}{\xi^{k+1} \Gamma(\xi)} \left(\left[(1-z)^{\xi-1} \right]_+ + \frac{1}{\xi} \delta(1-z) \right) \quad (\text{B.4.21b})$$

and in the second case, Eq. (B.4.20c),

$$\mathcal{M}^{-1} \left[\log^k \frac{1}{N} \right] \simeq \Delta^{(k)}(1) \delta(1-z) + \frac{d^k}{d\xi^k} \frac{z^{-\xi/2} \left[(1-z)^{\xi-1} \right]_+}{\Gamma(\xi)} \Big|_{\xi=0} \quad (\text{B.4.22a})$$

$$= \frac{k!}{2\pi i} \oint \frac{d\xi}{\xi^{k+1} \Gamma(\xi)} \left(z^{-\xi/2} \left[(1-z)^{\xi-1} \right]_+ + \frac{1}{\xi} \delta(1-z) \right). \quad (\text{B.4.22b})$$

The presence of the $\delta(1-z)$ term in Eqs. (B.4.21), (B.4.22), is crucial for the equalities to hold up to power suppressed terms: indeed, in threshold resummation, $\delta(1-z)$ terms (constants in N space) are considered enhanced at large N , since they don't vanish, and hence they must not be neglected. Note that, in both cases, the z dependence can be simplified using the relation

$$\left[(1-z)^{\xi-1} \right]_+ + \frac{1}{\xi} \delta(1-z) = (1-z)^{\xi-1} \quad (\text{B.4.23})$$

which holds for $\text{Re } \xi > 0$. Since the integral involves values of ξ with negative real part, this substitution is in principle not allowed; nevertheless, Eq. (B.4.23) can be continued analytically to the relevant values of ξ , obtaining expressions equivalent to Eqs. (B.4.21), (B.4.22) without the $\delta(1-z)$ term and without the plus distribution symbol. This can be used, for instance, if one performs a convolution analytically *before* the ξ integration; otherwise, if the ξ integral is computed before, the convolution would not be convergent anymore.

We now move to the Mellin transform of suppressed logarithms. In particular we consider

$$(1-z)^p \log^k(1-z), \quad p \geq 0; \quad (\text{B.4.24})$$

its Mellin transform is

$$\mathcal{M} \left[(1-z)^p \log^k(1-z) \right] = \frac{d}{d\xi} \mathcal{M} \left[(1-z)^{p+\xi} \right]_{\xi=0} \quad (\text{B.4.25})$$

$$= \frac{d}{d\xi} \left[\frac{\Gamma(N) \Gamma(p+1+\xi)}{\Gamma(N+p+1+\xi)} \right]_{\xi=0} \quad (\text{B.4.26})$$

$$= \Gamma(N) \sum_{j=0}^k \binom{k}{j} \Gamma^{(j)}(1+p) \Delta^{(k-j)}(N+1+p). \quad (\text{B.4.27})$$

The prefactor can be written as

$$\Gamma(N) = \frac{\Gamma(N+1+p)}{N(N+1) \cdots (N+p)} \quad (\text{B.4.28})$$

from which we have a clear large- N interpretation in terms of powers of $\log \frac{1}{N}$:

$$\mathcal{M} \left[(1-z)^p \log^k(1-z) \right] \stackrel{N \rightarrow \infty}{\simeq} \frac{1}{N^{p+1}} \sum_{j=0}^k \binom{k}{j} \Gamma^{(j)}(1+p) \log^{k-j} \frac{1}{N}. \quad (\text{B.4.29})$$

With the same technique we can compute the Mellin transform of a power of $\log z$ divided by $1-z$, which turns out to be

$$\mathcal{M} \left[\frac{\log^k z}{1-z} \right] = \frac{d^k}{d\eta^k} \frac{d}{d\epsilon} \left[\frac{\Gamma(N+\eta)}{\Gamma(N+\eta+\epsilon)} \right]_{\eta=\epsilon=0} = -\psi_k(N). \quad (\text{B.4.30})$$

Finally, the Mellin transform of a power of $\log z$ is

$$\mathcal{M} \left[\log^k z \right] = \psi_k(N+1) - \psi_k(N) = (-)^k \frac{k!}{N^{k+1}}. \quad (\text{B.4.31})$$

B.4.1 Explicit computation of Mellin transforms for the first few orders

We now turn to the explicit computation of the Mellin transforms Eqs. (B.4.9) in terms of elementary special functions. Using the recursion

$$\Delta^{(k+1)}(N) = - \sum_{j=0}^k \binom{k}{j} \Delta^{(j)}(N) \psi_{k-j}(N) \quad (\text{B.4.32})$$

we get for the first few terms of Eq. (B.4.9a)

$$\Gamma(N) \Delta^{(1)}(N) = -\psi_0(N) \quad (\text{B.4.33a})$$

$$\Gamma(N) \Delta^{(2)}(N) = -\psi_1(N) + \psi_0^2(N) \quad (\text{B.4.33b})$$

$$\Gamma(N) \Delta^{(3)}(N) = -\psi_2(N) + 3\psi_1(N)\psi_0(N) - \psi_0^3(N) \quad (\text{B.4.33c})$$

$$\Gamma(N) \Delta^{(4)}(N) = -\psi_3(N) + 4\psi_2(N)\psi_0(N) + 3\psi_1^2(N) - 6\psi_1(N)\psi_0^2(N) + \psi_0^4(N) \quad (\text{B.4.33d})$$

and, when $N = 1$, we have

$$\Delta^{(1)}(1) = \gamma_E \quad (\text{B.4.34a})$$

$$\Delta^{(2)}(1) = \gamma_E^2 - \zeta_2 \quad (\text{B.4.34b})$$

$$\Delta^{(3)}(1) = \gamma_E^3 - 3\gamma_E\zeta_2 + 2\zeta_3 \quad (\text{B.4.34c})$$

$$\Delta^{(4)}(1) = \gamma_E^4 - 6\gamma_E^2\zeta_2 + 8\gamma_E\zeta_3 + 3\zeta_2^2 - 6\zeta_4, \quad (\text{B.4.34d})$$

having used

$$\psi_0(1) = -\gamma_E \quad (\text{B.4.35a})$$

$$\psi_1(1) = \zeta_2 \quad (\text{B.4.35b})$$

$$\psi_2(1) = -2\zeta_3 \quad (\text{B.4.35c})$$

$$\psi_3(1) = 6\zeta_4. \quad (\text{B.4.35d})$$

Using instead the recursion

$$\Gamma^{(k+1)}(N) = \sum_{j=0}^k \binom{k}{j} \Gamma^{(j)}(N) \psi_{k-j}(N) \quad (\text{B.4.36})$$

and Eqs. (B.4.35), we get for the Γ derivatives in $N = 1$

$$\Gamma^{(1)}(1) = -\gamma_E \quad (\text{B.4.37a})$$

$$\Gamma^{(2)}(1) = \gamma_E^2 + \zeta_2 \quad (\text{B.4.37b})$$

$$\Gamma^{(3)}(1) = -\gamma_E^3 - 3\gamma_E\zeta_2 - 2\zeta_3 \quad (\text{B.4.37c})$$

$$\Gamma^{(4)}(1) = \gamma_E^4 + 6\gamma_E^2\zeta_2 + 8\gamma_E\zeta_3 + 3\zeta_2^2 + 6\zeta_4. \quad (\text{B.4.37d})$$

Concerning Eq. (B.4.9c) and Eq. (B.4.9d), we can find the recursion

$$\Upsilon_{k+1}(N, 0) = - \sum_{j=0}^k \binom{k}{j} \frac{1}{2} \left[\frac{1}{2^j} + \frac{1}{(-2)^j} \right] \Upsilon_{k-j}(N, 0) \psi_j(N)$$

$$= - \sum_{j=0, \text{ even}}^k \binom{k}{j} \frac{1}{2^j} \Upsilon_{k-j}(N, 0) \psi_j(N), \quad (\text{B.4.38})$$

from which we get

$$\Upsilon_1(N, 0) = -\psi_0(N) \quad (\text{B.4.39a})$$

$$\Upsilon_2(N, 0) = \psi_0^2(N) \quad (\text{B.4.39b})$$

$$\Upsilon_3(N, 0) = -\psi_0^3(N) - \frac{1}{4}\psi_2(N) \quad (\text{B.4.39c})$$

$$\Upsilon_4(N, 0) = \psi_0^4(N) + \psi_2(N)\psi_0(N). \quad (\text{B.4.39d})$$

Finally, the constant difference Eq. (B.4.15) can be easily computed from the recursion

$$C^{(k+1)}(0) = \sum_{j=0}^k \binom{k}{j} C^{(k-j)}(0) \left[1 - \frac{1 + (-1)^j}{2^{j+1}} \right] \psi_j(1) \quad (\text{B.4.40})$$

and can be expressed in terms of the Riemann ζ function according to Eq. (E.1.21). The first few terms are then given by

$$C^{(1)}(0) = 0 \quad (\text{B.4.41a})$$

$$C^{(2)}(0) = \zeta_2 \quad (\text{B.4.41b})$$

$$C^{(3)}(0) = -\frac{3}{2}\zeta_3 \quad (\text{B.4.41c})$$

$$C^{(4)}(0) = 3\zeta_2^2 + 6\zeta_4. \quad (\text{B.4.41d})$$

C Analytical expressions

Contents

C.1 Drell-Yan process at fixed perturbative order	151
C.1.1 Rapidity distribution	151
C.1.2 Invariant mass distribution	152
C.1.3 x_F distribution	153
C.2 Higgs production at fixed perturbative order	154
C.2.1 Finite top mass	156
C.3 Soft-gluons resummation formulae.	156
C.3.1 Resummed cross-section for the Drell-Yan process	157
C.3.2 Resummed cross-section for the Higgs production	159
C.3.3 Matching	159
C.4 High-energy resummation at NLO	160
C.4.1 BFKL kernel at NLO	160
C.4.2 Resummation at NLO	170
C.4.3 Resummation of quark anomalous dimension with running coupling	172
C.4.4 Resummation of coefficient functions	173

We collect in this Appendix various explicit analytical expressions which complete the discussions throughout the text.

C.1 Drell-Yan process at fixed perturbative order

To begin with, we present the LO and NLO expressions for the rapidity distribution and inclusive cross-section; the NNLO has been computed in Ref. [91] for the inclusive cross-section and in Ref. [72] for the rapidity distribution, but we won't report their lengthy expressions here.

C.1.1 Rapidity distribution

Recalling the notation introduced in Sect. 2.2, we have

$$\frac{1}{\tau} \frac{d\sigma}{dM^2 dY} = \sum_{i,j} \int_{\tau}^1 \frac{dz}{z} \int_0^1 du \mathcal{L}_{ij}^{\text{rap}}(z, u, \mu_F^2) \bar{C}_{ij} \left(z, u, \alpha_s(\mu_R^2), \frac{M^2}{\mu_F^2}, \frac{M^2}{\mu_R^2} \right) \quad (\text{C.1.1})$$

where Y is the hadronic rapidity and we restored the full dependence on renormalization and factorization scales (the dependence of $\mathcal{L}_{ij}^{\text{rap}}$ on τ and Y , Eq. (2.2.6), is implicitly understood). At next-to-leading order, the rapidity distribution receives contributions from quark-antiquark and quark-gluon subprocesses:

$$\frac{d\sigma^{\text{NLO}}}{dM^2 dY} = \frac{d\sigma_{q\bar{q}}^{\text{NLO}}}{dM^2 dY} + \frac{d\sigma_{qg+gq}^{\text{NLO}}}{dM^2 dY}. \quad (\text{C.1.2})$$

The $q\bar{q}$ contribution is given by

$$\bar{C}_{q\bar{q}} \left(z, u, \alpha_s, \frac{M^2}{\mu_F^2}, \frac{M^2}{\mu_R^2} \right) = \delta(1-z) + \frac{\alpha_s}{\pi} C_F F_q \left(z, u, \frac{M^2}{\mu_F^2} \right) + \mathcal{O}(\alpha_s^2) \quad (\text{C.1.3})$$

where

$$\begin{aligned} F_q \left(z, u, \frac{M^2}{\mu_F^2} \right) &= \frac{\delta(u) + \delta(1-u)}{2} \left[\delta(1-z) \left(\frac{\pi^2}{3} - 4 \right) + 2(1+z^2) \left(\frac{\log(1-z)}{1-z} \right)_+ \right. \\ &\quad \left. + \log \frac{M^2}{\mu_F^2} \left(\frac{1+z^2}{1-z} \right)_+ - \frac{1+z^2}{1-z} \log z + 1-z \right] \\ &\quad + \frac{1}{2} \frac{1+z^2}{1-z} \left[\left(\frac{1}{u} \right)_+ + \left(\frac{1}{1-u} \right)_+ \right] - (1-z). \end{aligned} \quad (\text{C.1.4})$$

The qg and gq contribution are given by

$$\bar{C}_{qg} \left(z, u, \alpha_s, \frac{M^2}{\mu_F^2}, \frac{M^2}{\mu_R^2} \right) = \frac{\alpha_s}{2\pi} T_F F_g \left(z, u, \frac{M^2}{\mu_F^2} \right) + \mathcal{O}(\alpha_s^2) \quad (\text{C.1.5})$$

$$\bar{C}_{gq} \left(z, u, \alpha_s, \frac{M^2}{\mu_F^2}, \frac{M^2}{\mu_R^2} \right) = \frac{\alpha_s}{2\pi} T_F F_g \left(z, 1-u, \frac{M^2}{\mu_F^2} \right) + \mathcal{O}(\alpha_s^2) \quad (\text{C.1.6})$$

where

$$\begin{aligned} F_g \left(z, u, \frac{M^2}{\mu_F^2} \right) &= \delta(u) \left[(z^2 + (1-z)^2) \left(\log \frac{(1-z)^2}{z} + \log \frac{M^2}{\mu_F^2} \right) + 2z(1-z) \right] \\ &\quad + (z^2 + (1-z)^2) \left(\frac{1}{u} \right)_+ + 2z(1-z) + (1-z)^2 u. \end{aligned} \quad (\text{C.1.7})$$

C.1.2 Invariant mass distribution

The inclusive coefficient functions are found integrating over the hadronic rapidity Y , whose dependence is all contained in the definition Eq. (2.2.6) of $\mathcal{L}_{ij}^{\text{rap}}$. We get

$$\frac{d\sigma^{\text{NLO}}}{dM^2} = \frac{d\sigma_{q\bar{q}}^{\text{NLO}}}{dM^2} + \frac{d\sigma_{qg+gq}^{\text{NLO}}}{dM^2} \quad (\text{C.1.8})$$

with

$$\frac{1}{\tau} \frac{d\sigma_{q\bar{q}}^{\text{NLO}}}{dM^2} = \int_{\tau}^1 \frac{dz}{z} \mathcal{L}_{q\bar{q}} \left(\frac{\tau}{z} \right) \left[\delta(1-z) + \frac{\alpha_s}{\pi} C_F F_q^{\text{int}} \left(z, \frac{M^2}{\mu_F^2} \right) \right] \quad (\text{C.1.9})$$

$$\frac{1}{\tau} \frac{d\sigma_{qg+gq}^{\text{NLO}}}{dM^2} = \frac{\alpha_s}{2\pi} T_F \int_{\tau}^1 \frac{dz}{z} \left[\mathcal{L}_{qg} \left(\frac{\tau}{z} \right) + \mathcal{L}_{gq} \left(\frac{\tau}{z} \right) \right] F_g^{\text{int}} \left(z, \frac{M^2}{\mu_F^2} \right) \quad (\text{C.1.10})$$

and

$$F_q^{\text{int}}\left(z, \frac{M^2}{\mu_F^2}\right) = 2(1+z^2) \left(\frac{\log \frac{1-z}{\sqrt{z}}}{1-z}\right)_+ - 4\delta(1-z) + 2 \log \frac{M^2}{\mu_F^2} \left(\frac{1+z^2}{1-z}\right)_+ \quad (\text{C.1.11})$$

$$F_g^{\text{int}}\left(z, \frac{M^2}{\mu_F^2}\right) = (z^2 + (1-z)^2) \left(\log \frac{(1-z)^2}{z} + \log \frac{M^2}{\mu_F^2}\right) + \frac{1}{2} + 3z - \frac{7}{2}z^2. \quad (\text{C.1.12})$$

It is interesting to rewrite the NLO $q\bar{q}$ coefficient function in several forms ($\mu_F = M$):

$$C_{q\bar{q}}^{(1)}(z, 1) = \frac{2C_F}{\pi} \left\{ (1+z^2) \left(\frac{\log \frac{1-z}{\sqrt{z}}}{1-z}\right)_+ + (2\zeta_2 - 2)\delta(1-z) \right\} \quad (\text{C.1.13a})$$

$$= \frac{2C_F}{\pi} \left\{ (1+z^2) \left(\frac{\log \frac{1-z}{\sqrt{z}}}{1-z}\right)'_+ + (\zeta_2 - 2)\delta(1-z) \right\} \quad (\text{C.1.13b})$$

$$= \frac{2C_F}{\pi} \left\{ (1+z^2) \left(\frac{\log(1-z)}{1-z}\right)_+ - \frac{1+z^2}{1-z} \log \sqrt{z} + (\zeta_2 - 2)\delta(1-z) \right\} \quad (\text{C.1.13c})$$

$$= \frac{2C_F}{\pi} \left\{ 2 \left(\frac{\log(1-z)}{1-z}\right)_+ - \frac{\log z}{1-z} - (1+z) \log \frac{1-z}{\sqrt{z}} + (\zeta_2 - 2)\delta(1-z) \right\} \quad (\text{C.1.13d})$$

where we have used the definition of the primed plus distribution, Eq. (B.4.1b), and the result Eq. (B.3.8).

C.1.3 x_F distribution

Especially in fixed-target experiments, distributions sometimes are given in terms of the Feynman x_F variable instead of rapidity. The variable x_F is defined by

$$x_F = \frac{2k_L}{\sqrt{s}}, \quad (\text{C.1.14})$$

where k_L is the longitudinal momentum of the Drell-Yan pair ($k = k_1 + k_2$), and it is related to the rapidity Y and the transverse momentum k_T by

$$Y = \frac{1}{2} \log \frac{\sqrt{x_F^2 + 4\tau(1 + \hat{k}_T^2)} + x_F}{\sqrt{x_F^2 + 4\tau(1 + \hat{k}_T^2)} - x_F} \quad (\text{C.1.15})$$

where $\hat{k}_T^2 = k_T^2/M^2$. At leading order $k_T = 0$, and at NLO k_T is fixed uniquely in terms of x_F by the kinematics, so up to this order the x_F and rapidity distributions are simply proportional:

$$\left. \frac{d\sigma}{dM^2 dY} \right|_{\text{NLO}} = \sqrt{x_F^2 + 4\tau(1 + \hat{k}_T^2)} \left. \frac{d\sigma}{dM^2 dx_F} \right|_{\text{NLO}}, \quad (\text{C.1.16})$$

though at higher orders they will be different.

C.2 Higgs production at fixed perturbative order

In the large- m_t limit, i.e. when the Higgs mass m_H is less than $2m_t$ enough (typically $m_H \lesssim 200$ GeV) we can use the effective lagrangian

$$\mathcal{L} = -\frac{1}{4v} W G_{\mu\nu}^a G^{a,\mu\nu} H, \quad v = (2G_F^2)^{-1/4} \quad (\text{C.2.1})$$

for the computation of the Higgs production at hadron colliders. The Wilson coefficient in the $\overline{\text{MS}}$ scheme up to order α_s^3 [92, 93] is given by

$$W = -\frac{\alpha_s}{3\pi} \left[1 + \frac{11}{4} \frac{\alpha_s}{\pi} + \left[\frac{2777}{288} + \frac{19}{16} \log \frac{\mu^2}{m_t^2} + n_f \left(-\frac{67}{96} + \frac{1}{3} \log \frac{\mu^2}{m_t^2} \right) \right] \left(\frac{\alpha_s}{\pi} \right)^2 + \mathcal{O}(\alpha_s^3) \right]. \quad (\text{C.2.2})$$

The total cross-section for the Higgs production at hadron colliders can be written as

$$\begin{aligned} \sigma(\tau, M^2) &= \sum_{i,j} \int_0^1 dx_1 \int_0^1 dx_2 \int_0^1 dz f_i(x_1) f_j(x_2) \hat{\sigma}_{ij}(z) \delta \left(z - \frac{\tau}{x_1 x_2} \right) \\ &= \tau \sigma_0 \alpha_s^2 \sum_{i,j} \int_\tau^1 \frac{dz}{z} \mathcal{L}_{ij} \left(\frac{\tau}{z} \right) C_{ij}(z) \end{aligned} \quad (\text{C.2.3})$$

where

$$\tau = \frac{M^2}{s} \quad (\text{C.2.4})$$

$$\sigma_0 = \frac{G_F}{288\pi\sqrt{2}} \left| \sum_q A(x_q) \right|^2, \quad x_q = \frac{4m_q^2}{m_H^2} \quad (\text{C.2.5})$$

$$A(x) = \frac{3}{2} x [1 + (1-x)f(x)] \quad (\text{C.2.6})$$

$$f(x) = \begin{cases} \arcsin^2 \frac{1}{\sqrt{x}} & x \geq 1 \\ -\frac{1}{4} \left[\log \frac{1+\sqrt{1-x}}{1-\sqrt{1-x}} - i\pi \right]^2 & x < 1 \end{cases} \quad (\text{C.2.7})$$

$$\mathcal{L}_{ij}(z) = \int_z^1 \frac{dx}{x} f_i(x) f_j \left(\frac{z}{x} \right) \quad (\text{C.2.8})$$

The partonic cross-section is

$$\hat{\sigma}_{ij}(z) = \sigma_0 z \alpha_s^2 C_{ij}(z, \alpha_s) \quad (\text{C.2.9})$$

and the coefficient functions $C_{ij}(z)$ have an expansion in α_s :

$$C_{ij} = C_{ij}^{(0)} + \alpha_s C_{ij}^{(1)} + \alpha_s^2 C_{ij}^{(2)} + \dots \quad (\text{C.2.10})$$

At LO only C_{gg} contributes

$$C_{ij}^{(0)}(z) = \delta_{ig} \delta_{jg} \delta(1-z). \quad (\text{C.2.11})$$

At NLO, in the large- m_t limit, we have [94, 95]¹

$$C_{gg}^{(1)}(z) = \bar{C}_1(z) + 2\tilde{P}_{gg}^{(0)}(z) \log \frac{M^2}{\mu_F^2} + 2\beta_0 \delta(1-z) \log \frac{\mu_R^2}{\mu_F^2} \quad (\text{C.2.12})$$

¹Actually there is a missing term in these references: the correct result can be found for example in Refs. [96, 97].

$$C_{gq}^{(1)}(z) = P_{gq}^{(0)}(z) \left[\log \frac{(1-z)^2}{z} + \log \frac{M^2}{\mu_F^2} \right] + \frac{C_F}{2\pi} z - \frac{3C_F}{4\pi} \frac{(1-z)^2}{z} \quad (\text{C.2.13})$$

$$= P_{gq}^{(0)}(z) \left[1 + \log \frac{(1-z)^2}{z} + \log \frac{M^2}{\mu_F^2} \right] - \frac{C_F}{4\pi} (1-z)(7-3z) \quad (\text{C.2.14})$$

$$C_{qq}^{(1)}(z) = C_{gq}^{(1)}(z) \quad (\text{C.2.15})$$

$$C_{q\bar{q}}^{(1)}(z) = 0 \quad (\text{C.2.16})$$

$$C_{q\bar{q}}^{(1)}(z) = \frac{32}{27\pi} \frac{(1-z)^3}{z} \quad (\text{C.2.17})$$

where

$$\begin{aligned} \bar{C}_1(z) &= \frac{2C_A}{\pi} \left(2 \left[\frac{\log(1-z)}{1-z} \right]_+ - \frac{\log z}{1-z} + \zeta_2 \delta(1-z) \right) + \frac{11}{2\pi} \delta(1-z) \\ &\quad + 2P_{gg}^{\text{reg}}(z) \log \frac{(1-z)^2}{z} - \frac{11}{2\pi} \frac{(1-z)^3}{z} \\ &= \frac{4C_A}{\pi} \left(\frac{\log \frac{1-z}{\sqrt{z}}}{1-z} \right)_+ + \left(\frac{4C_A}{\pi} \zeta_2 + \frac{11}{2\pi} \right) \delta(1-z) \\ &\quad + 2P_{gg}^{\text{reg}}(z) \log \frac{(1-z)^2}{z} - \frac{11}{2\pi} \frac{(1-z)^3}{z} \end{aligned} \quad (\text{C.2.18})$$

and

$$P_{gg}^{(0)}(z) = \tilde{P}_{gg}^{(0)}(z) + \beta_0 \delta(1-z), \quad P_{gq}^{(0)}(z) = \frac{C_F}{2\pi} \frac{1+(1-z)^2}{z} \quad (\text{C.2.19})$$

with

$$\tilde{P}_{gg}^{(0)}(z) = \frac{C_A/\pi}{(1-z)_+} + P_{gg}^{\text{reg}}(z), \quad P_{gg}^{\text{reg}}(z) = \frac{C_A}{\pi} \left[\frac{1}{z} - 2 + z(1-z) \right]. \quad (\text{C.2.20})$$

With the help of the results of Sect. B.4.1, the Mellin transforms of each contribution to $\bar{C}_1(z)$ are

$$\begin{aligned} \frac{4C_A}{\pi} \mathcal{M} \left[\left(\frac{\log(1-z)}{1-z} \right)_+ \right] &= \frac{2C_A}{\pi} [\psi_0^2(N) - \psi_1(N) + 2\gamma_E \psi_0(N) + \zeta_2 + \gamma_E^2] \\ - \frac{2C_A}{\pi} \mathcal{M} \left[\frac{\log z}{1-z} \right] &= \frac{2C_A}{\pi} \psi_1(N) \\ \left(\frac{11}{2\pi} + \frac{2C_A}{\pi} \zeta_2 \right) \mathcal{M} [\delta(1-z)] &= \left(\frac{11}{2\pi} + \frac{2C_A}{\pi} \zeta_2 \right) \\ 2 \mathcal{M} \left[P_{gg}^{\text{reg}}(z) \log \frac{(1-z)^2}{z} \right] &= \frac{2C_A}{\pi} [L(N-1) - 2L(N) + L(N+1) - L(N+2)] \\ - \frac{11}{2\pi} \mathcal{M} \left[\frac{(1-z)^3}{z} \right] &= -\frac{11}{2\pi} \left[\frac{1}{N-1} - \frac{3}{N} + \frac{3}{N+1} - \frac{1}{N+2} \right] \end{aligned} \quad (\text{C.2.21})$$

where we have defined

$$L(N) \equiv \mathcal{M} \left[\log \frac{(1-z)^2}{z} \right] = -\frac{2}{N} [\psi_0(N+1) + \gamma_E] + \frac{1}{N^2}. \quad (\text{C.2.22})$$

The full NNLO correction has been computed in [96] in the large- m_t approximation. The soft part is correctly reproduced in the large- m_t approximation [93].

C.2.1 Finite top mass

The large- m_t is good for the study of the threshold limit but fails in the description of the small- x region. At NLO, the full m_t dependence can be found in [69]. In practice, getting rid correctly of the top mass amounts to the substitutions

$$\frac{11}{2\pi} \delta(1-z) \rightarrow \frac{\mathcal{G}}{\pi} \delta(1-z) \quad (\text{C.2.23})$$

$$-\frac{11}{2\pi} \frac{(1-z)^3}{z} \rightarrow \frac{C_A}{\pi} \mathcal{R}_{gg}(z) \quad (\text{C.2.24})$$

in Eq. (C.2.18) for the gg channel. The constant \mathcal{G} can be found in Ref. [98] and the function \mathcal{R}_{gg} is given by [69]

$$\mathcal{R}_{gg}(z) = \frac{1}{z(1-z)} \int_0^1 \frac{dv}{v(1-v)} \left\{ \frac{z^4}{B} r_{gg}(s_t, t_t, u_t) - \frac{1}{4} [1 + z^2 + (1-z)^2]^2 \right\} \quad (\text{C.2.25})$$

where B is proportional to the Born contribution and r_{gg} is a function of

$$s_t = \frac{1}{yz}, \quad t_t = -\frac{1-z}{yz}(1-v), \quad u_t = -\frac{1-z}{yz}v; \quad y = \frac{m_t^2}{m_H^2} \quad (\text{C.2.26})$$

(see Ref. [69] for details). From this expression it is easy to see that the limits $m_t \rightarrow \infty$ and $z \rightarrow 0$ do not commute. Indeed, $m_t \rightarrow \infty$ means

$$y^{-1} \rightarrow 0, \quad (\text{C.2.27})$$

which conflicts with $z \rightarrow 0$, because they appear in the combination y^{-1}/z , which can be either 0 (if the limit $m_t \rightarrow \infty$ is taken before) or ∞ (if the limit $z \rightarrow 0$ is taken before).

C.3 Soft-gluons resummation formulae

The general structure valid for both Drell-Yan pair and Higgs production for the resummed coefficient function is given by [99]

$$C^{\text{res}}(N, \alpha_s(M^2)) = g_0(\alpha_s(M^2)) \exp G(N, M^2) \quad (\text{C.3.1})$$

where G is just the Sudakov exponent

$$G(N, M^2) = \mathcal{S} \left(\bar{\alpha} \log \frac{1}{N}, \bar{\alpha} \right) \quad (\text{C.3.2})$$

with a redefinition of the arguments. Formally, G is given by

$$G(N, M^2) = \int_0^1 dz \frac{z^{N-1} - 1}{1-z} \left[2 \int_{M^2}^{(1-z)^2 M^2} \frac{d\mu^2}{\mu^2} A(\alpha_s(\mu^2)) + D(\alpha_s([1-z]^2 M^2)) \right], \quad (\text{C.3.3})$$

where the functions $A(\alpha_s)$ and $D(\alpha_s)$ have the expansions

$$A(\alpha_s) = A_1 \alpha_s + A_2 \alpha_s^2 + A_3 \alpha_s^3 + \dots \quad (\text{C.3.4})$$

$$D(\alpha_s) = D_1 \alpha_s + D_2 \alpha_s^2 + \dots \quad (\text{C.3.5})$$

and, for Drell-Yan and Higgs, $D_1 = 0$. The function $A(\alpha_s)$, sometimes called $\Gamma_{\text{cusp}}(\alpha_s)$, is given by the coefficient of the distributional part of the GLAP splitting function:

$$P_{ii}(\alpha_s, x) = \frac{A(\alpha_s)}{(1-x)_+} + \dots \quad (\text{C.3.6})$$

with $i = q$ for Drell-Yan and $i = g$ for Higgs. The corresponding A functions are related by the colour-charge relation, Eq. (1.3.39). To N^kLL accuracy, the function $A(\alpha_s)$ must be included up to order α_s^{k+1} , and the function $D(\alpha_s)$ up to order α_s^k .

In the computation of $G(N, M^2)$ from Eq. (C.3.3) the Mellin integral hits the Landau singularity of the strong coupling. Therefore, Eq. (C.3.3) is only a formal definition and a prescription is needed to compute the functions g_i . This is done computing the Mellin transform in the large- N limit and keeping only terms up to the desired accuracy. Using Eq. (B.4.9a) we have in the large- N limit [20]

$$\begin{aligned} \mathcal{M} \left[\left(\frac{\log^p(1-z)}{1-z} \right)_+ \right] &= \frac{1}{p+1} \sum_{j=0}^{p+1} \binom{p+1}{j} \Gamma^{(j)}(1) \log^{p+1-j} \frac{1}{N} + \mathcal{O} \left(\frac{1}{N} \right) \\ &= - \sum_{j=0}^{p+1} \frac{\Gamma^{(j)}(1)}{j!} \frac{d^j}{d \log^j \frac{1}{N}} \int_0^{1-1/N} dz \frac{\log^p(1-z)}{1-z} + \mathcal{O} \left(\frac{1}{N} \right); \end{aligned} \quad (\text{C.3.7})$$

a N^kLL accuracy is then obtained truncating the sum at $j = k$. Hence, we finally have

$$\begin{aligned} G_k(N, M^2) &= - \sum_{j=0}^k \frac{\Gamma^{(j)}(1)}{j!} \frac{d^j}{d \log^j \frac{1}{N}} \\ &\quad \int_0^{1-1/N} dz \frac{1}{1-z} \left[2 \int_{M^2}^{(1-z)^2 M^2} \frac{d\mu^2}{\mu^2} A(\alpha_s(\mu^2)) + D(\alpha_s([1-z]^2 M^2)) \right]. \end{aligned} \quad (\text{C.3.8})$$

For technical reasons, the constant terms in N -space are usually all included in g_0 , and then the $(p+1)$ -th term in the sum must not contribute in the computation of $G(N, M^2)$. Then, at N^kLL , for those terms with a power p of $\log(1-z)$ smaller than k , the sum must be truncated at $j = p$ in order not to include the constant term.

C.3.1 Resummed cross-section for the Drell-Yan process

In this Appendix we give the explicit expressions of the functions g_i which appear in the resummed Drell-Yan cross-section, Eq. (2.1.23). We have [99]

$$g_0(\alpha_s) = 1 + \alpha_s g_{01} + \alpha_s^2 g_{02} + \mathcal{O}(\alpha_s^3) \quad (\text{C.3.9a})$$

$$g_1(\lambda) = \frac{2A_1}{\beta_0} [(1+\lambda) \log(1+\lambda) - \lambda] \quad (\text{C.3.9b})$$

$$\begin{aligned} g_2(\lambda) &= \frac{A_2}{\beta_0^2} [\lambda - \log(1+\lambda)] + \frac{A_1}{\beta_0} \left[\log(1+\lambda) \left(\log \frac{M^2}{\mu_R^2} - 2\gamma_E \right) - \lambda \log \frac{\mu_F^2}{\mu_R^2} \right] \\ &\quad + \frac{A_1 b_1}{\beta_0^2} \left[\frac{1}{2} \log^2(1+\lambda) + \log(1+\lambda) - \lambda \right] \end{aligned} \quad (\text{C.3.9c})$$

$$\begin{aligned}
g_3(\lambda) = & \frac{1}{4\beta_0^3} (A_3 - A_1 b_2 + A_1 b_1^2 - A_2 b_1) \frac{\lambda^2}{1+\lambda} \\
& + \frac{A_1 b_1^2}{2\beta_0^3} \frac{\log(1+\lambda)}{1+\lambda} \left[1 + \frac{1}{2} \log(1+\lambda) \right] + \frac{A_1 b_2 - A_1 b_1^2}{2\beta_0^3} \log(1+\lambda) \\
& + \left(\frac{A_1 b_1}{\beta_0^2} \gamma_E + \frac{A_2 b_1}{2\beta_0^3} \right) \left[\frac{\lambda}{1+\lambda} - \frac{\log(1+\lambda)}{1+\lambda} \right] \\
& - \left(\frac{A_1 b_2}{2\beta_0^3} + \frac{A_1}{\beta_0} (\gamma_E^2 + \zeta_2) + \frac{A_2}{\beta_0^2} \gamma_E - \frac{D_2}{4\beta_0^2} \right) \frac{\lambda}{1+\lambda} \\
& + \left[\left(\frac{A_1}{\beta_0} \gamma_E + \frac{A_2 - A_1 b_1}{2\beta_0^2} \right) \frac{\lambda}{1+\lambda} + \frac{A_1 b_1}{2\beta_0^2} \frac{\log(1+\lambda)}{1+\lambda} \right] \log \frac{M^2}{\mu_R^2} \\
& - \frac{A_2}{2\beta_0^2} \lambda \log \frac{\mu_F^2}{\mu_R^2} + \frac{A_1}{4\beta_0} \left[\lambda \log^2 \frac{\mu_F^2}{\mu_R^2} - \frac{\lambda}{1+\lambda} \log^2 \frac{M^2}{\mu_R^2} \right]. \tag{C.3.9d}
\end{aligned}$$

The coefficients g_{0k} can be found in [100], but without scale-dependent terms. Their full expression is given by

$$g_{01} = \frac{C_F}{\pi} \left[4\zeta_2 - 4 + 2\gamma_E^2 + \left(\frac{3}{2} - 2\gamma_E \right) \log \frac{M^2}{\mu_F^2} \right] \tag{C.3.10a}$$

$$\begin{aligned}
g_{02} = & \frac{C_F}{16\pi^2} \left\{ C_F \left(\frac{511}{4} - 198 \zeta_2 - 60 \zeta_3 + \frac{552}{5} \zeta_2^2 - 128 \gamma_E^2 + 128 \gamma_E^2 \zeta_2 + 32 \gamma_E^4 \right) \right. \\
& + C_A \left(-\frac{1535}{12} + \frac{376}{3} \zeta_2 + \frac{604}{9} \zeta_3 - \frac{92}{5} \zeta_2^2 + \frac{1616}{27} \gamma_E - 56 \gamma_E \zeta_3 \right. \\
& \quad \left. + \frac{536}{9} \gamma_E^2 - 16 \gamma_E^2 \zeta_2 + \frac{176}{9} \gamma_E^3 \right) \\
& + n_f \left(\frac{127}{6} - \frac{64}{3} \zeta_2 + \frac{8}{9} \zeta_3 - \frac{224}{27} \gamma_E - \frac{80}{9} \gamma_E^2 - \frac{32}{9} \gamma_E^3 \right) \\
& + \log^2 \frac{M^2}{\mu_F^2} \left[C_F (32\gamma_E^2 - 48\gamma_E + 18) + C_A \left(\frac{44}{3} \gamma_E - 11 \right) + n_f \left(2 - \frac{8}{3} \gamma_E \right) \right] \\
& + \log \frac{M^2}{\mu_F^2} \left[C_F (48\zeta_3 + 72\zeta_2 - 93 - 128\gamma_E \zeta_2 + 128\gamma_E + 48\gamma_E^2 - 64\gamma_E^3) \right. \\
& \quad + C_A \left(\frac{193}{3} - 24\zeta_3 - \frac{88}{3} \zeta_2 + 16\gamma_E \zeta_2 - \frac{536}{9} \gamma_E - \frac{88}{3} \gamma_E^2 \right) \\
& \quad \left. + n_f \left(\frac{16}{3} \zeta_2 - \frac{34}{3} + \frac{80}{9} \gamma_E + \frac{16}{3} \gamma_E^2 \right) \right] \left. \right\} \\
& - \frac{\beta_0 C_F}{\pi} \left[4\zeta_2 - 4 + 2\gamma_E^2 + \left(\frac{3}{2} - 2\gamma_E \right) \log \frac{M^2}{\mu_F^2} \right] \log \frac{\mu_F^2}{\mu_R^2}. \tag{C.3.10b}
\end{aligned}$$

The coefficients appearing in the previous functions are

$$A_1 = \frac{C_F}{\pi} = \frac{4}{3\pi} \tag{C.3.11}$$

$$A_2 = \frac{C_F}{2\pi^2} \left[C_A \left(\frac{67}{18} - \frac{\pi^2}{6} \right) - \frac{10}{9} T_F n_f \right] = \frac{201 - 10n_f}{27\pi^2} - \frac{1}{3} \tag{C.3.12}$$

$$A_3 = \frac{C_F}{4\pi^3} \left[C_A^2 \left(\frac{245}{24} - \frac{67}{9} \zeta_2 + \frac{11}{6} \zeta_3 + \frac{11}{5} \zeta_2^2 \right) + \left(-\frac{55}{24} + 2\zeta_3 \right) C_F n_f \right]$$

$$+ \left(-\frac{209}{108} + \frac{10}{9} \zeta_2 - \frac{7}{3} \zeta_3 \right) C_A n_f - \frac{1}{27} n_f^2 \Big] \quad (\text{C.3.13})$$

$$D_2 = \frac{C_F}{16\pi^2} \left[C_A \left(-\frac{1616}{27} + \frac{88}{9} \pi^2 + 56\zeta_3 \right) + \left(\frac{224}{27} - \frac{16}{9} \pi^2 \right) n_f \right]. \quad (\text{C.3.14})$$

C.3.2 Resummed cross-section for the Higgs production

The Higgs resummation coefficients are simply related to those of the Drell-Yan process. The coefficient for the Higgs are obtained as [99]

$$A_k^{\text{H}} = \frac{C_A}{C_F} A_k^{\text{DY}}, \quad D_k^{\text{H}} = \frac{C_A}{C_F} D_k^{\text{DY}}. \quad (\text{C.3.15})$$

The function g_0 collecting constant terms is instead different; the first two coefficients can be found in Ref. [97]² with full scale-dependence. We report here for completeness the first:

$$g_{01} = \frac{C_A}{\pi} \left[4\zeta_2 + 2\gamma_{\text{E}}^2 + \frac{2}{3} \pi \beta_0 \log \frac{\mu_{\text{R}}^2}{\mu_{\text{F}}^2} - 2\gamma_{\text{E}} \log \frac{M^2}{\mu_{\text{F}}^2} \right] + \frac{11}{2\pi}. \quad (\text{C.3.16})$$

C.3.3 Matching

Here we compute the terms to be subtracted in the resummed result in order to avoid double counting. The first step consists in expanding Eqs. (C.3.9) in powers of their argument λ :

$$g_1(\lambda) = \frac{A_1}{\beta_0} \left[\lambda^2 - \frac{1}{3} \lambda^3 + \mathcal{O}(\lambda^4) \right] \quad (\text{C.3.17a})$$

$$g_2(\lambda) = \frac{A_1}{\beta_0} \left(\log \frac{M^2}{\mu_{\text{F}}^2} - 2\gamma_{\text{E}} \right) \lambda + \left(\frac{A_2}{2\beta_0^2} + \frac{A_1}{2\beta_0} \left(2\gamma_{\text{E}} - \log \frac{M^2}{\mu_{\text{R}}^2} \right) \right) \lambda^2 + \mathcal{O}(\lambda^3) \quad (\text{C.3.17b})$$

$$g_3(\lambda) = \left(-\frac{A_1}{\beta_0} (\gamma_{\text{E}}^2 + \zeta_2) - \frac{A_2}{\beta_0^2} \gamma_{\text{E}} + \frac{D_2}{4\beta_0^2} \right) \lambda \\ + \left(\frac{A_1}{\beta_0} \gamma_{\text{E}} \log \frac{M^2}{\mu_{\text{R}}^2} + \frac{A_2}{2\beta_0^2} \log \frac{M^2}{\mu_{\text{F}}^2} - \frac{A_1}{4\beta_0} \left(\log^2 \frac{M^2}{\mu_{\text{R}}^2} - \log^2 \frac{\mu_{\text{F}}^2}{\mu_{\text{R}}^2} \right) \right) \lambda + \mathcal{O}(\lambda^2). \quad (\text{C.3.17c})$$

The double counting term are found as the Taylor expansion of $g_0(\alpha_s) \exp \mathcal{S}(\lambda, \bar{\alpha})$ in powers of α_s :

$$g_0(\alpha_s) \exp \mathcal{S}(\lambda, \bar{\alpha}) = (1 + \alpha_s g_{01} + \alpha_s^2 g_{02} + \dots) e^{\alpha_s \mathcal{S}_1 + \alpha_s^2 \mathcal{S}_2 + \dots} \\ = 1 + (\mathcal{S}_1 + g_{01}) \alpha_s + \left(\frac{\mathcal{S}_1^2}{2} + \mathcal{S}_2 + \mathcal{S}_1 g_{01} + g_{02} \right) \alpha_s^2 + \mathcal{O}(\alpha_s^3). \quad (\text{C.3.18})$$

²These constants can be also found in Ref. [100]; there, however, the constant contributions from the Wilson coefficient in the large- m_t approximation are not included. However, also such constants must be there in order to reproduce correctly the fixed-order result. Therefore one could use the constants from Ref. [100] provided the Wilson coefficient is left in front of the resummed expression, or (more consistently) of the whole matched result.

Using the expansions above, we get

$$\alpha_s \mathcal{S}_1 = \left[\frac{A_1}{\beta_0} \left(\frac{\lambda}{\bar{\alpha}} + \log \frac{M^2}{\mu_F^2} - 2\gamma_E \right) \right] \lambda \quad (\text{C.3.19})$$

$$\begin{aligned} \alpha_s^2 \mathcal{S}_2 = & \left[-\frac{A_1}{3\beta_0} \frac{\lambda}{\bar{\alpha}} + \left(\frac{A_2}{2\beta_0^2} + \frac{A_1}{2\beta_0} \left(2\gamma_E - \log \frac{M^2}{\mu_R^2} \right) \right) + \left\{ -\frac{A_1}{\beta_0} (\gamma_E^2 + \zeta_2) - \frac{A_2}{\beta_0^2} \gamma_E + \frac{D_2}{4\beta_0^2} \right. \right. \\ & \left. \left. + \frac{A_1}{\beta_0} \gamma_E \log \frac{M^2}{\mu_R^2} + \frac{A_2}{2\beta_0^2} \log \frac{M^2}{\mu_F^2} - \frac{A_1}{4\beta_0} \left(\log^2 \frac{M^2}{\mu_R^2} - \log^2 \frac{\mu_F^2}{\mu_R^2} \right) \right\} \frac{\bar{\alpha}}{\lambda} \right] \lambda^2. \end{aligned} \quad (\text{C.3.20})$$

Note that, since $\lambda = \bar{\alpha} \log \frac{1}{N}$, it can be seen as an expansion in λ with $\lambda/\bar{\alpha}$ fixed.

C.4 High-energy resummation at NLO

In this Appendix we collect many details on the construction of the full resummed NLO anomalous dimensions.

C.4.1 BFKL kernel at NLO

The NLO BFKL kernel $\chi_1^\sigma(M) = \chi_1^L(M) + \chi_1^R(M)$ in symmetric variables and in the scheme used by Ref. [52] is given by [54]³

$$\begin{aligned} \chi_1^\sigma(M) = & -\frac{N_c \beta_0}{2\pi} \left(\frac{\pi^2}{N_c^2} \chi_0^2(M) - \psi_1(M) - \psi_1(1-M) \right) \\ & + \frac{N_c^2}{4\pi^2} \left\{ \left(\frac{67}{9} - \frac{\pi^2}{3} - \frac{10}{9} \frac{n_f}{N_c} \right) [\psi(1) - \psi(M)] + \psi_2(M) + 3\zeta_3 - 4\phi^+(M) \right. \\ & + \frac{\pi^2}{2} \left[\psi \left(\frac{1+M}{2} \right) - \psi \left(\frac{M}{2} \right) \right] \\ & + \left[\frac{3}{4(1-2M)} + \frac{2+3M(1-M)}{32} \left(1 + \frac{n_f}{N_c^3} \right) \right. \\ & \quad \left. \times \left(\frac{2}{1-2M} + \frac{1}{1+2M} - \frac{1}{3-2M} \right) \right] \\ & \quad \left. \times \left[\psi_1 \left(\frac{1+M}{2} \right) - \psi_1 \left(\frac{M}{2} \right) \right] \right. \\ & \left. + (M \rightarrow 1-M) \right\} \end{aligned} \quad (\text{C.4.1})$$

where $\chi_0(M)$ is the LO BFKL kernel, Eq. (3.2.11), β_0 is the first coefficient of the β -function, Eq. (A.1.4), ζ_k is the Riemann Zeta function (see App. E.2), and $\phi^+(M)$ is given by

$$\phi^+(M) = -\int_0^1 \frac{dx}{1+x} x^{M-1} \int_x^1 \frac{dt}{t} \log(1-t); \quad (\text{C.4.2})$$

³There are some misprints in Ref. [54] that we correct here.

series representation of this function will be given in Sec. C.4.1.1.

Taking into account the reshuffling due to operator ordering in the running coupling, the kernel acquires the non-symmetric term given in Eq. (3.5.17). Passing to DIS variables, Eq. (3.4.8), one then gets

$$\chi_1(M) = \frac{N_c^2}{4\pi^2} \delta(M) - \frac{1}{2} \chi_0(M) \chi_0'(M) \quad (\text{C.4.3})$$

where

$$\begin{aligned} \delta(M) = & -\frac{2\pi\beta_0}{N_c} \left(\frac{\pi^2}{N_c^2} \chi_0^2(M) - \psi_1(M) + \psi_1(1-M) \right) + \left(\frac{67}{9} - \frac{\pi^2}{3} - \frac{10}{9} \frac{n_f}{N_c} \right) \bar{\psi}(M) \\ & + \frac{\pi^3}{\sin(\pi M)} - \frac{\pi^2 \cos(\pi M)}{\sin^2(\pi M)(1-2M)} \left[3 + \left(1 + \frac{n_f}{N_c^3} \right) \frac{2+3M(1-M)}{(3-2M)(1+2M)} \right] \\ & - 4\phi(M) + \psi_2(M) + \psi_2(1-M) + 6\zeta_3, \end{aligned} \quad (\text{C.4.4})$$

having used (C.4.18) and

$$\frac{4\pi^2 \cos(\pi M)}{\sin^2(\pi M)} = \psi_1\left(\frac{M}{2}\right) - \psi_1\left(\frac{M+1}{2}\right) - (M \rightarrow 1-M) \quad (\text{C.4.5})$$

and defining

$$\phi(M) = \phi^+(M) + \phi^-(M) \quad (\text{C.4.6})$$

where $\phi^-(M) = \phi^+(1-M)$, see Sect. C.4.1.1.

To change scheme to the $\overline{\text{MS}}$ scheme, a further term must be added [101]:

$$\chi_1^{\overline{\text{MS}}}(M) = \chi_1(M) + \frac{\beta_0 N_c}{2\pi} [\bar{\psi}^2(M) + 2\psi_1(1) - \psi_1(M) - \psi_1(1-M)]. \quad (\text{C.4.7})$$

C.4.1.1 Series representation of $\phi(M)$

The function $\phi^+(M)$, Eq. (C.4.2), has a series representation given by

$$\phi^+(M) = \sum_{n=0}^{\infty} (-)^n \frac{\psi(n+1+M) - \psi(1)}{(n+M)^2}. \quad (\text{C.4.8})$$

It can be obtained expanding

$$\frac{1}{1+x} = \sum_{n=0}^{\infty} (-x)^n \quad (\text{C.4.9})$$

and computing the integrals in reverse order

$$\begin{aligned} \phi^+(M) &= - \sum_{n=0}^{\infty} (-)^n \int_0^1 \frac{dt}{t} \log(1-t) \int_0^t dx x^n x^{M-1} \\ &= - \sum_{n=0}^{\infty} (-)^n \int_0^1 \frac{dt}{t} \log(1-t) \frac{t^{n+M}}{n+M}. \end{aligned} \quad (\text{C.4.10})$$

The computation of the second integral can be done with the trick

$$\begin{aligned} \int_0^1 dt t^{c-1} \log(1-t) &= \frac{d}{d\epsilon} \int_0^1 dt t^{c-1} (1-t)^\epsilon \Big|_{\epsilon=0} \\ &= \Gamma(c) \frac{d}{d\epsilon} \frac{\Gamma(1+\epsilon)}{\Gamma(c+1+\epsilon)} \Big|_{\epsilon=0} \\ &= \frac{\psi(1) - \psi(c+1)}{c}, \end{aligned} \quad (\text{C.4.11})$$

bringing directly to Eq. (C.4.8) (remember that $\psi(1) = -\gamma_E$, see App. E.1). From Eq. (C.4.8) it is clear that $\phi^+(M)$ has poles in $M = 0, -1, -2, \dots$ coming from the collinear region; the function $\phi^-(M) = -\phi^+(1-M)$ has instead poles in $M = 1, 2, 3, \dots$ coming from the anti-collinear region.

An alternative expansion can be obtained noting that

$$\int_x^1 \frac{dt}{t} \log(1-t) = \text{Li}_2(x) - \zeta(2) \quad (\text{C.4.12})$$

as one can verify expanding the logarithm

$$\log(1-t) = - \sum_{k=1}^{\infty} \frac{t^k}{k} \quad (\text{C.4.13})$$

and recalling the definitions

$$\text{Li}_s(x) = \sum_{k=1}^{\infty} \frac{x^k}{k^s}, \quad \zeta(s) = \sum_{k=1}^{\infty} \frac{1}{k^s} = \text{Li}_s(1). \quad (\text{C.4.14})$$

Then we can write

$$\phi(M) = \frac{\pi \zeta(2)}{\sin(\pi M)} - \phi_L^+(M) - \phi_L^-(M) \quad (\text{C.4.15})$$

where

$$\phi_L^+(M) = \int_0^1 \frac{dx}{1+x} x^{M-1} \text{Li}_2(x) = \sum_{k=1}^{\infty} \frac{1}{2k^2} \left[\psi\left(\frac{M+1+k}{2}\right) - \psi\left(\frac{M+k}{2}\right) \right] \quad (\text{C.4.16})$$

$$\phi_L^-(M) = \phi_L^+(1-M). \quad (\text{C.4.17})$$

Using the relation

$$\frac{2\pi}{\sin(\pi M)} = 2 \int_0^1 \frac{dx}{1+x} (x^{M-1} + x^{-M}) = \psi\left(\frac{M+1}{2}\right) - \psi\left(\frac{M}{2}\right) + (M \rightarrow 1-M) \quad (\text{C.4.18})$$

we have the identification

$$\phi^+(M) = \frac{\zeta(2)}{2} \left[\psi\left(\frac{M+1}{2}\right) - \psi\left(\frac{M}{2}\right) \right] - \phi_L^+(M). \quad (\text{C.4.19})$$

Also in this case, even if in a less transparent way, the collinear and anticollinear poles are separated.

Practically, it seems that the convergence of expansion (C.4.8) is faster, and hence we use it for numerical applications.

C.4.1.2 Expansion around $M = 0$ and relation with the singular expansion

By using Eq. (E.1.21) and the series representation of ϕ^+ Eq. (C.4.8), the behaviour of the kernel χ_1 can be found. By writing the Laurent expansion as⁴

$$\chi_k(M) = \sum_{j=-\infty}^{k+1} \frac{\chi_{k,j}}{M^j} \quad (\text{C.4.20})$$

we have

$$\chi_{0,1} = \frac{N_c}{\pi} \quad (\text{C.4.21a})$$

$$\chi_{0,0} = 0 \quad (\text{C.4.21b})$$

$$\chi_{1,2} = -\frac{11N_c^2 + 2n_f/N_c}{12\pi^2} \quad (\text{C.4.21c})$$

$$\chi_{1,1} = -\frac{n_f}{36\pi^2 N_c} (10N_c^2 + 13). \quad (\text{C.4.21d})$$

On the other hand, the functions χ_s and χ_{ss} have a series expansion⁵

$$\chi_s\left(\frac{\alpha_s}{M}\right) = \sum_{k=0}^{\infty} \chi_{s,k} \frac{\alpha_s^k}{M^k} \quad (\text{C.4.22})$$

$$\chi_{ss}\left(\frac{\alpha_s}{M}\right) = \sum_{k=0}^{\infty} \chi_{ss,k} \frac{\alpha_s^k}{M^k}. \quad (\text{C.4.23})$$

To obtain the coefficients $\chi_{s,k}$, we put the series (C.4.22) as argument of γ_0 and match the coefficients order by order in α_s/M (a general procedure is described in App. C.4.1.3). We obtain for the first three coefficient

$$\chi_{s,0} = 0, \quad \chi_{s,1} = \frac{C_A}{\pi}, \quad \chi_{s,2} = -\frac{11C_A^2}{12\pi^2} + \frac{n_f}{6\pi^2}(2C_F - C_A) \quad (\text{C.4.24})$$

or, using the definitions $C_F = (N_c^2 - 1)/2N_c$, $C_A = N_c$,

$$\chi_s(\alpha_s/M) = \frac{N_c}{\pi} \frac{\alpha_s}{M} - \frac{11N_c^2 + 2n_f/N_c}{12\pi^2} \frac{\alpha_s^2}{M^2} + \dots \quad (\text{C.4.25})$$

Note that this result is the same if the largest eigenvalue is taken to be the largest at each N or just in $N = 0$ (see discussion at the end of Sect. 1.3.2.1); higher orders will depend on the choice used. For the $n_f = 0$ case there are no ambiguities and these results can be established just by looking at γ_{gg} . The coefficients $\chi_{ss,k}$ can be simply obtained from the knowledge of the expansion of χ_s and the definition (3.3.15); using the general form

$$\gamma_1(N) = \frac{a_0}{N^2} + \frac{a_1}{N} + a_2 + \mathcal{O}(N) \quad (\text{C.4.26})$$

we get

$$\chi_{ss,0} = \frac{a_0\pi}{C_A}, \quad \chi_{ss,1} = a_1. \quad (\text{C.4.27})$$

⁴We know that the $\mathcal{O}(\alpha_s^{k+1})$ BFKL kernel $\chi_k(M)$ has a $(k+1)$ -th order pole in $M = 0$.

⁵Note that from a formal point of view the function $\chi_s(\alpha_s/M)$ and $\chi_{ss}(\alpha_s/M)$ could be expanded in positive powers of M/α_s ; however, for our purposes we are interested in a perturbative expansion in α_s .

From Eq. (1.3.37b) we have

$$a_0 = 0, \quad a_1 = -\frac{n_f(23C_A - 26C_F)}{36\pi^2} \quad (\text{C.4.28})$$

and hence (using again $C_F = (N_c^2 - 1)/2N_c$, $C_A = N_c$)

$$\chi_{ss,0} = 0, \quad \chi_{ss,1} = -\frac{n_f}{36\pi^2 N_c} (10N_c^2 + 13). \quad (\text{C.4.29})$$

With the help of Fig. 3.2 it is simple to match these coefficients to those of χ_0 and χ_1 :

$$\chi_{0,1} = \chi_{s,1} \quad \chi_{0,0} = \chi_{ss,0} \quad (\text{C.4.30})$$

$$\chi_{1,2} = \chi_{s,2} \quad \chi_{1,1} = \chi_{ss,1}. \quad (\text{C.4.31})$$

Of course, they coincide.

C.4.1.3 Computing the inverse function of χ_0 or γ_0

We now want to solve the duality relation

$$\gamma_0(\chi_s(z)) = \frac{1}{z} \quad (\text{C.4.32})$$

in an algorithmic way. We concentrate on χ_s , but the procedure applies to γ_s as well. Using the expansion

$$\gamma_0(N) = \sum_{k=-1}^{\infty} \gamma_k N^k \quad (\text{C.4.33})$$

we have ($\chi_{s,0} = 0$)

$$\sum_{k=-1}^{\infty} \gamma_k \left(\sum_{j=1}^{\infty} \chi_{s,j} z^j \right)^k = \frac{1}{z} \quad (\text{C.4.34})$$

or, rearranging terms,

$$\sum_{k=0}^{\infty} \gamma_{k-1} z^k \left(\sum_{j=0}^{\infty} \chi_{s,j+1} z^j \right)^k = \sum_{j=0}^{\infty} \chi_{s,j+1} z^j \quad (\text{C.4.35})$$

Using the result Eq. (D.1.14) with $a_j = \chi_{s,j+1}$ we get

$$\sum_{n=0}^{\infty} \left[\chi_{s,n+1} - \sum_{k=0}^n \gamma_{k-1} c_{k,n-k} \right] z^n = 0 \quad (\text{C.4.36})$$

where

$$c_{k,0} = \chi_{s,1}^k, \quad c_{k,p} = \frac{1}{\chi_{s,1}^p} \sum_{j=1}^p (jk + j - p) \chi_{s,j+1} c_{k,p-j}. \quad (\text{C.4.37})$$

Then, for $n = 0$ we get

$$\chi_{s,1} = \gamma_{-1} \quad (\text{C.4.38})$$

while for $n > 0$ we can compute recursively the coefficients

$$\chi_{s,n+1} = \sum_{k=1}^n \gamma_{k-1} c_{k,n-k}. \quad (\text{C.4.39})$$

C.4.1.4 Subtract double counting

From the computational point of view, it is better to subtract double counting between the fixed-order kernel and the singular expansion directly from the ψ_k functions in the fixed-order kernels, in order to avoid differences of huge numbers. Using the results

$$\chi_0^2(M) - \text{d.c.} = \tilde{\chi}_0^2(M) + 2 \frac{N_c}{\pi} \frac{\tilde{\chi}_0(M) + N_c/\pi}{M(1-M)} \quad (\text{C.4.40})$$

$$\phi^+(M) - \text{d.c.} = \tilde{\phi}^+(M) = \phi^+(M) - \frac{\zeta(2)}{M} \quad (\text{C.4.41})$$

$$\frac{1}{1-2M} \psi_1(M/2) - \text{d.c.} = \frac{1}{1-2M} [\psi_1(1+M/2) + 16] \quad (\text{C.4.42})$$

$$\frac{2+3M(1-M)}{1-2M} \psi_1(M/2) - \text{d.c.} = \frac{2+3M(1-M)}{1-2M} \psi_1(1+M/2) + \frac{44}{1-2M} \quad (\text{C.4.43})$$

$$\frac{2+3M(1-M)}{1+2M} \psi_1(M/2) - \text{d.c.} = \frac{2+3M(1-M)}{1+2M} \psi_1(1+M/2) - \frac{4}{1+2M} \quad (\text{C.4.44})$$

$$\frac{2+3M(1-M)}{3-2M} \psi_1(M/2) - \text{d.c.} = \frac{2+3M(1-M)}{3-2M} \psi_1(1+M/2) - \frac{4/9}{3-2M} \quad (\text{C.4.45})$$

we get⁶

$$\begin{aligned} \tilde{\chi}_1^\sigma(M) &= \chi_1^\sigma(M) - \text{d.c.} \\ &= -\frac{N_c \beta_0}{2\pi} \left(\frac{\pi^2}{N_c^2} \tilde{\chi}_0^2(M) + 2 \frac{\pi \tilde{\chi}_0(M)/N_c + 1}{M(1-M)} - \psi_1(1+M) - \psi_1(2-M) \right) \\ &\quad + \frac{N_c^2}{4\pi^2} \left\{ \left(\frac{67}{9} - \frac{\pi^2}{3} - \frac{10 n_f}{9 N_c} \right) [\psi(1) - \psi(1+M)] \right. \\ &\quad + \psi_2(1+M) + 3\zeta(3) - 4\tilde{\phi}^+(M) \\ &\quad + \frac{\pi^2}{2} \left[\psi\left(\frac{1+M}{2}\right) - \psi\left(1+\frac{M}{2}\right) \right] \\ &\quad + \frac{3}{4(1-2M)} \left[\psi_1\left(\frac{1+M}{2}\right) - \psi_1\left(1+\frac{M}{2}\right) - 16 \right] \\ &\quad + \frac{2+3M(1-M)}{32} \left(1 + \frac{n_f}{N_c^3} \right) \\ &\quad \times \left(\frac{2}{1-2M} \left[\psi_1\left(\frac{1+M}{2}\right) - \psi_1\left(1+\frac{M}{2}\right) \right] \right. \\ &\quad \left. + \frac{1}{1+2M} \left[\psi_1\left(\frac{1+M}{2}\right) - \psi_1\left(1+\frac{M}{2}\right) \right] \right. \\ &\quad \left. - \frac{1}{3-2M} \left[\psi_1\left(\frac{1+M}{2}\right) - \psi_1\left(1+\frac{M}{2}\right) \right] \right) \end{aligned}$$

⁶In this equation there are some terms which cancel with the analogous in the $M \rightarrow 1-M$ part; however we are not going to use this expression for numerical computations, but we will use Eq. (C.4.48), which is optimized.

$$\begin{aligned}
& + \frac{1}{32} \left(1 + \frac{n_f}{N_c^3} \right) \left(-\frac{88}{1-2M} + \frac{4}{1+2M} - \frac{4/9}{3-2M} \right) \\
& + (M \rightarrow 1-M) \left. \vphantom{\frac{1}{32}} \right\} \tag{C.4.46}
\end{aligned}$$

where

$$\tilde{\chi}_0(M) = \chi_0(M) - \text{d.c.} = \frac{N_c}{\pi} [2\psi(1) - \psi(1+M) - \psi(2-M)]. \tag{C.4.47}$$

Eq. (C.4.46) has no poles in the range $-1 < M < 2$; however, there are simple poles in the expression for $M = -\frac{1}{2}, \frac{3}{2}$ that cancel adding the $M \rightarrow 1-M$ contribution. For numerical convenience, it is better to subtract these poles directly in each collinear and anticollinear contributions. The resulting expression is (see Sect. C.4.1.5 for details)

$$\begin{aligned}
\tilde{\chi}_1^\sigma(M) = & -\frac{N_c\beta_0}{2\pi} \left(\frac{\pi^2}{N_c^2} \tilde{\chi}_0^2(M) + 2 \frac{\pi\tilde{\chi}_0(M)/N_c + 1}{M(1-M)} - \psi_1(1+M) - \psi_1(2-M) \right) \\
& + \frac{N_c^2}{4\pi^2} \left\{ \left(\frac{67}{9} - \frac{\pi^2}{3} - \frac{10}{9} \frac{n_f}{N_c} \right) [\psi(1) - \psi(1+M)] \right. \\
& + \psi_2(1+M) + 3\zeta(3) - 4\tilde{\phi}^+(M) \\
& + \frac{\pi^2}{2} \left[\psi\left(\frac{1+M}{2}\right) - \psi\left(1 + \frac{M}{2}\right) \right] \\
& + \frac{3}{4(1-2M)} \left[\psi_1\left(\frac{1+M}{2}\right) - \psi_1\left(1 + \frac{M}{2}\right) - \psi_1\left(\frac{3}{4}\right) + \psi_1\left(\frac{5}{4}\right) \right] \\
& + \frac{2+3M(1-M)}{32} \left(1 + \frac{n_f}{N_c^3} \right) \\
& \quad \times \left(\frac{2}{1-2M} \left[\psi_1\left(\frac{1+M}{2}\right) - \psi_1\left(1 + \frac{M}{2}\right) - \psi_1\left(\frac{3}{4}\right) + \psi_1\left(\frac{5}{4}\right) \right] \right. \\
& \quad + \frac{1}{1+2M} \left[\psi_1\left(\frac{1+M}{2}\right) - \psi_1\left(1 + \frac{M}{2}\right) - \psi_1\left(\frac{1}{4}\right) + \psi_1\left(\frac{3}{4}\right) \right] \\
& \quad \left. - \frac{1}{3-2M} \left[\psi_1\left(\frac{1+M}{2}\right) - \psi_1\left(1 + \frac{M}{2}\right) - \psi_1\left(\frac{5}{4}\right) + \psi_1\left(\frac{7}{4}\right) \right] \right) \\
& + \frac{2}{3} \left(1 + \frac{n_f}{N_c^3} \right) \\
& \left. + (M \rightarrow 1-M) \right\} \tag{C.4.48}
\end{aligned}$$

where the constant term in the second-last line arises from the asymmetric contributions of the previous two lines.

Following Ref. [54], we define

$$\check{\chi}_1(M) = \chi_1^\sigma(M) - \frac{N_c}{2\pi} \chi_0(M) [2\psi_1(1) - \psi_1(M) - \psi_1(1-M)]; \tag{C.4.49}$$

after subtracting double counting we have

$$\tilde{\chi}_1(M) = \check{\chi}_1(M) - \chi_{1,2} \left(\frac{1}{M^2} + \frac{1}{(1-M)^2} \right) - \chi_{1,1} \left(\frac{1}{M} + \frac{1}{1-M} \right) \quad (\text{C.4.50})$$

with $\chi_{1,1}, \chi_{1,2}$ defined in (C.4.21). Using for numerical convenience the previous results, we can write

$$\begin{aligned} \tilde{\chi}_1(M) = & \tilde{\chi}_1^\sigma(M) - \frac{N_c}{2\pi} \tilde{\chi}_0(M) [2\psi_1(1) - \psi_1(1+M) - \psi_1(2-M)] \\ & + \frac{N_c}{2\pi} \left[\frac{\tilde{\chi}_0(M) + N_c(1+M)/\pi}{M^2} + \frac{\tilde{\chi}_0(M) + N_c(2-M)/\pi}{(1-M)^2} \right. \\ & \left. - \frac{N_c}{\pi} \frac{2\psi_1(1) - \psi_1(1+M) - \psi_1(2-M) - 1}{M(1-M)} \right]. \end{aligned} \quad (\text{C.4.51})$$

C.4.1.5 Spurious poles subtraction in Eq. (C.4.48)

In Eqs. (C.4.1), (C.4.46) there are explicit simple poles in $M = -\frac{1}{2}, \frac{3}{2}$ that cancel adding the $M \rightarrow 1-M$ contribution. When extending off-shell, the cancellation no longer takes place; for this it is useful to add some terms in order for the cancellation to take place directly in each collinear and anticollinear term. Let us recall Eq. (C.4.5) and define

$$g(M) = \psi_1 \left(\frac{M}{2} \right) - \psi_1 \left(\frac{1+M}{2} \right) \quad (\text{C.4.52})$$

such that

$$\frac{4\pi^2 \cos(\pi M)}{\sin^2(\pi M)} = g(M) - g(1-M). \quad (\text{C.4.53})$$

The structure of the terms in Eq. (C.4.1) containing this function is

$$h(M) = f(M) \frac{4\pi^2 \cos(\pi M)}{\sin^2(\pi M)} = f(M)g(M) + (M \rightarrow 1-M) \quad (\text{C.4.54})$$

with

$$f(1-M) = -f(M). \quad (\text{C.4.55})$$

Let us consider first the case in which

$$f_1(M) = \frac{A(M)}{1-2M} \quad (\text{C.4.56})$$

where $A(M) = A(1-M)$ can be identified either with a constant or with $2+3M(1-M)$, but it is irrelevant for this discussion. Both $f_1(M)g(M)$ and $f_1(1-M)g(1-M)$ have a simple pole in $M = \frac{1}{2}$, but this pole cancels in the sum, because $g(M) - g(1-M)$ has a zero in $M = \frac{1}{2}$. We can subtract the pole in each term

$$h_1(M) = f_1(M) \left[g(M) - g \left(\frac{1}{2} \right) \right] + (M \rightarrow 1-M) \quad (\text{C.4.57})$$

without adding any other term (the $g(1/2)$ term cancels with the analogous in the $M \rightarrow 1-M$ part).

Now let us move to

$$f_2(M) = (2 + 3M(1 - M)) \left[\frac{1}{1 + 2M} - \frac{1}{3 - 2M} \right]. \quad (\text{C.4.58})$$

This case is a bit more complicated, because in order to preserve the anti-symmetry (C.4.55) we cannot separate $f_2(M)$ into the sum of two functions with just one pole each. Indeed, for the symmetry $M \rightarrow 1 - M$, the first term in the square brackets goes into (minus) the second and vice-versa. For the same reason as before, also in this case the sum has no poles, since $g(M) - g(1 - M)$ has zeros in $M = -\frac{1}{2}$ and $M = \frac{3}{2}$, where $f_2(M)$ has poles. The subtraction must be done separately for the two terms in the square brackets

$$h_2(M) = (2 + 3M(1 - M)) \left[\frac{g(M) - g(-1/2)}{1 + 2M} - \frac{g(M) - g(3/2)}{3 - 2M} \right] + (M \rightarrow 1 - M). \quad (\text{C.4.59})$$

This expression is exact again, but now the cancellation of the auxiliary terms takes place thanks to the relation

$$g\left(\frac{3}{2}\right) - g\left(-\frac{1}{2}\right) = 0 \quad (\text{C.4.60})$$

peculiar of the actual form of g , as one can verify using

$$\psi_1\left(\frac{3}{4}\right) = \psi_1\left(-\frac{1}{4}\right) - 16, \quad \psi_1\left(\frac{5}{4}\right) = \psi_1\left(\frac{1}{4}\right) - 16 \quad (\text{C.4.61})$$

coming from the recursion formula

$$\psi_k(x + 1) = \psi_k(x) + \frac{(-)^k k!}{x^{k+1}}. \quad (\text{C.4.62})$$

Also in this case, the numerator hasn't played any role.

Now turn to the case in which the double counting poles in $M = 0, 1$ are removed from $h(M)$, leading to Eq. (C.4.46). In this case we can define

$$\tilde{g}(M) = g(M) + \frac{4}{M^2} = \psi_1\left(1 + \frac{M}{2}\right) - \psi_1\left(\frac{1 + M}{2}\right) \quad (\text{C.4.63})$$

which is free of poles. The poles of $h(M)$ can be found by considering its divergent behaviour

$$h(M) \sim -\frac{4f(M)}{M^2} + (M \rightarrow 1 - M) \sim -\frac{4f(0)}{M^2} - \frac{4f'(0)}{M} + (M \rightarrow 1 - M) \quad (\text{C.4.64})$$

and then after subtracting these poles we get

$$\begin{aligned} \tilde{h}(M) &= h(M) - \text{d.c.} \\ &= \tilde{g}(M)f(M) - 4 \frac{f(M) - f(0) - f'(0)M}{M^2} + (M \rightarrow 1 - M) \end{aligned} \quad (\text{C.4.65})$$

(with this formula we have obtained Eqs. (C.4.42)÷(C.4.45)). Considering now again f_1 , Eq. (C.4.56), we have

$$\frac{f_1(M) - f_1(0) - f_1'(0)M}{M^2} \propto f_1(M) \quad (\text{C.4.66})$$

in both cases for $A(M)$; in fact, this proportionality holds as long as $A(M)$ is a polynomial of order 2 at most. This means that the second term in Eq. (C.4.65) cancels with the analogous in the $M \rightarrow 1 - M$ part, since $f(1 - M) = -f(M)$. Going to \tilde{h}_1 we have then, similarly to Eq. (C.4.57),

$$\tilde{h}_1(M) = f_1(M) \left[\tilde{g}(M) - \tilde{g}\left(\frac{1}{2}\right) \right] + (M \rightarrow 1 - M). \quad (\text{C.4.67})$$

In this case, as before, the $\tilde{g}(1/2)$ term cancels with the analogous in the $M \rightarrow 1 - M$ term. Consider instead f_2 , Eq. (C.4.58); this case is now non-trivial, for two facts:

- the second term in Eq. (C.4.65) doesn't cancel
- $\tilde{g}\left(\frac{3}{2}\right) - \tilde{g}\left(-\frac{1}{2}\right) \neq 0$.

Defining for convenience \tilde{h}_2^{res} as

$$\tilde{h}_2(M) = \left\{ (2 + 3M(1 - M)) \left[\frac{\tilde{g}(M) - \tilde{g}(-1/2)}{1 + 2M} - \frac{\tilde{g}(M) - \tilde{g}(3/2)}{3 - 2M} \right] + (M \rightarrow 1 - M) \right\} + \tilde{h}_2^{\text{res}}(M) \quad (\text{C.4.68})$$

we find, after a tedious but straightforward computation,

$$\tilde{h}_2^{\text{res}}(M) = \frac{128}{3}. \quad (\text{C.4.69})$$

We can then more conveniently write

$$\tilde{h}_2(M) = \left\{ (2 + 3M(1 - M)) \left[\frac{\tilde{g}(M) - \tilde{g}(-1/2)}{1 + 2M} - \frac{\tilde{g}(M) - \tilde{g}(3/2)}{3 - 2M} \right] + \frac{64}{3} \right\} + (M \rightarrow 1 - M). \quad (\text{C.4.70})$$

All together, this brings to Eq. (C.4.48).

C.4.1.6 Off-shell extension of $\chi_1(M)$

The off shell extension (in symmetric variables) of Eq. (C.4.1) can be simply obtained by substituting in the first line

$$\begin{aligned} \frac{\pi^2}{N_c^2} \chi_0^2(M) - \psi_1(M) - \psi_1(1 - M) \rightarrow \\ \frac{\pi^2}{N_c^2} \bar{\chi}_0^2(M, N) - \psi_1\left(M + \frac{N}{2}\right) - \psi_1\left(1 - M + \frac{N}{2}\right) \end{aligned} \quad (\text{C.4.71})$$

and in the following

$$M \rightarrow M + \frac{N}{2} \quad (\text{C.4.72})$$

but in the last line, which should remain $(M \rightarrow 1 - M)$. The off-shell extension of Eq. (C.4.48) can be done in the same way, but the first line transforms as

$$\begin{aligned} & \frac{\pi^2}{N_c^2} \tilde{\chi}_0^2(M) + \left[2 \frac{\pi \tilde{\chi}_0(M)/N_c + 1}{M} - \psi_1(1+M) + (M \rightarrow 1-M) \right] \rightarrow \\ & \frac{\pi^2}{N_c^2} \tilde{\chi}_0^2(M, N) + 2 \frac{(1+N)\pi \tilde{\chi}_0(M, N)/N_c + 1}{(M+N/2)(1-M+N/2)} - \psi_1\left(1+M+\frac{N}{2}\right) - \psi_1\left(2-M+\frac{N}{2}\right) \end{aligned} \quad (\text{C.4.73})$$

The off-shell extension of $\check{\chi}_1$, Eq. (C.4.49), is

$$\check{\chi}_1(M, N) = \bar{\chi}_1^\sigma(M, N) - \frac{N_c}{\pi} \bar{\chi}_0(M, N) \left[2\psi_1(1+N) - \psi_1\left(M+\frac{N}{2}\right) - \psi_1\left(1-M-\frac{N}{2}\right) \right] \quad (\text{C.4.74})$$

which do not to introduce spurious singularities. After subtracing double counting, the off-shell extension of Eq. (C.4.51) is

$$\begin{aligned} \tilde{\chi}_1(M, N) = & \tilde{\chi}_1^\sigma(M, N) - \frac{1}{2} \tilde{\chi}_0(M, N) \tilde{\psi}(M, N) \\ & + \frac{N_c}{2\pi} \left\{ \frac{1}{(M+N/2)^2} \left[\tilde{\chi}_0(M, N) - \tilde{\chi}_0\left(-\frac{N}{2}, N\right) - \left(M+\frac{N}{2}\right) \tilde{\chi}'_0\left(-\frac{N}{2}, N\right) \right] \right. \\ & \quad \left. - \frac{1}{M+N/2} \left[\tilde{\psi}(M, N) - \tilde{\psi}\left(-\frac{N}{2}, N\right) \right] \right. \\ & \quad \left. + (M \rightarrow 1-M) \right\} \end{aligned} \quad (\text{C.4.75})$$

where we have defined for convenience

$$\tilde{\psi}(M, N) = \frac{N_c}{\pi} \left[2\psi_1(1+N) - \psi_1\left(1+M+\frac{N}{2}\right) - \psi_1\left(2-M+\frac{N}{2}\right) \right] \quad (\text{C.4.76})$$

and the prime denotes derivatives with respect to the first argument:

$$\tilde{\chi}'_0\left(-\frac{N}{2}, N\right) = \frac{N_c}{\pi} [\psi_1(2+N) - \psi_1(1)] \quad (\text{C.4.77})$$

It is very important, from a numerical point of view, to provide an analytic evaluation of some critical points, i.e.

$$M + \frac{N}{2} = 0, \frac{1}{2}, -\frac{1}{2}, \frac{3}{2}, \quad (\text{C.4.78})$$

and the same with $M \rightarrow 1-M$.

C.4.2 Resummation at NLO

We now present the construction of the NLO resummed anomalous dimension. We do not pretend to explain the construction in detail, but just to show the result: full details can be found on Ref. [54].

The resummed anomalous dimension at NLO is given by

$$\begin{aligned} \gamma_{\text{res}}^{\text{NLO}}(\alpha_s, N) = & \gamma_B(\alpha_s, N) - \gamma_{B,s}(\alpha_s, N) - \gamma_{B,ss}(\alpha_s, N) \\ & + \gamma_{\text{DL}}^\sigma(\alpha_s, N) - \gamma_{ss}^{\text{rc}}(\alpha_s, N) + \frac{N}{2} + \gamma_{\text{match}}(N) + \gamma_{\text{mom}}(N), \end{aligned} \quad (\text{C.4.79})$$

which has the same structure of the LO result Eq. (3.6.1), with some modifications that we are going to discuss.

First, the coefficients $c(\alpha_s)$ and $\kappa(\alpha_s)$ in the Bateman anomalous dimension and its asymptotic subtracted terms are obtained from a NLO off-shell kernel given by

$$\begin{aligned}\bar{\chi}_B^\sigma(\alpha_s, M, N) &= \bar{\chi}_s^\sigma(\alpha_s, M, N) + \alpha_s \bar{\chi}_{ss}^\sigma(\alpha_s, M, N) \\ &\quad + \alpha_s \tilde{\chi}_0(M, N) + \alpha_s^2 \left[\tilde{\chi}_1(M, N) - \tilde{\chi}_1\left(-\frac{N}{2}, N\right) + \tilde{\chi}_1(0, 0) \right] \\ &\quad + \bar{\chi}_s^{\beta_0}(\alpha_s, M, N) + \bar{\chi}_0^{\beta_0}(\alpha_s, M, N) + \bar{\chi}_i^{\beta_0}(\alpha_s, M, N),\end{aligned}\quad (\text{C.4.80})$$

where the functions in the last line are due to running coupling commutators at LO and are given by

$$\begin{aligned}\bar{\chi}_s^{\beta_0}(\alpha_s, M, N) &= \frac{\beta_0}{2} \left[\left(\frac{\alpha_s}{M + \frac{N}{2}} \right)^3 \chi_s'' \left(\frac{\alpha_s}{M + \frac{N}{2}} \right) - \left(\frac{\alpha_s}{1 - M + \frac{N}{2}} \right)^3 \chi_s'' \left(\frac{\alpha_s}{1 - M + \frac{N}{2}} \right) \right. \\ &\quad \left. - 2 \left(\frac{\alpha_s}{1 - M + \frac{N}{2}} \right)^2 \chi_s' \left(\frac{\alpha_s}{1 - M + \frac{N}{2}} \right) \right]\end{aligned}\quad (\text{C.4.81})$$

$$\bar{\chi}_0^{\beta_0}(\alpha_s, M, N) = -\alpha_s^2 \beta_0 \frac{C_A}{\pi} \psi_1 \left(2 - M + \frac{N}{2} \right) \quad (\text{C.4.82})$$

$$\bar{\chi}_i^{\beta_0}(\alpha_s, M, N) = \frac{1}{M + \frac{N}{2}} \alpha_s^2 \beta_0 \left[c'_{\text{LO}}(\alpha_s) + \frac{1}{2} \kappa'_{\text{LO}}(\alpha_s) \left(M - \frac{1}{2} \right)^2 \right]. \quad (\text{C.4.83})$$

Note that the minimum is no longer in $M = \frac{1}{2}$.

The function $\gamma_{\text{DL}}^\sigma(\alpha_s, N)$ is obtained instead from the following NLO off-shell kernel (remember that for $n_f \neq 0$ the approximation described in Sect. 3.6.1 is used)

$$\begin{aligned}\bar{\chi}_B^\sigma(\alpha_s, M, N) &= \bar{\chi}_s^\sigma(\alpha_s, M, N) + \alpha_s \bar{\chi}_{ss}^\sigma(\alpha_s, M, N) \\ &\quad + \alpha_s \tilde{\chi}_0(M, N) + \alpha_s^2 \left[\tilde{\chi}_1(M, N) - \tilde{\chi}_1\left(-\frac{N}{2}, N\right) + \tilde{\chi}_1(0, 0) \right] \\ &\quad + \bar{\chi}_0^{\beta_0}(\alpha_s, M, N) + \bar{\chi}_{\text{int}}^{\beta_0}(\alpha_s, M, N),\end{aligned}\quad (\text{C.4.84})$$

with

$$\bar{\chi}_{\text{int}}^{\beta_0}(\alpha_s, M, N) = \frac{\alpha_s^2 \beta_0}{M + \frac{N}{2}} \frac{C_A}{\pi} \left[\psi(1) + \psi(1 + N) - \psi\left(1 + M + \frac{N}{2}\right) - \psi\left(1 - M + \frac{N}{2}\right) \right]. \quad (\text{C.4.85})$$

The function γ_{ss}^{rc} is given by

$$\gamma_{ss}^{\text{rc}}(\alpha_s, N) = \beta_0 \left[\frac{N \chi_0''(\gamma_s)}{2 [\chi_0'(\gamma_s)]^2} - \alpha_s \right]. \quad (\text{C.4.86})$$

Finally, since the parameters $c(\alpha_s)$ and $\kappa(\alpha_s)$ are different between the Bateman and the DL parts of the result, in order to allow the cancellation of spurious square-root branch-cut the function γ_{match} is added. It is given by

$$\gamma_{\text{match}}(N) = \sqrt{\frac{N - c_1}{\kappa_1/2}} - \sqrt{\frac{N + 1}{\kappa_1/2}} + \frac{1 + c_1}{\sqrt{2\kappa_1(1 + N)}} - (1 \rightarrow 2) \quad (\text{C.4.87})$$

where c_1 and κ_1 are the parameters from $\gamma_{\text{DL}}^\sigma$ and c_2 and κ_2 from γ_B .

C.4.3 Resummation of quark anomalous dimension with running coupling

The qg anomalous dimension is resummed as in Eq. (3.6.7), which needs the computation of the series

$$h([\gamma]) = \sum_{k=0}^{\infty} h_k [\gamma^k] \quad (\text{C.4.88})$$

where $[\gamma^k]$ are defined by

$$[\gamma^k] = \left(\frac{\dot{\gamma}}{\gamma}\right)^k \frac{\Gamma(\gamma^2/\dot{\gamma} + k)}{\Gamma(\gamma^2/\dot{\gamma})} = \left(\frac{\dot{\gamma}}{\gamma}\right)^k \left(\frac{\gamma^2}{\dot{\gamma}}\right)_k, \quad (\text{C.4.89})$$

where $(a)_k = \Gamma(a+k)/\Gamma(a)$ is the Pochhammer symbol, or, recursively,

$$[\gamma^{k+1}] = \gamma \left(1 + k \frac{\dot{\gamma}}{\gamma^2}\right) [\gamma^k] = \frac{\dot{\gamma}}{\gamma} \left(\frac{\gamma^2}{\dot{\gamma}} + k\right) [\gamma^k], \quad [\gamma] = \gamma. \quad (\text{C.4.90})$$

Note that, if all $h_k = 1$, we get a divergent series

$$\sum_{k=0}^{\infty} [\gamma^k] = t^a e^t \Gamma(1-a, t), \quad t = -\frac{\gamma}{\dot{\gamma}}, \quad a = \frac{\gamma^2}{\dot{\gamma}} = -t\gamma, \quad (\text{C.4.91})$$

which is the asymptotic expansion of the incomplete Gamma function. Note also that, at fixed coupling, $\dot{\gamma} = 0$, which corresponds to the limit $|t| \rightarrow \infty$; taking the limit on both sides we get

$$\sum_{k=0}^{\infty} \gamma^k = \frac{1}{1-\gamma}, \quad (\text{C.4.92})$$

which is of course correct (geometric series). This series converges for $|\gamma| < 1$, and in particular a pole in $\gamma = 1$ is present. The running coupling result is instead well defined for all γ ($t > 0$), even if the series has zero radius of convergence:

$$\lim_{k \rightarrow \infty} \left| \frac{[\gamma^{k+1}]}{[\gamma^k]} \right| = \lim_{k \rightarrow \infty} \left| \gamma + k \frac{\dot{\gamma}}{\gamma} \right| = \infty. \quad (\text{C.4.93})$$

Hence, the running of the coupling constant α_s reduces the convergence radius of the series by a factorial term.

This computation suggests that the series with $h_k = 1$ could be B_1 -summable and B_2^* -summable (see App. D.3 for notations). The order-1 Borel transform is

$$\sum_{k=0}^{\infty} \frac{1}{k!} [\gamma^k] w^k = \sum_{k=0}^{\infty} \frac{1}{k!} \left(w \frac{\dot{\gamma}}{\gamma}\right)^k \left(\frac{\gamma^2}{\dot{\gamma}}\right)_k = {}_1F_0\left(\frac{\gamma^2}{\dot{\gamma}}; ; w \frac{\dot{\gamma}}{\gamma}\right) = \left(1 - w \frac{\dot{\gamma}}{\gamma}\right)^{-\gamma^2/\dot{\gamma}} \quad (\text{C.4.94})$$

with radius of convergence $|w| < \gamma/\dot{\gamma}$. The order-2 Borel transform is

$$\sum_{k=0}^{\infty} \frac{1}{(k!)^2} [\gamma^k] w^k = \sum_{k=0}^{\infty} \frac{1}{k!} \left(w \frac{\dot{\gamma}}{\gamma}\right)^k \frac{(\gamma^2/\dot{\gamma})_k}{(1)_k} = {}_1F_1\left(\frac{\gamma^2}{\dot{\gamma}}; 1; w \frac{\dot{\gamma}}{\gamma}\right) \quad (\text{C.4.95})$$

with infinite radius of convergence. In the first case ($n_{\text{rc}} = 1$), the Borel inversion integral converges provided γ and $\dot{\gamma}$ are not both real and positive, otherwise the

branch-cut of Eq. (C.4.94) lies on the integration path. In the second case ($n_{\text{rc}} = 2$), the Borel inversion integral converges only for $\text{Re} [\gamma^2/\dot{\gamma}] > 0$.

The series $h(M)$ has a finite radius of convergence [10, 45]: then one would expect that even the actual series Eq. (C.4.88) is B_1 - and B_2^* -summable. However, the coefficients h_k are only known recursively, and it's pretty hard to work many of them out. Then, only a truncated method can be adopted. Originally [10], the truncated Borel method described in App. D.3.2 was adopted:

$$h([\gamma]) \simeq \int_0^\Lambda dw B_2(w) \sum_k^K h_k [\gamma^k] \frac{w^k}{(k!)^2}. \quad (\text{C.4.96})$$

However, it turns out that this is not enough for the result to be stable. For some values of γ and $\dot{\gamma}$, the integral is not convergent at infinity, and its truncation up to $w = \Lambda$ is not stable for variations of Λ . One could try to improve the approximation if the behaviour at large w of the Borel transform is known analytically somehow. In this case we could consider the step-defined Borel transform

$$\hat{s}_2(w) = \begin{cases} \sum_k^K h_k [\gamma^k] \frac{w^k}{(k!)^2} & \text{for } w \leq \Lambda \\ \hat{s}_2^{\text{asympt}}(w) & \text{for } w > \Lambda \end{cases} \quad (\text{C.4.97})$$

and extend the integration to infinity,

$$h(M) \simeq \int_0^\infty dw B_2(w) \hat{s}_2(w). \quad (\text{C.4.98})$$

However, it is not clear whether this approximation is good or not.

A better method consists in using the Borel-Padé method described in App. D.3.3. This method works also with an order-1 Borel, since the Borel transform is approximated with a Padé approximant which is analytically defined. Then one can consider the order- n Borel transform

$$\hat{s}_n = \sum_k^\infty h_k [\gamma^k] \frac{w^k}{(k!)^n} \quad (\text{C.4.99})$$

and approximate it with a $[p/p]$ Padé (obtained using the terms up to $K = 2p$ of the series), obtaining

$$h(\gamma) \simeq \int_0^\infty dw B_n(w) [p/p]_{\hat{s}_n}(w). \quad (\text{C.4.100})$$

As already said, this method works for both $n = 1, 2$.

C.4.4 Resummation of coefficient functions

The resummation of coefficient functions has been performed in Ref. [45] and extended to include running coupling resummation in Ref. [10]. In the $Q_0\overline{\text{MS}}$ scheme the coefficients functions at fixed coupling are given at NLL by

$$C_{Lg}(\alpha_s, N) = \frac{\alpha_s}{2\pi} \frac{2n_f}{3} \tilde{h}_L(M) \Big|_{M=\gamma_s(\alpha_s/N)} \quad (\text{C.4.101a})$$

$$C_{2g}(\alpha_s, N) = \frac{\alpha_s}{2\pi} \frac{2n_f}{3} \frac{\tilde{h}_2^{\text{CH}}(M) - \tilde{h}_{qg}(M)}{M} \Big|_{M=\gamma_s(\alpha_s/N)} \quad (\text{C.4.101b})$$

$$= \frac{\alpha_s}{2\pi} \frac{n_f}{3} \tilde{h}_2(M) \Big|_{M=\gamma_s(\alpha_s/N)} \quad (\text{C.4.101c})$$

$$(\text{C.4.101d})$$

where (the superscript CH stands for Catani-Hautmann, Ref. [45])

$$\tilde{h}_L(M) = \frac{3(1-M)}{3-2M} \frac{\Gamma^3(1-M)\Gamma^3(1+2M)}{\Gamma(2-2M)\Gamma(2+2M)} \quad (\text{C.4.102})$$

$$\tilde{h}_2^{\text{CH}}(M) = \frac{3(2+3M-3M^2)}{2(3-2M)} \frac{\Gamma^3(1-M)\Gamma^3(1+2M)}{\Gamma(2-2M)\Gamma(2+2M)} \quad (\text{C.4.103})$$

$$h_{qg}(M) = \frac{\alpha_s}{2\pi} \frac{2n_f}{3} \tilde{h}_{qg}(M) \quad (\text{C.4.104})$$

$$\tilde{h}_2(M) = 2 \frac{\tilde{h}_2^{\text{CH}}(M) - \tilde{h}_{qg}(M)}{M}. \quad (\text{C.4.105})$$

With these definitions, all the functions \tilde{h}_i have a series expansion starting with 1, i.e. $\tilde{h}_i(0) = 1$. The coefficients of the series expansion of \tilde{h}_{qg} can be worked out as described in Ref. [45]: with these coefficients at the hand, it is straightforward to obtain also the coefficient of the series expansion of \tilde{h}_2 . Then, one can use the procedure described in Sect. C.4.3 for the resummation of the quark anomalous dimensions to resum the coefficient functions as well.

The singular part of the quark-singlet coefficient functions is obtained from Eqs. (C.4.101) by colour-charge relation [45]

$$C_{Lq}(\alpha_s, N) = \frac{C_F}{C_A} \left[C_{Lg}(\alpha_s, N) - \frac{\alpha_s}{2\pi} \frac{2n_f}{3} \right] \quad (\text{C.4.106})$$

$$C_{2q}(\alpha_s, N) = \frac{C_F}{C_A} \left[C_{2g}(\alpha_s, N) - \frac{\alpha_s}{2\pi} \frac{n_f}{3} \right]. \quad (\text{C.4.107})$$

D Series and divergent series

Contents

D.1 Series	175
D.1.1 Power series	176
D.1.2 Asymptotic expansions	177
D.1.3 Operation with series	177
D.2 Divergent series and their sum	178
D.2.1 Linear transformation and regularity	179
D.2.2 Summation methods	179
D.3 Borel summation	180
D.3.1 Applications of the Borel method: some examples	182
D.3.2 Truncated Borel sum	187
D.3.3 Padé approximants and the Borel-Padé method	193

In this Appendix we will mainly talk about divergent series, which recur several times throughout the text. A complete reference on the subject is [102].

D.1 Series

Definition D.1.1. *The series*

$$\sum_k c_k \tag{D.1.1}$$

is said to be convergent if, given the partial sums

$$s_n = \sum_k^n c_k, \tag{D.1.2}$$

the limit

$$s = \lim_{n \rightarrow \infty} s_n \tag{D.1.3}$$

exists and is finite; in this case such limit s is called the sum of the series. Otherwise, the series is said to be divergent.

Definition D.1.2. *The series*

$$\sum_k c_k \quad (\text{D.1.4})$$

is said to be absolutely convergent if the series

$$\sum_k |c_k| \quad (\text{D.1.5})$$

is convergent.

The sum of a series which is convergent but not absolutely convergent can be any number. Hence, we could recast the definition of absolute convergence by the requirement that the limit of partial sums exists, is finite and is *unique*.

There are several convergence test. We are not going to review all of them; we will just show one of them, which is quite common and useful: the *ratio test*. Defining

$$\rho = \lim_{k \rightarrow \infty} \left| \frac{c_{k+1}}{c_k} \right| \quad (\text{D.1.6})$$

we have that

- if $\rho < 1$ the series converges absolutely
- if $\rho > 1$ the series diverges
- if $\rho = 1$ the test is inconclusive, and we need to use another test.

A typical example in which the test is inconclusive is the case of $c_k = k^\sigma$: indeed $\rho = 1$ for any σ , and we know from other tests (for instance, the root test) that for $\sigma < -1$ the series of c_k converges.

D.1.1 Power series

Sometimes it is useful to talk about power series, i.e. series in which the k -th coefficient c_k is splitted into a numeric coefficient (we will call it c_k again) times the k -th power of a generic complex variable z :

$$s(z) = \sum_k c_k z^k. \quad (\text{D.1.7})$$

Of course, this definition doesn't add anything to the discussion above: indeed, for any fixed z we have again a series with k -th coefficient $c_k z^k$ and everything is like before.

However, power series are very useful, since they arise in functional analysis and in perturbation theory. In particular, we can introduce the concept of *radius of convergence*. Indeed, using the ratio test, we get

$$\rho = \lim_{k \rightarrow \infty} \left| \frac{c_{k+1} z^{k+1}}{c_k z^k} \right| = |z| \lim_{k \rightarrow \infty} \left| \frac{c_{k+1}}{c_k} \right| = \frac{|z|}{r} \quad (\text{D.1.8})$$

where we have defined

$$r = \lim_{k \rightarrow \infty} \left| \frac{c_k}{c_{k+1}} \right|; \quad (\text{D.1.9})$$

then, the convergence condition $\rho < 1$ gives

$$|z| < r, \quad (\text{D.1.10})$$

i.e. the power series $s(z)$ converges in a circle of radius r . Since the series converges inside such a circle, the sum $s(z)$ is analytic in the same region. Then, reversing the argument, if we are going to expand a function $f(z)$ around some point z_0 and this function has poles in the complex plane, the radius of convergence of the expansion can be at most the distance between z_0 and the closest pole to it.

D.1.2 Asymptotic expansions

It happens in some cases that we are able to find a series expansion of a function $f(z)$ around some values of z which is actually a divergent series. In these cases, we will call it an *asymptotic expansion*. Formally (supposing for simplicity to consider an expansion around $z = 0$) we have the following

Definition D.1.3. *A series expansion*

$$s(z) = \sum_k c_k z^k \quad (\text{D.1.11})$$

is said to be asymptotic to $f(z)$ in the sense of Poincaré if

$$\lim_{z \rightarrow 0} z^{-n} [f(z) - s_n(z)] = 0 \quad (\text{D.1.12})$$

for all $n > 0$ (s_n is the n -th partial sum).

A stronger definition of asymptotic series can be obtained by requiring that there exists a constant C such that

$$|f(z) - s_n(z)| \leq C c_{k+1} |z|^{k+1} \quad (\text{D.1.13})$$

for all n .

D.1.3 Operation with series

Raising a series to a power gives

$$\left(\sum_{j=0}^{\infty} a_j z^j \right)^n = \sum_{k=0}^{\infty} c_{n,k} z^k \quad (\text{D.1.14})$$

with

$$c_{n,0} = a_0^n, \quad c_{n,k} = \frac{1}{a_0^k} \sum_{j=1}^k (jn + j - k) a_j c_{n,k-j}. \quad (\text{D.1.15})$$

D.2 Divergent series and their sum

When the limit of the partial sums of a series does not exist or is not finite the series is said to be *divergent* (Def. D.1.1). This, however, doesn't mean that the sum of the series is infinite; indeed, it simply means that the definition of the sum of the series as the limit of the partial sums is not a good definition. Then, we need a definition for the sum of a divergent series.

As an example, let's consider a classical divergent series

$$\sum_{k=0}^{\infty} (-1)^k = 1 - 1 + 1 - 1 + \dots; \quad (\text{D.2.1})$$

it diverges because the partial sums

$$s_n = \sum_{k=0}^n (-1)^k = \begin{cases} 0 & \text{for } n \text{ even} \\ 1 & \text{for } n \text{ odd} \end{cases} \quad (\text{D.2.2})$$

oscillate between 0 and 1, and the limit for $n \rightarrow \infty$ of s_n does not exist. However there are some simple arguments to believe that the sum *should* be $1/2$. For example, if we call s the sum of the series, we can manipulate it to obtain an equation for s :

$$s = \sum_{k=0}^{\infty} (-1)^k \quad (\text{D.2.3})$$

$$= 1 + \sum_{k=1}^{\infty} (-1)^k \quad (\text{D.2.4})$$

$$= 1 + \sum_{k=0}^{\infty} (-1)^{k+1} \quad (\text{D.2.5})$$

$$= 1 - \sum_{k=0}^{\infty} (-1)^k \quad (\text{D.2.6})$$

$$= 1 - s \quad (\text{D.2.7})$$

from which we get immediately $s = 1/2$. Of course, such manipulations are allowed if the series is convergent; here they might be not allowed. However there are other ways to obtain $s = 1/2$. For example, consider the power series

$$s(z) = \sum_{k=0}^{\infty} (-z)^k \quad (\text{D.2.8})$$

which converges in the complex circle $|z| < 1$, where the sum is

$$s(z) = \frac{1}{1+z}; \quad (\text{D.2.9})$$

this result can be analytically continued to the whole complex plane but $z = -1$. The series (D.2.1) is recovered when $z = 1$, which is outside the convergence circle, but using the analytical extension of the sum we get again $s = s(1) = 1/2$.

In the following we will provide the necessary mathematical theorems and tools to *define* the sum of a divergent series in such a way that we can really *prove* that the sum of the series (D.2.1) is $1/2$.

D.2.1 Linear transformation and regularity

The way forward the definition of the sum of a divergent series starts by considering a linear transformation T of the sequence $\{s_n\}_{n \geq 0}$ of the partial sums into the sequence $\{t_m\}_{m \geq 0}$:

$$t_m = \sum_n a_{mn} s_n, \quad (\text{D.2.10})$$

where a_{mn} are complex coefficients. This transformation can be generalized to the case in which m is a continuous index:

$$t(x) = \sum_n a_n(x) s_n. \quad (\text{D.2.11})$$

We have the following

Definition D.2.1. *The linear transformation (D.2.10) is said to be regular if, whenever*

$$\lim_{n \rightarrow \infty} s_n = s \quad (\text{D.2.12})$$

(that is, the original series converges), we have

$$\lim_{m \rightarrow \infty} t_m = s. \quad (\text{D.2.13})$$

A regular linear transformation is then a transformation which doesn't change the sum for convergent series. Applying a regular linear transformation to a divergent series may lead to a finite limit

$$t = \lim_{m \rightarrow \infty} t_m. \quad (\text{D.2.14})$$

When this is the case, we are then tempted to consider t as the sum of the divergent series. Of course, if different linear transformation gave different sums, this would not be a good definition.

Let's call the entire set of sequences S , and $C \subset S$ the subset of convergence sequences. A regular linear transformation T gives a finite result at least in C , but possibly in a wider subset $S_T \subseteq S$. Now consider two regular linear transformation T_1 and T_2 : when the results obtained with both transformations coincide for all the sequences in $S_{T_1} \cap S_{T_2}$ the two transformations are said to be *consistent*. Consistent transformations are good candidates for extending the definition of the sum of a series to divergent series. In the literature, several regular linear transformations are known to be consistent.

D.2.2 Summation methods

Several summation methods have been proposed for long; the most well known are by Cesaro, Abel, Euler, etc. For a complete review, we refer the Reader to Ref. [102]. All these methods are based on regular linear transformations. There exists other summation methods which are not linear, but they are not supported by strong theorems, and therefore we do not discuss them here: some details can be found in Ref. [103].

In the following, we will concentrate on one method, by Borel, which turns out to be very flexible especially for physical application and for numerical implementations.

D.3 Borel summation

The Borel method for summing divergent series is based on a continuous linear transformation. In its original form it can be formulated as

$$\sum_k c_k \stackrel{\text{B}}{=} \int_0^\infty dw e^{-w} \sum_k \frac{c_k}{k!} w^k. \quad (\text{D.3.1})$$

Its regularity can be easily proven by noting that, for absolutely convergent series, the integral and the sum can be exchanged and

$$\frac{1}{k!} \int_0^\infty dw e^{-w} w^k = 1; \quad (\text{D.3.2})$$

pictorially, a nice way to view the Borel method is to start from the divergent series, multiply each term by 1, write 1 as above with the appropriate k in each term, and finally exchange the sum and the integral.

It can be useful to introduce the following

Definition D.3.1. *The inner power series in the right-hand-side of Eq. (D.3.1),*

$$\hat{s}(w) = \sum_k \frac{c_k}{k!} w^k, \quad (\text{D.3.3})$$

is called the Borel transform of the series $\sum_k c_k$.

Since in the Borel transform there is a $k!$ factorial in the denominator, this sum has more chances to converge, even if the original sum is divergent. Hence, we have the following

Definition D.3.2. *Given a divergent series,*

- *if its Borel transform converges*
- *if its sum $\hat{s}(w)$ is defined on (or can be analytically extended to) $0 \leq w \leq \infty$*
- *if the integral converges*

the series is said to be Borel-summable or B-summable. If the second requirement is made stronger by requiring that the Borel transform actually has infinite radius of convergence we will call the series B-summable.*

The Borel method can be generalized for “more divergent” series, by iterating the standard method:

$$\sum_k c_k \stackrel{\text{B}_n}{=} \int_0^\infty dw_1 \cdots \int_0^\infty dw_n e^{-w_1 \cdots w_n} \sum_k \frac{c_k}{(k!)^n} (w_1 \cdots w_n)^k. \quad (\text{D.3.4})$$

In this way, because at the denominator there is a $(k!)^n$ the inner sum (which we’ll call generalized Borel transform $\hat{s}_n(w_1 \cdots w_n)$) has many more chances to converge, provided n is large enough. A divergent series which can be summed with this generalized Borel method of order n is said B_{*n*}-summable (or B_{*n*}*-summable in the stronger case). The standard method Eq. (D.3.1) is recovered for $n = 1$.

We can recast Eq. (D.3.4) in a form more similar to the original one: by changing integration variables $w_n = w/(w_1 \cdots w_{n-1})$ we get

$$\sum_k c_k \stackrel{\text{B}_n}{=} \int_0^\infty dw B_n(w) \sum_k \frac{c_k}{(k!)^n} w^k. \quad (\text{D.3.5})$$

where

$$B_n(w) = \int_0^\infty \frac{dw_1}{w_1} \cdots \int_0^\infty \frac{dw_{n-1}}{w_{n-1}} \exp \left[-w_1 \cdots - w_{n-1} - \frac{w}{w_1 \cdots w_{n-1}} \right] \quad (\text{D.3.6})$$

$$= \int_0^\infty \frac{dw_1}{w_1} \cdots \int_0^\infty \frac{dw_{n-k}}{w_{n-k}} \exp [-w_1 \cdots - w_{n-k}] B_k \left(\frac{w}{w_1 \cdots w_{n-k}} \right) \quad (\text{D.3.7})$$

which satisfy, for regularity,

$$(k!)^n = \int_0^\infty dw B_n(w) w^k. \quad (\text{D.3.8})$$

Explicit expressions of $B_n(w)$ for the first few $n = 1, 2$ are

$$B_1(w) = e^{-w} \quad (\text{D.3.9})$$

$$B_2(w) = 2K_0(2\sqrt{w}) \quad (\text{D.3.10})$$

but no explicit expressions in terms of common functions are available for higher orders. Anyway, we can recast the integrals for a generic n into a single integral

$$B_n(w) = \frac{1}{2\pi i} \int ds w^{-s} \Gamma^n(s) = G_{0n}^{n0}(w; ; ; \underbrace{0, \dots, 0}_n;) \quad (\text{D.3.11})$$

where the integration contour is the same as for a Mellin inversion (passing to the right of $s = 0$), and the function is called a Meijer G function. The proof of Eq. (D.3.11) can be easily obtained from Eq. (D.3.6) by using the formula

$$e^{-x} = \frac{1}{2\pi i} \int ds x^{-s} \Gamma(s) \quad (\text{D.3.12})$$

to rewrite $\exp \left[-\frac{w}{w_1 \cdots w_{n-1}} \right]$ and computing the w_i integrals. We may then recast the order n Borel method in a third form

$$\sum_k c_k \stackrel{\text{B}_n}{=} \frac{1}{2\pi i} \int ds \Gamma^n(s) \int_0^\infty dw w^{-s} \sum_k \frac{c_k}{(k!)^n} w^k \quad (\text{D.3.13})$$

which may be more convenient for some applications. Indeed, whence Eqs. (D.3.4) and (D.3.5) are completely equivalent, this equation is somehow different because we have swapped the two integrals. In particular, we have to specify the integration path: after the w integral some other s -singularities may arise, and we need a prescription how the contour has to pass through them.¹

Note that we may also consider the case in which $n = 0$: in practice, it means that we add to the original series a w^k in each term, obtaining then a power series;

¹The correct choice seems to be that the path has to cross the real axis to the right of the rightmost singularity of $\Gamma(s)$, i.e. $s = 0$, and to the left of any other singularity which may appear out of the w integral.

if this power series can be summed, the Borel sum consists in computing this 0-order Borel transform in $w = 1$. Formally, this is obtained with $B_0(w) = \delta(1 - w)$, which can be also obtained from the general expression Eq. (D.3.11). This is, for example, the second way we used to find a sum of the series Eq. (D.2.1), see Eq. (D.2.8) and discussion there.

If a series is B_n -summable it is also B_k -summable, $\forall k > n$ (the same for B_n^*). Indeed, in order for a series to be B_n -summable, the Borel transform $\hat{s}_k(w)$ for any $k > n$ must have an infinite radius of convergence (since $\hat{s}_n(w)$ has, at least, a finite radius of convergence). Then, in the B_k expression for the sum, one can swap back one of the integrals with the sum without problems (because the series converges everywhere), obtaining a completely equivalent expression: the integral can now be computed explicitly, giving the formal expression for the B_{k-1} sum of the series. Since these manipulations are all completely legal, the result will be the same: this completes the proof.

Therefore, it is useful to consider the minimal value of n for which a series is B_n -summable (or B_n^* -summable). For a wide class of divergent series, it happens that if a series is minimally B_n -summable, then it is also minimally B_{n+1}^* -summable. This comes simply from the fact that, often, the Borel transform $\hat{s}_n(w)$ has a finite radius of convergence, and then straightforwardly $\hat{s}_n(w)$ has infinite radius of convergence. However there are special cases in which the same n is minimal for both B - and B^* -summability, but they are not so common.

Note that this is valid for a divergent series; conversely, if a series is convergent, it is for sure B_0 -summable, but it can be or not B_0^* -summable, depending on the radius of convergence of its 0-order Borel transform $\hat{s}_0(w)$. We now see some examples.

D.3.1 Applications of the Borel method: some examples

D.3.1.1 Example 0

Consider as first example the series Eq. (D.2.1). With standard Borel method ($n = 1$), we get

$$\hat{s}_1(w) = \sum_k \frac{(-w)^k}{k!} = e^{-w} \quad (\text{D.3.14})$$

with infinite radius of convergence, and then

$$s = \int_0^\infty dw e^{-w} e^{-w} = \frac{1}{2}, \quad (\text{D.3.15})$$

again. Higher order methods give, of course, the same result.

D.3.1.2 Example 1a

Consider the divergent series

$$s = \sum_{k=0}^{\infty} (-1)^k k!. \quad (\text{D.3.16})$$

Its Borel transform for $n = 1, 2, 3$ is

$$\hat{s}_1(w) = \frac{1}{1+w}, \quad \hat{s}_2(w) = e^{-w}, \quad \hat{s}_3(w) = J_0(2\sqrt{w}), \quad (\text{D.3.17})$$

where the first transform has convergence radius $|w| < 1$, while the others have infinite convergence radius ($J_0(x)$ is a cylindrical Bessel function). The Borel sums with $n = 1, 2$ are given by

$$s \stackrel{\text{B}_1}{=} \int_0^\infty dw e^{-w} \frac{1}{1+w}, \quad s \stackrel{\text{B}_2}{=} \int_0^\infty dw e^{-w} 2K_0(2\sqrt{w}); \quad (\text{D.3.18})$$

as expected, the result is the same

$$s = -e \text{Ei}(-1) = 0.596347. \quad (\text{D.3.19})$$

D.3.1.3 Example 1b

Consider now the divergent series, closely related to that of the previous example,

$$s = \sum_{k=0}^{\infty} k!. \quad (\text{D.3.20})$$

Its Borel transform for $n = 1, 2, 3$ is

$$\hat{s}_1(w) = \frac{1}{1-w}, \quad \hat{s}_2(w) = e^w, \quad \hat{s}_3(w) = I_0(2\sqrt{w}), \quad (\text{D.3.21})$$

where the first transform has again convergence radius $|w| < 1$, while the others have infinite convergence radius ($I_0(x)$ is a modified cylindrical Bessel function). However, in this case, for every n the Borel inversion integral does not converge: for $n = 1$, because of a pole in the integration path, $w = 1$, the others for the bad behaviour at $w \rightarrow \infty$.

However, the standard method $n = 1$

$$s \stackrel{\text{B}_1}{=} \int_0^\infty dw e^{-w} \frac{1}{1-w} \quad (\text{D.3.22})$$

can still give a result, by deforming the integration contour in the complex w -plane to avoid the pole in $w = 1$; nevertheless, the result has an ambiguity, given by the two possible way of avoiding the pole (above or below). The result is (a simple way to compute the integral is to deform the contour into the two straight lines $0 \rightarrow i\epsilon \rightarrow i\epsilon + \infty$)

$$s \stackrel{\text{B}_1}{=} e^{-1} [\text{Ei}(1) \pm i\pi]. \quad (\text{D.3.23})$$

Note that here, even if with $n = 1$ the convergence radius of the Borel transform is finite, we are nevertheless able to find a (even ambiguous) sum.

We could try to interpret the result of the $n \geq 2$ method imagining that in those case the pole appearing on the first approach is somehow pushed at infinity. Indeed, for $n = 2$, e^w has an essential singularity at the complex infinity, so we might try to

do the same job as in the $n = 1$ case by going to infinity in a different direction. For example, we choose a contour on the positive imaginary axis, giving as result

$$-e \operatorname{Ei}(-1) + 1.32387 \cdot 10^{-8}i. \quad (\text{D.3.24})$$

Using instead the negative imaginary axis, we get the opposite sign in the imaginary part. We may then quote as result

$$s \stackrel{\text{B}_2}{=} -e \operatorname{Ei}(-1) \pm 1.32387 \cdot 10^{-8}i, \quad (\text{D.3.25})$$

which however differs a lot from the $n = 1$: this may mean that the series is seriously too divergent, and hence any attempt to give it a meaning is going to fail, or to give meaningless results. We see in the next example which is the correct interpretation of these results.

D.3.1.4 Example 2

Of course, examples 1a and 1b are related, and we want to consider here their relation. Then we concentrate our attention on the power series

$$s(z) = \sum_{k=0}^{\infty} (-z)^k k!, \quad (\text{D.3.26})$$

which gives back the first two examples when $z = 1$ and $z = -1$, respectively. We can work on this series as in the examples above; for instance, the Borel transforms are essentially the same as for example 1a, but with $w \rightarrow wz$:

$$\hat{s}_1(w) = \frac{1}{1+wz}, \quad \hat{s}_2(w) = e^{-wz}, \quad \hat{s}_3(w) = J_0(2\sqrt{wz}). \quad (\text{D.3.27})$$

Of course, the radius of convergence of such series depends on z . Let's for a while forget about this radius and compute the integrals; each method gives

$$s(z) = \frac{1}{z} \Gamma\left(0, \frac{1}{z}\right) \exp \frac{1}{z} \quad (\text{D.3.28})$$

which reproduces the result Eq. (D.3.19) for $z = 1$.

As a function of z in the complex plane, $s(z)$ has a branch-cut along the negative real axis, where the real part could be analytically continued but the imaginary part has a discontinuity, see Fig. D.1. In particular, the imaginary part along the negative real axis is given by

$$\operatorname{Im} s(-x + i0^+) = -\frac{\pi}{x} e^{-1/x}, \quad (\text{D.3.29})$$

as one can easily find knowing that $\Gamma(0, -1/x)$ has a discontinuity of 2π .

If one consider now the limit $z \rightarrow -1$, the result depends (because of the discontinuity) if the point $z = -1$ is approached from imaginary part of z positive or negative, and hence it has an ambiguous imaginary part. The result is

$$s(-1) = e^{-1} [\operatorname{Ei}(1) \pm i\pi], \quad (\text{D.3.30})$$

which is exactly what we found in Eq. (D.3.23) with the standard Borel method $n = 1$. This means that, in this case, the $n = 1$ method gives the *correct* result also if the series

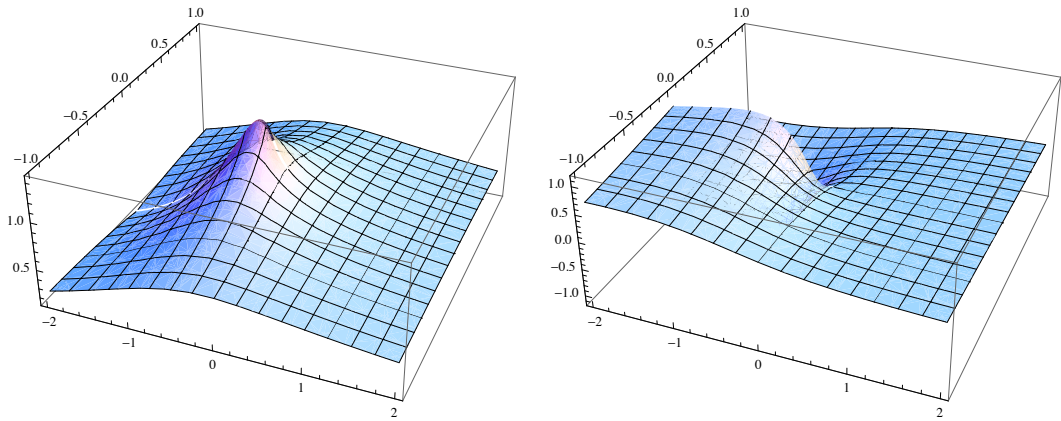


Figure D.1. Real and imaginary part of the function $s(z)$, Eq. (D.3.34)

is not B_1 -summable in the sense of Def. D.3.2. Of course, this is not a case: indeed, for instance, the upper sign of the imaginary part is obtained when approaching $z = -1$ from the lower half-plane, i.e. we have

$$s(-1 - i0^+) = e^{-1} [\text{Ei}(1) + i\pi]. \quad (\text{D.3.31})$$

If one builds the divergent series for $z = -1 - i0^+$, the Borel transform for $n = 1$ becomes

$$\hat{s}_1(w) = \frac{1}{1 - w(1 + i0^+)} = \frac{1}{1 - i0^+ - w} \quad (\text{D.3.32})$$

which automatically include a prescription to circumvent the pole. When $n = 2$, the Borel transform is

$$\hat{s}_2(w) = e^{w(1+i0^+)}, \quad (\text{D.3.33})$$

and again we automatically have a prescription to compute the inversion integral, different from the one we tried to use before. However, in this case, the integral cannot be computed even with the prescription, remarking again that higher orders in this case don't work.

Note, however, that there is no hope to find a numerical method to automatically extract the result for this sum: indeed, here we use analytic continuation, and before we deformed the contour of Borel inversion, having already analytically computed the Borel transform.

Note that the function can be continued to $z = 0$ giving as result

$$s(0) = 1, \quad (\text{D.3.34})$$

as one would naively expect from the series (only the first term remains for $z = 0$). However, the function is not analytical in z , because of the presence of the branch-cut from $z = 0$ down to the negative real axis: indeed, the series (D.3.26) has the form of the Taylor expansion of $s(z)$ around $z = 0$, and the fact that the series has zero radius of convergence (is divergent for all z) is related to the non-analyticity of $s(z)$ in $z = 0$. To exploit this relation, we have to show that because of the branch-cut the derivatives of $s(z)$ in $z = 0$ give the coefficients of the divergent series. However, since $s(z)$ is not analytical in $z = 0$, we cannot compute such derivatives in a straightforward way. The

idea here is to use the Cauchy formula for derivatives

$$s^{(k)}(z) = \frac{k!}{2\pi i} \oint dx \frac{s(x)}{(x-z)^{k+1}} \quad (\text{D.3.35})$$

where the integration contour encircles the point z . Then we can modify the contour to a Pac-Man contour eating the negative real axis, and, if

- $zs(z) \rightarrow 0$ as $z \rightarrow 0$ and
- $s(z) \rightarrow 0$ as $z \rightarrow \infty$,

(as it is in the present case), the contribution from the circles at infinity and around $z = 0$ vanishes, leaving

$$s^{(k)}(z) = \frac{k!}{\pi} \int_{-\infty}^0 dx \frac{\text{Im } s(x + i0^+)}{(x-z)^{k+1}}. \quad (\text{D.3.36})$$

We can then push this expression to be valid also in the limit $z = 0$, from which we can obtain the coefficients of the Taylor expansion:

$$c_k = \frac{1}{k!} s^{(k)}(0) = \frac{1}{\pi} \int_{-\infty}^0 dx \frac{\text{Im } s(x + i0^+)}{x^{k+1}}. \quad (\text{D.3.37})$$

Using Eq. (D.3.29), with a straightforward calculation we find

$$c_k = (-1)^k k!, \quad (\text{D.3.38})$$

which are exactly the coefficient of the power series Eq. (D.3.26), as expected. Summarizing, this computation shows a deep connection between the non-analyticity of a function and a divergent power series, and in particular it relates the discontinuity along a cut of the non-analytic function to the large- k behaviour of the terms of its power series.

D.3.1.5 Example 3

There are many other examples that may be built out of example 2 above, by choosing different values of the variable z . For example, let us choose $z = -i$ to obtain

$$s = \sum_{k=0}^{\infty} (-i)^k k! = \sum_{k=0}^{\infty} (-1)^k (2k)! + i \sum_{k=0}^{\infty} (-1)^k (2k+1)!. \quad (\text{D.3.39})$$

We know that the sums of the two series are, respectively, the real and the imaginary parts of

$$i \Gamma(0, i) e^i. \quad (\text{D.3.40})$$

However, separately, the two series are not B_1 -summable, because the terms of the series diverge more than $k!$. Of course, we know that this is due to the fact that we have separated the two sums: the original sum is a special case of the one we have already resummed before, Eq. (D.3.26). As a toy exercise, we can then try to use

$n = 2$ Borel method. Concentrating on the real part (the other series has the same properties), we have

$$\hat{s}_2(w) = \sum_{k=0}^{\infty} \frac{(2k)!}{(k!)^2} (-w)^k = \frac{1}{\sqrt{1+4w}} \quad (\text{D.3.41})$$

with convergence radius $|w| < 1/4$, and hence

$$s \stackrel{\text{B}_2}{=} \int_0^{\infty} dw \frac{2K_0(2\sqrt{w})}{\sqrt{1+4w}} = 0.62145 \quad (\text{D.3.42})$$

which is numerically equal to what expected.

D.3.1.6 Example 4

Now let's consider a more divergent series like

$$\sum (-1)^k (k!)^p, \quad p > 1. \quad (\text{D.3.43})$$

From the last examples, we immediately understand that the series is B_p -summable and B_{p+1}^* -summable. Its order p and $p+1$ Borel transforms are trivially

$$\hat{s}_p(w) = \frac{1}{1+w}, \quad \hat{s}_{p+1}(w) = e^{-w}. \quad (\text{D.3.44})$$

However, here the standard formulae Eqs. (D.3.4) and (D.3.5) are complicated because of the many integrals to be computed. Indeed, for general p , it's better to use Eq. (D.3.13): the w integral gives, in the p and $p+1$ cases respectively,

$$\frac{\pi}{\sin(\pi s)}, \quad \text{and} \quad \Gamma(1-s), \quad (\text{D.3.45})$$

and the sum of the series is

$$\sum (-1)^k (k!)^p \stackrel{\text{B}_p}{=} \frac{1}{2i} \int ds \frac{\Gamma^p(s)}{\sin(\pi s)} \quad (\text{D.3.46})$$

$$\stackrel{\text{B}_{p+1}^*}{=} \frac{1}{2\pi i} \int ds \Gamma^{p+1}(s) \Gamma(1-s), \quad (\text{D.3.47})$$

and the two results are trivially related by the Euler reflection formula. Note the presence of the poles for positive integer values of s : the integration path has to cross the real axis in the region $0 < s < 1$. Even if an analytical expression of the integrals can't be found, the numerical result for any given p is very easy to compute.

D.3.2 Truncated Borel sum

Sometimes, even if a series is B_n -summable, it is not possible to analytically compute the sum of the Borel transform. In these cases, it's impossible to use the (generalized) Borel method in a straightforward way, since any truncation of the Borel transform series would reproduce a truncation of the original divergent series.

A way to use the Borel method in such cases is to truncate the w integral up to some cutoff Λ : if the series is B_n -summable, the integral is convergent, and it means

that the truncated integral can give an arbitrarily precise result provided Λ is large enough. With the cutoff Λ , we have then

$$\begin{aligned} \sum_k c_k &\stackrel{B_n}{=} \int_0^\infty dw B_n(w) \sum_k c_k \frac{w^k}{(k!)^n} \\ &\simeq \int_0^\Lambda dw B_n(w) \sum_k c_k \frac{w^k}{(k!)^n} \\ &= \sum_k c_k D_k^{(n)}(\Lambda) \end{aligned} \quad (\text{D.3.48})$$

where

$$\begin{aligned} D_k^{(n)}(\Lambda) &= \frac{1}{(k!)^n} \int_0^\Lambda dw B_n(w) w^k \\ &= \frac{1}{2\pi i} \int ds \frac{\Lambda^{k+1-s}}{k+1-s} \left(\frac{\Gamma(s)}{k!} \right)^n \end{aligned} \quad (\text{D.3.49})$$

is a damping factor for k , showed in Fig. D.2; the second row is obtained using Eq. (D.3.13). If this damping is enough to suppress the divergent terms in the se-

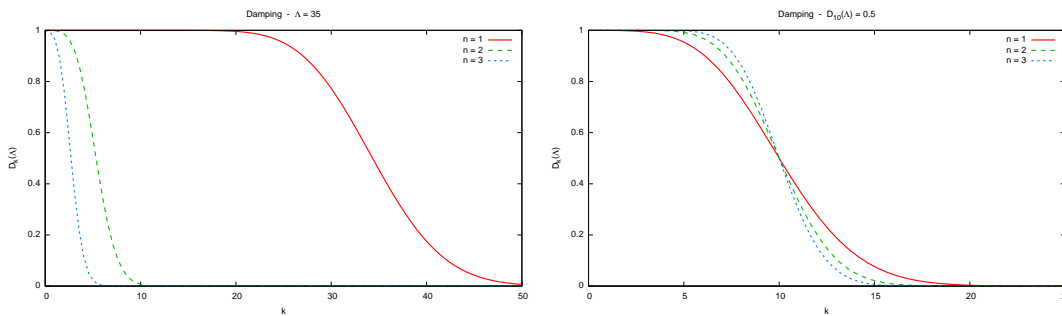


Figure D.2. The function $D_k^{(n)}(\Lambda)$ defined in Eq. (D.3.49) for $n = 1, 2, 3$. In the left plot $\Lambda = 35$ for all curves, while in the right plot Λ is chosen in such a way to have the medium damping point at the same value $k = 10$.

ries, we can truncate the series at some $k = K$, and the subsequent terms would give smaller and smaller contributions. Then we are again able to have a result as accurate as needed by choosing K large enough. We have then

$$\begin{aligned} \sum_k c_k &\simeq \sum_k^K c_k D_k^{(n)}(\Lambda) \\ &= \int_0^\Lambda dw B_n(w) \sum_k^K c_k \frac{w^k}{(k!)^n} \\ &= \frac{1}{2\pi i} \int ds \Gamma^n(s) \sum_k^K c_k \frac{\Lambda^{k+1-s}}{(k+1-s)(k!)^n} \end{aligned} \quad (\text{D.3.50})$$

which can be used to evaluate the Borel sum of a divergent series to arbitrary precision by choosing appropriate values for Λ and K . In particular, using the last row, always just one single integral has to be computed, independently on the order n .

We emphasize that for the applicability of Eq. (D.3.50) there is the strong requirement that the damping be enough to cure the divergence of the series, that is, the series in the last line of Eq. (D.3.48) has to be convergent. This is related to the radius of convergence of the Borel transform: indeed, between the second and third lines of Eq. (D.3.48) we exchanged the integral and the sum, and this can be done provided the sum is absolutely convergent for all values of w in the integration range $0 \leq w \leq \infty$, that is to say that the Borel transform $\hat{s}_n(w)$ has infinite radius of convergence. We conclude that the truncated Borel method Eq. (D.3.50) applies only to those divergent series which are, according to Def. D.3.2, B_n^* -summable. Fortunately, if a series is not B_n^* -summable for a given n , there are chances that it is for a larger n .

D.3.2.1 Damping factor

The damping factor is, for $n = 1$,

$$D_k^{(1)}(\Lambda) = 1 - \frac{\Gamma(k+1, \Lambda)}{\Gamma(k+1)} \quad (\text{D.3.51})$$

where $\Gamma(k+1, \Lambda)$ is the incomplete Gamma function. It can be computed directly (and easily) from the integral in the first row of Eq. (D.3.49); otherwise, we can use the second row formulation, deform the contour to encircle the poles of $\Gamma(s)$, obtaining

$$D_k^{(1)}(\Lambda) = \frac{1}{k!} \sum_{j=0}^{\infty} \frac{(-1)^j \Lambda^{k+1+j}}{(k+1+j)j!} \quad (\text{D.3.52})$$

which gives the same result.

The same kind of double computation may be done for $n = 0$: indeed, recalling that $B_0(w) = \delta(1-w)$, from the integral we get

$$D_k^{(0)}(\Lambda) = \Theta(\Lambda - 1). \quad (\text{D.3.53})$$

This is not a damping, but this is expected, since $n = 0$ does not manipulate the original series: it simply means that, provided $\Lambda > 1$, the cutoff is ineffective, while $\Lambda < 1$ is meaningless (too small). With the second formulation, the same result is obtained by noting that the only pole is at $s = k+1$, with residue 1: then, when $\Lambda > 1$, we can close the path on the right, where the contribution is given only by the pole, and we get 1, while for $\Lambda < 1$ we can deform the path to the left where there are no singularities, and we get 0.

In the case of $n = 2$ we have instead a complicated analytical expression in terms of hypergeometric functions; for practical purposes it's easier to numerically compute the integral. For $n = 3$ or higher no analytic results are available.

The approximation Eq. (D.3.50) is good provided K is larger than the point where the damping starts to suppress the terms in the series. Let's call such a point $k_\Lambda^{(n)}$. Of course it may depend also on the series, hence it's impossible to have a general expression for it. Nevertheless, as one can see from Fig. D.2, there is a relatively small region in which the damping factor goes from being approximately 1 to be approximately 0 (the larger n , the smaller this region). Hence, $k_\Lambda^{(n)}$ cannot be too far

from the medium point of this damping: then, to have a precise definition of $k_\Lambda^{(n)}$, let's define it as the value

$$D_{k_\Lambda^{(n)}}^{(n)}(\Lambda) = \frac{1}{2}. \quad (\text{D.3.54})$$

For $n = 1$, we have (numerically)

$$k_\Lambda^{(1)} \simeq \Lambda \quad (\text{D.3.55})$$

For $n = 2, 3$ see Fig. D.3.

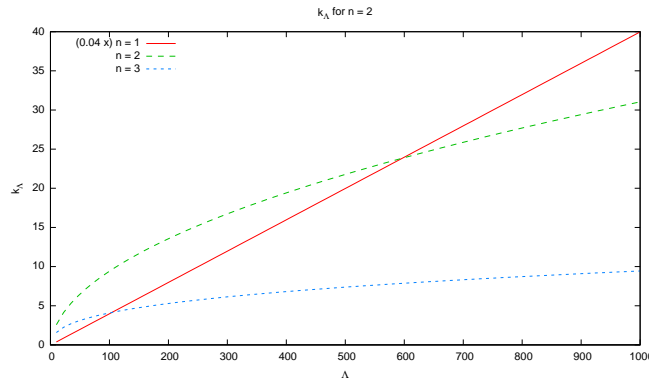


Figure D.3. $k_\Lambda^{(n)}$ as defined in Eq. (D.3.54) for $n = 1, 2, 3$.

D.3.2.2 Example

Let's consider again the divergent series discussed in the example 1a,

$$s = \sum_{k=0}^{\infty} (-1)^k k!. \quad (\text{D.3.56})$$

We have seen that this series is minimally B_1 -summable and B_2^* -summable. Hence, we expect that the truncated Borel method can be used only for $n \geq 2$. To begin with, we show in Fig. D.4 the dependence on the cutoff Λ for $n = 1, 2, 3$ of

$$\int_0^\Lambda dw B_n(w) \hat{s}_n(w) \quad (\text{D.3.57})$$

in the case in which we still use the exact (non-truncated) Borel transforms Eq. (D.3.17). The faster convergence is obtained for $n = 2$, which is the minimal value for B_n^* -summability. We will consider this fact as an hint that the minimal n for which a series is B_n^* -summable is the best one for numerical applications. Nevertheless, at this level also the other values of n can be used as well. In particular, for $n = 3$, we need to go to much larger values of Λ (outside the plot range) to obtain the same accuracy as with $n = 1, 2$; this can be easily understood by looking at Fig. D.2 or Fig. D.3, where we see that the damping for $n = 3$ is much stronger and we need larger Λ to effectively include the first few terms in the sum (if the included terms are too few, the asymptotic behaviour of the coefficients is not probed and the method cannot accurately guess the correct sum).

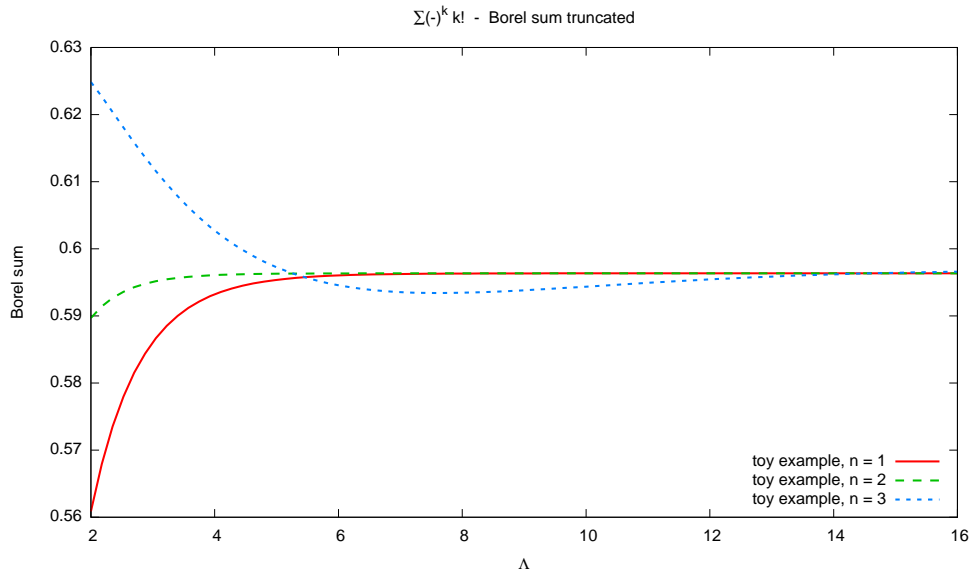


Figure D.4. Dependence of Eq. (D.3.57) on the cutoff Λ .

Now, let's fix $\Lambda = 10$, and look at the partial sums in the series obtained exchanging sum and integral in Eq. (D.3.57):

$$\sum_k^K (-1)^k k! D_k^{(n)}(\Lambda). \quad (\text{D.3.58})$$

These are shown in Fig. D.5 for $n = 1, 2, 3$. We see immediately from this plot that method $n = 1$ has no chances to work at the truncated level, as expected. The other two converge rapidly to the appropriate value given $\Lambda = 10$, which can be read out of the plot in Fig. D.4.

D.3.2.3 On the domain of analyticity

Borel summation extends the convergence radius of a power series: for divergent series (radius zero) it may find a sum for values of the variable z in some domain, but also if the series is convergent with finite radius it may extend this convergence domain.

Let's see this with an example. Consider the geometric series

$$\sum_k (-z)^k = \frac{1}{1+z}, \quad |z| < 1; \quad (\text{D.3.59})$$

the convergence radius 1 means that any truncated sum would converge to the sum if z is within the convergence circle, and would have no limit if z is outside. Of course, having an analytical result for the sum, it can be extended analytically to the whole complex plane but $z = -1$.

Using a Borel of order $n = 1$, we get

$$\sum_k (-z)^k = \int_0^\infty dw e^{-w} \sum \frac{(-zw)^k}{k!}$$

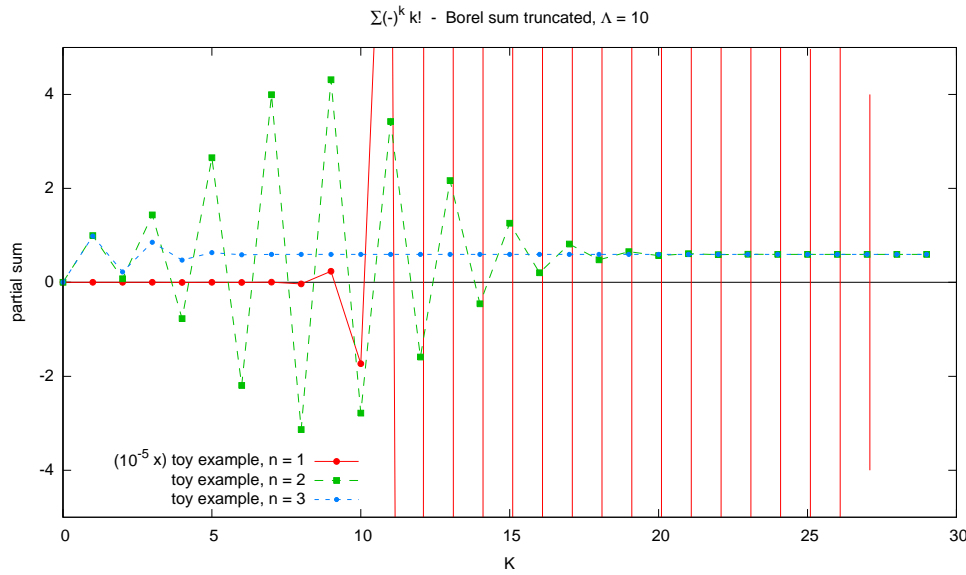


Figure D.5. Behaviour of the partial sums Eq. (D.3.58) as a function of K for $\Lambda = 10$.

$$\begin{aligned}
 &= \int_0^{\infty} dw e^{-w(1+z)} \\
 &= \frac{1}{1+z}, \quad \text{Re } z > -1, \quad (\text{D.3.60})
 \end{aligned}$$

which converges in the whole half-plane $\text{Re } z > -1$. This means that, provided $\text{Re } z > -1$, the integral can be computed numerically, or equivalently that cutoffting the integral to an upper value Λ the limit $\Lambda \rightarrow \infty$ can be safely taken only for $\text{Re } z > -1$. Also in this case, of course, being the sum the same as before, the result can be analytically extended everywhere but in $z = -1$.

We are now interested in what happens when considering a truncated Borel sum. We then consider

$$\sum_k (-z)^k \simeq \sum_k^K (-z)^k D_k^{(1)}(\Lambda); \quad (\text{D.3.61})$$

strictly speaking, this series has still convergence radius 1, as one can see immediately with the square ratio test:

$$\frac{1}{\rho} = \lim_{k \rightarrow \infty} \frac{D_{k+1}^{(1)}(\Lambda)}{D_k^{(1)}(\Lambda)} = \lim_{k \rightarrow \infty} \frac{\gamma(k+2, \Lambda)}{(k+1) \gamma(k+1, \Lambda)} = 1. \quad (\text{D.3.62})$$

This is a consequence of the fact that, after truncating the series, the integral and the sum has been exchanged back to their original position; otherwise stated, the extension in the analyticity domain in Eq. (D.3.60) is achieved thanks to the fact that the Borel transform is explicitly summed and analytically continued. However, for any given finite Λ , when $|z| > 1$ one could treat the sum as an asymptotic expansion, and find the optimal value of K which stabilizes the sum. Then, at least for Λ reasonably small, the truncated Borel sum could give an approximation of the result even outside the convergence region.

D.3.3 Padé approximants and the Borel-Padé method

A very powerful method to compute numerically the sum of a divergent series consists in mixing the use of a minimal Borel method with a Padé approximant [104].

Indeed, as discussed above, when a series is minimally B_n -summable the Borel transform has a finite radius of convergence. Hence, numerically, any truncation of the series cannot reproduce the Borel transform outside the convergence radius, while it would be required for the Borel integral. Here comes the idea to use a Padé approximant to the Borel transform.

A Padé approximant to a function $f(z)$ is a ratio of two polynomials

$$[p/m]_f(z) = \frac{a_0 + a_1z + \dots + a_pz^p}{1 + b_1z + \dots + b_mz^m} \quad (\text{D.3.63})$$

of order p and m , respectively, such that its Taylor expansion corresponds up to the $(p+m)$ -th order to that of $f(z)$:

$$[p/m]_f(z) - f(z) = \mathcal{O}(z^{p+m+1}). \quad (\text{D.3.64})$$

This equation can be easily solved multiplying $f(z)$ by the denominator

$$a_0 + a_1z + \dots + a_pz^p = (1 + b_1z + \dots + b_mz^m) f(z) + \mathcal{O}(z^{p+m+1}) \quad (\text{D.3.65})$$

and equating term by term; one gets a system of equations to express the $p+m+1$ coefficients a_k, b_k in terms of the first $p+m+1$ coefficients c_k of the Taylor expansion of $f(z)$:

$$\begin{aligned} a_0 &= c_0 \\ a_1 &= c_1 + c_0b_1 \\ a_2 &= c_2 + c_1b_1 + c_0b_2 \\ &\vdots \\ a_p &= c_p + c_{p-1}b_1 + \dots + c_0b_p \\ 0 &= c_{p+1} + c_pb_1 + \dots + c_{p-m+1}b_m \\ &\vdots \\ 0 &= c_{p+m} + c_{p+m-1}b_1 + \dots + c_pb_m \end{aligned}$$

(we intend that if the index of a coefficient is less than zero the coefficient is zero). Actually, the system splits into two pieces: the second set of equations are m equations for the m unknowns b_1, \dots, b_m , and we can solve it first. Then, with the b_k , we can compute the a_k directly using the first set of $p+1$ equations.

The Borel-Padé method can then be formulated in this way:

$$s \stackrel{B_n}{=} \int_0^\infty dw B_n(w) [p/m]_{\hat{s}_n}(w) \quad (\text{D.3.66})$$

where $[p/m]_{\hat{s}_n}(w)$ is the Padé approximant of the Borel transform $\hat{s}_n(w)$. Since the Padé approximant has a polynomial at the denominator, it will produce poles in the complex plane. It has been observed [104] that for diagonal ($p=m$) or quasi-diagonal

($p + 1 = m$) Padé's such poles reproduce quite well the poles in the Borel transform, and, if the Borel transform has a branch-cut, its Padé approximant mimics the cut with a sequence of poles along it. This would mean that, using a Padé approximant to the Borel transform, even few terms in the series (which, remember, has finite radius of convergence) can actually provide a good approximation even outside the convergence radius. Moreover, where some poles lie on the real axis, by deforming the integral path to avoid the singularities one can obtain [105] the correct (ambiguous) sum (see Example 1b of Sect. D.3.1); note that increasing the order doesn't help in this case (see the same example), meaning that this method is more powerful than the truncated method described in Sect. D.3.2.

Numerically, a very efficient and fast way for computing a diagonal or quasi-diagonal Padé approximant is the Wynn epsilon algorithm (for a review, see [103]). However, it computes the full approximant at a given z , and not the coefficients, so it is not convenient to use it here, since the result must be integrated (Borel integral). Hence, for practical purposes of computing Borel sums using few coefficients of the series, it is better to solve the system once for all in order to have all the coefficients available, and then we compute the Borel integral.

E Special functions

Contents

E.1 Euler Gamma and related functions	195
E.1.1 PolyGamma functions	197
E.1.2 Generalized Gamma functions	198
E.2 Riemann Zeta function	198
E.3 Hypergeometric and related functions	199
E.3.1 Airy functions	200
E.3.2 Bateman functions	200

In this Appendix we collect properties and relation of some special functions which appear in the text. We will mainly concentrate on those properties which are useful in the context of resummation. This Appendix is *not* intended as a complete overview on the subject.

E.1 Euler Gamma and related functions

The Euler Gamma function is defined as

$$\Gamma(z) \equiv \int_0^{\infty} dt e^{-t} t^{z-1}; \quad (\text{E.1.1})$$

the integral converges in the half-plane $\text{Re } z > 0$. The Gamma function is a real function, i.e. it satisfies

$$\Gamma(\bar{z}) = \overline{\Gamma(z)}; \quad (\text{E.1.2})$$

in particular, $\text{Im } \Gamma(x) = 0$ for $x \in \mathbb{R}$. Integrating by parts, it is easy to show that $\Gamma(z)$ satisfy the recursion relation

$$\Gamma(z+1) = z \Gamma(z). \quad (\text{E.1.3})$$

Then, because additionally $\Gamma(1) = 1$, for $z = n \in \mathbb{N}$ we have

$$\Gamma(n+1) = n! \quad (\text{E.1.4})$$

extending the factorial to complex values. Eq. (E.1.3) in reverse allows to analytically extend the Gamma function to the whole complex plane, apart from some singular

points. Indeed, the Gamma function has poles for non-positive integer values of its argument: more precisely, for $n \in \mathbb{N}$ $\Gamma(-n)$ has a simple pole with residue

$$\operatorname{Res}_{z=-n} \Gamma(z) = \frac{(-1)^n}{n!}. \quad (\text{E.1.5})$$

Around one of such poles, the Gamma function satisfies the expansion

$$\Gamma(z - n) = \frac{(-1)^n}{n!} \left[\frac{1}{z} + \psi(n + 1) + \mathcal{O}(z) \right] \quad (\text{E.1.6})$$

where ψ is the DiGamma function, defined in Eq. (E.1.15).

The Gamma function satisfies the so called *Euler reflection formula*

$$\Gamma(z) \Gamma(1 - z) = \frac{\pi}{\sin(\pi z)}, \quad (\text{E.1.7})$$

which is useful to relate the region of convergence of the integral in Eq. (E.1.1) to the other half-plane; also the pole structure is evident from such formula.

At large $|z|$, for $|\arg z| < \pi$, the Gamma function has the asymptotic expansion

$$\Gamma(z) = e^{-z} z^{z-\frac{1}{2}} \sqrt{2\pi} \left[1 + \frac{1}{12z} + \frac{1}{288z^2} + \dots \right] \quad (\text{E.1.8})$$

which reduces to the well known Stirling approximation keeping only the first term. It has to be noticed that even the Stirling approximation is very precise also for small values of z : for example, in the Stirling approximation we have

$$\Gamma(2) \simeq 0.96 \dots \quad (\text{E.1.9})$$

which is very close to the exact value $\Gamma(2) = 1$.

The inverse Gamma function

$$\Delta(z) \equiv \frac{1}{\Gamma(z)} \quad (\text{E.1.10})$$

is an entire function, which satisfies the recursion relation

$$\Delta(z) = z \Delta(z + 1). \quad (\text{E.1.11})$$

An integral representation is given by

$$\Delta(z) = \frac{1}{2\pi i} \int_{c-i\infty}^{c+i\infty} ds e^s s^{-z}. \quad (\text{E.1.12})$$

From the recursion relation we can derive a relation for its derivatives,

$$\Delta^{(k)}(z) = z \Delta^{(k)}(z + 1) + k \Delta^{(k-1)}(z + 1) \quad (\text{E.1.13})$$

from which it follows, in particular, for $z = 0$

$$\Delta^{(k)}(0) = k \Delta^{(k-1)}(1). \quad (\text{E.1.14})$$

E.1.1 PolyGamma functions

The logarithmic derivative of the Gamma function is usually called DiGamma function:

$$\psi(z) \equiv \frac{d}{dz} \log \Gamma(z). \quad (\text{E.1.15})$$

Form the recursion relation (E.1.3) it follows that

$$\psi(z+1) = \psi(z) + \frac{1}{z}; \quad (\text{E.1.16})$$

for a positive integer n , we can iterate the recursion to obtain

$$\psi(n+1) = \psi(1) + 1 + \frac{1}{2} + \frac{1}{3} + \dots + \frac{1}{n}. \quad (\text{E.1.17})$$

The value of $-\psi(1)$ is called the Euler-Mascheroni constant and is

$$\gamma_E \equiv -\psi(1) = 0.577216\dots \quad (\text{E.1.18})$$

Higher order derivatives, the PolyGamma functions, are usually indicated as

$$\psi_n(z) \equiv \psi^{(n)}(z) = \frac{d^{n+1}}{dz^{n+1}} \log \Gamma(z); \quad (\text{E.1.19})$$

with this notation, the DiGamma function is also indicated as ψ_0 . Derivating Eq. (E.1.16) we obtain the recursion relation

$$\psi_n(z+1) = \psi_n(z) + (-1)^n n! \frac{1}{z^{n+1}}. \quad (\text{E.1.20})$$

From this relation one can write a Laurent expansion of $\psi_n(z)$ around $z=0$,

$$\psi_n(z) = \frac{(-)^{n+1} n!}{z^{n+1}} + \sum_{k=0}^{\infty} \frac{\psi_{n+k}(1)}{k!} z^k, \quad \psi_k(1) = (-)^{k+1} k! \zeta(k+1) \quad (\text{E.1.21})$$

where ζ is the Riemann Zeta function defined in Sect. E.2.

An asymptotic expansion at large $|z|$, for $|\arg z| < \pi$, is given by

$$\psi(1+z) = \log z + \frac{1}{2z} + \sum_{j=1}^{\infty} \frac{\zeta(1-2j)}{z^{2j}} \quad (\text{E.1.22a})$$

$$= \log z + \frac{1}{2z} + 2 \sum_{j=1}^{\infty} \frac{(-1)^k (2k-1)! \zeta(2j)}{(2\pi z)^{2j}}, \quad (\text{E.1.22b})$$

where in the second equality we have used Eq. (E.2.4). By shifting the argument of the logarithm, we can mimic the first subleading term in the expansion, obtaining the approximation

$$\psi(1+z) = \log \left(\frac{1}{2} + z \right) + \mathcal{O} \left(\frac{1}{z^2} \right), \quad (\text{E.1.23})$$

which is surprisingly good even for small z (apart along the negative real axis, where the log has a cut and the DiGamma a sequence of poles). All the PolyGamma ψ_k with $k \geq 1$ vanish as $1/z^k$ at large $|z|$, $|\arg z| < \pi$.

E.1.2 Generalized Gamma functions

The incomplete Gamma function (or plica function) is defined as

$$\Gamma(z, a) \equiv \int_a^\infty dt e^{-t} t^{z-1}; \quad (\text{E.1.24})$$

it has a branch-cut on the negative real axis in the a complex plane. Its complement to the Gamma function is sometimes called the truncated Gamma function,

$$\gamma(z, a) \equiv \int_0^a dt e^{-t} t^{z-1}, \quad (\text{E.1.25})$$

and of course

$$\Gamma(z) = \Gamma(z, a) + \gamma(z, a). \quad (\text{E.1.26})$$

For $z = k + 1$ integer, integrating repeatedly by parts we get

$$\frac{\Gamma(k+1, a)}{\Gamma(k+1)} = e^{-a} \sum_{n=0}^k \frac{a^n}{n!}, \quad (\text{E.1.27})$$

where $\Gamma(k+1) = k!$.

Another useful function is the so called Beta function, defined by

$$B(a, b) \equiv \int_0^1 dx x^{a-1} (1-x)^{b-1}, \quad (\text{E.1.28})$$

which can be written in terms of Gamma functions as

$$B(a, b) = \frac{\Gamma(a)\Gamma(b)}{\Gamma(a+b)}. \quad (\text{E.1.29})$$

E.2 Riemann Zeta function

A commonly appearing function is the so called Riemann Zeta function, defined by the series

$$\zeta(s) = \sum_{k=1}^{\infty} k^{-s}. \quad (\text{E.2.1})$$

The series converges for $\text{Re } s > 1$, but the function can be analytically extended to the whole complex plane, apart from $s = 1$, where it reduces to the divergent harmonic series. The analytic continuation is based on the reflection formula

$$\zeta(1-s) = 2(2\pi)^{-s} \cos\left(\frac{\pi s}{2}\right) \Gamma(s)\zeta(s); \quad (\text{E.2.2})$$

in particular we can relate the Zeta function for values of its argument less than 1 to the Zeta function computed values where the series (E.2.1) converges. For positive integers $s = k > 0$, we have two cases: when $k = 2j + 1$ is odd, the cosine vanishes and we get

$$\zeta(-2j) = 0, \quad j \in \mathbb{N}, j > 0, \quad (\text{E.2.3})$$

while when $k = 2j$ is even, we have

$$\zeta(1 - 2j) = \frac{2(2j - 1)!}{(2\pi)^{2j}} \zeta(2j), \quad j \in \mathbb{N}, j > 0. \quad (\text{E.2.4})$$

An integral expression for the Zeta function valid for real $s > 1$ is

$$\zeta(s) = \frac{1}{\Gamma(s)} \int_0^\infty dt \frac{t^{s-1}}{e^t - 1}; \quad (\text{E.2.5})$$

by expanding the denominator as a geometric series and exchanging the integral and the sum we get back the series definition Eq. (E.2.1).

Special values of the Zeta function are

$$\zeta(2) = \frac{\pi^2}{6} \quad (\text{E.2.6})$$

$$\zeta(3) = 1.2020569 \dots \quad (\text{E.2.7})$$

$$\zeta(4) = \frac{\pi^4}{90}. \quad (\text{E.2.8})$$

In the text, the values of the Zeta function for integer arguments are usually indicated as

$$\zeta_k \equiv \zeta(k). \quad (\text{E.2.9})$$

E.3 Hypergeometric and related functions

The hypergeometric functions are a class of very general functions, which reduces to simpler special functions in various cases. The most general definition can be given in term of the power series

$${}_pF_q(a_1, \dots, a_p; b_1, \dots, b_q; z) = \sum_{k=0}^{\infty} \frac{(a_1)_k \cdots (a_p)_k}{(b_1)_k \cdots (b_q)_k} \frac{z^k}{k!} \quad (\text{E.3.1})$$

where $(a)_k$ is the Pochhammer symbol

$$(a)_k = \frac{\Gamma(a + k)}{\Gamma(a)} = a(a + 1) \cdots (a + k - 1). \quad (\text{E.3.2})$$

When $p > q + 1$, the series has zero radius of convergence, but with some analytical relations a meaning can be given also to these functions, and the power series serves as an asymptotic expansion.

To see some examples, the easiest case is given by $p = q = 0$, for which

$${}_0F_0(; ; z) = e^z. \quad (\text{E.3.3})$$

We discuss in the following other special cases which appear in the text.

E.3.1 Airy functions

The (regular) Airy function can be written in terms of hypergeometric functions as

$$\text{Ai}(z) = \frac{1}{3^{2/3}\Gamma(2/3)} {}_0F_1\left(\begin{matrix} \\ \frac{2}{3} \end{matrix}; \frac{1}{9}z^3\right) - \frac{z}{3^{1/3}\Gamma(1/3)} {}_0F_1\left(\begin{matrix} \\ \frac{4}{3} \end{matrix}; \frac{1}{9}z^3\right) \quad (\text{E.3.4})$$

and is one of the two linearly independent solutions of the Airy equation

$$f''(z) - zf(z) = 0. \quad (\text{E.3.5})$$

It is an entire function, with infinitely zeros on the negative real axis. The first zero (closest to the origin) is located at $z = -2.33811$.

E.3.2 Bateman functions

The Bateman function $K_\nu(z)$ is a solution of the Bateman equation

$$-K_\nu''(z) + \left(1 - \frac{\nu}{z}\right) K_\nu(z) = 0. \quad (\text{E.3.6})$$

It can be expressed in integral form and written in terms of hypergeometric functions as

$$K_\nu(z) = \frac{2}{\pi} \int_0^{\pi/2} d\theta \cos(z \tan \theta - \nu\theta) \quad (\text{E.3.7})$$

$$= \frac{e^{-z}}{\Gamma\left(1 + \frac{\nu}{2}\right)} U\left(-\frac{\nu}{2}, 0, 2z\right) \quad (\text{E.3.8})$$

where $U(a, b, z)$ is the *confluent hypergeometric function of the second kind*

$$U(a, b, z) = z^{-a} {}_2F_0(a, 1 + a - b; ; -z^{-1}) \quad (\text{E.3.9})$$

$$= \frac{\pi}{\sin(\pi b)} \left[\frac{{}_1F_1(a; b; z)}{\Gamma(a - b + 1)\Gamma(b)} - \frac{z^{1-b} {}_1F_1(a - b + 1; 2 - b; z)}{\Gamma(a)\Gamma(2 - b)} \right] \quad (\text{E.3.10})$$

and satisfies

$$U(a, b, z) = z^{1-b} U(a + 1 - b, 2 - b, z). \quad (\text{E.3.11})$$

The first form for exists only as a formal power series, but can be used as an asymptotic expansion.

The z -derivative is related to the function itself:

$$\frac{d}{dz} U(a, b, z) = -a U(a + 1, b + 1, z). \quad (\text{E.3.12})$$

From this, the logarithmic derivative of the Bateman function can be written as

$$\frac{d}{dz} \log K_\nu(z) = -1 + \nu \frac{U\left(1 - \frac{\nu}{2}, 1, 2z\right)}{U\left(-\frac{\nu}{2}, 0, 2z\right)}. \quad (\text{E.3.13})$$

F Numerical methods

Contents

F.1 Numerical derivatives.	201
F.2 Root finding	202
F.3 Chebyshev polynomials.	202
F.3.1 Minimal Prescription	203
F.3.2 Borel Prescription	204

In this Appendix we collect some numerical method used in developing the codes used in the text.

F.1 Numerical derivatives

Numerical derivatives are usually approximated to the finite differences

$$f'(x) \sim \frac{f(x+h) - f(x-h)}{2h} \quad (\text{F.1.1})$$

$$f''(x) \sim \frac{f(x+h) + f(x-h) - 2f(x)}{h^2} \quad (\text{F.1.2})$$

where h is a “small” parameter: the smaller h is, the better should be the approximation. However, if h is too small, a roundoff error probably takes place. Then, a better way to compute the derivative is to compute the finite differences for different values of h not too small, and then use a polynomial interpolation to $h = 0$. Using 3 values of h we can use a quadratic interpolation, and get as a best estimate

$$f'(x) \sim \frac{1}{h_2 - h_1} \left[h_2 \frac{h_1 y_0 - h_0 y_1}{h_1 - h_0} - h_1 \frac{h_2 y_0 - h_0 y_2}{h_2 - h_0} \right] \quad (\text{F.1.3})$$

where

$$y_i = \frac{f(x+h_i) - f(x-h_i)}{2h_i}, \quad i = 0, 1, 2. \quad (\text{F.1.4})$$

If h_i are chosen as

$$h_i = \frac{h_0}{2^i} \quad (\text{F.1.5})$$

we get the easier expression

$$f'(x) \sim \frac{y_0 - 6y_1 + 8y_2}{3}. \quad (\text{F.1.6})$$

The same technique also applies for the second derivative.

F.2 Root finding

For the computation of the inverse function which defines χ_s , Eq. (3.3.14), and for putting on-shell the off-shell kernels, we use a root finding algorithm.

If we know the analytic derivative, the Newton algorithm is quite good (even if not so fast), and moreover it is applicable also in the complex plane.

However, typically the analytic derivative is not known (or hard to work out) and we use the secant method, which uses finite differences instead of the actual derivative. The secant method is also valid in the complex plane, but it is not much robust, and quite accurate initial guesses are needed in order for the algorithm not to fail.

In the (rare) cases in which we just need to find a root in the real axis the falsi regula method works pretty well, since it is fast and robust. However, the two initial guesses must surround the root, and this may be not simple to realize.

We do not discuss these algorithms here, since the Reader can find very accurate description of them throughout the web.

F.3 Chebyshev polynomials

In this Appendix we recall the definition and the main properties of Chebyshev polynomials. The Chebyshev polynomials

$$T_i(z) = \sum_{k=0}^i T_{ik} z^k, \quad (\text{F.3.1})$$

are defined in the range $z \in [-1, 1]$ recursively by

$$T_0(z) = 1 \quad (\text{F.3.2a})$$

$$T_1(z) = z \quad (\text{F.3.2b})$$

$$T_2(z) = 2z^2 - 1 \quad (\text{F.3.2c})$$

$$T_i(z) = 2z T_{i-1}(z) - T_{i-2}. \quad (\text{F.3.2d})$$

A generic function $G(u)$ can be approximated in the range $u \in [u_{\min}, u_{\max}]$ by its expansion on the basis of Chebyshev polynomials (F.3.2), truncated at some order n :

$$G(u) \simeq -\frac{c_0}{2} + \sum_{i=0}^n c_i T_i(Au + B), \quad (\text{F.3.3})$$

where

$$A = \frac{2}{u_{\max} - u_{\min}}, \quad B = -\frac{u_{\max} + u_{\min}}{u_{\max} - u_{\min}}. \quad (\text{F.3.4})$$

Simple numerical algorithms for the calculation of the coefficients c_i are available (we have used the routines of the `gs1`).

Simple algebra leads to

$$G(u) \simeq \sum_{k=0}^n \tilde{c}_k (Au + B)^k \quad (\text{F.3.5})$$

where

$$\tilde{c}_k = -\frac{c_0}{2} \delta_{k0} + \sum_{i=k}^n c_i T_{ik}. \quad (\text{F.3.6})$$

F.3.1 Minimal Prescription

We have shown in Sect. 2.3 that the minimal prescription can be conveniently implemented by means of an analytic expression for the Mellin transform of the luminosity $\mathcal{L}(z)$ (which can be either $\mathcal{L}_{q\bar{q}}(z)$ in the case of invariant mass distributions or $\mathcal{L}^{\text{rap}}(z, 1/2)$ in the case of rapidity distributions). This can be obtained by expanding $\mathcal{L}(z)$ on the basis of Chebyshev polynomials, truncated at some finite order n , and then taking its analytical Mellin transform. The luminosity itself, however, is very badly behaved in the range $(0, 1)$: it is singular at $z = 0$, and varies by orders of magnitude in the range

$$0 \leq z \leq z_{\text{max}}; \quad z_{\text{max}} = \begin{cases} 1 & \text{for the rapidity-integrated cross-section} \\ e^{-2|Y|} & \text{for the rapidity distribution} \end{cases} \quad (\text{F.3.7})$$

It is therefore convenient to expand a regularized function

$$F(z) = \frac{z^\beta}{(z_{\text{max}} - z)^\delta} \mathcal{L}(z). \quad (\text{F.3.8})$$

Values of β and δ in the range $3 \div 7$ are normally suited to make $F(z)$ smooth enough to be approximated by a reasonably small number of Chebyshev polynomials. Equation (F.3.4) gives

$$A = \frac{2}{z_{\text{max}}}, \quad B = -1. \quad (\text{F.3.9})$$

and the approximation is

$$F(z) = \sum_{k=0}^n \tilde{c}_k \left(2 \frac{z}{z_{\text{max}}} - 1\right)^k = \sum_{p=0}^n \hat{c}_p z^p, \quad (\text{F.3.10})$$

where

$$\hat{c}_p = \left(\frac{2}{z_{\text{max}}}\right)^p \sum_{k=p}^n \binom{k}{p} (-1)^{k-p} \tilde{c}_k. \quad (\text{F.3.11})$$

The luminosity is easily recovered:

$$\mathcal{L}(z) = (z_{\text{max}} - z)^\delta \sum_{p=0}^n \hat{c}_p z^{p-\beta} = \sum_{j=0}^{\delta} \binom{\delta}{j} z_{\text{max}}^{\delta-j} (-1)^j \sum_{p=0}^n \hat{c}_p z^{p+j-\beta}, \quad (\text{F.3.12})$$

where the last equality holds for δ integer. It is now immediate to obtain the Mellin transform:

$$\mathcal{L}(N) = \int_0^{z_{\max}} dz z^{N-1} \mathcal{L}(z) = \sum_{p=0}^n \sum_{j=0}^{\delta} \hat{c}_p \binom{\delta}{j} (-1)^j \frac{z_{\max}^{N+p+\delta-\beta}}{N+p+j-\beta}. \quad (\text{F.3.13})$$

Alternatively, one may introduce the variable u

$$z = z_{\max} e^u \quad (\text{F.3.14})$$

and approximate the function

$$F(u) = z \mathcal{L}(z) = z_{\max} e^u \mathcal{L}(z_{\max} e^u) \quad (\text{F.3.15})$$

by an expansion on the basis of Chebyshev polynomials. The variable u ranges from $-\infty$ to 0 when $0 \leq z \leq z_{\max}$; however, for practical purposes one only needs the luminosity for $z \geq z_{\min} = z_{\max} e^{u_{\min}}$. We have therefore

$$A = -\frac{2}{u_{\min}}, \quad B = 1, \quad (\text{F.3.16})$$

and

$$F(u) = \sum_{k=0}^n \tilde{c}_k \left(1 - 2 \frac{u}{u_{\min}}\right)^k. \quad (\text{F.3.17})$$

We can now reconstruct $\mathcal{L}(z)$ through the replacement $u = \log \frac{z}{z_{\max}}$. We get

$$\mathcal{L}(z) = \frac{1}{z} \sum_{p=0}^n (-2)^p u_{\min}^{-p} \log^p \frac{z}{z_{\max}} \sum_{k=p}^n \binom{k}{p} \tilde{c}_k. \quad (\text{F.3.18})$$

The Mellin transform is computed using the result

$$\int_0^{z_{\max}} dz z^{N-2} \log^p \frac{z}{z_{\max}} = z_{\max}^{N-1} \frac{(-1)^p p!}{(N-1)^{p+1}}. \quad (\text{F.3.19})$$

We obtain

$$\mathcal{L}(N) = \int_0^{z_{\max}} dz z^{N-1} \mathcal{L}(z) = z_{\max}^{N-1} \sum_{p=0}^n \frac{\bar{c}_p}{(N-1)^{p+1}}, \quad (\text{F.3.20})$$

where

$$\bar{c}_p = \frac{2^p}{u_{\min}^p} \sum_{k=p}^n \frac{k!}{(k-p)!} \tilde{c}_k. \quad (\text{F.3.21})$$

In practice, we have found that the second method is to be preferred for small values of τ , $\tau \lesssim 0.1$, while the previous one works better for $\tau \gtrsim 0.1$.

F.3.2 Borel Prescription

In this case, we look for an approximation of the function $g(z, \tau)$, Eq. (2.3.5), as a function of $z \in [\tau, 1]$. We have

$$g(z, \tau) = \sum_{k=0}^n \tilde{c}_k (Az + B)^k = \sum_{p=0}^n b_p (1-z)^p \quad (\text{F.3.22})$$

where

$$b_p = (-A)^p \sum_{k=p}^n \binom{k}{p} (A+B)^{k-p} \tilde{c}_k \quad (\text{F.3.23})$$

and

$$A = \frac{2}{1-\tau}, \quad B = -\frac{1+\tau}{1-\tau}. \quad (\text{F.3.24})$$

Note that $A+B=1$ in this case. Therefore

$$b_p = \left(\frac{-2}{1-\tau}\right)^p \sum_{k=p}^n \binom{k}{p} \tilde{c}_k. \quad (\text{F.3.25})$$

In the case of the rapidity distributions, the variable z is in the range $z \in [\tau e^{2|Y|}, 1]$; therefore

$$b_p = \left(\frac{-2}{1-\tau e^{2|Y|}}\right)^p \sum_{k=p}^n \binom{k}{p} \tilde{c}_k. \quad (\text{F.3.26})$$

For the original Borel prescription, Eq. (2.1.46), it proves useful to approximate the function $\tilde{g}(z, \tau)$, Eq. (2.3.14), in powers of $\log \frac{1}{z}$. Defining

$$t = \log \frac{1}{z} \quad (\text{F.3.27})$$

we get

$$\tilde{g}(z, \tau) = \sum_{k=0}^n \tilde{c}_k (At+B)^k = \sum_{p=0}^n \tilde{b}_p t^p \quad (\text{F.3.28})$$

where

$$\tilde{b}_p = \sum_{k=p}^n \binom{k}{p} \tilde{c}_k A^p B^{k-p}. \quad (\text{F.3.29})$$

Approximating the function in the range $0 < t < t_{\max}$, corresponding to $z_{\min} < z < 1$, with $z_{\min} = e^{-t_{\max}}$, we have

$$A = \frac{2}{t_{\max}}, \quad B = -1, \quad (\text{F.3.30})$$

and hence

$$\tilde{b}_p = \left(-\frac{2}{t_{\max}}\right)^p \sum_{k=p}^n \binom{k}{p} (-)^k \tilde{c}_k. \quad (\text{F.3.31})$$

Acknowledgments

Here I am, at the end of my Ph.D. thesis, my last opportunity to informally thank on a formal document all the people around me, who helped me somehow in preparing this work. I will try to do all my best to use this opportunity properly.

First, as usual, I would like to thank my supervisors: of course, without them this thesis would not exist at all. In particular, I am really grateful to Giovanni, who I worked with for four years, and who has been a great teacher and a friend: most things I know on the subject of this thesis I have learnt from him, but most importantly he introduced me to the research world. I also want to thank Stefano a lot: unfortunately we didn't spend so much time working together face-to-face, but I'm always surprised by the amount of things I can learn from almost every e-mail he sends me (even if often I need some time to decrypt them...).

Then, I move to the other collaborators, or simply people who I interacted with for the preparation of this thesis. A first special thank goes to Tiziano Peraro, who wrote a small- x code complementary to mine, which made possible several checks and allowed us to optimize the codes as much as possible; moreover, I'm grateful to him 'cause I felt (and still, I feel) free to complain with him whenever something is puzzling me. The second thank is definitely for Richard Ball, who gave us his first version of a small- x code, and who helped me in understanding how he practically realized several of the dark steps of small- x resummation. Then, I want to thank Guido Altarelli, who underlined me the relevance of high-energy resummation and the importance of completing the resummation task. A thank goes to Alessandro Vicini, who gave me his code on Higgs at NLO with full m_t dependence, explaining it to me in detail. Several thanks are for Juan Rojo, who I discussed with several times and who is always interested in my codes, for Maria Ubiali for useful discussions on the Talbot algorithm, and for Fabrizio Caola, who discussed with me small- x resummation at the beginning. I thank Robert Harlander for giving me a piece of his code on Higgs at NNLO with full m_t dependence.

Finally, I have some formal thanks: to the GGI, where I spent almost two months learning many stringy stuff and having much fun; to the CERN Theory division, where I spent nine months last year, having the opportunity to meet people, to participate to seminars and conferences, and to enjoy staying in a very friendly and pleasing place; and to DESY, where I'm going to stay a couple of years, which is giving me the opportunity to complete my thesis.

Now I move to friends. I don't exactly know where to start from, then I will choose the easiest way. So, the first thank is for Ludovica Aperio Bella and Davide Caffari, aka *the Conquis*: I don't have to specify anything more, they were my family, and it was

really funny. Then, of course, I have to thank my band, *the Suspenders*, i.e. Alexandros, Matias, Samir, Valerio, Lillian and Georgios: I really miss them all, Friday's practices were the best moment of the week. Maybe I should also thank the CERN Musicclub, which made all this possible. Staying at CERN, I have many many other people to thank as well. Riccardo Torre, for many things, often not related to physics (he knows what I mean); Ennio Salvioni, even if he uses Windows sometimes; Andrea Coccaro, because he always laughs; Roberto Di Nardo, because he did it; Manuela Venturi, for the jingle; all the others...

Moving to the University, I have several persons to thank. A special thank goes to Guido Fernandes, who is really a good friend, and who knows everything about almost everything, including product codes, and can always help me because he already had that problem, or he possesses that tool. I want to thank Francesco Sanfilippo for his infinite knowledge on C++ and BASH tricks, and for having studied QFT with me. A thank goes to Stefano Davini, for many useful discussions about elegant coding, and for having shared with me the teaching experience. I thank Daniele Musso, mainly for *Blues in D-branes*, but also because he made my exam on instantons much more interesting with his questions. I'm also grateful to Giulia Piovano, who'll do all the Ph.D. exam paperwork for me. Of course I want to thank also my lunch friends, my office mates, and all the people with which I shared these years.

I don't have time to thank all my local friends from Sant'Olcese, and more widely from Genova. I'm actually really sorry that in the last years we didn't have many opportunities to meet, because it was really nice when we were young and we went out until the wee hours of the morning.

I don't know exactly which category he should belong to, so I thank Matteo Casu in a separate paragraph: for the endless conversations, and because we always end up with very nerdy strange ideas.

Of course, a great thank goes to my parents and my relatives: even if they stopped understanding what I'm doing long ago, they have always supported me, and I'm pretty sure they are proud of me.

Last, but definitely not least, comes Sara. To thank her is not enough, since what she gave and she's giving me is priceless. I could spend an undefined amount of words to describe why she occupies a special place in this page, but I don't want to be rhetorical. She perfectly knows why, and not only her, and that's fine. But just to satisfy her, let me just thank her for a specific topic. Then, I want to thank Sara because she allowed me to cut and paste from her thesis the description of the Drell-Yan process that *I wrote* for her.

Marco Bonvini

Bibliography

- [1] CDF Collaboration, F. Abe et al., *Observation of top quark production in $\bar{p}p$ collisions*, *Phys.Rev.Lett.* **74** (1995) 2626–2631, [arXiv:hep-ex/9503002 \[hep-ex\]](#).
- [2] D0 Collaboration, S. Abachi et al., *Search for high mass top quark production in $p\bar{p}$ collisions at $\sqrt{s} = 1.8$ TeV*, *Phys.Rev.Lett.* **74** (1995) 2422–2426, [arXiv:hep-ex/9411001 \[hep-ex\]](#).
- [3] R. Peccei and H. R. Quinn, *CP Conservation in the Presence of Instantons*, *Phys.Rev.Lett.* **38** (1977) 1440–1443.
- [4] R. Ellis, W. Stirling, and B. Webber, *QCD and collider physics*, vol. 8. Camb.Monogr.Part.Phys.Nucl.Phys.Cosmol., 1996.
- [5] T. Kinoshita, *Mass singularities of Feynman amplitudes*, *J.Math.Phys.* **3** (1962) 650–677.
- [6] T. Lee and M. Nauenberg, *Degenerate Systems and Mass Singularities*, *Phys.Rev.* **133** (1964) B1549–B1562.
- [7] S. Moch, J. Vermaseren, and A. Vogt, *The Three loop splitting functions in QCD: The Nonsinglet case*, *Nucl.Phys.* **B688** (2004) 101–134, [arXiv:hep-ph/0403192 \[hep-ph\]](#).
- [8] A. Vogt, S. Moch, and J. Vermaseren, *The Three-loop splitting functions in QCD: The Singlet case*, *Nucl.Phys.* **B691** (2004) 129–181, [arXiv:hep-ph/0404111 \[hep-ph\]](#).
- [9] G. Altarelli, R. D. Ball, and S. Forte, *Small x resummation and HERA structure function data*, *Nucl.Phys.* **B599** (2001) 383–423, [arXiv:hep-ph/0011270 \[hep-ph\]](#).
- [10] G. Altarelli, R. D. Ball, and S. Forte, *Small x Resummation with Quarks: Deep-Inelastic Scattering*, *Nucl.Phys.* **B799** (2008) 199–240, [arXiv:0802.0032 \[hep-ph\]](#).
- [11] G. Korchemsky, *Asymptotics of the Altarelli-Parisi-Lipatov Evolution Kernels of Parton Distributions*, *Mod.Phys.Lett.* **A4** (1989) 1257–1276.
- [12] NNPDF Collaboration, R. D. Ball et al., *A Determination of parton distributions with faithful uncertainty estimation*, *Nucl.Phys.* **B809** (2009) 1–63, [arXiv:0808.1231 \[hep-ph\]](#).

- [13] Y. Dokshitzer, D. D'yakonov, and S. Troyan, *On the transverse momentum distribution of massive lepton pairs*, *Physics Letters B* **79** (1978) no. 3, 269 – 272.
- [14] G. Parisi and R. Petronzio, *Small Transverse Momentum Distributions in Hard Processes*, *Nucl.Phys.* **B154** (1979) 427.
- [15] G. Curci, M. Greco, and Y. Srivastava, *COHERENT QUARK - GLUON JETS*, *Phys.Rev.Lett.* **43** (1979) 834–837.
- [16] J. C. Collins, D. E. Soper, and G. F. Sterman, *Transverse Momentum Distribution in Drell-Yan Pair and W and Z Boson Production*, *Nucl.Phys.* **B250** (1985) 199.
- [17] M. Bonvini, S. Forte, and G. Ridolfi, *Borel resummation of transverse momentum distributions*, *Nucl.Phys.* **B808** (2009) 347–363, [arXiv:0807.3830 \[hep-ph\]](#).
- [18] G. F. Sterman, *Summation of Large Corrections to Short Distance Hadronic Cross-Sections*, *Nucl.Phys.* **B281** (1987) 310.
- [19] S. Catani and L. Trentadue, *Resummation of the QCD Perturbative Series for Hard Processes*, *Nucl.Phys.* **B327** (1989) 323.
- [20] S. Forte and G. Ridolfi, *Renormalization group approach to soft gluon resummation*, *Nucl.Phys.* **B650** (2003) 229–270, [arXiv:hep-ph/0209154 \[hep-ph\]](#).
- [21] S. Catani, *Higher order QCD corrections in hadron collisions: Soft gluon resummation and exponentiation*, *Nucl.Phys.Proc.Suppl.* **54A** (1997) 107–113, [arXiv:hep-ph/9610413 \[hep-ph\]](#).
- [22] S. Weinberg, *The Quantum theory of fields. Vol. 1: Foundations*, .
- [23] V. Sudakov, *Vertex parts at very high-energies in quantum electrodynamics*, *Sov.Phys.JETP* **3** (1956) 65–71.
- [24] H. Contopanagos, E. Laenen, and G. F. Sterman, *Sudakov factorization and resummation*, *Nucl.Phys.* **B484** (1997) 303–330, [arXiv:hep-ph/9604313 \[hep-ph\]](#).
- [25] M. Bonvini, S. Forte, and G. Ridolfi, *Soft gluon resummation of Drell-Yan rapidity distributions: Theory and phenomenology*, *Nucl.Phys.* **B847** (2011) 93–159, [arXiv:1009.5691 \[hep-ph\]](#).
- [26] A. V. Manohar, *Deep inelastic scattering as $x \rightarrow 1$ using soft collinear effective theory*, *Phys.Rev.* **D68** (2003) 114019, [arXiv:hep-ph/0309176 \[hep-ph\]](#).
- [27] T. Becher and M. Neubert, *Threshold resummation in momentum space from effective field theory*, *Phys.Rev.Lett.* **97** (2006) 082001, [arXiv:hep-ph/0605050 \[hep-ph\]](#).
- [28] T. Becher, M. Neubert, and G. Xu, *Dynamical Threshold Enhancement and Resummation in Drell-Yan Production*, *JHEP* **0807** (2008) 030, [arXiv:0710.0680 \[hep-ph\]](#).

- [29] M. Bonvini, S. Forte, M. Ghezzi, and G. Ridolfi, *Threshold resummation in SCET vs. perturbative QCD: an analytic comparison*, [arXiv:1201.6364](#) [[hep-ph](#)].
- [30] S. Forte, G. Ridolfi, J. Rojo, and M. Ubiali, *Borel resummation of soft gluon radiation and higher twists*, *Phys.Lett.* **B635** (2006) 313–319, [arXiv:hep-ph/0601048](#) [[hep-ph](#)].
- [31] S. Catani, M. L. Mangano, P. Nason, and L. Trentadue, *The Resummation of soft gluons in hadronic collisions*, *Nucl.Phys.* **B478** (1996) 273–310, [arXiv:hep-ph/9604351](#) [[hep-ph](#)].
- [32] R. Abbate, S. Forte, and G. Ridolfi, *A New prescription for soft gluon resummation*, *Phys.Lett.* **B657** (2007) 55–63, [arXiv:0707.2452](#) [[hep-ph](#)].
- [33] R. Bonciani, S. Catani, M. L. Mangano, and P. Nason, *NLL resummation of the heavy quark hadroproduction cross-section*, *Nucl.Phys.* **B529** (1998) 424–450, [arXiv:hep-ph/9801375](#) [[hep-ph](#)].
- [34] A. Mukherjee and W. Vogelsang, *Threshold resummation for W-boson production at RHIC*, *Phys.Rev.* **D73** (2006) 074005, [arXiv:hep-ph/0601162](#) [[hep-ph](#)].
- [35] P. Bolzoni, *Threshold resummation of Drell-Yan rapidity distributions*, *Phys.Lett.* **B643** (2006) 325–330, [arXiv:hep-ph/0609073](#) [[hep-ph](#)].
- [36] E. Laenen and G. F. Sterman, *Resummation for Drell-Yan differential distributions*, .
- [37] D. Bourilkov, R. C. Group, and M. R. Whalley, *LHAPDF: PDF use from the Tevatron to the LHC*, [arXiv:hep-ph/0605240](#) [[hep-ph](#)].
- [38] W. Furmanski and R. Petronzio, *A METHOD OF ANALYZING THE SCALING VIOLATION OF INCLUSIVE SPECTRA IN HARD PROCESSES*, *Nucl.Phys.* **B195** (1982) 237.
- [39] R. Ellis, H. Georgi, M. Machacek, H. Politzer, and G. G. Ross, *Factorization and the Parton Model in QCD*, *Phys.Lett.* **B78** (1978) 281.
- [40] R. Ellis, H. Georgi, M. Machacek, H. Politzer, and G. G. Ross, *Perturbation Theory and the Parton Model in QCD*, *Nucl.Phys.* **B152** (1979) 285.
- [41] S. Catani, M. Ciafaloni, and F. Hautmann, *Gluon contributions to small x heavy flavor production*, *Phys.Lett.* **B242** (1990) 97.
- [42] S. Catani, M. Ciafaloni, and F. Hautmann, *High-energy factorization and small x heavy flavor production*, *Nucl.Phys.* **B366** (1991) 135–188.
- [43] S. Catani, M. Ciafaloni, and F. Hautmann, *High-energy factorization in QCD and minimal subtraction scheme*, *Phys.Lett.* **B307** (1993) 147–153.
- [44] S. Catani and F. Hautmann, *Quark anomalous dimensions at small x*, *Phys.Lett.* **B315** (1993) 157–163.

- [45] S. Catani and F. Hautmann, *High-energy factorization and small x deep inelastic scattering beyond leading order*, *Nucl.Phys.* **B427** (1994) 475–524, [arXiv:hep-ph/9405388](#) [[hep-ph](#)].
- [46] D. Colferai, *Small x processes in perturbative quantum chromodynamics*, [arXiv:hep-ph/0008309](#) [[hep-ph](#)]. Ph.D thesis (Advisor: M. Ciafaloni).
- [47] R. D. Ball and S. Forte, *Asymptotically free partons at high-energy*, *Phys.Lett.* **B405** (1997) 317–326, [arXiv:hep-ph/9703417](#) [[hep-ph](#)].
- [48] L. Lipatov, *Reggeization of the Vector Meson and the Vacuum Singularity in Nonabelian Gauge Theories*, *Sov.J.Nucl.Phys.* **23** (1976) 338–345.
- [49] E. Kuraev, L. Lipatov, and V. S. Fadin, *Multi - Reggeon Processes in the Yang-Mills Theory*, *Sov.Phys.JETP* **44** (1976) 443–450.
- [50] E. Kuraev, L. Lipatov, and V. S. Fadin, *The Pomeron Singularity in Nonabelian Gauge Theories*, *Sov.Phys.JETP* **45** (1977) 199–204.
- [51] I. Balitsky and L. Lipatov, *The Pomeron Singularity in Quantum Chromodynamics*, *Sov.J.Nucl.Phys.* **28** (1978) 822–829.
- [52] V. S. Fadin and L. Lipatov, *BFKL pomeron in the next-to-leading approximation*, *Phys.Lett.* **B429** (1998) 127–134, [arXiv:hep-ph/9802290](#) [[hep-ph](#)].
- [53] G. Altarelli, R. D. Ball, and S. Forte, *Resummation of singlet parton evolution at small x* , *Nucl.Phys.* **B575** (2000) 313–329, [arXiv:hep-ph/9911273](#) [[hep-ph](#)].
- [54] G. Altarelli, R. D. Ball, and S. Forte, *Perturbatively stable resummed small x evolution kernels*, *Nucl.Phys.* **B742** (2006) 1–40, [arXiv:hep-ph/0512237](#) [[hep-ph](#)].
- [55] G. Salam, *A Resummation of large subleading corrections at small x* , *JHEP* **9807** (1998) 019, [arXiv:hep-ph/9806482](#) [[hep-ph](#)].
- [56] G. Altarelli, R. D. Ball, and S. Forte, *Factorization and resummation of small x scaling violations with running coupling*, *Nucl.Phys.* **B621** (2002) 359–387, [arXiv:hep-ph/0109178](#) [[hep-ph](#)].
- [57] G. Camici and M. Ciafaloni, *k factorization and small x anomalous dimensions*, *Nucl.Phys.* **B496** (1997) 305–336, [arXiv:hep-ph/9701303](#) [[hep-ph](#)].
- [58] L. Lipatov, *The Bare Pomeron in Quantum Chromodynamics*, *Sov.Phys.JETP* **63** (1986) 904–912.
- [59] R. D. Ball and S. Forte, *All order running coupling BFKL evolution from GLAP (and vice-versa)*, *Nucl.Phys.* **B742** (2006) 158–175, [arXiv:hep-ph/0601049](#) [[hep-ph](#)].
- [60] M. Ciafaloni, *$k(T)$ factorization versus renormalization group: A Small x consistency argument*, *Phys.Lett.* **B356** (1995) 74–78, [arXiv:hep-ph/9507307](#) [[hep-ph](#)].

- [61] M. Ciafaloni and D. Colferai, *Dimensional regularisation and factorisation schemes in the BFKL equation at subleading level*, *JHEP* **0509** (2005) 069, [arXiv:hep-ph/0507106](#) [hep-ph].
- [62] R. D. Ball and S. Forte, *Momentum conservation at small x* , *Phys.Lett.* **B359** (1995) 362–368, [arXiv:hep-ph/9507321](#) [hep-ph].
- [63] D. Appell, G. F. Sterman, and P. B. Mackenzie, *SOFT GLUONS AND THE NORMALIZATION OF THE DRELL-YAN CROSS-SECTION*, *Nucl.Phys.* **B309** (1988) 259.
- [64] R. D. Ball, L. Del Debbio, S. Forte, A. Guffanti, J. I. Latorre, et al., *A first unbiased global NLO determination of parton distributions and their uncertainties*, *Nucl.Phys.* **B838** (2010) 136–206, [arXiv:1002.4407](#) [hep-ph].
- [65] M. Grazzini, *QCD Effects in Higgs Boson Production at Hadron Colliders*, *PoS RADCOR2009* (2010) 047, [arXiv:1001.3766](#) [hep-ph].
- [66] C. W. Bauer, N. D. Dunn, and A. Hornig, *On the effectiveness of threshold resummation away from hadronic endpoint*, [arXiv:1010.0243](#) [hep-ph].
- [67] P. Collins, *An Introduction to Regge Theory and High-Energy Physics*, .
- [68] H. Abarbanel, M. Goldberger, and S. Treiman, *Asymptotic properties of electroproduction structure functions*, *Phys.Rev.Lett.* **22** (1969) 500–502.
- [69] R. Bonciani, G. Degrossi, and A. Vicini, *Scalar particle contribution to Higgs production via gluon fusion at NLO*, *JHEP* **0711** (2007) 095, [arXiv:0709.4227](#) [hep-ph].
- [70] S. Marzani, R. D. Ball, V. Del Duca, S. Forte, and A. Vicini, *Higgs production via gluon-gluon fusion with finite top mass beyond next-to-leading order*, *Nucl.Phys.* **B800** (2008) 127–145, [arXiv:0801.2544](#) [hep-ph].
- [71] W. van Neerven and E. Zijlstra, *The $O(\alpha_s^2)$ corrected Drell-Yan K factor in the DIS and MS scheme*, *Nucl.Phys.* **B382** (1992) 11–62.
- [72] C. Anastasiou, L. J. Dixon, K. Melnikov, and F. Petriello, *High precision QCD at hadron colliders: Electroweak gauge boson rapidity distributions at NNLO*, *Phys.Rev.* **D69** (2004) 094008, [arXiv:hep-ph/0312266](#) [hep-ph].
- [73] S. Catani, G. Ferrera, and M. Grazzini, *W boson production at hadron colliders: the lepton charge asymmetry in NNLO QCD*, *JHEP* **1005** (2010) 006, [arXiv:1002.3115](#) [hep-ph]. * Temporary entry *.
- [74] M. Grazzini, *Transverse-momentum resummation at hadron colliders*, [arXiv:0908.1338](#) [hep-ph].
- [75] FNAL E866/NuSea Collaboration, R. Towell et al., *Improved measurement of the anti-d / anti-u asymmetry in the nucleon sea*, *Phys.Rev.* **D64** (2001) 052002, [arXiv:hep-ex/0103030](#) [hep-ex].
- [76] J. C. Webb, *Measurement of continuum dimuon production in 800-GeV/C proton nucleon collisions*, [arXiv:hep-ex/0301031](#) [hep-ex]. Ph.D. Thesis (Advisor: Vassili Papavassiliou).

- [77] NuSea Collaboration, J. Webb et al., *Absolute Drell-Yan dimuon cross-sections in 800 GeV / c pp and pd collisions*, Phys.Rev.Lett. (2003) , [arXiv:hep-ex/0302019 \[hep-ex\]](#).
- [78] A. Martin, W. Stirling, R. Thorne, and G. Watt, *Parton distributions for the LHC*, Eur.Phys.J. **C63** (2009) 189–285, [arXiv:0901.0002 \[hep-ph\]](#).
- [79] H.-L. Lai, M. Guzzi, J. Huston, Z. Li, P. M. Nadolsky, et al., *New parton distributions for collider physics*, Phys.Rev. **D82** (2010) 074024, [arXiv:1007.2241 \[hep-ph\]](#).
- [80] G. Balossini, G. Montagna, C. M. Carloni Calame, M. Moretti, O. Nicrosini, et al., *Combination of electroweak and QCD corrections to single W production at the Fermilab Tevatron and the CERN LHC*, JHEP **1001** (2010) 013, [arXiv:0907.0276 \[hep-ph\]](#).
- [81] S. Catani, L. Cieri, G. Ferrera, D. de Florian, and M. Grazzini, *Vector boson production at hadron colliders: A Fully exclusive QCD calculation at NNLO*, Phys.Rev.Lett. **103** (2009) 082001, [arXiv:0903.2120 \[hep-ph\]](#).
- [82] PDF4LHC working group.
https://wiki.terascale.de/index.php?title=PDF4LHC_WIKI.
- [83] Particle Data Group, K. Nakamura et al., *Review of particle physics*, J.Phys.G **G37** (2010) 075021.
- [84] S. Bethke, *The 2009 World Average of alpha(s)*, Eur.Phys.J. **C64** (2009) 689–703, [arXiv:0908.1135 \[hep-ph\]](#).
- [85] H.-L. Lai, J. Huston, Z. Li, P. Nadolsky, J. Pumplin, et al., *Uncertainty induced by QCD coupling in the CTEQ global analysis of parton distributions*, Phys.Rev. **D82** (2010) 054021, [arXiv:1004.4624 \[hep-ph\]](#).
- [86] CDF Collaboration, T. A. Aaltonen et al., *Measurement of $d\sigma/dy$ of Drell-Yan e^+e^- pairs in the Z Mass Region from $p\bar{p}$ Collisions at $\sqrt{s} = 1.96$ TeV*, Phys.Lett. **B692** (2010) 232–239, [arXiv:0908.3914 \[hep-ex\]](#).
- [87] CDF Collaboration, T. Aaltonen et al., *Direct Measurement of the W Production Charge Asymmetry in $p\bar{p}$ Collisions at $\sqrt{s} = 1.96$ TeV*, Phys.Rev.Lett. **102** (2009) 181801, [arXiv:0901.2169 \[hep-ex\]](#).
- [88] T. van Ritbergen, J. Vermaseren, and S. Larin, *The Four loop beta function in quantum chromodynamics*, Phys.Lett. **B400** (1997) 379–384, [arXiv:hep-ph/9701390 \[hep-ph\]](#).
- [89] M. Czakon, *The Four-loop QCD beta-function and anomalous dimensions*, Nucl.Phys. **B710** (2005) 485–498, [arXiv:hep-ph/0411261 \[hep-ph\]](#).
- [90] J. Abate and P. P. Valkó, *Multi-precision Laplace transform inversion*, International Journal for Numerical Methods in Engineering **60** (2004) no. 5, 979–993.

- [91] R. Hamberg, W. van Neerven, and T. Matsuura, *A Complete calculation of the order $\alpha - s^2$ correction to the Drell-Yan K factor*, *Nucl.Phys.* **B359** (1991) 343–405.
- [92] K. Chetyrkin, B. A. Kniehl, and M. Steinhauser, *Decoupling relations to $O(\alpha_s^3)$ and their connection to low-energy theorems*, *Nucl.Phys.* **B510** (1998) 61–87, [arXiv:hep-ph/9708255](#) [hep-ph].
- [93] R. V. Harlander and W. B. Kilgore, *Soft and virtual corrections to $pp \rightarrow H + X$ at NNLO*, *Phys.Rev.* **D64** (2001) 013015, [arXiv:hep-ph/0102241](#) [hep-ph].
- [94] S. Dawson, *Radiative corrections to Higgs boson production*, *Nucl.Phys.* **B359** (1991) 283–300.
- [95] S. Dawson and R. Kauffman, *QCD corrections to Higgs boson production: nonleading terms in the heavy quark limit*, *Phys.Rev.* **D49** (1994) 2298–2309, [arXiv:hep-ph/9310281](#) [hep-ph].
- [96] C. Anastasiou and K. Melnikov, *Higgs boson production at hadron colliders in NNLO QCD*, *Nucl.Phys.* **B646** (2002) 220–256, [arXiv:hep-ph/0207004](#) [hep-ph].
- [97] S. Catani, D. de Florian, M. Grazzini, and P. Nason, *Soft gluon resummation for Higgs boson production at hadron colliders*, *JHEP* **0307** (2003) 028, [arXiv:hep-ph/0306211](#) [hep-ph].
- [98] U. Aglietti, R. Bonciani, G. Degrossi, and A. Vicini, *Analytic Results for Virtual QCD Corrections to Higgs Production and Decay*, *JHEP* **0701** (2007) 021, [arXiv:hep-ph/0611266](#) [hep-ph].
- [99] S. Moch, J. Vermaseren, and A. Vogt, *Higher-order corrections in threshold resummation*, *Nucl.Phys.* **B726** (2005) 317–335, [arXiv:hep-ph/0506288](#) [hep-ph].
- [100] S. Moch and A. Vogt, *Higher-order soft corrections to lepton pair and Higgs boson production*, *Phys.Lett.* **B631** (2005) 48–57, [arXiv:hep-ph/0508265](#) [hep-ph].
- [101] R. D. Ball and S. Forte, *The Small x behavior of Altarelli-Parisi splitting functions*, *Phys.Lett.* **B465** (1999) 271–281, [arXiv:hep-ph/9906222](#) [hep-ph].
- [102] G. Hardy, *Divergent series*. Chelsea Publishing Series. American Mathematical Society, 1991.
- [103] E. J. Weniger, *Nonlinear sequence transformations for the acceleration of convergence and the summation of divergent series*, [arXiv:math/0306302v1](#).
- [104] S. Graffi, V. Grecchi, and B. Simon, *Borel summability: Application to the anharmonic oscillator*, *Phys.Lett.* **B32** (1970) 631–634.
- [105] U. D. Jentschura, *The Resummation of nonalternating divergent perturbative expansions*, *Phys.Rev.* **D62** (2000) 076001, [arXiv:hep-ph/0001135](#) [hep-ph].